NASA Tech Briefs

National
Aeronautics and
Space
Administration

Steel is one of the many industries that has used data from NASA's network of Industrial Applications Centers to reduce costs and improve products and services. Large and small companies throughout the U.S. purchase individually tailored searches of more than 8 million documents to help solve their technical and managerial problems. *See page A6 inside.*

Vol. 2, No. 4

WINTER 1977

About the NASA Technology Utilization Program

The National Aeronautics and Space Act of 1958, which established NASA and the United States civilian space program, requires that "The Administration shall provide for the widest practicable and appropriate dissemination of information concerning its activities and the results thereof."

To help carry out this objective the NASA Technology Utilization (TU) Program was established in 1962. It offers a variety of valuable services to facilitate the transfer of aerospace technology to nonaerospace applications, thus assuring American taxpayers maximum return on their investment in space research; thousands of spinoffs of NASA research have already occurred in virtually every area of our economy.

The TU Program has worked for engineers, scientists, technicians, and businessmen. And it can work for you.

NASA Tech Briefs

Tech Briefs is published quarterly and is free to any U.S. citizen or organization. It is both a current-awareness medium and a problem-solving tool. Potential products ... industrial processes ... basic and applied research ... shop and lab techniques ... computer software ... new sources of technical data ... concepts ... you will find them all in NASA Tech Briefs. The first section highlights a few of the potential new products contained in Tech Briefs. The remainder of the volume is organized by technical category to help you quickly review new developments in your areas of interest. Finally, a subject index makes each issue a convenient permanent reference file.

Further Information on Innovations

Although many articles are complete in themselves, others are backed up by Technical Support Packages (TSP's). TSP's are available without charge and may be ordered by simply completing the enclosed TSP Request Card. Further information on some innovations is available for a nominal fee from other sources, as indicated at the ends of the articles. In addition, Technology Utilization Officers at NASA Field Centers will assist you directly when necessary. (See page A4.)

Patent Licenses

Many of the inventions described are under consideration for patents or have been patented by NASA. Unless NASA has decided not to apply for a patent, the patent status is described at the end of each article. For further information about the Patent Program see page A8.

Other Technology Utilization Services

To assist engineers, industrial researchers, business executives, city officials, and other potential users in applying space technology to their problems, NASA sponsors six Industrial Applications Centers. Their services are described on page A6. In addition, an extensive library of computer programs is available through COSMIC, the Technology Utilization Program's outlet for NASA-developed software. (See page A5.)

Applications Program

To help solve public-sector problems in such areas as safety, health, transportation, and environmental protection, NASA TU Applications Teams, staffed by professionals from a variety of disciplines, work with Federal agencies, local governments, and health organizations to identify critical problems amenable to technical solutions. Among their many significant contributions are a rechargeable heart pacemaker, a lightweight fireman's breathing apparatus, aids for the handicapped, and safer highways.

Reader Feedback

We hope you find the information in NASA Tech Briefs useful. A reader feedback card has been included because we want your comments and suggestions on how we can further help you apply NASA innovations and technology to your needs. Please use it, or if you need more space, write us a letter.

NASA Tech Briefs

National Aeronautics and Space Administration

WINTER 1977
Volume 2, Number 4

COVERS: The photographs on the front and back covers illustrate commercial and nonaerospace advances made with the assistance of NASA's Technology Utilization program and from new technology developed by NASA and its contractors. For information about NASA's Industrial Applications Centers, [front cover], see pages A6 and A7. The Solar Concentrator [back cover] is described on page 461 [Circle 18]; and the communications Terminal [back cover], on page 497 [Circle 40].

About This NASA Publication

NASA Tech Briefs, a quarterly publication, is distributed free to U.S. citizens to encourage commercial application of U.S. space technology. For information on publications and services available through the NASA Technology Utilization Program, write to the Director, Technology Utilization Office, P. O. Box 8757, Baltimore/Washington International Airport, Maryland 21240.

"The Administrator of National Aeronautics and Space Administration has determined that the publication of this periodical is necessary in the transaction of the public business required by law of this Agency. Use of funds for printing this periodical has been approved by the Director of the Office of Management and Budget through December 31, 1978."

Change of Address

Change of Address: If you wish to have NASA Tech Briefs forwarded to your new address, use one of the Subscriptions cards enclosed in the back of this volume of NASA Tech Briefs. Be sure to check the appropriate box indicating change of address.

Communication Concerning Editorial Matter

For editorial comments or general communications about NASA Tech Briefs, you may use the self-addressed Feedback card in the back of NASA Tech Briefs, or write to: The Publications Manager, Technology Utilization Office (Code KT), NASA Headquarters, Washington, DC 20546. Technical questions concening specific articles should be directed to the Technology Utilization Officer of the sponsoring NASA Center (addresses listed on page A4.)

NASA TU SERVICES

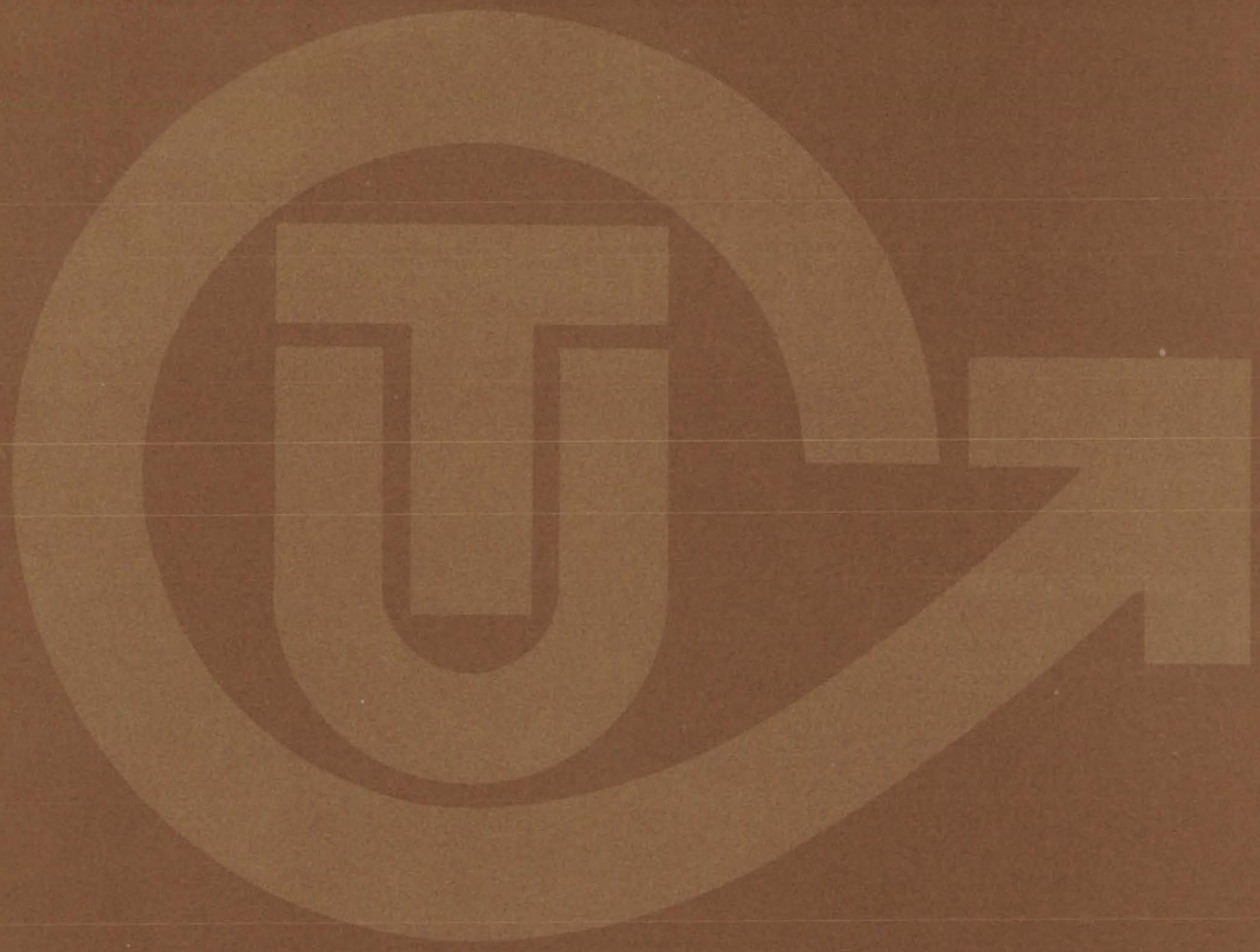

THE NASA TECHNOLOGY UTILIZATION OFFICERS

They will help you apply the innovations described in Tech Briefs.

The Technology Utilization Officer (TUO)
Each NASA Center has a Technology Utilization Officer — An applications engineer whose job is to help you make use of new technology developed at his center. He brings you the NASA Tech Briefs and other special publications, sponsors conferences, and arranges for expert assistance in solving technical problems.

Technical Assistance
Working together with NASA Scientists and Engineers and the Industrial Applications Centers, the center TUO's can answer specific questions about innovations and related NASA technology.

Technical Support Package (TSP's)
For many of the innovations described in Tech Briefs, the center TUO has prepared additional material that will help you in detailed evaluation and actual use or construction of the new technology. You may get TSP's free of cost by using the TSP Request Card or writing the center TUO.

Who to Contact. Of course, many technical questions about Tech Briefs are answered in the TSP's, but when no TSP is available, or you have further questions, write the Technology Utilization Officer at the center that sponsored the research at the address listed below.

Charles K. Kubokawa
Ames Research Center
Code AU: 230-2
Moffett Field, CA 94035
(415) 965-5554

Donald S. Friedman
Goddard Space Flight Center
Code 704.1
Greenbelt, MD 20771
(301) 982-6242

John T. Wheeler
Johnson Space Center
Code AT3
Houston, TX 77058
(713) 483-3809

Raymond J. Cerrato
John F. Kennedy Space Center
Code SA-RTP
Kennedy Space Center, FL 32899
(305) 867-2780

John Samos
Langley Research Center
Mail Stop 139A
Hampton, VA 23665
(804) 827-3281

Paul Foster
Lewis Research Center
21000 Brookpark Rd.
Cleveland, OH 44135
(216) 433-4000, Ext. 6832

Aubrey D. Smith
Marshall Space Flight Center
Code AT01
Marshall Space Flight Center, AL 35812
(205) 453-2224

John C. Drane
NASA Resident Legal Office-JPL
4800 Oak Grove Drive
Pasadena, CA 91103
(213) 354-6420

Gilmore H. Trafford
Wallops Flight Center
Wallops Island, VA 23337
(804) 824-3411, Ext 201

Louis Mogavero, Director
Technology Utilization Office
Code KT
NASA Headquarters
Washington, DC 20546
(202) 755-3103

COSMIC

(Computer Software Management & Information Center)

AN ECONOMICAL SOURCE OF COMPUTER PROGRAMS DEVELOPED BY THE GOVERNMENT.

COSMIC is sponsored by NASA to give you access to over 1400 computer programs developed by NASA and the Department of Defense, and selected programs from other government agencies. It is one of the Nation's largest software libraries.

COSMIC charges very reasonable fees for programs to help cover part of their expenses—and NASA pays for the remainder. Programs generally cost from $500 to $1000, but a few are more expensive and many are less. Documentation is available separately and very inexpensively.

COSMIC collects and stores software packages, insures that they are complete, prepares special announcements (such as Tech Briefs), publishes an indexed software catalog, and reproduces programs for distribution. COSMIC helps customers to identify their software needs, follows up to determine the successes and problems, and provides updates and error corrections. In some cases, NASA engineers can offer guidance to users in installing or running a program.

COSMIC programs range from management (pert scheduling) to information science (retrieval systems) and computer operations (hardware and software). Hundreds of engineering programs perform such tasks as structural analysis, electronic circuit design, chemical analysis, and design of fluid systems. Others determine building energy requirements, optimize mineral exploration, and draw maps of water-covered areas using NASA satellite data. In fact, the chances are, if you use a computer, you can use COSMIC.

COSMIC is eager to help you get the programs you need. For more information about services or software available from COSMIC, fill out and mail the COSMIC Request Card in this issue.

COSMIC: Computer Software Management and Information Center

Suite 112, Barrow Hall, University of Georgia, Athens, Georgia 30602 Phone: (404) 542-3265

WHERE IS THE WORLD'S LARGEST BANK OF TECHNICAL DATA ?

It's in Indianapolis and Pittsburgh, it's in Storrs, Connecticut and Research Triangle Park, North Carolina; and it's in Albuquerque and Los Angeles.

NASA IAC's — INDUSTRIAL

You can get more information and more data on more technical subjects through NASA's network of IAC's than anywhere else in the world. About 8,000,000 documents and growing at the rate of 50,000 more each month!

Major sources include:

- 750,000 NASA Technical Reports
- Selected Water Resources Abstracts
- NASA Scientific and Technical Aerospace Reports
- Air Pollution Technical Information Center
- NASA International Aerospace Abstracts
- Chem Abstracts Condensates
- Engineering Index
- Nuclear Science Abstracts
- NASA Tech Briefs
- Government Reports Announcements

and many other specialized files on food technology, textile technology, metallurgy, medicine, business, economics, social sciences, and physical science.

The IAC's are one of the most economical ways of staying competitive in today's world of exploding technology. The help available from the network ranges from literature searches through expert technical assistance.

Literature Searches
Help in designing your search, typically from 30 to 300 abstracts in as narrow or broad an area as you need, and complete reports when you need them. The most complete "search before research" available!

Current Awareness
Consult with our applications engineers to design your personal program — selected monthly or quarterly abstracts on new developments in your speciality. It's like having your own journal!

Technical Assistance
Our applications engineers will help you evaluate and apply your literature-search results. They can help find answers to your technical problems and put you in touch with scientists and engineers at NASA Field Centers.

To obtain more information about how NASA's IAC's can help you —
Check the IAC box on the TSP Request Card in this issue,
Or write or call the IAC nearest you.

APPLICATIONS CENTERS

How to get reports and other documents discussed in this issue of Tech Briefs

Many of the innovations in Tech Briefs are described in detail in reports available at a reasonable cost through one or more of the IAC's. To order a report, call or write the IAC referenced at the end of the Tech Brief article at the address below. Be sure to list the titles and accession numbers (N76-..., N75-..., etc.) of those you wish to purchase.

Aerospace Research Application Center (ARAC)
Indiana University-Purdue University at Indianapolis
1201 E. 38th St.
Indianapolis, IN 46205
E. Guy Buck, Director
(317) 264-4644

Knowledge Availability Systems Center (KASC)
University of Pittsburgh
Pittsburgh, PA 15260
Dr. Edmond Howle, Director
(412) 624-5211

New England Research Application Center (NERAC)
Mansfield Professional Park
Storrs, CT 06268
Dr. Daniel U. Wilde, Director
(203) 486-4533

North Carolina Science & Technology
Research Center (NC/STRC)
P. O. Box 12235
Research Triangle Park, NC 27709
Peter J. Chenery, Director
(919) 549-0671

Technology Application Center (TAC)
University of New Mexico
Albuquerque, NM 87131
Stanley A. Morain, Director
(505) 277-4000

Western Research Application Center (WESRAC)
901 Exposition Boulevard, Room 205
University of Southern California
University Park
Los Angeles, CA 90007
Radford King, Director
(213) 741-6132

NASA INVENTIONS AVAILABLE FOR LICENSING

Over 3,500 NASA inventions are available for licensing in the United States - both exclusive and nonexclusive.

Nonexclusive Licenses

Nonexclusive licenses for commercial use are encouraged to promote competition and to achieve the widest use of inventions. They must be used by a negotiated target date but are usually royalty free.

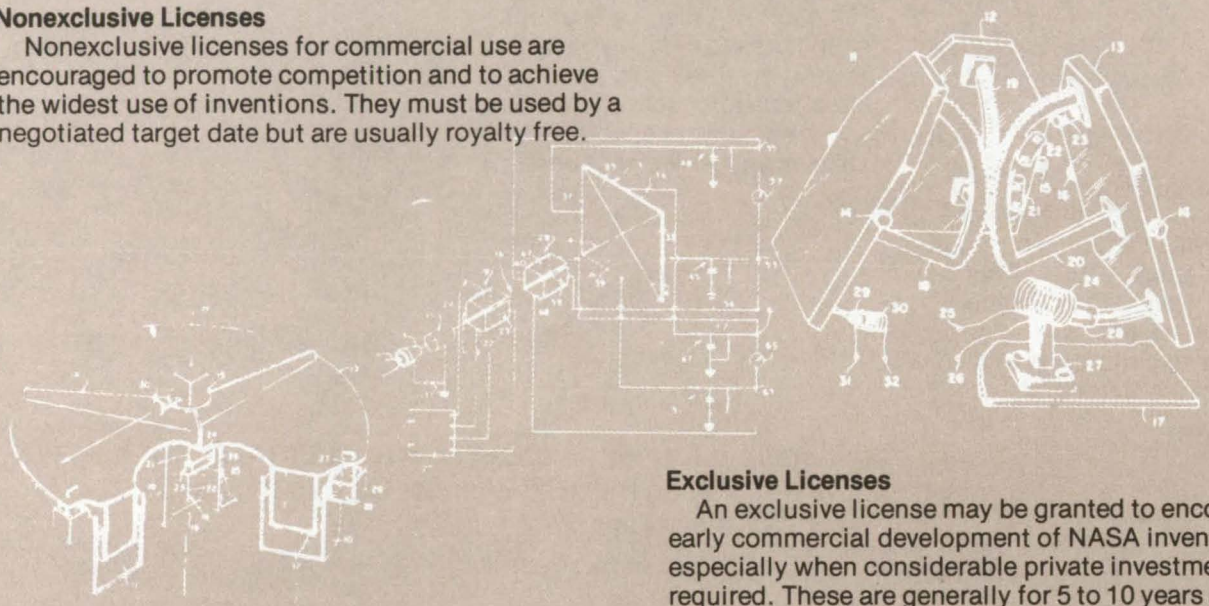

Exclusive Licenses

An exclusive license may be granted to encourage early commercial development of NASA inventions, especially when considerable private investment is required. These are generally for 5 to 10 years and usually require royalties based on sales or use.

The NASA patent licensing program also provides for licensing of NASA-owned foreign patents. In addition to inventions described in Tech Briefs, "NASA Patent Abstract Bibliography," containing abstracts of all NASA inventions, can be purchased from: National Technical Information Service, Springfield, Va., 22161. This document is updated semi-annually.

Patent Licenses and the NASA Tech Brief

Many of the inventions reported in Tech Briefs are patented or are under consideration for a patent at the time they are published. When this is the case, the current patent status is described at the end of the article; otherwise, there is no statement about patents. **If you want to know more about the patent program or are interested in license for a particular invention, write the Patent Counsel at the NASA Field Center** that sponsored the research. Be sure to refer to the NASA reference number in parenthesis at the end of the Tech Brief.

Robert F. Kempf
NASA Headquarters, Code GP
400 Maryland Ave., S.W.
Washington, DC 20546
(202) 755-3932

Darrell G. Brekke
Ames Research Center
Mail Code: 200-11A
Moffett Field, CA 94035
(415) 965-5104

John O. Tresansky
Goddard Space Flight Center
Mail Code: 204
Greenbelt, MD 20771
(301) 982-2351

Marvin F. Matthews
Lyndon B. Johnson Space Center
Mail Code: AM
Houston, TX 77058
(713) 483-4871

James O. Harrell
John F. Kennedy Space Center
Mail Code: SA-PAT
Kennedy Space Center, FL 32899
(305) 867-2544

Howard J. Osborn
Langley Research Center
Mail Code: 313
Hampton, VA 23665
(804) 827-3725

Norman T. Musial
Lewis Research Center
Mail Code: 500-113
21000 Brookpark Road
Cleveland, OH 44135
(216) 433-4000

Leon D. Wofford, Jr.
Marshall Space Flight Center
Mail Code: CC01
Marshall Space Flight Center, AL 35812
(205) 453-0020

Monte F. Mott
NASA Resident Legal Office-JPL
4800 Oak Grove Drive
Pasadena, CA 91103
(213) 354-2700

NEW PRODUCT IDEAS

NEW PRODUCT IDEAS are just a few of the many innovations described in this issue of NASA Tech Briefs and having promising commercial applications. Each is discussed further on the referenced page in the appropriate section in this issue. If you are interested in developing a product from these or other NASA innovations, you can receive further technical information by requesting the TSP referenced at the end of the full-length article or by writing the Technology Utilization Office of the sponsoring NASA center (see page A4). NASA's patent-licensing program to encourage commercial development is described on page A8.

New Process Produces High-Power Schottky Diodes

A new high-yield process produces mesa-geometry Schottky diodes with high reverse breakdown voltage and low reverse leakage current. The diodes can carry currents up to 50 amperes with less than 0.7-volt forward voltage drop.

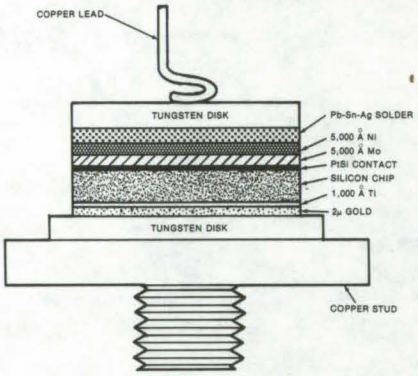

Switching times are typically less than 50 nanoseconds. The new process involves forming a Schottky barrier by depositing a film of platinum on epitaxially-grown silicon wafers while they are help at an elevated temperature. The platinum reacts with the silicon to form platinum silicide over the entire mesa top right up to the surrounding silicon oxide boundary. This metalization prevents edge breakdown and minimizes surface leakage.
(See page 431.)

No-Spill Touchup Paint Container

Small paint cans used for touchup painting can be converted to "spill-proof" containers with a new threaded spout that is installed in a hole in a standard paint-can lid. The spout has a funnel that makes it easier to dip the brush and a central tubular part that extends almost to the bottom of the container. If the can

tips, the seal between the spout and the lid prevents spillage. The device is simple and can be made is most shops.
(See page 529.)

Rotating Optical Coupler for Signal Transmission

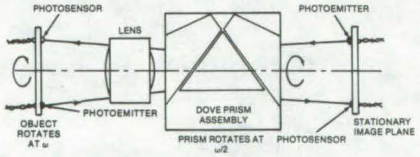

Data can be transmitted across a rotating interface without sliprings or other mechanical contacts using a new optical coupler able to handle simultaneously many high bit-rate signal channels. This coupler could be incorporated into several types of optical-communications and data-transfer equipment. A rotating Dove prism assembly, which forms a stationary image of a rotating object (such as the output of many optical transmitters), is the heart of the coupler. The stationary image is picked up by detectors at the receiving end of the system. The interface is bidirectional so that the roles of object and image can be reversed.
(See page 468.)

Miniature Diaphragm Valve for Medical Equipment

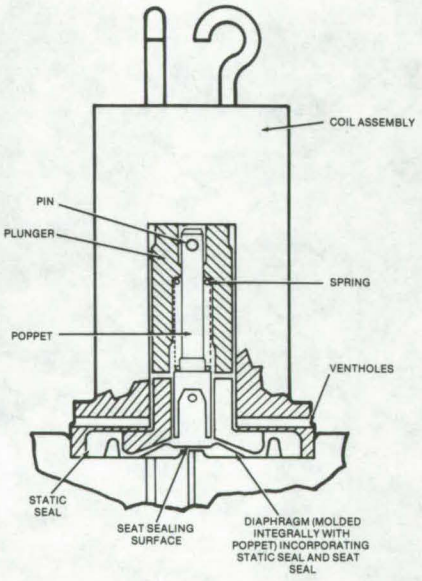

A proposed new valve isolates the moving parts of the valve assembly from the valved fluid. This feature is useful in biomedical applications where fluids that are subjected to sterilization temperatures might leave a residue that could degrade the performance of the valve. The fluid is isolated by molding the poppet and diaphragm in a single unit that separates the plunger mechanism from inlet and outlet ports. The design also gives a positive locking action for effective seating and unseating of the diaphragm.
(See page 498.)

"Either-Side-Up" Inflatable Liferaft

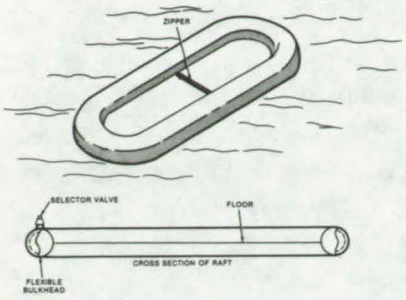

A new one-man liferaft can be thrown into the water and boarded regardless of which side falls up when it lands. The "both-sides-up" feature is made possible by positioning the floor midway between the top and bottom of the inflatable float tube. The raft is symmetrical about a horizontal plane through its midheight and can be ridden on either side. Other features include a zippered entry door in the floor of the raft that is easily fabricated and makes boarding easier and a double-sectioned float tube that provides an extra margin of safety against punctures.
(See page 518.)

Versatile Communications Terminal

Many widely separated parties are joined in an efficient communications network by a versatile new control terminal that handles voice and data transmissions via both telephone lines and radio-frequency channels. The system combines commercially available subassemblies into an attractive package that is easily operated by nontechnical personnel. Special features include a telephone autodialer, three radio and three telephone channels, and a telephone-to-radio "patch." A prototype is presently being used to link hospitals, ambulances, and special-care centers for rapid communications in emergency medical services operations.
(See page 497.)

Space-Age Cleaning Devices

Imaginative concepts in cleaning devices, originally developed for space applications, may find use in industry, research, and medicine.

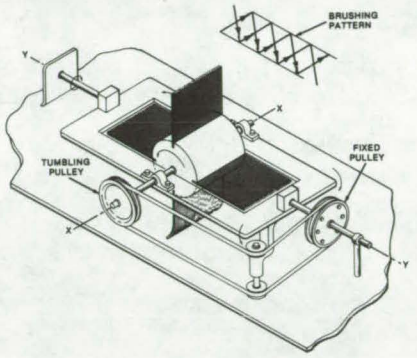

Included in the proposals and developments for more effective brushes and air handling are: a tapered-bristle brush that uses flowing air and an electrostatic-charge neutralizer to remove tiny surface particles, a cross-sweeping brush that sweeps in two directions simultaneously, an aerodynamically designed brush with a low sharp-edged tuftholder shaped like a diverging nozzle, and a notched-nozzle cleaning head that directs air into twin counterrotating vortexes to detach and entrain particles.
(See page 544.)

Biotelemetry System for Ambulatory Patients

A new system for multichannel transmission of EEG, EKG, and other biomedical information is so compact that it can be carried in a patient's belt. Pulse-code modulation is used for a high-quality signal, and CMOS integrated circuits make

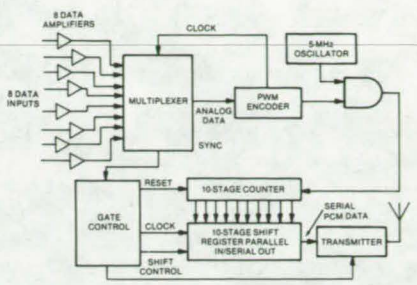

miniaturization possible. The present design can accept up to eight analog signals (blood pressure, blood flow, respiration, or oxygen consumption, for example). The data are converted to digital information and relayed to an RF transmission stage. The electronics are packaged in three units, each only 2 by 5 by 8 cm in size, and power is supplied by two 9-volt batteries.
(See page 500.)

Cryogenic Liquid-Level Detector

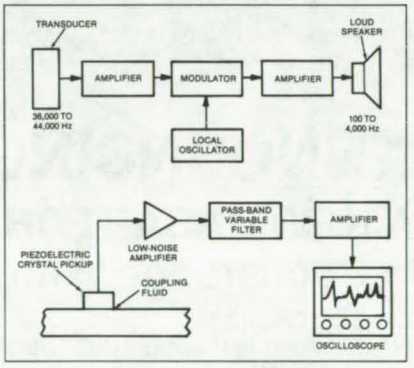

A new continuous-reading cappcitance sensor is an accurate level detector for cryogenic liquids. The detector has been designed for quick assembly, fast response, and good performance even when there is sloshing, boiling, or other disturbance in the liquid. The sensor, essentially a long parallel-plate capacitor with a specially-designed dielectric spacer, gives an accuracy of better than 1 percent when used with any of several simple signal-conditioning circuits. It has been successfully tested in liquid oxygen and liquid hydrogen in rocket propellant tanks.
(See page 510.)

PATENT LICENSES RECENTLY GRANTED BY NASA FOR COMMERCIAL USE OF NASA-OWNED INVENTIONS

The patent licenses listed below have been recently awarded by NASA as part of its program to encourage the commercial application of its new technology. For information on how you may obtain nonexclusive or exclusive license for the commercial use of NASA inventions, see page A8 of this issue.

A nonexclusive license to Applied Power Research, Indianapolis, Indiana, for U.S. Patent No. 3,964,928, covering an invention entitled "Lead-Oxygen DC Power Supply System Having A Closed Loop Oxygen and Water System."

A nonexclusive license to Hopkins International Company, Elmsford, New York, for U.S. Patent Application Serial No. 739,914, covering an invention entitled "Hearing Aid Malfunction Unit."

A nonexclusive license to Berkeley Bio-Engineering, San Leandro, California, for U.S. Patent Application Serial No. 779,428, covering an invention entitled "Flow Compensating Pressure Regulator."

A nonexclusive license to Xytel Corporation, Lombard, Illinois, for U.S. Patent Application Serial No. 754,066, covering an invention entitled "ROUS Bolt Tensioning Monitor."

A nonexclusive license to Advanced Life Sciences, Inc., New York, New York, for U.S. Patent No. 3,814,083, covering an invention entitled "Apparatus and Method for Processing Korotkov Sounds."

A nonexclusive license to Fiber Materials, Incorporated, Biddeford, Maine, for U.S. Patent Application Serial No. 658,487, covering an invention entitled "Improved Nozzle for Use With Abrasive and/or Corrosive Materials."

A nonexclusive license to Bison Instruments, Incorporated, Minneapolis, Minnesota, for U.S. Patent No. 3,814,083, covering an invention entitled "Apparatus and Method for Processing Korotkov Sounds."

A nonexclusive license to Ferro Corporation, Cleveland, Ohio for U.S. Patent No. 3,745,149, covering an invention entitled "Preparation of Polyimides From Mixtures of Monomeric Diamines and Esters of Polycarboxylic Acids."

A nonexclusive license to U.S. Polymeric, Santa Ana, California, for U.S. Patent No. 3,745,149, covering an invention entitled "Preparation of Polyimides From Mixtures of Monomeric Diamines and Esters of Polycarboxylic Acids."

ANNOUNCING . . .

A NEW NASA TECHNOLOGY UTILIZATION SERVICE in Cooperation With STATE GOVERNMENTS

NASA recently inaugurated a State Technology Applications Center (STAC) program with the opening of facilities in Florida and Kentucky.

The purpose of the experimental STAC program is to provide technical information services to state and local government agencies as well as to industry within each state.

The STAC's differ from the NASA Industrial Applications Centers (see page A7) primarily in that the STAC's are integrated into existing state technical assistance programs and serve only the host state, whereas the Industrial Applications Centers serve multistate regions.

The STAC's have access to several commercial data bases, as well as the NASA data base, and they normally charge a fee for their services.

Persons wishing **further information** should write to:

In Florida

NASA/Florida State Technology Applications Center (STAC)
311 Weil Hall
University of Florida
Gainesville, Florida 32611

or phone, Gainesville: (904) 392-6760
Orlando: (305) 275-2706
Tampa: (813) 974-2499

or contact the local State Department of Commerce Business Development Representative

In Kentucky

NASA/University of Kentucky State Technology Applications Program (STAP)
109 Kinkead Hall
University of Kentucky
Lexington, Kentucky 40506

phone: (606) 258-4632

Electronic Components and Circuits

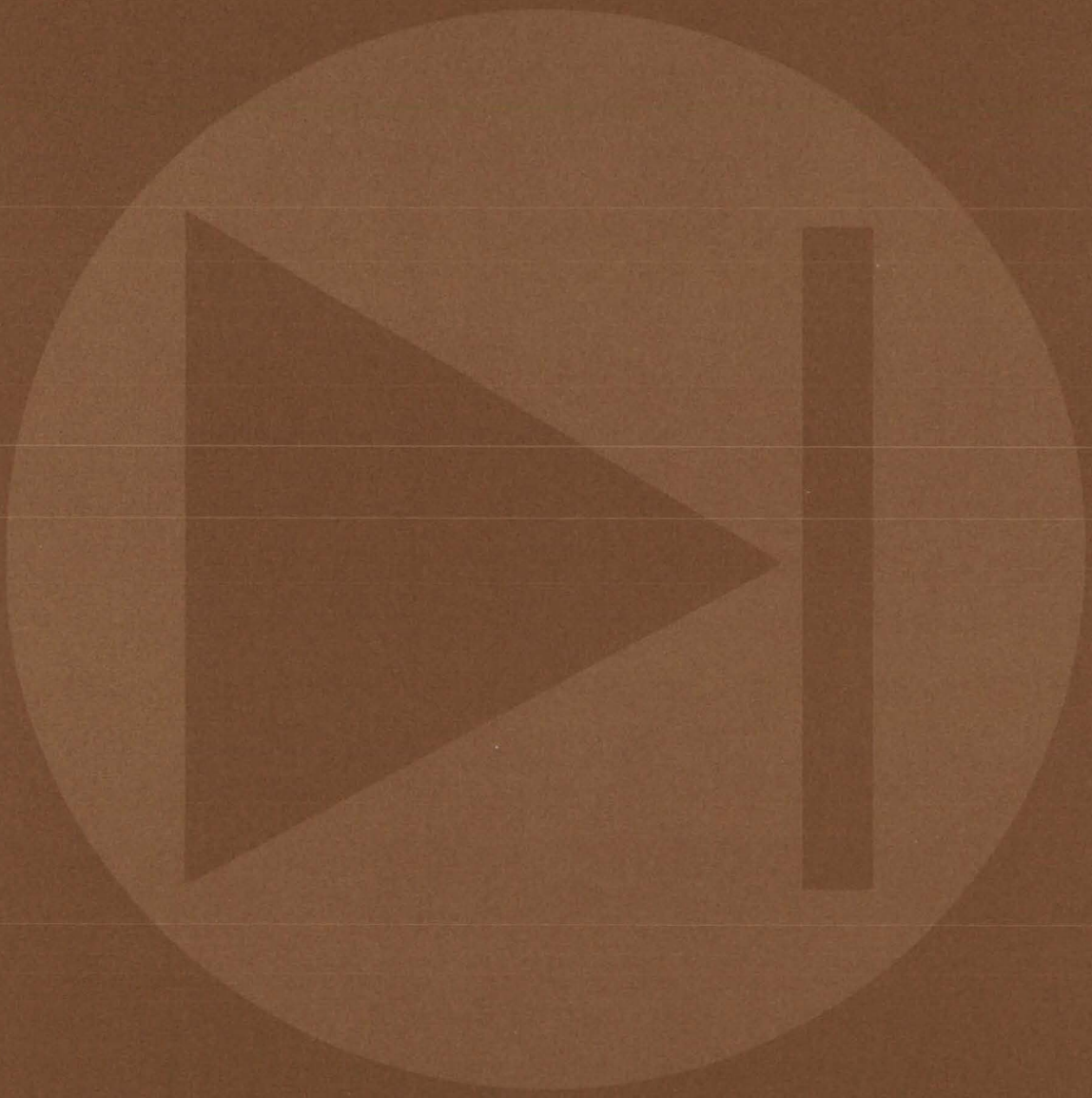

Simpler Process Produces More-Efficient Solar Cells

One-step process produces gallium arsenide solar cells with 18.5% efficiency.

Langley Research Center, Hampton, Virginia

A new process appears to be a major step toward producing a more-efficient solar cell at a lower cost. Cells of p-$Ga_{1-x}Al_xAs$, p-GaAs, and n-GaAs have been made by a single-step process, which replaces previous methods that required several more-involved growth sequences. In addition, the efficiency of the new cells is 18.5 percent compared to the about 15-percent efficiency that had been the best achievable previously.

The high efficiency of GaAs solar cells depends on large minority-carrier diffusion lengths (>3 μm) in the photoactive region of the cell plus a thin (<0.5-μm) $Ga_{1-x}Al_xAs$ layer. The GaAs required is necessary for high current collection efficiency, and the thin $Ga_{1-x}Al_xAs$ layer enhances the amount of solar radiation absorbed in the photoactive region of the GaAs. Earlier liquid-phase epitaxy (LPE) techniques utilized to grow the thin $Ga_{1-x}Al_xAs$ layer resulted in a deterioration in minority-carrier diffusion lengths in the region of the GaAs next to the $Ga_{1-x}Al_xAs$ layer. This lowered cell efficiency. Deterioration of the GaAs substrate could be prevented by contacting the substrate with a saturated LPE melt for a specific time followed by cooling, but the cooling leads to the growth of a discontinuous nonuniform layer of $Ga_{1-x}Al_xAs$ at the thin thicknesses desired.

The new one-step technique produces a solar cell with a uniform and continuous $Ga_{1-x}Al_xAs$ layer thinner than 0.5 μm and produces a minority diffusion length in the photoactive GaAs region greater than 3 μm. In its simplest form, this new technique involves bringing the substrate into contact with an undersaturated Ga-Al-As melt, causing etchback of the GaAs substrate. Interdiffusion of the freshly dissolved GaAs with the rest of the Ga-Al-As melt produces a supersaturated region near the substrate, which results in the growth of a thin (0.2- to 0.4-μm) graded layer of $Ga_{1-x}Al_xAs$. This graded layer has the effect of producing a drift field that enhances carrier separation.

Variations of this basic approach include zinc doping the p-GaAs layer and evaporating palladium and aluminum onto the $Ga_{1-x}Al_xAs$ surface. A 600-Å antireflective film of TiO_2 is then applied over the surface. The spectral response of such a cell is shown in the diagram.

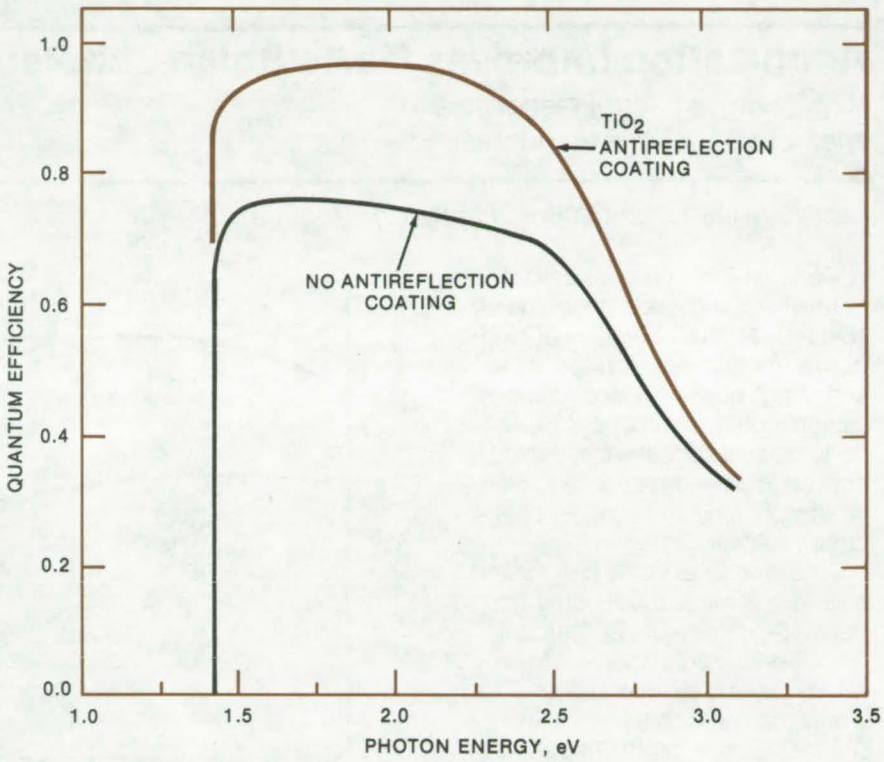

The Spectral Response of an Improved GaAs Solar Cell is shown with and without an antireflection coating. The cell is fabricated by a simplified process that promises lower production costs as well as improved efficiency.

Using an air mass 0 (AM0) extraterrestrial solar-spectrum simulation source, a cell fabricated with this technique exhibited a short-circuit current of 33 mA/cm^2, an open-circuit voltage of 0.99 volt, and a fill factor of 0.77. This cell has an AM0 efficiency of 18.5 percent as compared to about 15 percent for the best silicon cells in use. In addition, the one-step procedure is an improvement over the various multi-step procedures currently in use in

(continued next page)

the development of $Ga_{1-x}Al_xAs$-GaAs cells. Since solar cells are expected to be large-area devices, with cost an important consideration, this technique produces not only what is believed to be the best performing cell to date but shows promise to do so both efficiently and economically.

This work was done by H. J. Hovel and J. M. Woodall of IBM Corp. for **Langley Research Center.** *For further information, Circle 1 on the TSP Request Card.*

Title to this invention has been waived under the provisions of the National Aeronautics and Space Act [42 U.S.C. 2457(f)], to the IBM Corp., Yorktown Heights, New York 10598.
LAR-12180

Anodization Improves GaAs Solar-Cell Performance

High-energy spectral response and open-circuit voltage are increased.

Langley Research Center, Hampton, Virginia

GaAs pn-junction solar cells normally exhibit a poor high-energy spectral response because of high carrier-recombination rates at the surface. A newly-developed anodization technique produces GaAs pn-junction solar cells that exhibit both an improved response to high-energy photons and a higher open-circuit voltage.

A conventional GaAs pn-junction solar cell is made by diffusing zinc from a 5-percent-Ga, 50-percent-As, 45-percent-Zn source into an n-type GaAs substrate at 700° C for 2 minutes, yielding a pn junction 0.3 to 0.5 μm in depth. This structure is then fabricated into a solar cell by applying a Au-Ge-Ni alloy contact to the n-type surface and applying a p-type contact by the evaporation of, first, chromium, then aluminum. The decreasing spectral response with increasing energy (see Curve 1 in figure) for this type of cell is probably caused by carrier-recombination losses at the surface, where significant absorption of the high-energy photons occurs.

Anodizing the cell in a H_2O-H_3PO_4 solution of pH around 2.0 with an applied voltage of 40 V for 1 minute produces a $GaAsO_3$ layer about 750 Å thick and a refractive index of 1.8. This oxide layer reduces reflection losses from the GaAs surface; in addition, it greatly improves the high-energy response (Curve 2 in figure) and increases the open-circuit voltage by about 15 percent.

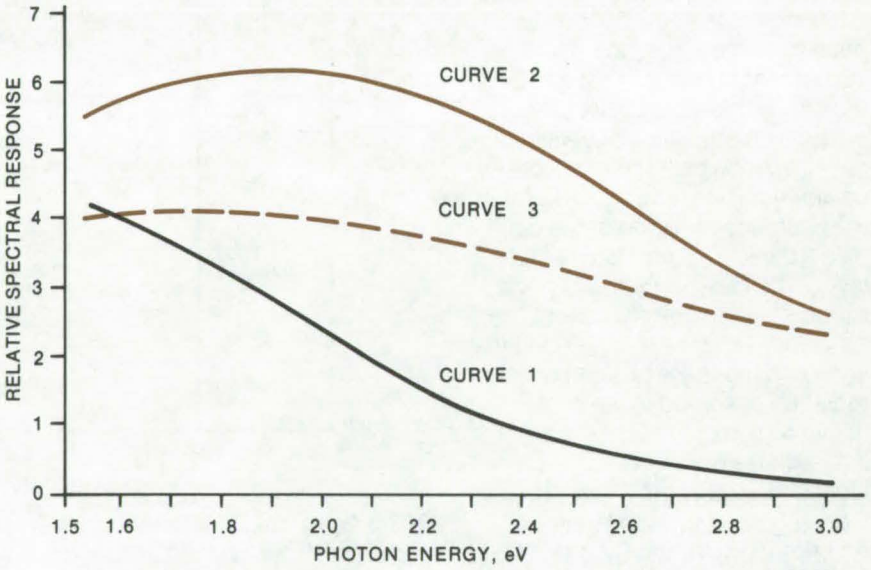

The Spectral Responses of three types of GaAs pn-junction solar cells show the effects of surface anodization and suggest the significance of carrier-recombination losses at the cell surface. Curve 1 refers to a conventional cell. The upper curve, Curve 2, is obtained after anodizing the cell as explained in the text. The anodization forms an antireflection layer and probably eliminates a surface layer of GaAs with high carrier-recombination rates. This conclusion is supported by Curve 3, the response after the anodization layer is removed. The removal of the antireflection coating reduces the response, compared to Curve 2, but the removal of a GaAs layer during the preceding anodization results in a response that is still higher than for the conventional cell in Curve 1.

Curve 3 shows the spectral response of the cell after the anodized layer has been removed by HCl, suggesting that anodization eliminates a GaAs layer with high carrier-recombination rates.

This single operation, which reduces reflection losses, improves high-energy response and increases open-circuit voltage, produces high-efficiency GaAs solar cells without the use of heterojunction structures such as $Ga_{1-x}Al_xAs$/GaAs.

This work was done by H. J. Hovel and J. M. Woodall of IBM Corp. for **Langley Research Center.** *No further documentation is available.*
LAR-12164

New Process Produces High-Power Schottky Diodes

High-yield process produces diodes with high reverse breakdown voltage and low reverse leakage current.

Lewis Research Center, Cleveland, Ohio

Reproducible methods have been developed for the fabrication of large-area (≅1 cm^2) mesa-geometry Schottky diodes that are free from defects. Processing procedures were demonstrated, using low-temperature platinum silicide to form the silicon/metal Schottky interface. Over 50 power Schottky diodes with forward and reverse characteristics that approach theoretical values have been built and tested.

Schottky diodes made by the new process have been operated with reverse breakdown voltages as high as 150 volts and leakage currents less than 5 milliamperes at 212° F (373 K). The diodes are rated to carry currents up to 50 amperes with a forward voltage drop less than 0.7 volt. Switching times are typically less than 50 nanoseconds.

Schottky diodes have long been attractive for high-power applications by virtue of their reduced power loss in forward conduction and their rapid recovery time compared with pn junction rectifiers. These advantages, however, are balanced by the inherent disadvantages of greater reverse leakage current, lower reverse-bias breakdown voltage, and far greater variability than their pn junction counterparts in electrical characteristics due to processing difficulties.

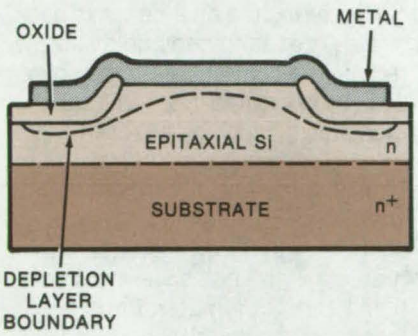

Figure 1. A **Mesa Schottky Diode** with no practical defects in the geometry is shown above. These diodes have breakdown voltages near 150V, leakage currents less than 5 mA, and carry currents up to 50 A with a forward voltage drop less than 0.7 V.

New-process Schottky diodes were fabricated in a mesa geometry as shown in Figure 1. Epitaxially-grown n-type silicon 10 to 15 microns thick, ranging in resistivity from 1 to 4 Ω-cm, was used as starting material. Silicon nitride (Si_3N_4) was used as an etch mask to define the mesa top, which eventually comprises the active device area. Mesas 8,000 Å high were formed by etching away the unprotected silicon with an HNO_3:HF etch. Wafers were oxidized at 1,832° F (1,273 K) in steam followed by a 1,832° F argon anneal to passivate the mesa sides and reduce leakage currents. The same Si_3N_4 mask that served to define the mesa top due to its resistance to the mesa etch also protects the silicon against oxidation. In this way, the SiO_2 mesa passivation is automatically prevented from extending onto the mesa top, and the metal barrier, to be formed later, will precisely cover the mesa top. A conventional $POCl_3$ gettering step was required in order to produce hard nonleaky junctions. It was performed either before or after mesa formation and passivation.

The barrier itself is formed as follows. First, the Si_3N_4 etch mask is removed with hot H_3PO_4. Next, the exposed silicon is lightly sputter-etched to remove surface impurities and any heavily doped regions at the surface formed during the getter

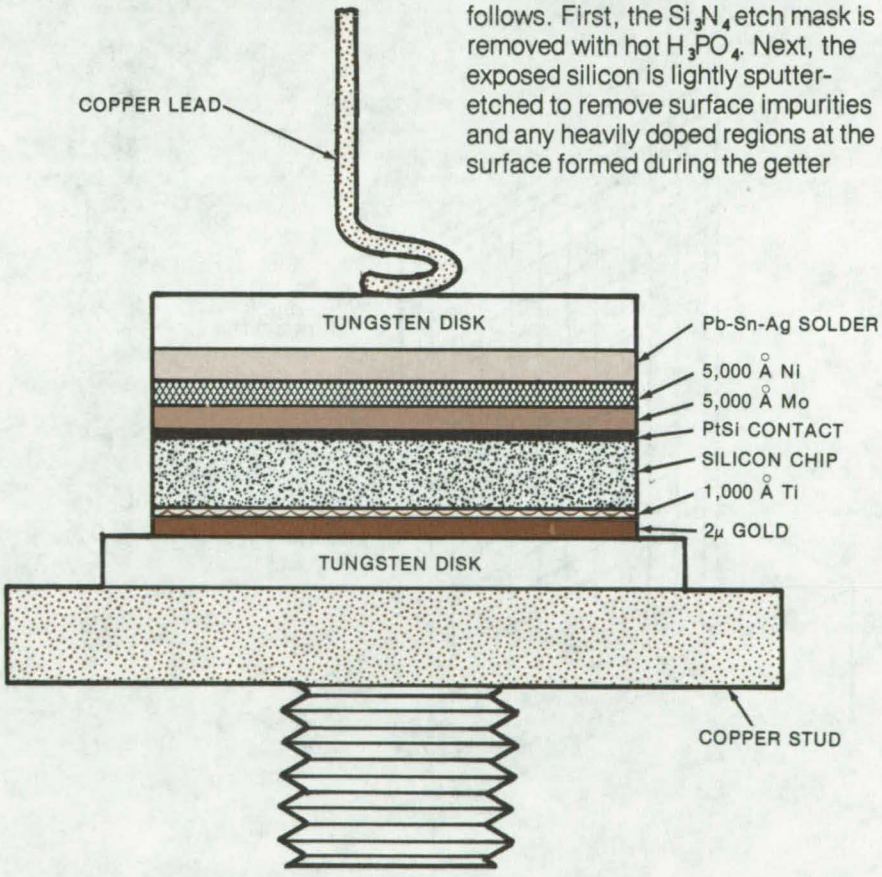

Figure 2. The **Assembled Diode** is eutectic-bonded between tungsten backup plates and is mounted to a copper header and lead-in wire. The entire assembly is soldered together in one step.

(continued next page)

cycle. Then, the Schottky barrier is formed by depositing 600 Å of platinum onto the silicon wafers while they are held at an elevated temperature. As the platinum is deposited on the hot silicon, some of it reacts with the silicon to form platinum silicide. In this way, the PtSi Schottky metalization covers the entire mesa top right up to the SiO_2 boundary and prevents edge breakdown and surface leakage.

In the assembly phase (Figure 2), the pretested chips were first eutectic-bonded to tungsten backup plates at a temperature of 932° F (773 K). The completed tested subassembly was then mounted to its copper header, and its top lead was applied. A tungsten toppiece is used to spread the current from the copper lead-in wire to the metalized Schottky barrier.

The entire assembly was soldered together in one step by heating it in hydrogen to a temperature of 662° F (623 K). The mounted diode was encapsulated in silicon rubber, leaving the top Cu lead accessible for measurements.

This new processing procedure, using low-temperature platinum silicide, resulted in a successful high-yield fabrication of large-area mesa-geometry Schottky diodes. Reproducible methods of silicon Schottky fabrication were also demonstrated for tungsten, aluminum, and conventional platinum silicide metalization.

This work was done by Linus F. Cordes, Marvin Garfinkel, and Ernest A. Taft of General Electric Co. for **Lewis Research Center.** *Further information may be found in NASA CR-134925 [N76-21391], "Development and Fabrication of Improves Schottky Power Diodes," a copy of which may be obtained at cost from the New England Research Application Center [see page A7].*
LEW-12749

Inexpensive Silicon Sheets for Solar Cells

Liquid silicon adheres to a graphite grid by surface tension.

Caltech/JPL, Pasadena, California

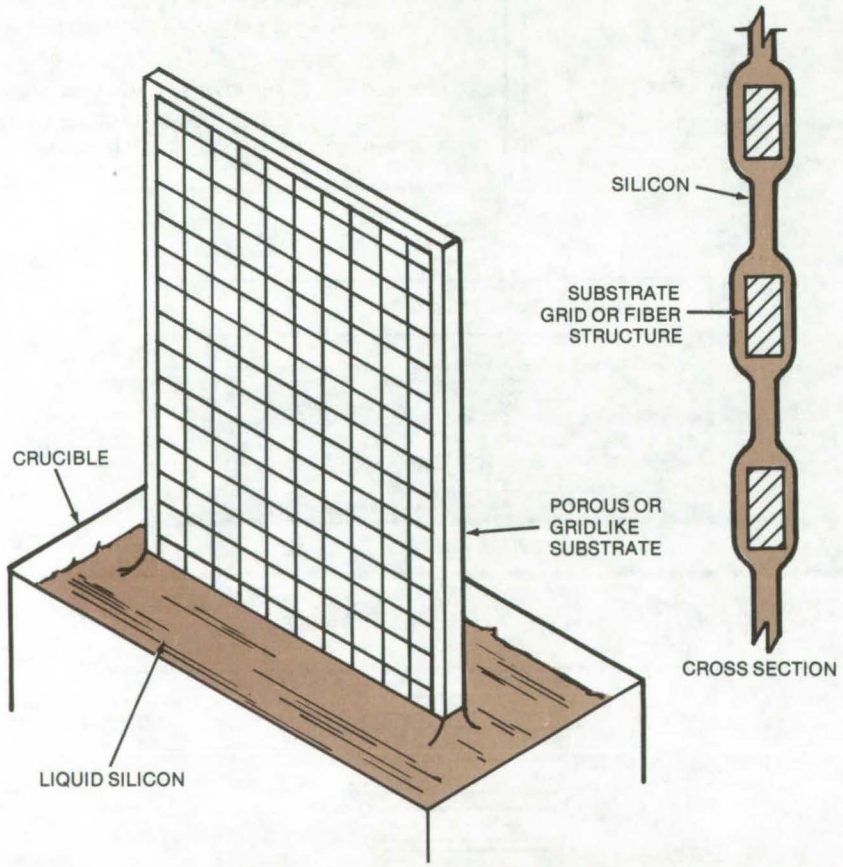

Figure 1. A **Graphite Grid Acquires a Coating of Silicon** as it is withdrawn from a melt. The coating is continuous and is accessible from either side, making it possible to attach electrodes for the fabrication of photovoltaic cells.

Inexpensive solar-cell arrays may become a reality, using a new method for growing thin sheets of silicon. In the method, a gridlike or porous sheet of graphite is dipped in molten silicon. As the graphite is withdrawn from the melt, silicon clings to it and solidifies as thin sheets in the holes, encasing the grid (Figure 1). Electrical contacts are easily attached to both surfaces of silicon sheets formed in this way, a feature not possible when the silicon is deposited on a ceramic substrate. The technique could sharply reduce the cost of producing solar cells by operating in a continuous mode using flexible gauzelike graphite or other flexible materials.

In an experiment, holes of various sizes were cut in a thin (127-μm) sheet of high-purity, high-density graphite. If the holes were no more than 2 mm in diameter, the surface tension of the liquid silicon was sufficient to form a stable film in the holes. In the experiment, the graphite was withdrawn at 1.5 cm/s, a speed that may be sufficiently fast for mass production.

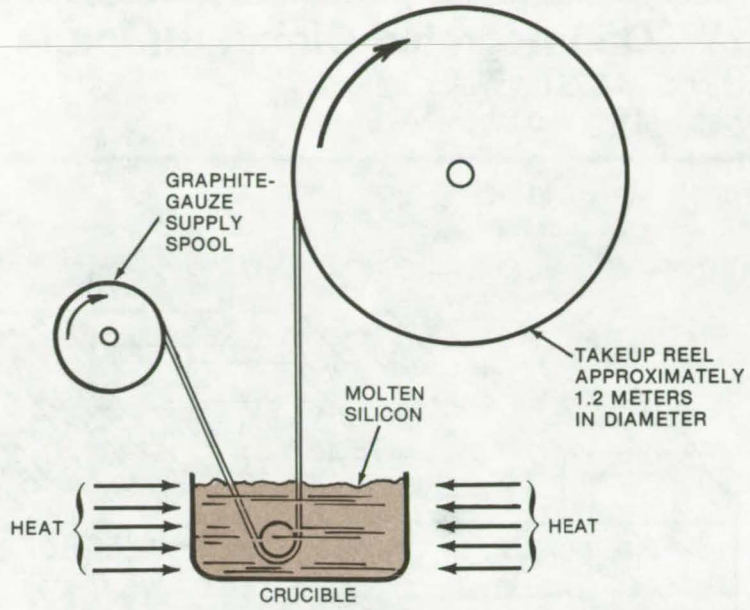

Figure 2. In a **Continuous Process,** a graphite gauze (or other flexible material) is immersed in liquid silicon, coated, and wound on a takeup spool.

The method is readily adaptable to a continuous process (Figure 2). The graphite can be supplied from a spool as a gauzelike strip, drawn through a pool of liquid silicon in a crucible, and taken up as a continuous silicon-coated sheet on a large reel. Other substrate materials may be suitable for mass production — possibly paper could be used to minimize costs.

This work was done by Theodore F. Ciszek and Guenter H. Schwuttke of IBM Corp. for **Caltech/JPL.** *For further information, Circle 2 on the TSP Request Card.*
NPO-14069

Low-Resistance Contacts for GaAlAs/GaAs Cells

A bimetallic contact such as palladium/aluminum lowers the series resistance and improves the reliability of $Ga_{1-x}Al_xAs$ solar cells.

Langley Research Center, Hampton, Virginia

In previous technology, achieving a low-resistance ohmic contact to p-type $Ga_{1-x}Al_xAs$ has proved difficult. Contacts that work well with p-type GaAs work poorly with $Ga_{1-x}Al_xAs$. For example, a Au-Zn contact works very well for p-type GaAs but is unsuccessful with $Ga_{0.3}Al_{0.7}As$, even when the latter is diffused with zinc to raise the acceptor concentration level. This contradiction in requirements has complicated the fabrication of reliable $Ga_{1-x}Al_xAs$/GaAs solar cells, particularly when the GaAlAs layer is less than 1μ in depth, due to the high series resistance resulting from the poor contacting. Diffusing the cell with zinc and annealing it at a high temperature after contact evaporation can lower the contact resistance to an acceptable level, but the high-temperature process often ruins the cell.

Low-resistance contacts for GaAlAs/GaAs cells have now been made by using palladium to contact the GaAlAs, followed by gold, silver, chromium, or aluminum for bonding. Typically, 500 Å of palladium are applied, followed by about 5,000 Å of aluminum. The palladium forms an ohmic contact of low resistance to undiffused GaAlAs, as well as to diffused materials. Low-temperature annealing at 300° C with aluminum strongly bonds the palladium and the GaAlAs. (Firing temperatures even as high as 500° C with gold or silver contacts does not produce equivalent results.) The palladium can be applied by evaporation, sputtering, or electroless plating, using a palladous chloride solution.

The ohmic contact obtained by this method greatly reduces the series resistance and increases the reliability of GaAlAs/GaAs solar cells. The results obtained have not been achieved by any other metallurgy to date, and this technique is also applicable to the fabrication of lasers such as the room-temperature heterojunction laser.

This work was done by H. J. Hovel and J. M. Woodall of IBM Corp. for **Langley Research Center.** *No further documentation is available.*

Inquiries concerning rights for the commercial use of this invention should be addressed to the Patent Counsel, Langley Research Center *[see page A8].* *Refer to LAR-12201.*

Complementary DMOS/VMOS Integrated-Circuit Structure

Asymmetric double diffusion in P-channel DMOS transistor and in N-channel VMOS transistor provides fast high-voltage CMOS.

Goddard Space Flight Center, Greenbelt, Maryland

A new complementary metal-oxide-semiconductor (CMOS) structure has relatively high speed, a high breakdown voltage, high transconductance, and high packing densities. Radiation-hardening techniques can be incorporated into its processing with no degradation in performance.

These results are achieved by forming an integrated-circuit CMOS including an asymmetrical double-diffused metal-oxide-semiconductor (DMOS) transistor as half of the complementary pair and a V-notched metal-oxide-semiconductor (VMOS) transistor as the other half of the pair. The figure shows this arrangement.

The device has a fast response time because both the DMOS and VMOS transistors have high-speed channels. The asymmetric DMOS has fast transit time across the channel because a carrier is accelerated as it crosses the n-type material between the p^+ layer and the p^- well. (In contrast, in a symmetric DMOS configuration, a carrier is both accelerated and decelerated as it crosses the relatively-short channel length.) Because double diffusion in the DMOS transistor occurs only on the p^+ side of the device where the source electrode is located, there is a relatively-high voltage breakdown between the source and drain electrodes of the DMOS transistor.

The V-notched transistor has a fast response time because it has a relatively-short channel length. The short channel is achieved without sacrificing the voltage breakdown characteristics of the device. It is made by diffusing successive p^+ and n^+ regions into the p^- well, and then cutting a V-shaped notch along the edge of the p^+ region (see figure). Thus there are three regions along one side of the V-notch — p^-, p^+, and n^+ — and only two regions along the other side. The channel is formed through the p^+ region on the three-region side, between the p^- well and the n^+ contacting region.

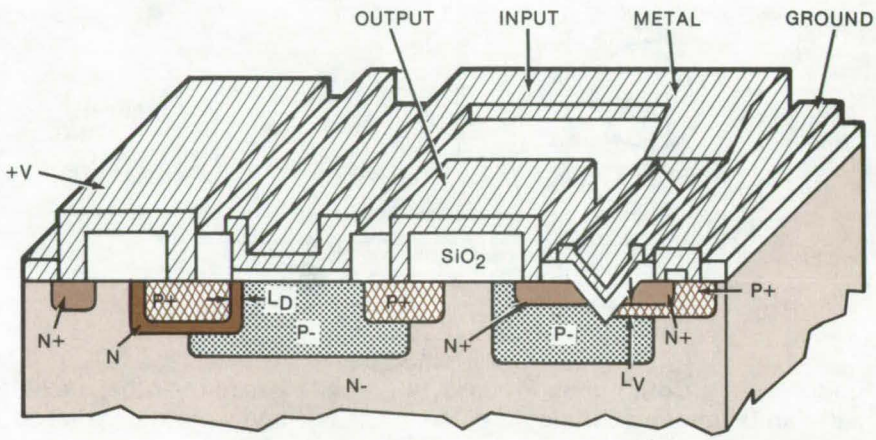

Complementary Transistors, a p-channel DMOS and an n-channel VMOS, both feature asymmetrical double diffusion for high-speed operation and high breakdown voltage. Their combination has all of the advantages of conventional CMOS devices.

The V-notch is formed on a plane having a crystalline surface state of <111> in a substrate having a crystalline structure of <100>. This structure results in a shift in the threshold voltage of the well; the well has a low impedance with zero bias applied to a metalized gate electrode that covers an oxide layer formed over exposed portions of the well and diffusion layers in the notch. With zero bias, there is no conduction through the p^+ region. Conduction occurs when a forward bias voltage at the gate electrode causes charges to flow across the relatively short length of this region. The breakdown voltage is relatively high because the avalance current, which must be achieved before breakdown results, must be through the relatively high concentration of the p^+ channel of the three-region edge to the diffusion layer along the other edge of the notch.

The DMOS and VMOS devices have been fabricated with channel lengths of between 0.5 and 1.0 micrometer. Devices having theoretical cutoff frequencies of approximately 2 GHz were formed, with maximum transconductances of 190 micromhos for the p-channel DMOS transistor and 490 micromhos for the n-channel VMOS transistor. The n-channel and p-channel transistor widths were 1.1 mils (28 micrometers) and 0.7 mil (18 micrometers), respectively. The absolute value of the threshold voltage of the individual devices was between 0.8 and 4.0 volts; the inverter was found to operate satisfactorily for supply voltages ranging from 2 to 15 volts.

This work was done by Murzban D. Jhabvala of **Goddard Space Flight Center.** *For further information, including details and illustrations on fabrication, Circle 3 on the TSP Request Card.*

This invention is owned by NASA, and a patent application has been filed. Inquiries concerning nonexclusive or exclusive license for its commercial development should be addressed to the Patent Counsel, Goddard Space Flight Center [see page A8]. *Refer to GSC-12190.*

Welding Single-Crystal Silicon to Molybdenum

Heating, followed by slow cooling, produces reliable bonds.

Caltech/JPL, Pasadena, California

In high-temperature diodes (used for thermionic generation of electric current), the anode or collector is a metal substrate, typically molybdenum. A wafer of a single-crystal semiconductor, such as silicon, may be bonded to the diode to produce a collector with an extremely low work function. It has been found that these materials can be bonded by raising the substrate temperature to around 1,100° C and cooling it at a slow controlled rate.

Before bonding, the interfacing surfaces must be carefully prepared. A typical as-received silicon wafer has a lapped and polished planar surface with a native-grown oxide; the oxide can be removed with a hydrofluoric acid dip and a distilled-water rinse immediately prior to processing. Surface oxidation is removed from the smooth-machined and lightly-polished molybdenum substrate by electrolytic cleaning in sulfuric acid and distilled-water rinsing just prior to processing.

The exact substrate temperature at which bonding begins is a function of the thermal conductivity at the interface; this depends on the cleanliness and flatness of the surfaces to be bonded. Once bonding begins in any small area (as evidenced by a glow in the area of the silicon), the entire silicon crystal bonds to the molybdenum in a period of about 10 minutes. A compressive force of from 1 to 10 dynes/cm^2 has been found helpful (but not necessary) for initiating the bond.

So far, processing has been carried out in a vacuum environment, but successful welding can probably be achieved in an inert gas or hydrogen atmosphere as well. When bonding is complete, the composite is slowly cooled, at about 25° C/min; otherwise, the silicon crystal can crack due to thermal stresses caused by differential expansion.

The bond withstands continuous operation at 1,100° C in a vacuum environment. The bonding mechanism is thought to be the diffusion of silicon into the molybdenum across the interface. The diffusion changes the coefficient of thermal expansion for the interface region, (see figure). This change is apparent from the fact that the molybdenum area into which the silicon has diffused is slightly raised with respect to the plane of the undiffused molybdenum.

This work was done by Keun-Ho Chang of **Caltech/JPL** *and Michael P. Donovan of The Boeing Co. No further documentation is available.*
NPO-13735

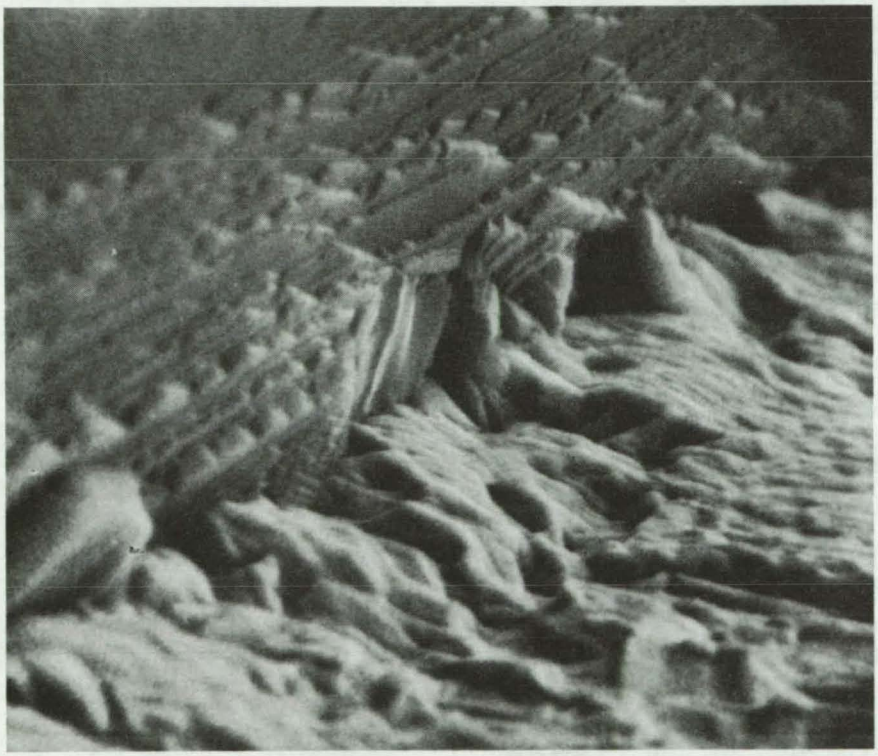

A **Silicon-to-Molybdenum Bond,** seen magnified 3,000X, is formed at elevated temperature, followed by slow cooling to prevent cracking. The silicon is the material above the interface.

Primary-Controlled AC-to-DC Power Converter

Synchronous switch in primary circuit allows transformer rewinding for increased power-handling capacity and regulates output voltage.

Marshall Space Flight Center, Alabama

Switched operation of a power-transformer/rectifier dc supply requires fewer turns of larger wire on a given transformer core, increasing its power-handling capability, and regulates the output voltage.

A synchronous switch, which can be a transistor, is placed in series with the transformer primary, as shown in Figure 1. The switch remains open during most of each half cycle and then is closed for a short time so that energy can be delivered to the load. The transformer primary voltage falls to zero while the switch is open, so the average primary voltage is greatly reduced. With fewer volt-seconds impressed on the transformer during each half cycle, a given core can have fewer turns per volt and therefore can use larger wire. The secondary voltage is regulated by varying the phase angle at which the switch is closed.

A conventional power-transformer/rectifier circuit was breadboarded and tested. Then a regulator employing the technique illustrated in Figure 1 was designed with a modified transformer that had fewer turns of larger wire. This circuit also was breadboarded and tested. The tests showed that for the same temperature rise of the transformer core, the circuit of Figure 1 delivered four times as much power as the unmodified transformer/rectifier circuit. These results are shown graphically in Figure 2.

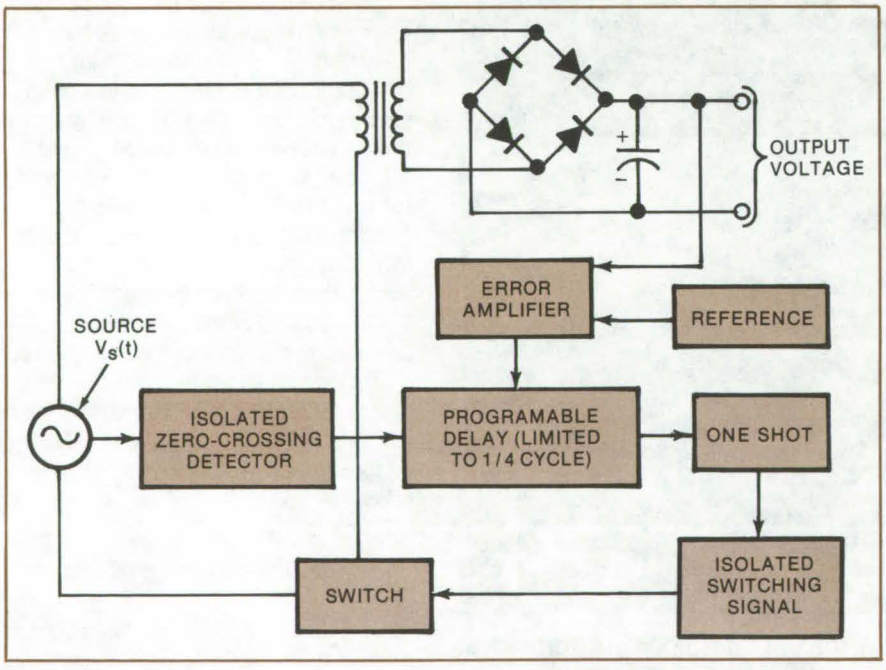

Figure 1. A **Synchronous Switch** circuit (shown in color) controls this ac-to-dc converter that has modified transformer windings. The power-handling capability is improved over a conventional transformer/rectifier circuit, and the output voltage is regulated.

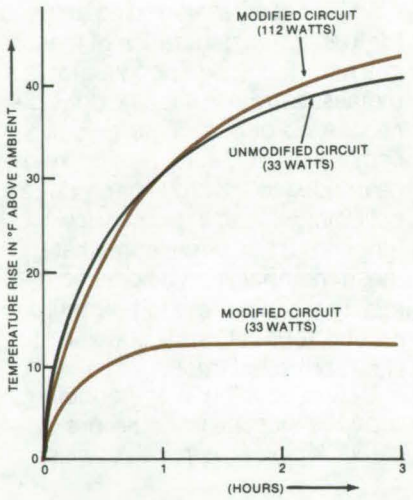

Figure 2. **Test Results** show that the modified circuit delivers four times as much power as the unmodified circuit for a given temperature rise of the transformer core. The black curve is for the unmodified circuit, and the curves in color are for the circuit of Figure 1.

The control circuit of Figure 1 regulates the output voltage by closing the switch at the appropriate time during each half cycle. In the tests, the output voltage was held to within 1.5 percent of nominal for a 10-percent input voltage variation and a 400-percent load variation.

This work was done by Paul Harper and L. N. Mercer of Sperry Rand Corp. for **Marshall Space Flight Center.** *For further information, including detailed circuit diagrams, Circle 4 on the TSP Request Card.*
MFS-23198

Differential Current Driver

Three op amps form a stable low-noise current source.

Lyndon B. Johnson Space Center, Houston, Texas

Three operational amplifiers in a closed-loop configuration form a stable current driver for variable non-ground-referenced loads. The circuit uses lower-voltage power supplies than other circuits of this type and provides constant voltage-to-current gain in a low-noise configuration. The use of operational amplifiers simplifies frequency compensation when driving reactive loads.

The uncompensated circuit is shown in the figure. The input voltage signal (E_{in}) is applied to the open-loop amplifier U_1. The output of U_1 goes to the input of unity-gain inverting amplifier U_2 and to one side of the load. The output of U_2 is applied to the other side of the load through a sensing resister (R_S). The sensed output is amplified by U_3 (gain = A) and is applied to the inverting input of U_1, completing the loop.

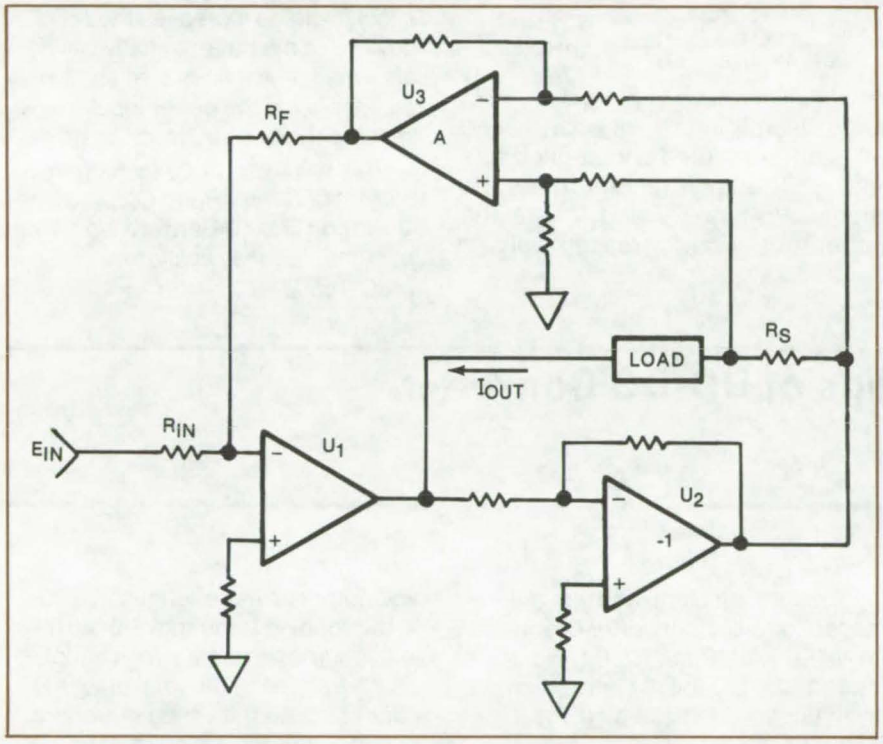

This **Differential Current Driver** provides stable voltage-to-current gain for a variable non-ground-referenced load. The voltage across the load is approximately twice that present at the output to U_1 (because of the inverting unity-gain amplifier U_2), so that low-voltage power supplies can be used.

Since the load is not referenced to ground, the susceptibility of the circuit to noise and electromagnetic interference is reduced. Also, since the voltage applied to the load is double that provided by a ground-referenced configuration (except for a small drop across R_S), a higher voltage range is available with lower-voltage power supplies; this can save weight, space, and cost in many applications. Reactive elements could easily be added to offer frequency compensation for complex loads. The closed-loop gain of the current driver is given by the following equation:

$$\frac{I_{out}}{E_{in}} = \frac{R_f}{R_{in}} \frac{1}{R_S A}$$

This work was done by Gerald F. Kopp of Honeywell Inc. for **Johnson Space Center.** *For further information, Circle 5 on the TSP Request Card.*
MSC-16475

Digital-Signal Transfer Between Isolated Systems

Simple circuit is compatible with CMOS logic.

Lyndon B. Johnson Space Center, Houston, Texas

A simple circuit that is compatible with CMOS logic can transfer digital signals between electrically isolated systems. The system uses no transistors and a minimum of discrete components. Its essential elements are a small transformer and a CMOS noninverting buffer.

As seen in the figure, the input signal (V_{in}) passes through the first buffer (B_1) and is differentiated to give positive and negative spikes (V_1) at the transformer primary. The spikes mark the leading and trailing edges of the input signal.

(continued next page)

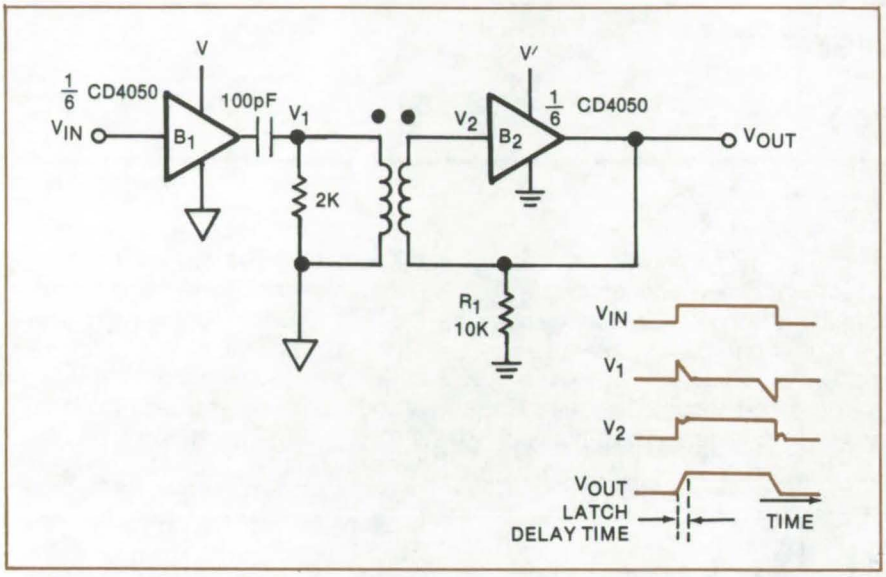

Digital-Signal Transfer Circuit requires a minimum of parts and consumes little power. The input signal is differentiated and applied to a bistable latch in the transformer secondary. The latch reconstitutes the input signal from the differentiated signal. Voltages V and V′ are the power supply voltages of the input and output circuits, respectively.

The output circuit is configured as a bistable latch. The output of the noninverting buffer (B_2) is connected back to its input through the transformer secondary. The buffer has two stable states: either input and output are both high or both low. If the latch is in the low state, a positive spike at the transformer primary will switch the buffer to its high state. Similarly, the buffer will be switched to the low state by a negative spike.

The resistor R_1 can be included to hold the latch in a known state when power is first turned on. As the supply voltage increases the MOS devices in the buffer initially will be off; when the devices turn on, the resistor holds the buffer input low, keeping the latch in its low state.

This work was done by Richard Harper of Sperry Rand Corp. for **Johnson Space Center.** *No further documentation is available.*
MSC-16508

Circuit Regulates Voltage of DC-DC Converter

Lightweight, efficient regulator requires no preregulator.

Lewis Research Center, Cleveland, Ohio

A new method of regulating a voltage-multiplier dc-dc converter eliminates the separate preregulator used in conventional practice. The regulating circuit directly controls only a fraction of the input voltage. The result is a lightweight, efficient regulator suitable for use with the lightweight, efficient, and versatile capacitor diode converter described in *NASA Tech Briefs,* Vol. 1, No. 2, page 152, "DC-to-DC Conversion With Voltage Multipliers" (LEW-12297).

The regulation compensates simultaneously for both input voltage and output power changes at a 70-kHz chopping frequency. An auxiliary inductor is used, which handles only a fraction of the total power to control the output voltage through a pulse-width modulation method in a buck/boost circuit.

No known means existed for direct control of a voltage-multiplier dc-dc converter prior to the development of this regulation method. The previous method was to control the input voltage of the capacitance diode voltage multiplier, and therefore the output voltage, by a separate preregulator using one of several well known methods such as buck or buck/boost regulation. This resulted in a serious penalty in weight and efficiency. The new method described here gives direct control of a voltage-multiplier dc-dc converter without the weight and efficiency penalties of a preregulator.

As shown in the schematic, the

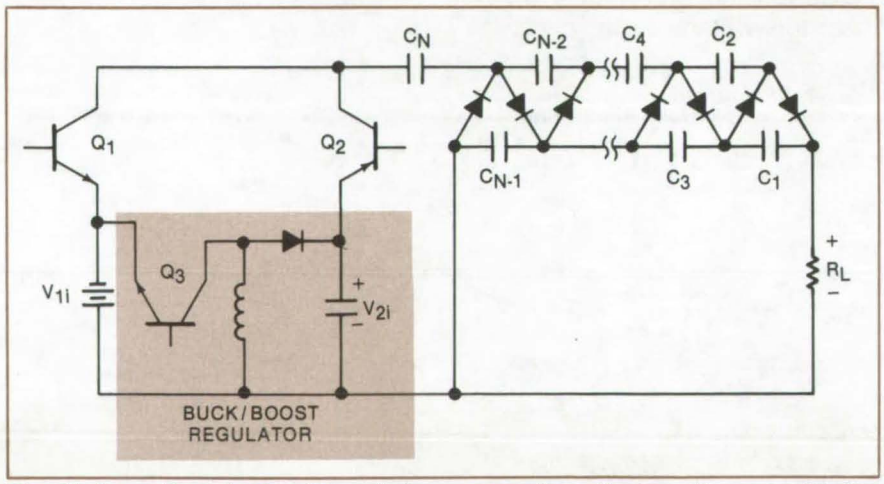

The **Voltage-Regulating Circuit** for a capacitor diode voltage multiplier uses the regulating voltage V_{2i} supplied by a buck/boost circuit.

circuit includes a small inductor in a special buck/boost regulator used in a unique way for output voltage regulation. The inductor with transistor Q_3 and the capacitor across which V_{2i} is developed form the regulating circuit.

The value of V_{2i} is controlled by controlling the "on" time of transistor Q_3. Since the load voltage is nominally $N/2\ (V_{1i} + V_{2i})$ where N is the number of capacitors in the multiplier, the output voltage can be regulated by controlling the "on" time of the transistor Q_3. Because the regulation part of the circuit handles only a fraction of the total output power, with most of the power being furnished by the voltage V_{1i} directly to the voltage multiplier, the weight penalty of the regulation part of the circuit can be made small. Regulation circuits other than the buck/boost circuit could be used to produce the regulation voltage input V_{2i}.

Other voltages, other frequencies, other powers, and high efficiencies are possible, with the parameters being determined according to the mathematical analysis developed for the purposes. Any of a variety of feedback controls could be used to control automatically the transistor Q_3 "on" time from changes in the output voltage.

This work was done by William T. Harrigill, Jr., and Ira T. Myers of **Lewis Research Center.** *Further information may be found in NASA TM-X-73427 (N76-27474), "Regulation of a Lightweight High Efficiency Capacitor Diode Voltage Multiplier DC-DC Converter," a copy of which may be obtained at cost from the New England Research Application Center (see page A7).*

This invention is owned by NASA, and a patent application has been filed. Inquiries concerning nonexclusive or exclusive license for its commercial development should be addressed to the Patent Counsel, Lewis Research Center (see page A8). Refer to LEW-12791.

Circuit Monitors Powerline Interruptions

Simple circuit and pulse detector indicate outages as short as 150 μs.

Lyndon B. Johnson Space Center, Houston, Texas

A simple circuit, when combined with a pulse detector, can detect momentary interruptions of a 400-cycle ac signal. The circuit has been used during vibration and shock testing of electronic hardware to determine if the tests caused interruptions of normal circuit operation. It replaces a complex computer system that had been used to perform the same function, allowing substantial cost savings and more efficient utilization of equipment.

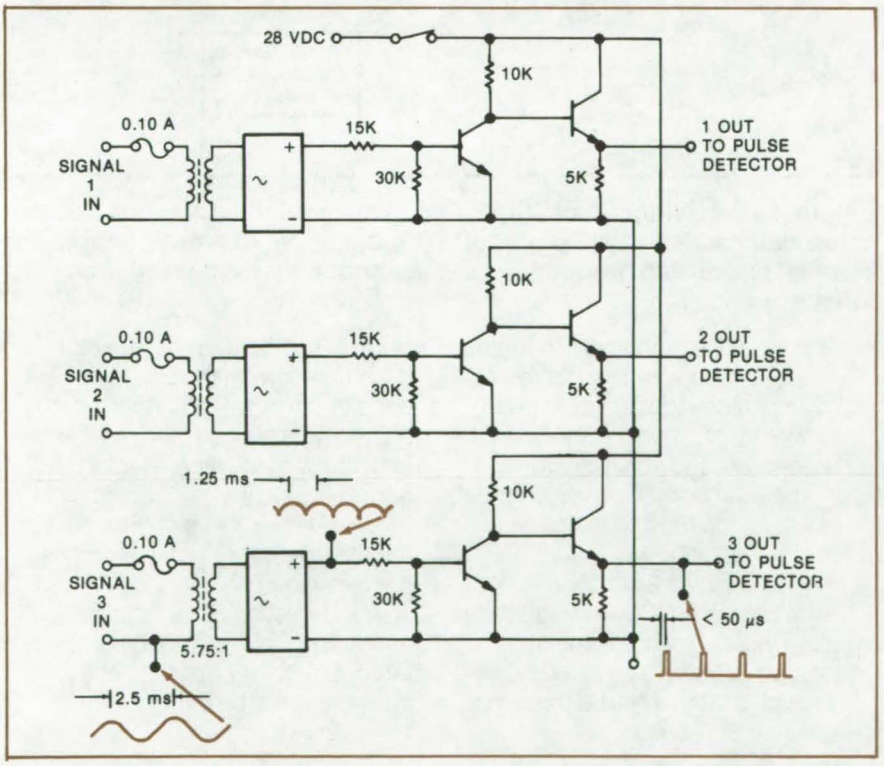

Powerline Monitoring Circuit detects momentary interruptions of 400-cycle signals from three independent inputs. Each output is fed to a pulse detector that triggers on 150-μs (or greater) pulses. Thus, the pulse detector is only activated when one of the input signals is interrupted.

In its present form (see figure) the circuit can monitor three independent powerlines, such as from three separate circuit-board assemblies. The 115-volt, 400-cycle input signal is reduced to 20 volts by the transformer and then is full-wave-rectified. The rectified signal is sent into a saturated two-transistor amplifier and is converted to a stream of 50-μs pulses. This signal is available to the pulse detector.

The pulse detector could be the type described in *NASA Tech Briefs*, Vol. 1, No. 4, p. 615, "Pulse Detector," (MSC-16268). This device will trigger on 150-μs pulses (positive or negative) to indicate a momentary interruption of the original signal.

This work was done by Norman E. Simmons and John O. Stricklen of Rockwell International Corp. for **Johnson Space Center.** *No further documentation is available. MSC-16763*

Improved Numerical Control of Oscillator Frequency

Precision oscillator for phase-locked loop generates exact frequency and phase of a noisy input signal.

Lyndon B. Johnson Space Center, Houston, Texas

The frequency and phase of the output signal from a newly-developed oscillator circuit can be controlled with extreme accuracy by a digital word. This numerically controlled oscillator (NCO) is a key element in a phase-locked loop that generates the exact frequency and phase of a noise-corrupted input signal and thus is of value in communications and tracking equipment.

Figure 1 is a functional diagram of the precision control circuit. It produces an output clock frequency f_S at a nominal center frequency, plus or minus some amount determined by the magnitude of a number (digital word) applied to its input. Like previous NCO's, this circuit accumulates the control word; but it does not reset the accumulator when a positive or negative overflow occurs and then delay or advance f_S by the phase corresponding to a single cycle of the reference oscillator. Instead, this NCO provides for the positive and negative output-frequency alterations by translating all input numbers so that they are positive (by adding "1") and by increasing the reference oscillator frequency to be such that corrections in only one direction (that of adding phase to the f_S clock) need to be made. If the control word with value 0.0 is applied to the input, "carries" will occur at a rate such that the effect of the $\div 3$ or $\div 4$, followed by the $\div 64$, is to produce an average dividing ratio of 193 to yield f_S. This concept has the advantage of providing a consistent correspondence between the phase alterations in the f_S clock output and the numerical amount removed from the accumulator.

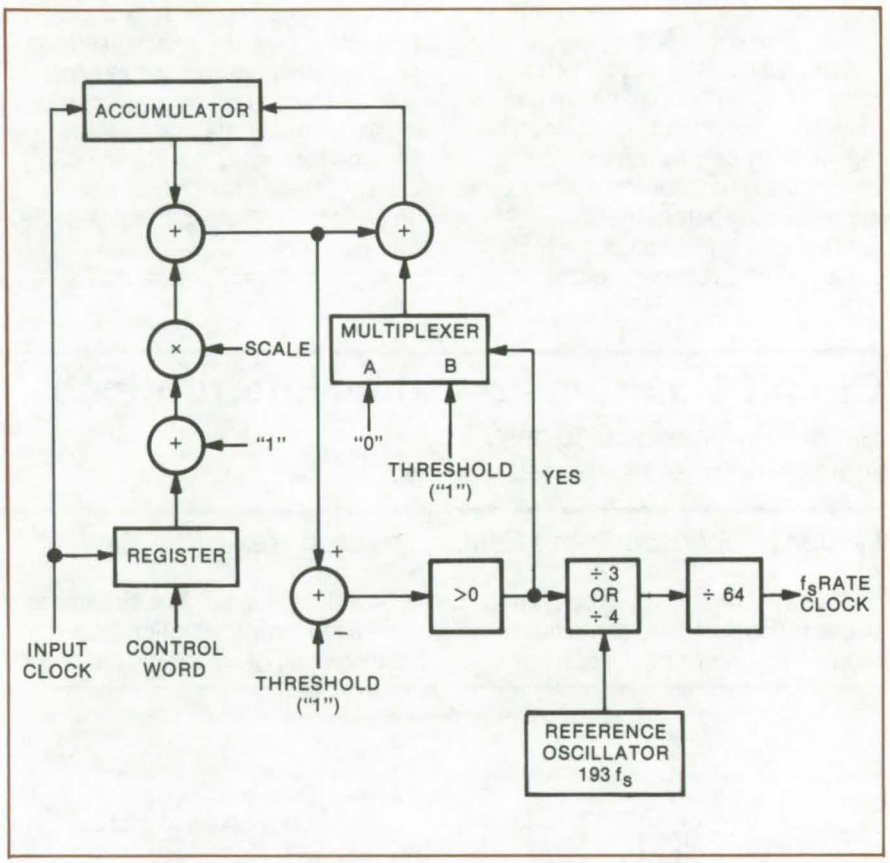

Figure 1. **Precision Clock Signal** is generated by this numerically-controlled oscillator (NCO) circuit. The digital input word controls the precise phase and frequency of the output clock derived from the reference oscillator.

The circuit arrangement in Figure 1 also has the advantages of easily allowing prescaling and of allowing numbers larger than the threshold to be added into the accumulator and the proper amount of phase change eventually imparted to the output clock.

Figure 2 shows a simple implementation of the NCO in digital hardware. The scaling constant is restricted to being a negative power of 2, such as 2^{-1}, and the threshold is 1.0. The addition of the factor "1" is combined with the scaling of 2^{-1}, each of the bits of the input word is shifted right by 1 bit, the most significant bit is made a constant "0," and the next most significant bit is inverted. The most significant bit of the accumulator simply becomes the carry logic.

The detection of threshold exceedance (now only in the positive direction) simply consists of examining the carry bit out of the most

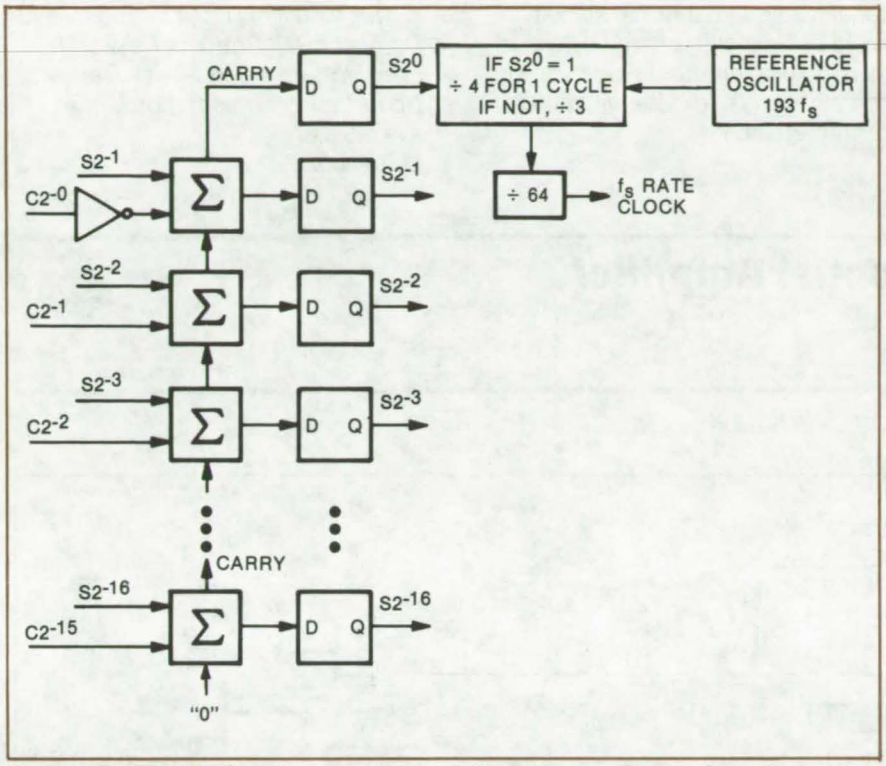

Figure 2. **Simple Implementation** of the circuit shown functionally in Figure 1 is achieved by making the threshold level "1" and restricting the scaling constant to negative powers of 2. Fewer integrated circuits and one discrete unit are required.

significant adder to see if it is a "1." If it is, the ÷3 or ÷4 counter is instructed to divide by 4 (from the reference oscillator output) for one cycle, thus inserting an extra reference oscillator period. A straightforward divide-by-64 follows to obtain the output at the frequency f_S.

Subtraction of the threshold from the accumulator when it has been exceeded requires no hardware, being the natural result in any binary number system when overflow occurs.

This NCO requires fewer parts (two integrated circuits and one discrete) than others, yet provides superior performance.

This work was done by Alfred Cellier, Douglas C. Huey, and Lit N. Ma of TRW, Inc., for **Johnson Space Center.** *No further documentation is available.*

Inquiries concerning rights for the commercial use of this invention should be addressed to the Patent Counsel, Johnson Space Center [*see page A8*]. *Refer to MSC-16747.*

Diodes Stabilize LED Output

Simple technique compensates for thermal fluctuations.

Lyndon B. Johnson Space Center, Houston, Texas

Small-signal diodes can be placed in series with light-emitting diodes (LED's) to stabilize the LED output against temperature fluctuations. The simple and inexpensive method compensates for thermal fluctuations over a broad temperature range. Since it requires only a few components, the technique should be particularly useful where circuit-board space is limited.

The method works because the luminous intensity of light-emitting diodes decreases with increasing temperature, while the intrinsic voltage drop across most small-signal diodes decreases with increasing temperature. Thus, if the series combination is placed across a constant-voltage source (see figure), the current will rise as the temperature rises, thereby offsetting the decrease in light output.

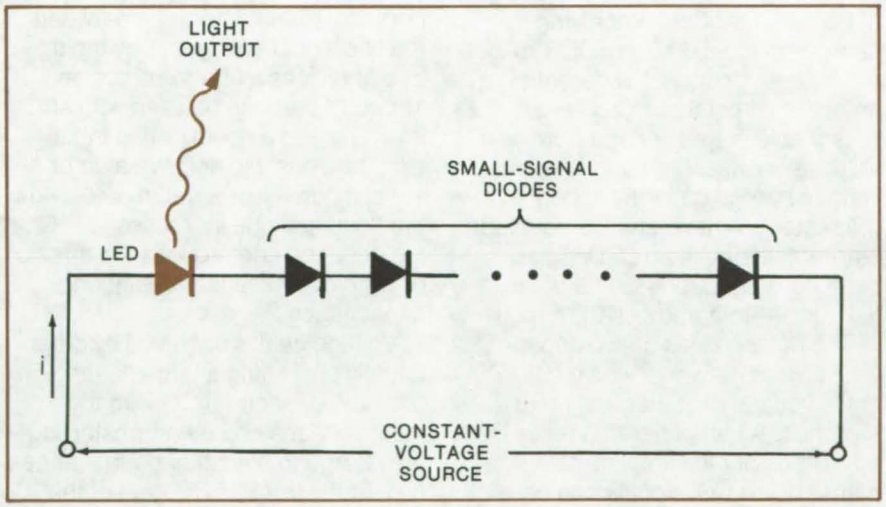

LED Output Is Stabilized with respect to temperature by placing one or more small-signal diodes in series with the LED. As the temperature rises, the light output normally drops (at constant current); however, since the voltage across the compensating diodes also decreases, the current (i) rises to offset the drop in intensity.

(continued next page)

In one application, an uncompensated LED intensity fluctuation of ±33 percent over 90° C was cut to ±5 percent by adding three 1N3600 diodes in series with an LED. It is conceivable that thermal stability could be further improved by experimenting with different diodes or with combinations of diodes with different characteristics.

This work was done by Richard A. Deters of Ball Brothers Research Corp. for **Johnson Space Center.** *No further documentation is available.*
MSC-16520

Charge-Coupled Differential Amplifier

Solid-state device designed as output amplifier for CCD transversal filters

Langley Research Center, Hampton, Virginia

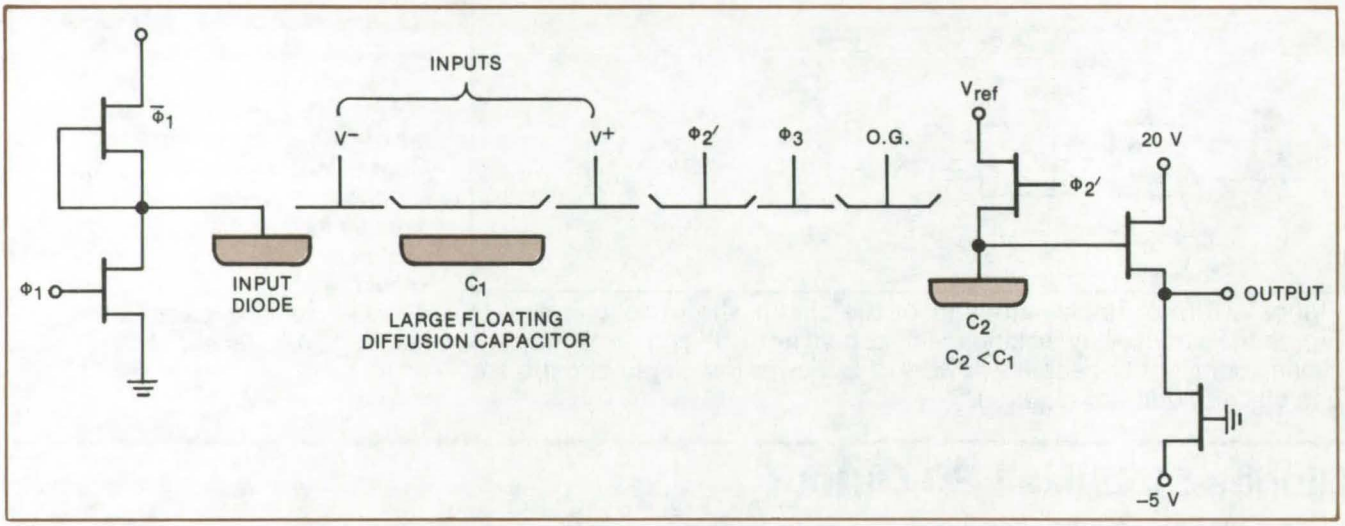

Charge-Coupled Differential Amplifier above is used in a differential current-integrator circuit. The amplifier is basically a one-stage CCD that has a differential floating diffusion input and a standard precharge output. Voltage gain is achieved by transferring charge from a large-capacitance node (C_1) to a smaller capacitance node (C_2).

A highly critical area in the design of transversal filters employing charge-coupled devices (CCD's) is the output circuitry. A differential amplifier is required to achieve reasonable output voltage from a CCD transversal filter and to reject voltage swings that may appear in the system. A new, charge-coupled differential amplifier (CCDA) has been developed for use in a differential current-integrator (DCI) circuit.

The DCI consists of two capacitive-divider networks with a differential voltage amplifier and reset switches. An amplifier that takes advantage of the sampled-data nature of the DCI signals can be obtained with a CCD structure. The CCDA is basically a one-delay-stage CCD with a differential-input circuit and a standard precharge output circuit. The inputs are applied to the gates (see diagram) labeled v^+ and v^- so that the injected charge is proportional to the difference between the two signal voltages. The input circuit utilizes a floating diffusion structure that can be used with an inverting and a noninverting input simultaneously to achieve a differential input. Also, a metal gate over the floating diode increases its capacitance and reduces the effects of the diode nonlinear depletion capacitance.

Voltage gain is achieved by differentially presetting a large floating diffusion capacitor (C_1) with the input voltages and then transferring the charge to a smaller capacitance (C_2) at the output. The gain of the amplifier is simply the capacitance ratio C_{in}/C_2, where C_{in} is the sum of the floating diffusion C_1 and the gate capacitance of the v^+ gate.

The maximum usable output signal of the amplifier is about 2 Vrms, with a dynamic range of about 74 dB. The noise level of the amplifier is about four times that generated in the CCD filter itself.

The CCDA solves the problem of differential voltage gain in sampled-data metal-oxide semiconductor (MOS) devices. It can produce gain at any frequency compatible with CCD operation, with low noise, low power, good linearity, and high stability. In these respects, it should prove superior to conventional MOS differential amplifiers.

This work was done by Charles R. Hewes of Texas Instruments Inc. for **Langley Research Center.** *For further information, Circle 6 on the TSP Request Card.*

Title to this invention has been waived under the provisions of the National Aeronautics and Space Act [42 U.S.C. 2457(f)], to Texas Instruments, Inc., Dallas, TX 75222.
LAR-12110

Simple, Accurate Analog Divider for Low Divisor Values

Current-exponential voltage characteristic of diode used for accuracy at low denominator values.

Lewis Research Center, Cleveland, Ohio

An electronic analog divider circuit has been developed that employs, over a certain range, the current-exponential voltage characteristics of a diode to obtain better accuracy at low denominator voltages.

Although many divider circuits are known, most use log and antilog techniques or multipliers with a feedback loop incorporating an operational amplifier. These divider circuits are inaccurate at low denominator voltages unless complicated circuits are used to insure accuracy.

The circuit shown in the figure uses the known exponential characteristic of a diode. The current, particularly at low forward voltages and currents, is an exponential function of the voltage applied across the diode. Therefore, the incremental impedance of the diode is inversely proportional to the current through the diode. The divider circuit employs a bias current through the diode proportional to the desired denominator and applies an incremental current to the diode proportional to the numerator. As a result, the incremental voltage across the diode is proportional to the desired quotient.

This work was done by Arthur G. Birchenough of **Lewis Research Center.** *Further information may be found in U.S. Patent No. 4,001,602, "Electronic Analog Divider," a copy of which may be obtained at cost from the U.S. Patent Office, Washington, DC 20231.*

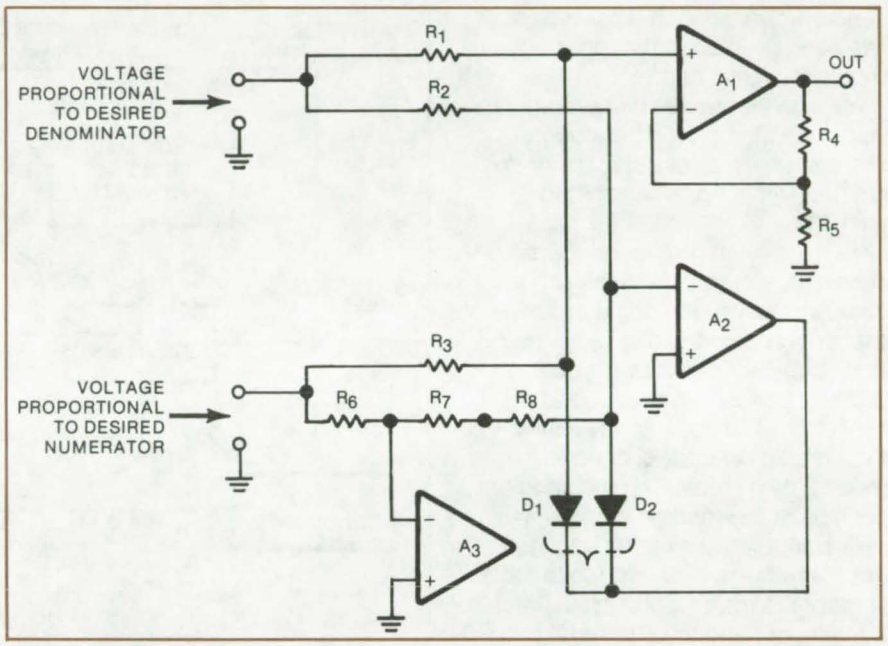

Analog Signal Divider uses the dynamic impedance of a pair of matched diodes. A voltage proportional to the desired denominator is applied between the junction of R_1 and R_2 and signal ground. With $R_1 = R_2$, equal currents flow into D_1 and D_2. The potential at D_2 is kept at 0 V by op amp A_2; for matched diodes, the anode of D_1 is also 0 V. A voltage proportional to the desired numerator is applied to the junction between R_3 and R_6; a current proportional to the numerator flows into the anode of D_1, and an equal but opposite current flows into the anode of D_2 if $R_3 = R_6 = R_7 = R_8$. These currents produce a voltage drop across the dynamic impedance of D_1 and D_2, which is amplified by A_1. (The input to A_1 is the differential signal produced across D_1 and D_2.)

This invention has been patented by NASA (U.S. Patent No. 4,001,602). Inquiries concerning nonexclusive or exclusive license for its commercial development should be addressed to the Patent Counsel, Lewis Research Center (see page A8). Refer to LEW-11881.

Electronic Shaft-Angle Encoder

"Contactless" encoder is useful at high angular velocities.

Lewis Research Center, Cleveland, Ohio

An electronic shaft-angle encoder has been developed that does not require physical connection to a shaft, can be used at higher angular velocities than existing encoders, and can be used for objects that do not have an integral supporting shaft.

Existing shaft-angle encoders consist of a coded disk in which the code varies with the angle around the disk. The coded disk is connected to the shaft of a rotating object with the disk axis concentric to the shaft axis. The code on the disk is then read by electrical or optical means, thus measuring the angular position of the rotating object. Two disadvantages of existing encoders are that access is needed to the shaft of the rotating object to attach the encoder and the structural properties of the encoder limit the angular velocity of the rotating object.

The new electronic shaft-angle encoder is shown in the figure. The encoded angular position of the rotating object is produced by the counter that is clocked by the frequency synthesizer. The synthesizer frequency is adjusted as necessary by the microcomputer so that the number of counts for each revolution (selected by the user) remains constant. A suitable sensor provides a once-per-revolution pulse. At the once-per-revolution pulse, the current count is read into the output buffer register of the counter, the counter is reset to zero, and the microcomputer is interrupted. The microcomputer checks if the count in the output buffer register is within a given tolerance of the desired count for 1 revolution; if not, it calculates a new clock frequency, using the equation:

$$F_n = (F_{n-1})(C_D/C_A)$$

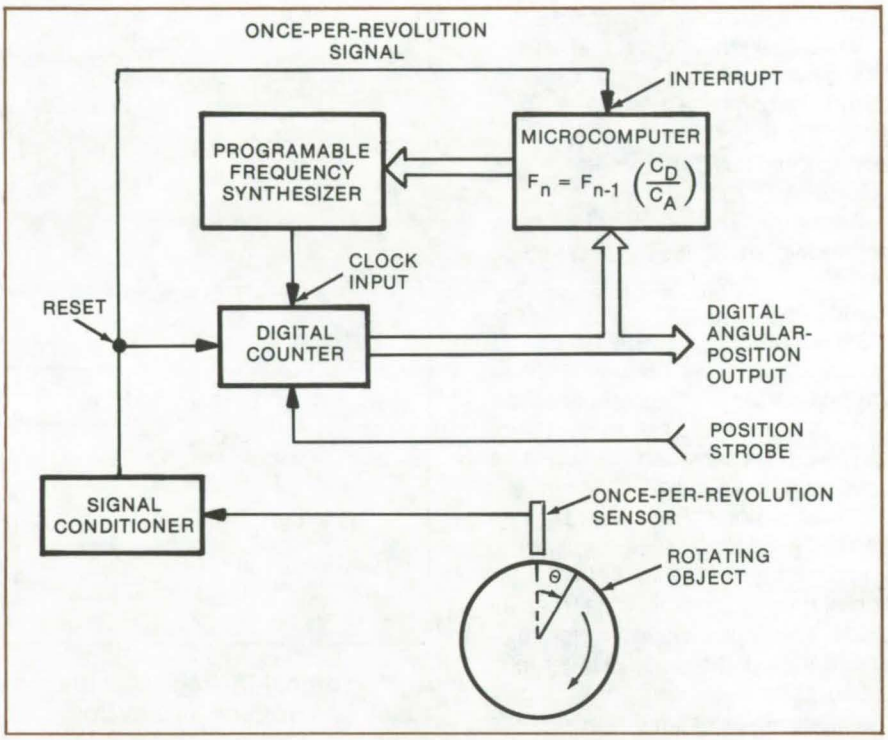

Shaft-Angle Encoder produces an encoded angular-position readout for a rotating object. The count in a digital counter is continuously proportional to the angular position of the object. A once-per-revolution pulse from a sensor resets the counter. A microcomputer and a programable frequency synthesizer keep the number of counts per revolution constant.

where:

F_n = new frequency
F_{n-1} = previous frequency
C_D = desired count for 1 revolution
C_A = actual count for 1 revolution

If necessary, the microcomputer programs the synthesizer with the new frequency. Therefore, the number of counts for each revolution will remain constant, independent of the angular velocity. At any time during each revolution, the counter can be read and the current count transferred to the output buffer register that is a measure of the angular position of the rotating object at the time the signal was read.

An operational requirement is that the fractional change in angular velocity of the rotating object for each revolution must be small compared to the desired resolution in the angular position expressed as a fractional part of 1 revolution. This requirement is easily met in applications involving high angular velocities or rotating objects with large amounts of inertia.

This work was done by J. Anthony Powell of **Lewis Research Center.** *For further information, Circle 7 on the TSP Request Card.*

Inquiries concerning rights for the commercial use of this invention should be addressed to the Patent Counsel, Lewis Research Center [see page A8]. Refer to LEW-12832.

Twisted Shielded-Pair Transmission Line

Lightweight cable with controlled electrical characteristics can replace coaxial cables for data transmission.

Lyndon B. Johnson Space Center, Houston, Texas

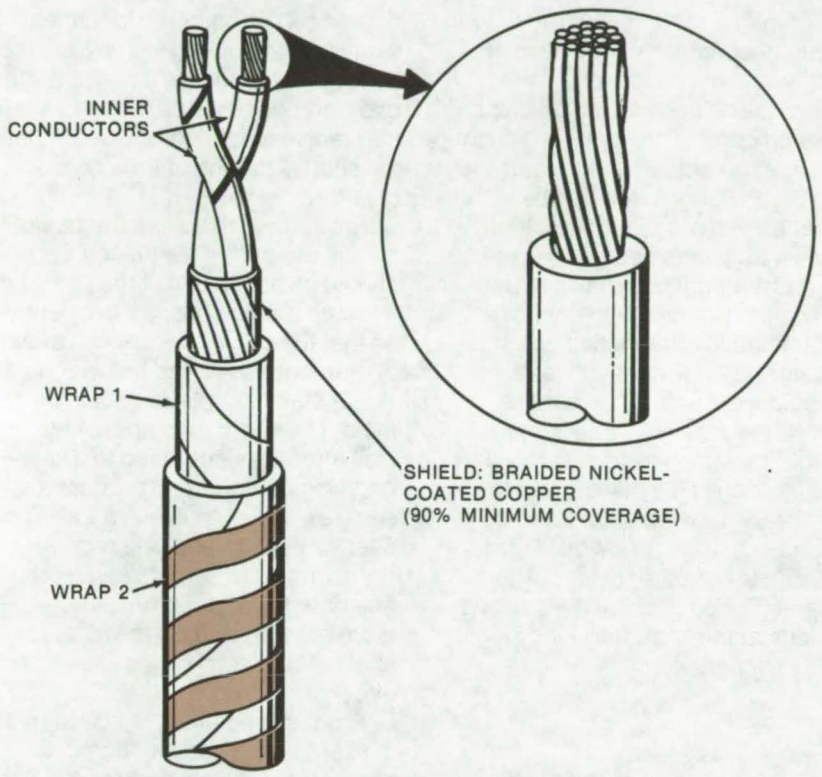

Twisted Shielded Two-Conductor Cable has Teflon-insulated stranded inner conductors, a braided shield, and a two-layer outer wrap. Electrical and physical characteristics are carefully controlled, making the cable a suitable replacement for coaxial cable in multiplexed-data transmission at frequencies to 10 MHz.

Resistance	30.1 Ω/1,000 ft (98.8 Ω/km)
Capacitance (conductor to conductor)	32 to 40 pF/ft (105 to 131 pF/m)
Capacitance (conductor to shield)	18 to 23 pF/ft(59.2 to 75.4 pF/m)
Characteristic Impedance	70 to 80 Ω
Attenuation at 100 kHz at 350 kHz at 1 MHz at 2.25 MHz	0.8 dB/100 ft (0.026 dB/m) 1.05 dB/100 ft (0.034 dB/m) 1.2 dB/100 ft (0.039 dB/m) 1.4 dB/100 ft (0.046 dB/m)

Electrical Characteristics of 24-gage twisted shielded-pair electrical cable

A twisted shielded-pair electrical cable forms a balanced transmission line and can replace costlier coaxial cables for multiplexed-signal transmission. Unlike other twisted pairs, this cable is fabricated with carefully-controlled electrical characteristics and can function without tuning networks at frequencies up to 10 MHz. It requires no special connectors, is lightweight, and is smaller in diameter than all-Teflon insulated cables. Attenuation is typically less than 1.5 dB per 100 ft.

Typical electrical characteristics of the cable, using 24-gage conductors, are shown in the table.

The construction of the cable is shown in the figure. The inner conductors are nickel-coated stranded copper alloy with extruded-Teflon insulation, twisted 15 to 20 turns per foot. High-strength copper is used for conductors smaller than 22-gage. The shield is braided nickel-coated copper with a minimum of 90 percent coverage for improved electromagnetic compatibility. A two-layer wrap of polyimide/fluorocarbon is provided. The outer layer is heat-sealed and color-coded.

The cable is more stable during significant thermal changes than other twisted shielded-pair systems. It is more economical than coaxial cables since it may be used with standard pin-and-socket connectors and without tuning networks.

The cable can be used for multiplexed-information and data-transmission systems, such as those in aircraft, closed-circuit television, computer systems, and automobiles. It is also applicable for audio communications.

This work was done by Wallace N. Lind and George H. Waddy of Rockwell International Corp. for **Johnson Space Center.** *For further information, Circle 8 on the TSP Request Card.*
MSC-16702

Brushless Tachometer Gives Speed and Direction

Its dc output is proportional to rpm and changes sign for counterrotation.

Marshall Space Flight Center, Alabama

A brushless electronic tachometer measures not only rotational speed but also rotational direction. Unlike conventional tachometers, the new unit is accurate at low speeds as well as high speeds and can be used in vacuum and applications requiring low friction. It is also lighter in weight than brush tachometers.

The tachometer uses two Hall-effect devices mounted in the flux path of a magnet on the rotating shaft (see figure). The Hall devices are arranged 90° apart with respect to the poles of the magnet and are supplied with excitation voltages of constant frequency and amplitude but 90° out of phase. The devices are connected in series, to produce an output frequency that increases for one rotational direction and decreases for the other. This signal is conditioned and filtered to give a dc output proportional to the speed. Its polarity indicates direction.

The Hall devices are small chips of silicon containing impurities such as indium arsenide. When a current is passed through each device in the presence of a magnetic field, it produces a transverse output voltage that has a magnitude that is dependent on the product of the excitation current and the magnetic field.

A signal generator supplies a sinusoidal excitation current at a carrier frequency ω_C. The signal is fed through an operational amplifier directly to one Hall device; and the resistor R_1 and capacitor C_1 shift the phase of the current by 90° at the input to the other device. The magnetic fields seen by the devices oscillate at the shaft frequency ω_S and are separated by 90 electrical degrees. Trigonometric identities verify that the output signal from the series combination is either the sum or difference of the carrier and shaft frequencies, depending on whether the shaft is turning clockwise or counterclockwise.

For zero shaft speed, the output is simply the carrier frequency. It should be at least five times greater than the maximum shaft frequency so that the output frequency varies 20 percent above and below the carrier. A stable oscillator should be used. The summed output of the two Hall-effect devices is fed to a zero-crossing detector that produces a square-wave output with a frequency that increases in proportion to increasing shaft speed for one direction of rotation and decreases in proportion to increasing shaft speed for the opposite direction.

From this point on, the circuitry is similar to that in conventional tachometers. The square wave is differentiated to form narrow voltage spikes that drive a one-shot multivibrator. Fixed-height, fixed-width

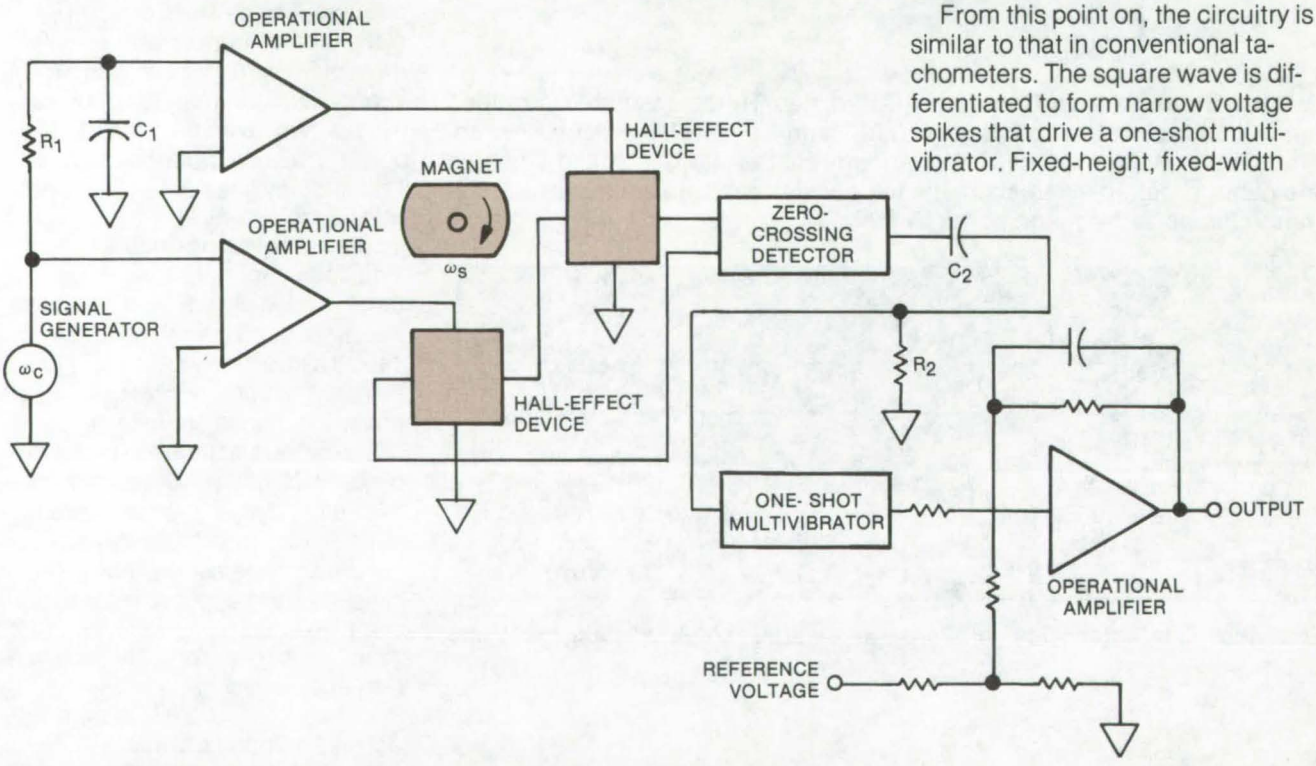

New **Tachometer Uses Two Hall-Effect Transducers** to superimpose the shaft frequency (ω_S) and a carrier frequency (ω_C). The shaft frequency is added to the carrier for clockwise rotation and is subtracted from it for counterclockwise rotation. The resulting signal is conditioned to give a dc output proportional to speed; its polarity gives the direction.

pulses from the multivibrator are filtered to produce a dc voltage proportional to shaft speed.

When the shaft is not turning, the frequency (ω_C) of the pulse train out of the multivibrator produces a constant bias voltage. This bias is nulled by introducing an equal and opposite voltage into the final op amp from a reference, so that the circuit output is zero volts for zero shaft speed. As the shaft turns, the dc output increases for clockwise rotation and increases negatively for counterclockwise rotation. Devices other than Hall-effect devices can be used for the transducers. For example, optical encoders, electromagnetic resolvers, or electronic multipliers might be substituted.

Unlike conventional tachometers, the ripple voltage of the new circuit is low because the frequency — even for zero rpm — is always high. Thus, the circuit is accurate even at very low turning speeds.

This work was done by Frank J. Nola of **Marshall Space Flight Center.** *For further information, Circle 68 on the TSP Request Card.*

This invention has been patented by NASA [U.S. Patent No. 4,039,946]. Inquiries concerning nonexclusive or exclusive license for its commercial development should be addressed to the Patent Counsel, Marshall Space Flight Center [see page A8]. Refer to MFS-23175.

Recording-Tape Lightning Detector

A length of prerecorded magnetic tape, doubled over on a plastic strip, forms a simple passive device for monitoring lightning strikes. The magnetic field around the lightning strike erases part of the recorded signal, and the length of the erased portion measures the current. The device has a wide range and is not "reset" when hit by two successive strikes.

(See page 454.)

Cast-in-Place Grommets for Honeycomb Substrates

A new Teflon grommet that is cast-in-place is easily installed in electronic subchassis that are fabricated out of lightweight honeycomb material. The cast-in-place grommets replace standard cable grommets, which weaken the honeycomb structural integrity. The cable hole, set at a minimum during casting, can be enlarged by drilling to accommodate a range of cable diameters.

(See page 548.)

Bonding Aluminum Beam Leads

Cost savings can be realized in the manufacture of beam-lead integrated circuits if aluminum rather than gold is used to fabricate the leads. When proper aluminum-bonding procedures are used, as outlined in the results of a new study, excellent-quality IC's at high yields can be produced. The changeover from gold can be made with only minor modifications of equipment and procedures.

(See page 546.)

Books and Reports

These reports, studies, and handbooks are available from NASA as Technical Support Packages (TSP's) when a Request Card number is cited; otherwise they are available from one of NASA's Industrial Application Centers or the National Technical Information Service.

Choosing the Right Connector

Handbook guides designers in selecting electrical connectors according to total system concept.

Electrical connectors should be part of the "total system"; they should be selected according to the same design objectives as the other components of a system. Selection should start early in the design cycle to allow rational tradeoffs with other design decisions, and reliability, maintainability, and service life should be consistent with other components used.

To aid designers in following this philosophy, the "User Design Handbook for Electrical Connectors" has been written. Although prepared for space vehicle applications, the information presented will be useful throughout industry. The handbook discusses general types of connectors, but does not provide data on specific connectors. It should be particularly helpful whenever fairly-complex electrical systems must be designed.

"User Design Handbook for Electrical Connectors" describes the general features of representtative connectors — their shell or body, insert, contacts, coupling, mounting, accessories. It discusses electrical performance and mechanical requirements.

A section is devoted to severe environments, such as extreme temperature, vibration, high and low pressure, and oxygen-rich surroundings.

A special feature of the handbook is a checklist for selecting connectors. The checklist covers electrical requirements, environmental considerations, reliability, assembly and installation, and maintainability. It reminds the user of basic project requirements (materials, finishes, and the like) and of basic design objectives (Is the goal lowest installed weight, for example, or smallest total installed volume?).

This work was done by C. R. Lynch of Martin Marietta Corp. for **Marshall Space Flight Center.** *To obtain a copy of the handbook, Circle 9 on the TSP Request Card. MFS-23785*

Computer Programs

These programs may be obtained at very reasonable cost from COSMIC, a facility sponsored by NASA to make new programs available to the public. For information on program price, size, and availability, circle the reference letter on the COSMIC Request Card in this issue.

Mask and Display Program

Designer aid for precise artwork

A new program aids designers of microelectronics, integrated optics, bubble memories, and practically any other devices that require precise artwork. It allows the circuit or mask designer to create data rapidly and easily and to arrange and format them for use on the Mann (1600 Series) or the Gerber (1000 and 2000 Series) pattern generators. The program can be used to create complex lines, shapes, circles, and alphanumeric characters; and it allows one to shift and repeat patterns without having to regenerate all of the data. To date, the program has been used to design monolithic masks for research and development devices, hybrid screening masks at final product sizes, and microwave conductor patterns and to generate grids and line patterns.

Inputs to the Mask and Display Program are a series of control cards that specify the shape, location, and repetition of a desired mask element. The different types of input cards allow the user: to add a teletype (TTY) text message to the Mann tape; to specify a scale factor, a center of mask, a border, and a true or mirror image mask; to create patterns, using either the modified Mann format or the strip format; to create the patterns of lines joining at any angle, arcs, and circles; to create alphanumeric characters to be put on the mask; and to create standard flareout patterns.

Outputs are a magnetic data tape and a listing of the input data cards. The output tape formats available are: a seven-track Mann tape that can be used to display the created mask on a Tektronix 611 CRT terminal for inspection before making the mask on the Mann Pattern Generator (MPG); a nine-track Mann tape that will be accepted by the Mann (1600 Series) Pattern Generator; or a seven-track Gerber tape that can be used to drive a Gerber (1000 or 2000 Series) Artwork Generator.

This program is written in modified Sigma 5 FORTRAN for the XDS Sigma 5 computer and has a core requirement of approximately 50K of 32-bit words.

This work was done by Donald Routh of **Marshall Space Flight Center** *and Dae-Shik Woo of Sperry Rand Corp. For further information, Circle A on the COSMIC Request Card.*
MFS-23625

Electronic Systems

Hardware, Techniques, and Processes

Autonomous Rendezvous and Feature Detection System

Standard TV signal is converted into directly-usable spatial and dimensional information.

Langley Research Center, Hampton, Virginia

Standard television imaging systems used on spacecraft for scientific imaging may now be used as sensors for deriving spacecraft steering signals, tracking, autonomous rendezvous and docking, and ranging. Algorithms and equations have been developed and tested for converting television-generated image data into directly-usable spatial and dimensional information, i.e., object position coordinates, object size, and elliptical object orientation and shape parameters. These basic data are then used to derive steering commands for rendezvous, to provide for stationkeeping and tracking, to perform object acquisition, and to allow feature detection. Range information can also be generated if separate images, such as those obtained with dual cameras, are provided.

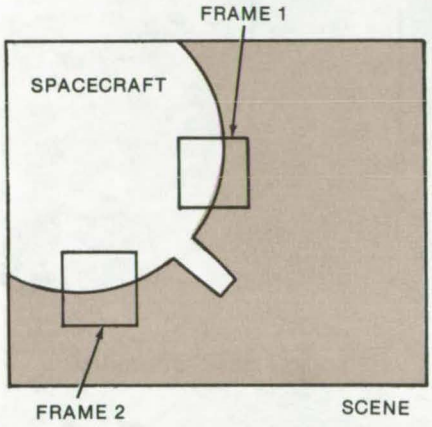

Figure 1. The **Near-Steering and Stationkeeping Technique** employs approximate data from previous scans. Accurate relative position is obtained by scanning an area covering object boundaries in two or more places. By knowing the command scan coordinates and the relative placement of the camera, frame 1 yields data on the X position of the spacecraft edge, and frame 2 shows what the Y coordinate is.

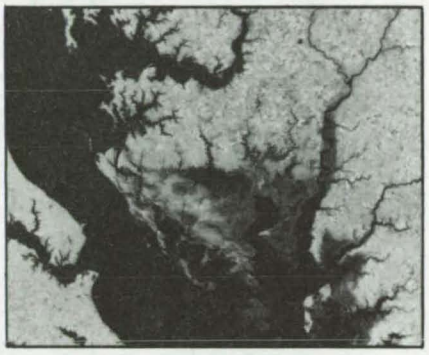

Figure 2. The **Test Scene** above was used to evaluate the capability to distinguish coastlines. A brightness map of this scene was quantized for deriving the threshold map in Figure 3.

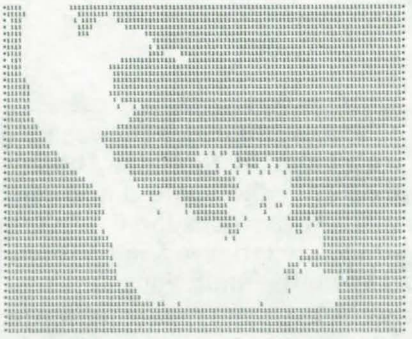

Figure 3. A **Thresholded Version** of the scene in Figure 2 was developed from brightness information.

Algorithms were tested in the laboratory and included calculations for area, object center, object orientation, and ranging. For near-steering and stationkeeping applications, a possible method is indicated in Figure 1. A representative television scene of surface features is shown in Figure 2. A brightness map of 5,000 pixels per frame, with the video signal quantized on a scale of 0 to 9, was then derived from this scene. The brightness information was then thresholded: If the video signal was larger than the threshold, a "1" was assigned to the pixel; if less than the threshold, a "0" was assigned to the pixel. Figure 3 is the converted version of the scene. Acquisition and tracking of a particular surface feature or other constituent of interest would greatly increase the use of directive sensors and significantly reduce data-transmission bandwidth and time requirements.

Further investigations appear warranted into the utility and capability of television imaging systems as sensors to augment the primary guidance, navigation, and attitude-control hardware of spacecraft and to enhance further the scientific data-gathering ability of these vehicles.

This work was done by Robert B. Rice, Jr., of Martin Marietta Corp. for **Langley Research Center.** *For further information, Circle 10 on the TSP Request Card.*

Inquiries concerning rights for the commercial use of this invention should be addressed to the Patent Counsel, Langley Research Center [*see page A8*]. *Refer to LAR-12050.*

Four-Quadrant Phase Detector

Logic-compatible circuit gives a linear indication over 360°.

Goddard Space Flight Center, Greenbelt, Maryland

Phase detectors, such as those used in phase-locked loops, usually only cover the range from zero to 180°. These circuits produce an output that is proportional to the cosine of the phase angle between the input signal and a reference, so that their indication is zero when the angle is 90°, has a maximum when it is 0°, and is a minimum when it is 180°. Thus, the phase is identified over only two quadrants, with one quadrant represented by a positive voltage and the other by a negative voltage.

For some applications, it is necessary to have a phase detector that covers all four quadrants, preferably with a linear rather than cosine indication. This requirement is met by the phase-detection circuit, shown in the figure. The circuit functions over a full 360° and gives a linear output that is proportional to the phase difference. In addition, its output has a single polarity; thus, it is compatible with logic circuitry without the need for additional processing.

As seen in the figure, the input signals (V_1 and V_2) are fed to operational amplifiers that are wired as zero-crossing detectors. The zero-crossing detectors produce negative voltages when their inputs swing positive. They can be selected so that the transitions occur for arbitrarily small input signals (limited only by the inherent noise of the devices). Thus the outputs are square waves with the same phase relationship as the original signals. One square wave is used to clock a JK flip-flop; the other is differentiated and applied to the clear input to provide the reference. For the 7476 TTL flip-flop shown, both transitions take place on the falling edges of the square wave; a positive-edge-triggered flip-flop could also be used with virtually the same effect.

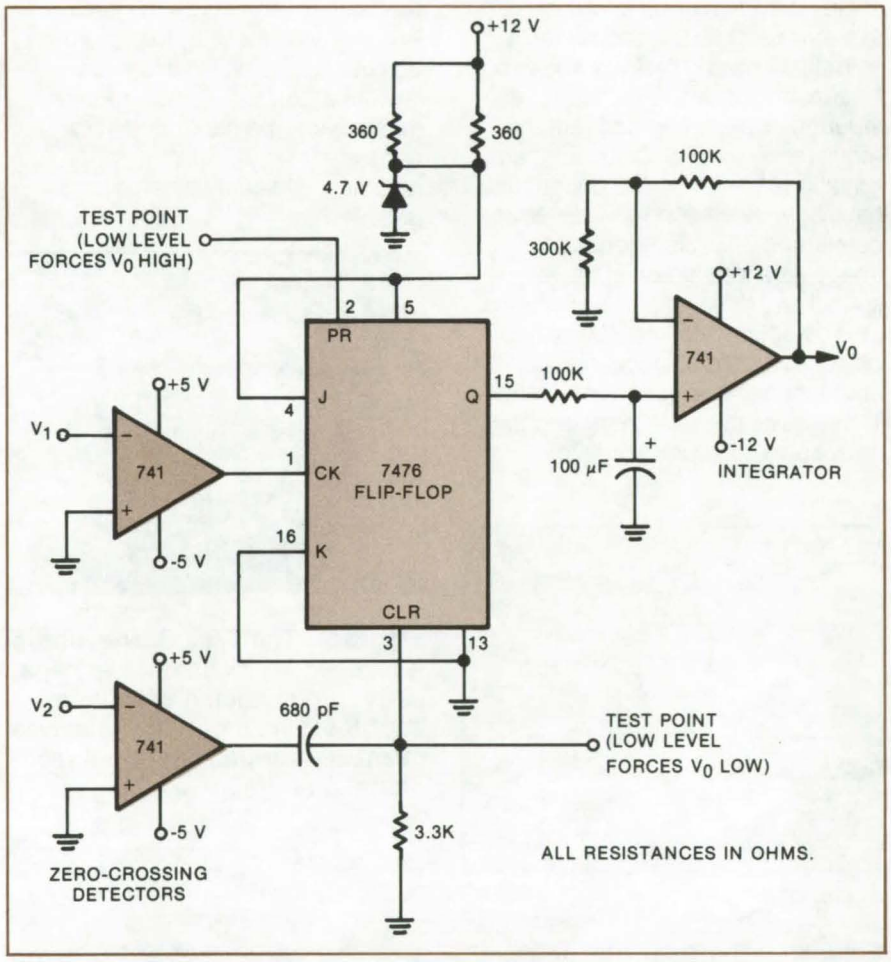

The Phase Difference Between Signals V_1 and V_2 is recorded in the "on" time of the JK flip-flop. The zero-crossing detectors produce square waves with the same phase relationship as the analog signals. One square wave clocks the flip-flop; the other clears it. The flip-flop output is integrated to give a linear signal proportional to the phase difference between the input signals.

The flip-flop produces a series of pulses with widths proportional to the phase difference between the original inputs. The final stage of the circuit is a low-pass filter followed by an operational amplifier. This combination produces a dc level proportional to the pulse width out of the JK flip-flop, and therefore to the phase difference between the input signals.

This work was done by Eugene A. Manus and P. H. Wiley of Virginia Polytechnic Institute & State University for **Goddard Space Flight Center.** *For further information, Circle 11 on the TSP Request Card.*
GSC-12179

Fast, Accurate Rangefinder

Computer-controlled laser system detects obstacles for collision avoidance, surveying, and other applications.

Caltech/JPL, Pasadena, California

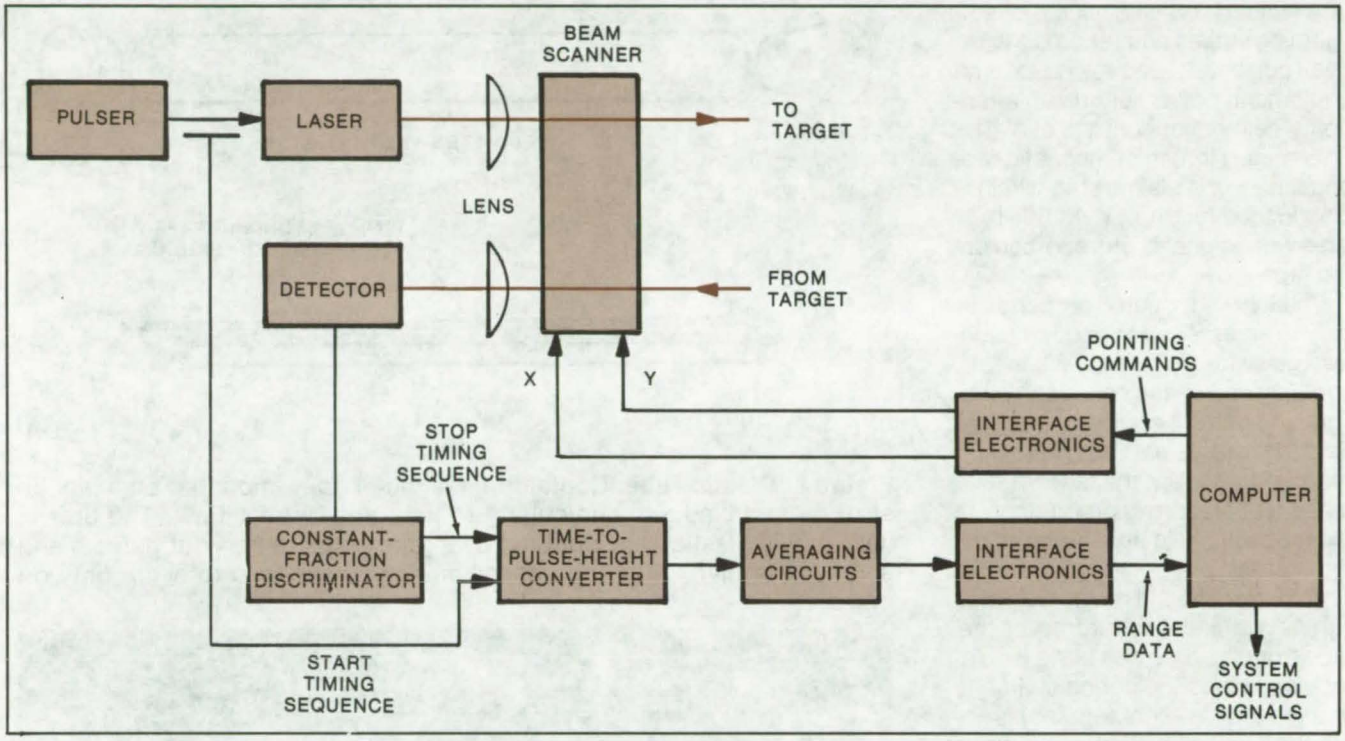

The Time of Flight of Many Laser Pulses is averaged to give one range datum. As the beam is scanned under computer control, the data are analyzed and used to generate control signals for a roving vehicle, for a manipulator, or for other purposes. The constant-fraction discriminator eliminates errors caused by the varying intensity of the returned pulses.

An optical ranging system can detect objects as close as 1 meter and as distant as 30 meters. Developed for robot planetary-surface explorers, the ranger may be used to sight obstacles or targets and to measure the positions of objects for manipulators. It may also be used to locate moving vehicles and for surveying.

The system laser emits short infrared pulses at a high repetition rate, allowing better accuracy and precision than previous rangefinders. At close range, it is accurate to 1 cm. A semiconductor injection laser is used, making the system rugged and compact.

The system is sufficiently sensitive to detect natural, diffusely reflecting objects at its maximum range. Favorable objects can theoretically be detected at distances of 100 meters or more.

A computer controls the laser beam, scanning it in a programed elevation and azimuthal pattern. The computer averages the reflection time of many laser pulses to make a range measurement and analyzes the measurements in real time. Approximately 10,000 measurements are made per second.

A gimbaled mirror scans the beam, as directed by the computer (see figure). A pulser drives the laser at a 10-kHz repetition rate with pulses 30 nanoseconds wide at their base. The injection laser produces 3 watts of light at a wavelength of 844 nanometers. (A higher-output-power laser can be substituted if required.) The light is collimated to a 2-milliradian beam before it goes to the scanning mirror. Each pulse starts a timing sequence that is terminated when the reflected pulse is received.

After passing through an optical filter, the return beam is picked up by a telescope that has a field of view carefully limited to the area illuminated. The filter passes 844-nanometer light; it rejects ambient light and thus improves the signal-to-noise ratio. A baffle prevents stray internal radiation from entering the telescope.

Finally, the beam strikes a photomultiplier having a gallium arsenide photo-cathode with a response peak at 830 nanometers. To further reduce noise, the empty space around the photomultiplier is filled with carbon-loaded spongy material.

This work was done by Alan R. Johnston of **Caltech/JPL.** *For further information, Circle 12 on the TSP Request Card.*
NPO-13460

Recording-Tape Lightning Detector

Prerecorded magnetic tape measures the current in lightning strikes.

John F. Kennedy Space Center, Florida

A simple passive device monitors lightning strikes and records their peak current. It requires no external equipment, power, or human attention. The monitor consists of a 4-foot (1.3-meter) length of magnetic tape doubled over a plastic strip within a plastic tube (Figure 1). An 8-kHz sine-wave signal is prerecorded on the tape.

The tube is mounted perpendicularly to an exposed conductor such as a guy wire (Figure 2). When lightning strikes the conductor, the lightning current creates a magnetic field that erases part of the prerecorded signal on the tape. The amount of erasure is proportional to the magnetic field and therefore to the current.

To determine the magnitude of a lightning strike, a user removes the tape from the tube and plays it on a tape machine. The period of time that the tape is silent (erased) is proportional to the lightning current. Current as high as 17,000 amperes on a single guy wire has been measured with the device.

The magnetic tape method replaces a technique that used cobalt/steel links with high retentivity. These links had serious disadvantages. If a link was struck by two or more bolts of lightning of opposite polarity, the residual magnetism would cancel and indicate zero net current flow; high currents from strong lightning bolts saturated the links, making it impossible to determine the true maximum current, and links had to be taken to a laboratory for measurement. The tape method avoids all of these problems.

A coil and flashbulb combination is wrapped around the conductor so that the user can identify tape

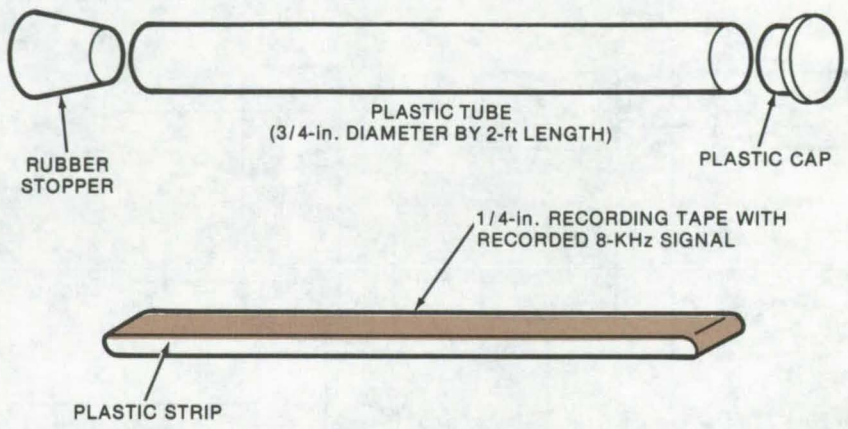

Figure 1. **Plastic Tube, Containing Magnetic Tape** mounted on a plastic strip, is installed perpendicularly to lightning-current flow. The unit is sealed by a plastic cap. Doubled-over tape helps to sort out defects and spurious signals in the tape; these noise sources tend to occur only on one side.

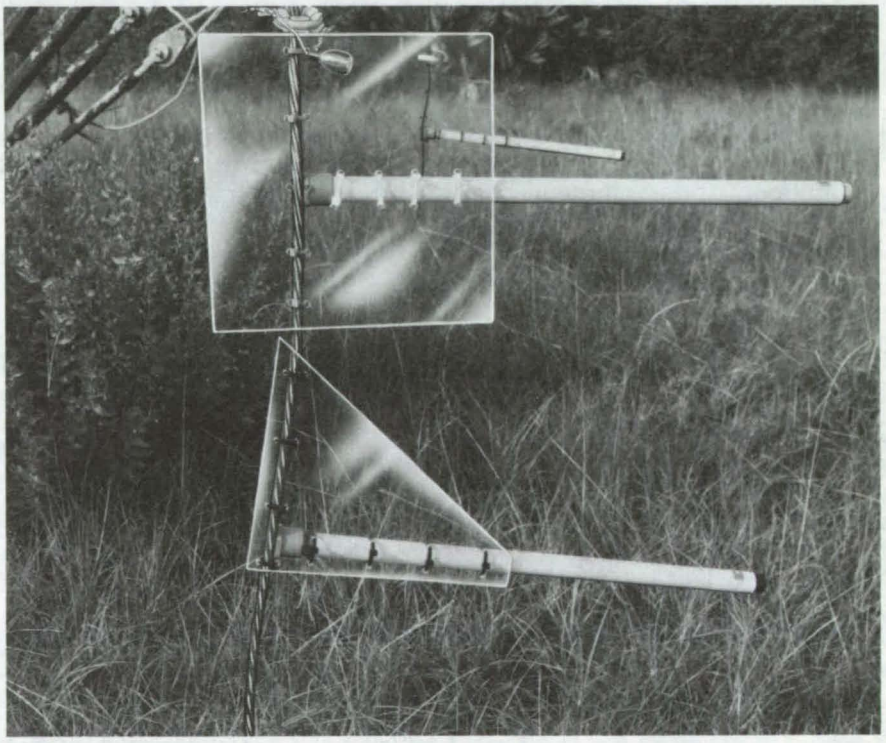

Figure 2. **Magnetic-Tape Lightning Detectors Are Used** on guy wires in Florida. The coil and flashbulb, seen near the top, aid in identifying guy wires hit by lightning.

devices that have been subjected to lightning. The lightning induces current in the coil and flashes the bulb. The user only has to look for burnt-out flashbulbs to find erased tapes for playback.

This work was done by Stephen Livermore of **Kennedy Space Center.** *For further information, Circle 13 on the TSP Request Card.*

This invention is owned by NASA, and a patent application has been filed. Inquiries concerning nonexclusive or exclusive license for its commercial development should be addressed to the Patent Counsel, Kennedy Space Center [see page A8]. Refer to KSC-11057.

Improving FM Transmitter Power and Efficiency

Tracking oscillator and amplifier act like wideband circuitry with narrow-band advantages.

Marshall Space Flight Center, Alabama

In wide-deviation FM transmitters developed for space-vehicle applications, the amplifier that follows the FM oscillator required a 1-dB bandwidth of 20 MHz. The conventional way of obtaining this broad frequency response is to use a broadband matching network — at a sacrifice of output power and efficiency.

To improve these parameters, an amplifier has been designed that tracks the oscillator frequency. This allows a narrow-band, high Q circuit to be used, increasing efficiency and power output and suppressing spurious output frequencies. Moreover, since the amplifier is in resonance with the instantaneous frequency, phase shifts are minimal.

In the transmitter circuit (see figure) the oscillator is frequency-modulated by a varactor diode, as is the amplifier. The tuned circuits in the oscillator and amplifier are similar; thus, standard tracking techniques can be used to ensure that both circuits are tuned in synchronism as they are frequency-modulated by the input signal.

In addition, it is possible to tune the amplifier to a harmonic of the oscillator — a possibility that could find application in signal generators. In this case the amplifier is tuned to a harmonic but is synchronized with the fundamental of the oscillator. For an oscillator frequency f_o, the amplifier produces an output at nf_o, where n is 2, 3, or some higher multiple. The amplifier thus functions as a tracking frequency multiplier.

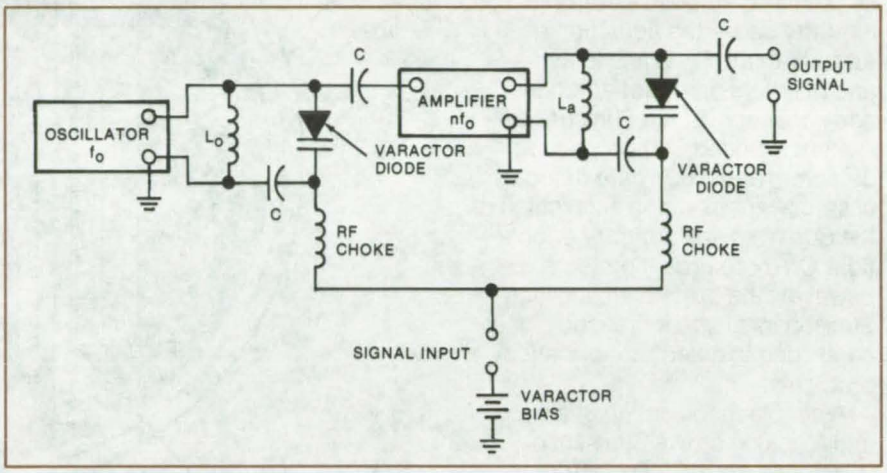

Varactor Diodes Continuously Tune the oscillator and amplifier of a TV transmitter. Amplifier output is precisely at the oscillator frequency (n = 1) or at a multiple of f_o (n = 2, 3, . . .). L_o and L_a are oscillator and amplifier tuning inductors, and C represents coupling and bypass capacitors.

This work was done by Martial A. Honnell of Auburn University for **Marshall Space Flight Center.** *For further information, Circle 14 on the TSP Request Card.*

Inquiries concerning rights for the commercial use of this invention should be addressed to the Patent Counsel, Marshall Space Flight Center [see page A8]. Refer to MFS-23517.

Acquisition and Cruise Sensing for Attitude Control

Solar sensor may be potentially useful in guidance and controls of a solar-energy collection system.

Caltech/JPL, Pasadena, California

On-course navigation of spacecraft flying interplanetary missions depends upon proper orientation of the spacecraft on its various axes. For pitch-and-yaw axis attitude control, for example, the Sun is used as a celestial reference, and Sun sensors and suitable electronic logic circuitry cause the actuation of attitude-control gas jets to achieve and maintain proper orientation. On early spacecraft, the Sun sensor system included Sun acquisition detectors and a Sun gate detector assembly for assuring acquisition of the Sun from any arbitrary orientation. On more recent projects, however, the costs of acquisition Sun sensors have increased significantly due to detector fabrication problems.

A simple modification of a wide-angle analog cruise Sun sensor [disclosed in NASA Tech Brief B72-10080, "Wide Angle Solar Sensor" (NPO-11341)], coupled with a change in the optics, and taken in conjunction with increased attitude-correction capabilities (resulting from development of the HYPACE programable attitude-control electronics, improvements in the inertial guidance system using the dry gyro, and the development of the aforementioned cruise sensor) now make it possible to eliminate the acquisition and Sun gate sensors, with minimal risk to the mission and with considerable savings. Furthermore, the operational characteristics of the cruise Sun sensor make it potentially useful as an alternate guidance and control means for a solar-energy collection system.

As shown in the figure, four sensor elements are laid down on the substrate instead of two. The outer two function as angle detectors, but the inner two have been provided as illumination detectors for testing the device. The elements are comprised of two parallel electrodes, which are adjacent to photoconductive cadmium sulfide (CdS) strips between them and which do not contain a resistor. Measuring the CdS resistance therefore does not give Sun angle position but does indicate if the Sun image is on or off the detectors.

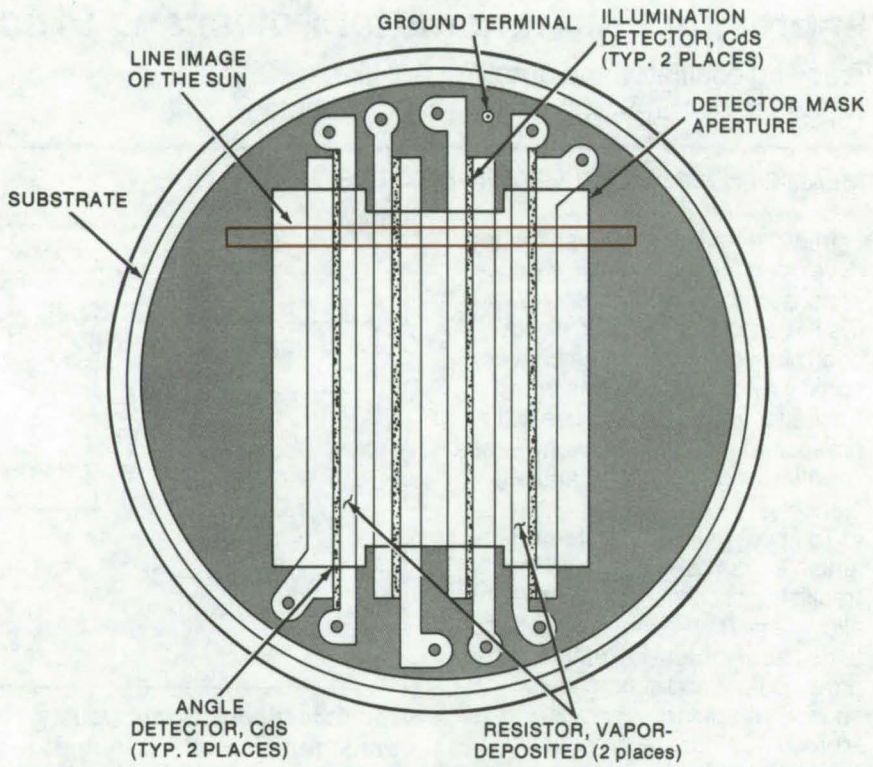

This Wide-Angle Analog Cruise Sun Sensor, a modified version of one disclosed previously, can, together with increased attitude-correction capabilities, eliminate the need for costly acquisition Sun sensors and Sun gate detectors. Loss of Sun acquisition is indicated when the resistance of the illumination detectors rises sharply; this occurs when the Sun image line, moving toward one end of the photoconductive CdS strips, becomes blocked by an aperture mask.

By using the illumination detectors in conjunction with an aperture mask that limits the field of view and with a modified optical field stop, the new design cruise sensors can also provide a Sun acquisition signal, to be used in combination with the aforementioned additional capabilities of the attitude-control system of the spacecraft. As the Sun moves out of the sensor field of view, the Sun image line moves toward one end of the photoconductive strips, and the resistance of the illumination detectors remains substantially the same until the Sun image is blocked; when that happens, the resistance rises sharply to indicate loss of Sun acquisition.

This work was done by George D. Pace, Jr., and Louis F. Schmidt of **Caltech/JPL.** *For further information, Circle 15 on the TSP Request Card.*

This invention has been patented by NASA, [U.S. Patent No. 4,018,532]. Inquiries concerning nonexclusive or exclusive license for its commercial development should be addressed to the Patent Counsel, NASA Resident Legal Office-JPL. Refer to NPO-13722.

Rate-of-Change Limiter for Quantized Signals

Voltage variations that occur in signal transfer applications are regulated without distorting signal fidelity.

Lyndon B. Johnson Space Center, Houston, Texas

An analog circuit may be employed to smooth the change between levels of a quantized voltage signal without adversely affecting its fidelity. The circuit consists of operational amplifiers, a diode bridge, a capacitor, and a series of resistors configured to form a feedback loop having rate-limiting capabilities. The circuit is useful in applications that require interface between digital and analog systems. Modified versions can be used to regulate the transmission of control signals between the computation and effector circuits in automated manufacturing systems and industrial robots, for instance.

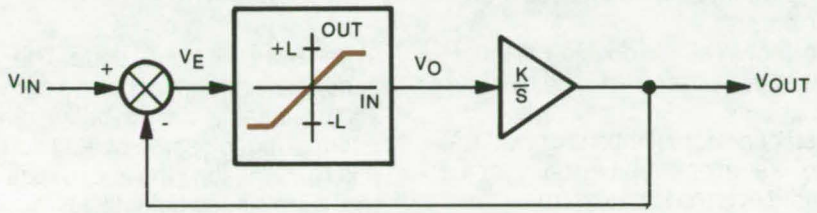

Figure 1. The **Analog Rate Limiter for Quantized Signals** retains signal fidelity of the output, compared to the input. The rate limiter consists of an operational amplifier, a diode bridge, a capacitor, and a series of resistors configured to form a feedback loop. For small-signal amplitudes, circuit bandwidth is determined by the loop gain.

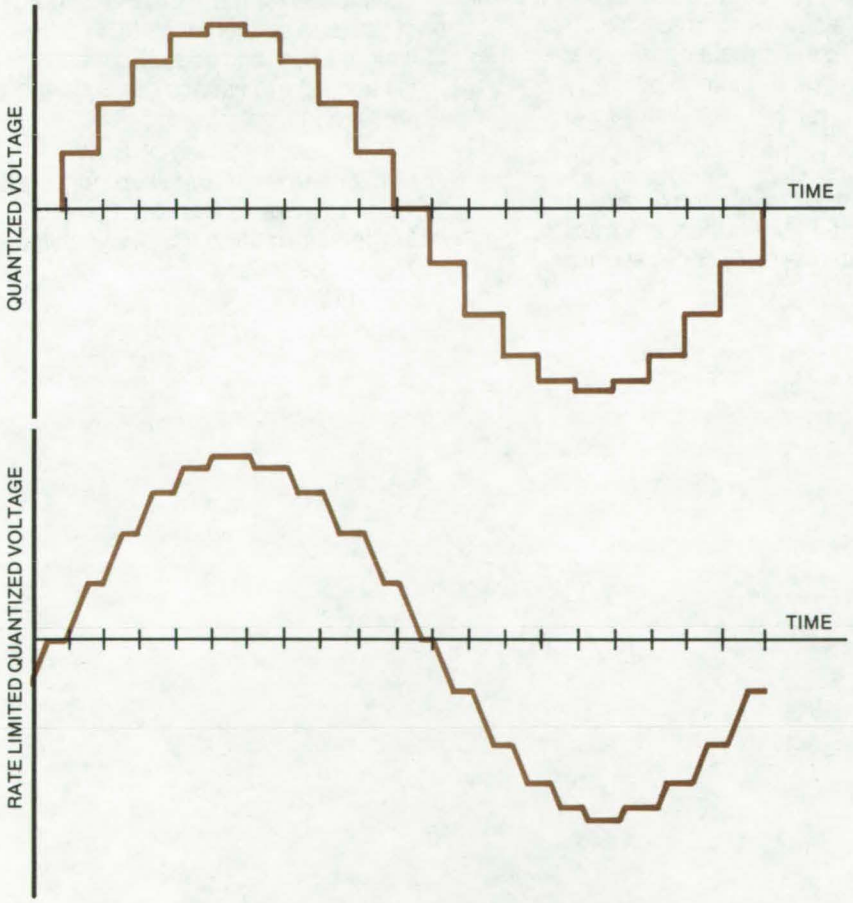

Figure 2. A **Quantized Signal is Smoothed** by the rate-of-change limiter. Noise pulses are also rate limited, reducing jitter on servo-control systems and wear on mechanical components.

The limiter finds particular application as an interface between digital-to-analog converter circuits. Converters normally output voltages that are incrementally (or decrementally) quantized in discrete steps. The discontinuity of the digitized signal creates problems for many types of control systems, especially those requiring a smooth input command to operate properly. The limiter smooths the discontinuities and thus enables the control signal to drive the controlled member more precisely.

The rate limiter, shown in Figure 1, is a nonlinear analog circuit that limits the time rate of change of the output voltage. As shown, an input voltage is applied to a summing junction, where the output voltage is subtracted. The error (difference) voltage is bounded by a limit circuit before being integrated to produce the output voltage. Characteristics of the closed-loop system force the output to be nearly equal to the input; the error signal is thus a time derivative of the input. By limiting this time derivative, the maximum rate of change of the output voltage is limited, and a waveform that varies in quantized steps, such as the one in Figure 2, is smoothed.

This work was done by Gerhard C. Streuding of Lockheed Electronics Corp. for **Johnson Space Center.** *For further information, Circle 16 on the TSP Request Card.*
MSC-16406

Efficient Bit-Error Detecting Code

Special codes detect and correct errors in computer-data transmission.

John F. Kennedy Space Center, Florida

Various codes have been developed to detect bit errors automatically in computer-data transmission. Bits can be received incorrectly due to hardware failures, noise, or other transmission faults. The error-detecting codes are implemented by transmitting the data according to a prescribed pattern; deviations from the pattern at the receiving end indicate that the data are faulty.

Two new codes have been developed to provide fail-safe operation of a launch processing and control system in which a common memory is the coordination point for the interconnection of up to 64 minicomputers. High reliability is clearly needed since a single failure in the memory could knock out the entire system.

The new codes, termed "modified b-adjacent interleaving codes," are more effective than the standard error-detecting codes, including the many varieties of Hamming and BCH codes. They are 16 bits in length and contain 8 data bits [denoted (16,8)]; the codes satisfy the following requirements:

- correct all single random-bit errors and detect all random double-bit errors,
- correct all single double-adjacent-bit errors on an even/odd hardware boundary,
- detect all combinations of two double-adjacent-bit errors over the same even/odd hardware boundary,
- convert to codes that can correct all single four-adjacent-bit errors on an even/odd hardware boundary, and
- detect a data stream of all 1's or all 0's as an uncorrectable error.

To implement code 1, a special symbol, δ, defined by

$$\delta \equiv \begin{bmatrix} 1 & 1 \\ 1 & 0 \end{bmatrix} \qquad (1)$$

is inserted into the data section of the parity matrix of any maximum distance (8,4) code, such that the code remains balanced (i.e., one δ per row). The 1's and 0's in the (8,4) code are then replaced by

$$1 \equiv \begin{bmatrix} 1 & 0 \\ 0 & 1 \end{bmatrix} \text{ and } 0 \equiv \begin{bmatrix} 0 & 0 \\ 0 & 0 \end{bmatrix} \qquad (2)$$

to generate the (16,8) code. The generator polynomial can be derived and used analytically to define direct interleaving to degree two. In addition to its meeting the above requirements, this code detects 94.1 percent of possible double-adjacent errors of 3, 4, 5, or 6 bits involving three hardware failures on an even/odd boundary.

For code 2, the δ symbols are substituted for the 1's in the diagonal of the data section of an (8,4) odd-weighted column code. Equations (1) and (2) are used to generate the (16,8) code.

This work was done by R. W. Hockenberger of IBM Corp. for **Kennedy Space Center.** *For further information, Circle 17 on the TSP Request Card.*
KSC-11039

Physical Sciences

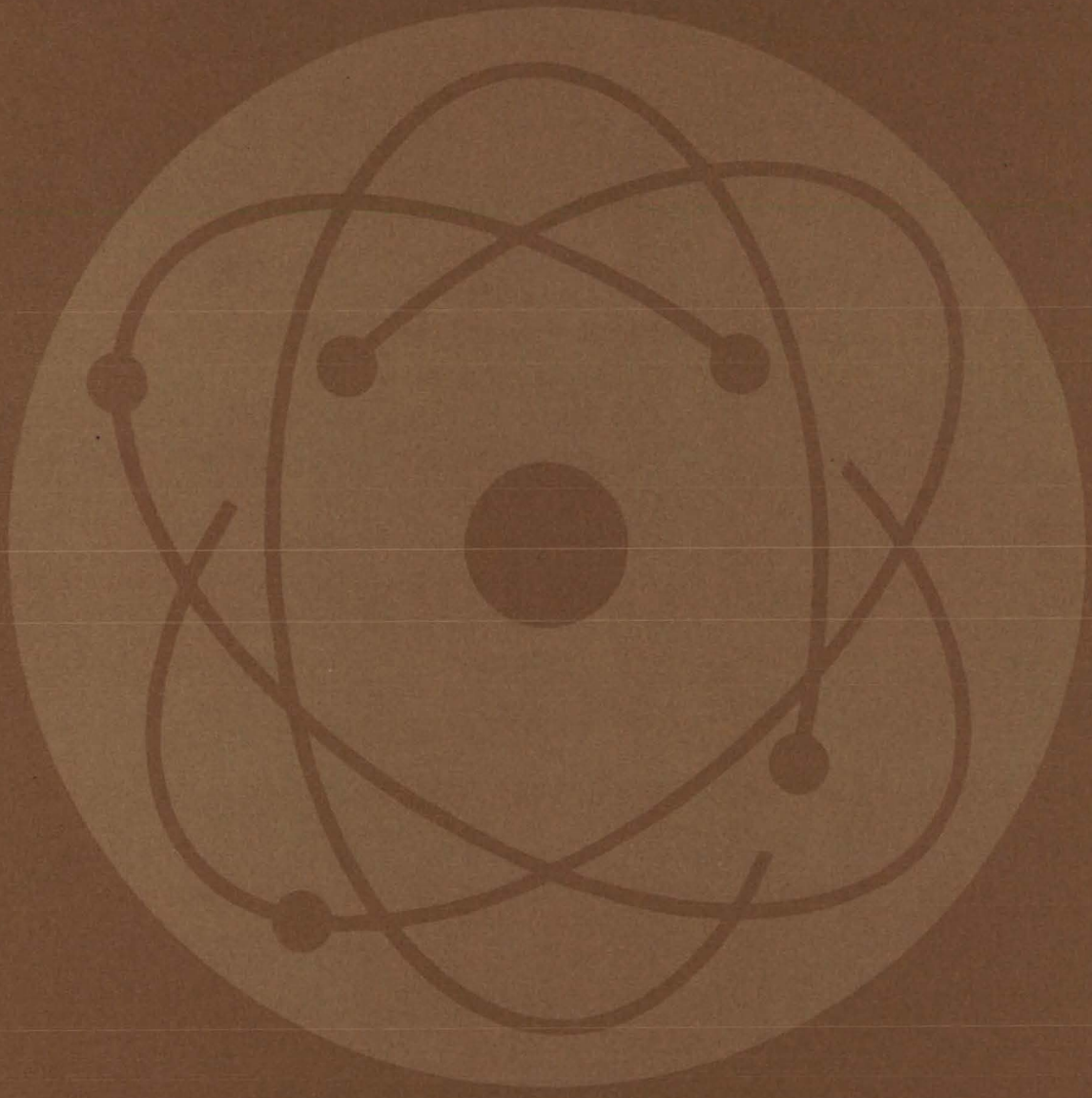

Hardware, Techniques, and Processes

Large-Scale Fresnel Lens Solar Concentrator

Acrylic lenses are lightweight, inexpensive, and relatively immune to atmospheric degradation.

Marshall Space Flight Center, Alabama

A solar-energy collection unit that employs a large acrylic Fresnel lens to concentrate the Sun's energy onto a receiver tube in a heat-collecting cavity has been tested recently. The lens is 6 by 12 ft (1.8 by 3.6 m) and consists of an array of panels 18 in. (46 cm) square, as shown in Figure 1.

The lenses follow the Sun with two-axis tracking and focus along the receiver assembly located approximately 5-1/2 ft (1.6 m) beneath the lenses. The collector longitudinal axis is alined in a north-south direction. The grooved surfaces of the lenses and the receiver assembly are protected from direct atmospheric exposure by an enclosure made of polyvinyl; both contamination/degradation and thermal convection losses due to wind are thus minimized.

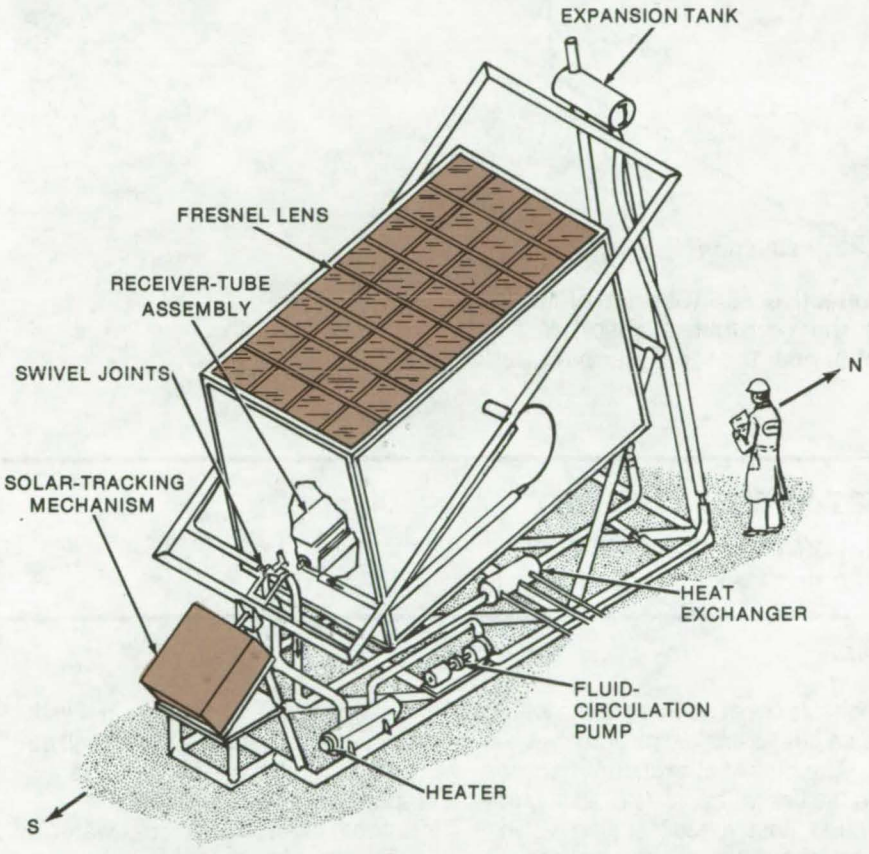

Figure 1. **Six- by Twelve-Foot Fresnel Lens** concentrates solar energy into a 5-cm-wide focal plane. Collector fluid temperatures of 300° C were obtained. This concentrator has provided performance data on the utilization of acrylic Fresnel lenses for high-temperature solar-energy applications (see back cover).

The receiver tube assembly (Figure 2) consists of an absorber tube mounted in a reflecting cavity. The absorber tube is stainless steel 0.75 in. (1.9 cm) in diameter that has been both corrugated to promote wall-to-fluid heat transfer and heat treated to produce a natural oxide absorptive coating. The reflecting cavity distributes the solar flux around the tube to reduce circumferential tube temperature gradients. By focusing on the 6.6-cm-wide cavity aperture rather than the tube, east-west Sun-tracking error effects are reduced. The cavity is normally covered with a transparent film, and a single-phase commercial thermal fluid is used as the heat-transport medium.

During the testing of the unit, solar collection efficiencies varied from 40 percent at an average fluid temperature of 125° C to 26 percent at 300° C. Redesign of the receiver assembly and placement of the absorber tube such that more energy is focused directly on the tube should, however, raise efficiency up to the 40- to 50-percent range at the latter temperature. Transverse (east-west) Sun-tracking errors up to 0.5° and longitudinal (north-south) deviations up to 5° led to no significant effects on collection efficiency.

(continued next page)

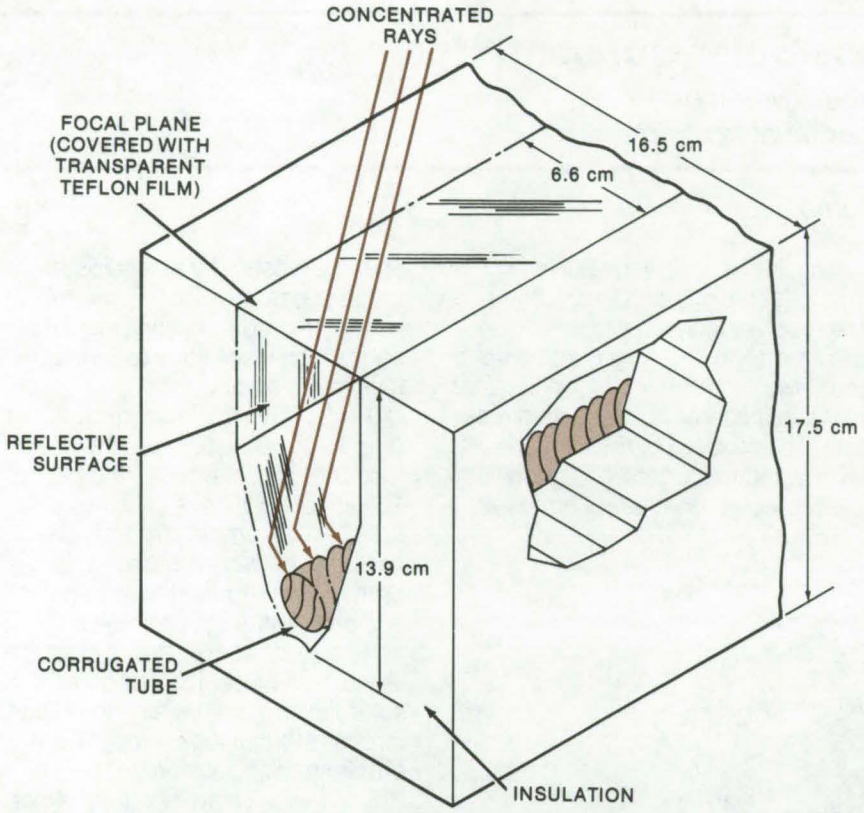

Figure 2. **Receiver Assembly** has a reflective surface that distributes incoming radiation uniformly around the corrugated absorber tube. Future designs will have the absorber at or near the focal plane for better efficiency.

This work was done by Steve L. Allums, Leon J. Hastings, and Warren S. Jensen of **Marshall Space Flight Center.** *For further information, Circle 18 on the TSP Request Card.*
MFS-23770

Heat Exchanger for Solar Water Heaters

Proposed efficient double-walled unit prevents contamination of domestic water-supply lines and indicates leakage automatically.

Marshall Space Flight Center, Alabama

Solar collectors, like other heating systems using water as a heat-transfer medium, require special precautions when used to heat water for homes. For instance, the heat exchanger must have two walls between the heated-water source and the potable water to be heated. Most heat exchangers employing this principle sacrifice considerable efficiency to gain the extra measure of insurance against contamination of the domestic water supply.

A double-walled heat-exchanger proposed for solar collectors would retain most of the efficiency of single-walled exchangers and includes an automatic indication of leaks in either of the two walls. Of course, it could be also used with nonsolar heat sources using water as a heat-transfer medium.

The new heat exchanger, shown in the figure, consists of four spiral-rolled metal tubes installed within concentric smooth metal tubes. Each spiral tube touches, or is very close to, the surrounding smooth tube. Heat-transfer fluid from the solar collector flows inside the spiral-walled tubes; the potable water to be heated flows around the outside of the smooth tubes. The many contact points between the two tubes transfer heat efficiently, yet the spiral void between the tubes serves as a path for any leaked fluid to leave the exchanger.

In operation, both the solar-collector loop and the domestic water are under pressure. If a leak occurs in either tube, water will be forced into the nonpressurized space between the spiral and smooth tubes. The excess water will ultimately flow out weep holes in the wall of the exchanger housing. By placing a nontoxic dye in the space between the tubes, leaks can be identified readily.

A potable liquid (e.g., glycerine) with a boiling point higher than that of water could be used between the tubes to improve heat transfer. A powdered metal, or metal granules, could also be placed between the tubes as long as they are porous and chemically compatible with the heat-exchanger walls and fluids. This would permit water to continue into

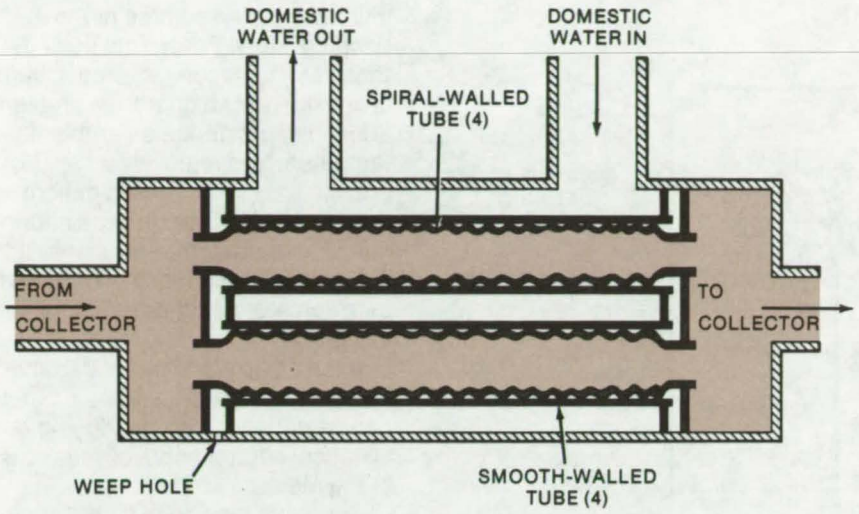

A **Double-Walled Heat Exchanger** (shown in cross section) consists of four smooth-walled tubes containing concentric spiral-walled tubes (only three of each shown). A leak in either wall allows water to flow into the space between the headers and out the weep hole, which can be monitored to detect leaks without risk of contaminating the domestic water supply. The heat-exchange properties are as good as, or better than, other double-walled designs.

the header void and out the weep holes, while improving heat transfer. The metal granules could be coated with a water-soluble dye that would show up at the weep hole in the event of a leak.

Leaks could also be detected with two electrical probes that are shorted by any water in the space between the headers and a warning device. Another alternate to the weep holes is to place a sight glass between void spaces to view the liquid level and permit the liquid to overflow in case of leakage.

This work was done by Mitchell Cash and Albert C. Krupnick of **Marshall Space Flight Center.** *For further information, Circle 19 on the TSP Request Card.*

Inquiries concerning rights for the commercial use of this invention should be addressed to the Patent Counsel, Marshall Space Flight Center [see page A8]. Refer to MFS-23711.

Simple Device Measures Solar Radiation

A modified thermometer measures the incident radiation intensity.

Marshall Space Flight Center, Alabama

The simple and inexpensive device shown in the figure can measure the intensity of solar radiation or the radiation from other sources, such as furnaces and ovens. The device is essentially a conventional thermometer that has been almost totally isolated from convective and conductive heat transfer with its surroundings. Therefore, its temperature (and its liquid level) is determined mainly by the incident radiation intensity and by radiative heat transfer. Its reading is somewhat dependent on the ambient temperature; however, this effect is predictable and can be accounted for by proper calibration.

The thermometer is encased in an evacuated transparent-glass or plastic jacket to isolate it from the surroundings. Its reservoir is spherical to present a constant surface area as the Sun moves across the sky. Thus it will maintain its calibration for any time of day or year (for a given ambient temperature).

Any liquid that does not freeze or boil at the combined radiation intensities and ambient temperatures to which it is exposed can be used. For the range of conditions encountered in the U.S., mercury is a good choice.

The capillary must be long enough to accommodate the expected expansion of the fluid. For example, mercury in a capillary 0.005 in. (0.13 mm) in diameter and a 0.20-in.^{3} (3.28-cm^3) reservoir will rise 6 in. (15 cm) as the radiation intensity increases from zero to 330 Btu/h-ft^2 (249 cal/s-m^2), the maximum solar intensity expected in the United States.

The mounting is coated with a low-reflectivity paint so that it does not reflect radiation into the reservoir. The reservoir is exposed to the Sun's rays; however, it may be necessary to shield the capillary.

For steady-state operation, the thermal energy into the device (determined by the solar intensity and constants such as the transmittance of the glass reservoir) is balanced by the thermal energy out (determined by the temperature difference between the reservoir and the air outside and the radiation properties of the reservoir). This energy balance allows the solar intensity to be related to the reservoir temperature and

(continued next page)

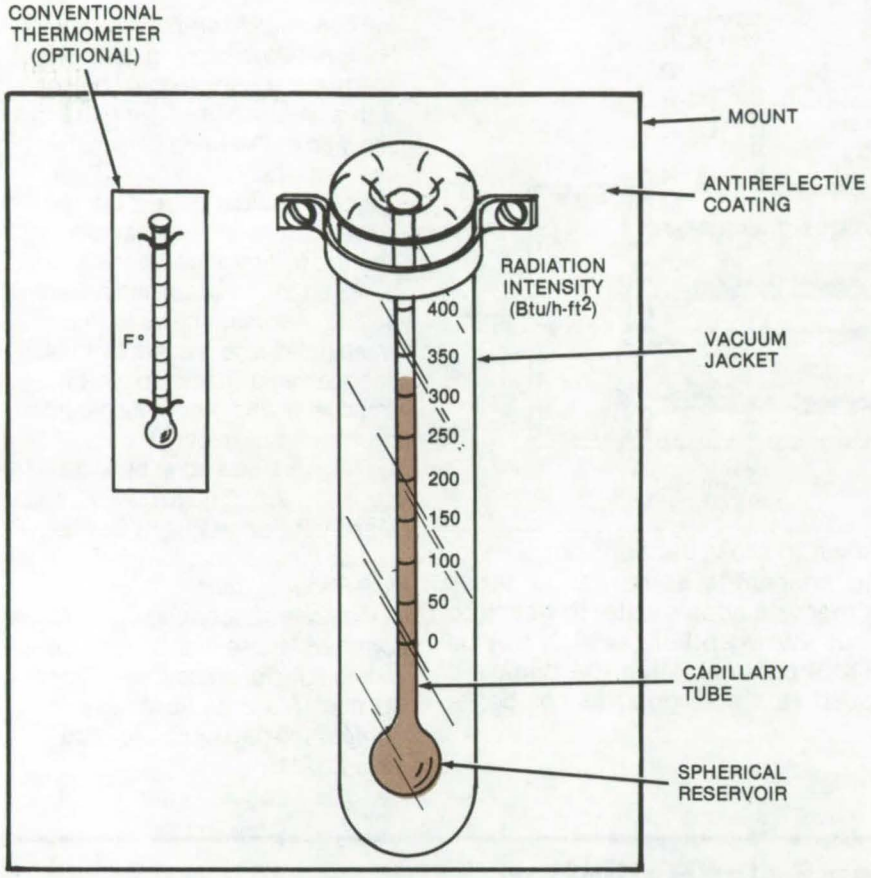

Radiation Thermometer uses an expanding liquid (such as mercury) to measure radiation intensity. The capillary tube and reservoir in a vacuum jacket can be made by techniques similar to those used for manufacturing electric light bulbs.

ultimately to the volume of the expanding liquid. For typical solar intensities, the reservoir temperature is considerably higher than ambient, and the dependence on ambient temperature is relatively weak. For precise measurements, a calibration curve that gives the error as a function of ambient temperature would be used. A conventionally mounted thermometer could be included for this purpose.

If the device is to be read from a remote location, an electrical output can be derived from the varying resistance, capacitance, or pressure of the mercury column.

This work was done by William R. Humphries of **Marshall Space Flight Center.** *For further information, Circle 20 on the TSP Request Card.*

Inquiries concerning rights for the commercial use of this invention should be addressed to the Patent Counsel, Marshall Space Flight Center [see page A8]. Refer to MFS-23751.

Direct-Heating Solar-Collector Dump Valve

Five-port ganged valve eliminates heat exchangers in pumped systems.

Marshall Space Flight Center, Alabama

Heat exchangers have been used in pumped solar thermal systems to preclude fouling of the collector waterways and to protect against freezing by decoupling the collector loop from line pressure. These reasons, however, are invalid in certain situations. Although less fouling should occur inside the collectors (through which the flow velocity is greater than that across a heat exchanger immersed in a storage tank), fouling would still be expected to occur on the exterior of the heat exchangers. In areas that rarely freeze, freeze protection is preferably provided by a frost cycle in the autocontrol; automatic circulation would occur when the collectors reach a preset temperature just above freezing. In these situations, the use of direct heating, rather than a heat exchanger, is possible.

For those installations that experience regular and frequent freezes, the use of direct heating and a frost cycle are not preferred, since too much energy is consumed operating the automatic circulation equipment. For these installations, a positive drainage system, such as a dump tank, is required.

A new five-port ganged valve isolates the collectors from the primary load (system pressure) and drains the collectors, allowing the use of direct heating with all its advantages. The valve, shown providing this direct-dump option in a collector flow line in the figure, could be opened and closed by the same switch that controls the pump, or by a temperature sensor set at 32° F (0° C) plus some small safety margin. A schematic of the flow pattern within the valve is also shown.

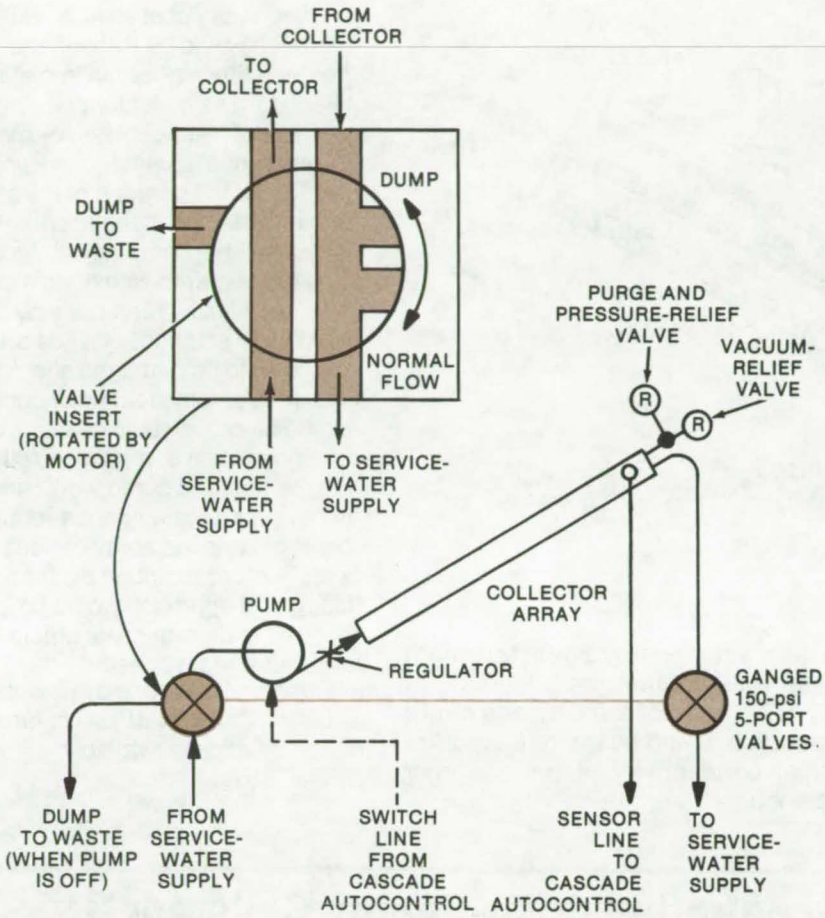

A **Five-Port Ganged Valve** provides direct dump (to prevent freezing) in this solar-collector fluid line. The flow schematic of the valve is also shown. Counterclockwise rotation by 90° opens the dump line and isolates the collector line from the service water-supply line.

The valve would be normally closed, since for the majority of its life cycle, it would not be in the dump mode. Synchronous clock motors have been used to drive similar valves. This method is relatively inexpensive, since the valve may be held open for long periods by stalling the motor without excessive power drain or overheating. A more powerful drive may be required if the valve is to restrict water from a public main, which may reach 100 psi (690×10^3 N/m^2).

This work was done by Terence C. Honikman of Elcam, Inc., for **Marshall Space Flight Center.** *For further information, Circle 21 on the TSP Request Card.*
MFS-23679

"Tubeless" Flat-Plate Solar Collector

A proposed solar collector could collect solar energy efficiently without metal tubing.

Caltech/JPL, Pasadena, California

Despite the large number of variations of the conventional flat-plate solar collector that have evolved recently, none are yet sufficiently cost-effective for widespread home use. This is largely due to the extensive use of formed metal parts for the collector plates and for the tubing, channeling, or the equivalent that circulate the energy-collection fluid (usually water) within the collector.

In a proposed design, heat would be removed from the collector plate effectively by bringing the collector fluid into direct contact with the absorber plate without the use of tubing or channeling. As can be seen in the figure, this could be accomplished by spraying the collector fluid onto the undersurface of the collector plate. This would produce a convective heat-transfer coefficient large enough so that only minimal spatial temperature variations would occur in the plane of the absorber. Consequently, the requirement for high in-plane thermal conductance, a necessity for collectors with absorbers that must conduct absorbed solar energy to attached fluid conduits, would be eliminated. Low-cost materials, summarily overlooked in the past because of low thermal conductivity (e.g., plastics), could thus be utilized in this novel design.

The heated fluid collects in a sump from which it is pumped through the system for space heating and/or domestic hot-water supply. The collector structure could employ the usual insulation and double glazing to reduce heat losses.

(continued next page)

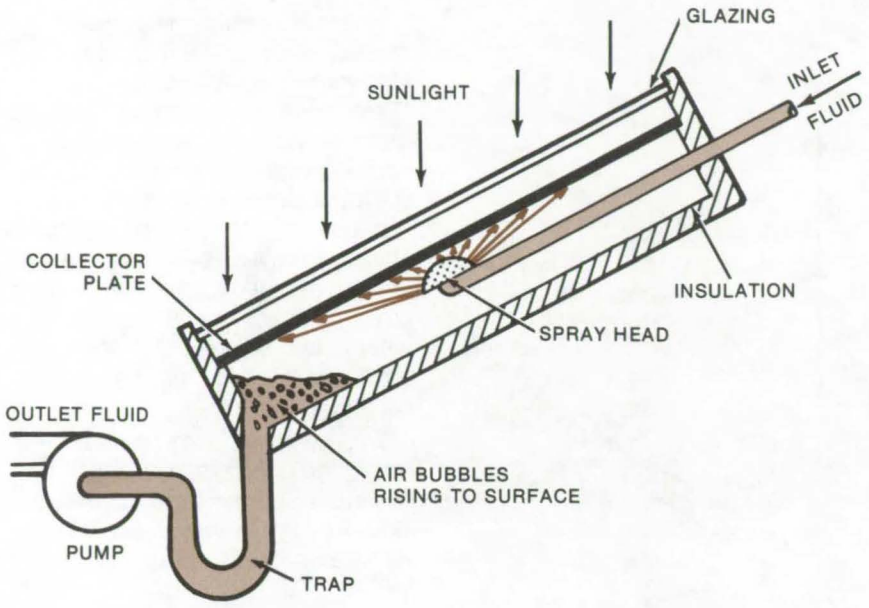

Efficient Heat Transfer Without Pipes in a solar-energy collector might be possible by spraying the heat-transfer fluid against the underside of the collector plate. A single spray head or an array of spray heads might be used. The chief advantage of this approach would be the relaxation of materials requirements, as high thermal conductivity of the absorber plate material is no longer a critical selection parameter.

The primary cost savings with this approach would be through the greater latitude possible in materials selection. The collector plate might be made of plastic, glass, or metal; however, one advantage in using plastics for the portions of the structure in contact with the absorber fluid is that the compatibility problems encountered with metals used in conventional structures may be avoided. In addition, plastics are less likely to be damaged should the fluid accidentally freeze. Of course additional costs would be incurred through the use of a spray nozzle and the required pump work, and there may be maintenance requirements to keep the spray orifices open. A more thorough evaluation of this type of approach would be required to determine its efficiency and cost-effectiveness.

This work was done by Burton Zeldin of **Caltech/JPL.** *No further documentation is available.*
NPO-13897

Two-Axis Movable Concentrating Solar-Energy Collector

Proposed construction eliminates need for flexible or slip connections between boiler and heat engine.

Caltech/JPL, Pasadena, California

Practical development of large-scale solar-energy collection systems, using collectors that concentrate the incident heat energy, has been hampered by requirements for flexible lines, complex rotary or slip joints, and other piping. Such connections are needed between the fluid boiler, which is mounted at the focal point of the parabolic collection surface, and the ground-supported heat engine that utilizes the collected energy.

These connections might be eliminated by mounting the boiler in fixed positon at the parabolic collector focuses. In a fixed position, hard line connections capable of withstanding the optimum high-temperature fluid flow can be utilized to connect the boiler and the heat engine.

A proposed type of solar-tracker collector assembly (shown in the figure) makes this possible. Two concentric circular tracks are placed about a vertical axis in a shallow spherical hole in the ground. The boiler is mounted in a fixed position over the hole. The tracks support a frame that can be moved around the perimeter of the hole (shifted in azimuth). This "azimuth frame" in turn supports an elevation frame that rides up and down the side of the bowl. The elevation frame supports the parabolic mirror or reflector, which focuses the incident solar energy on the fixed boiler at all azimuths and elevations.

The elevation frame is counterbalanced by a cable and a weight system. Pulleys for the cable are attached to the azimuth frame, and the cable is attached to the elevation frame. The weight falls into a circular ditch on the shady side of the bowl. The counterbalanced weight leaves the elevation drive system with only frictional losses to be overcome. The reflector elevates at a slow (sidereal) rate and can be readily driven by a small motor with a very large gear reduction.

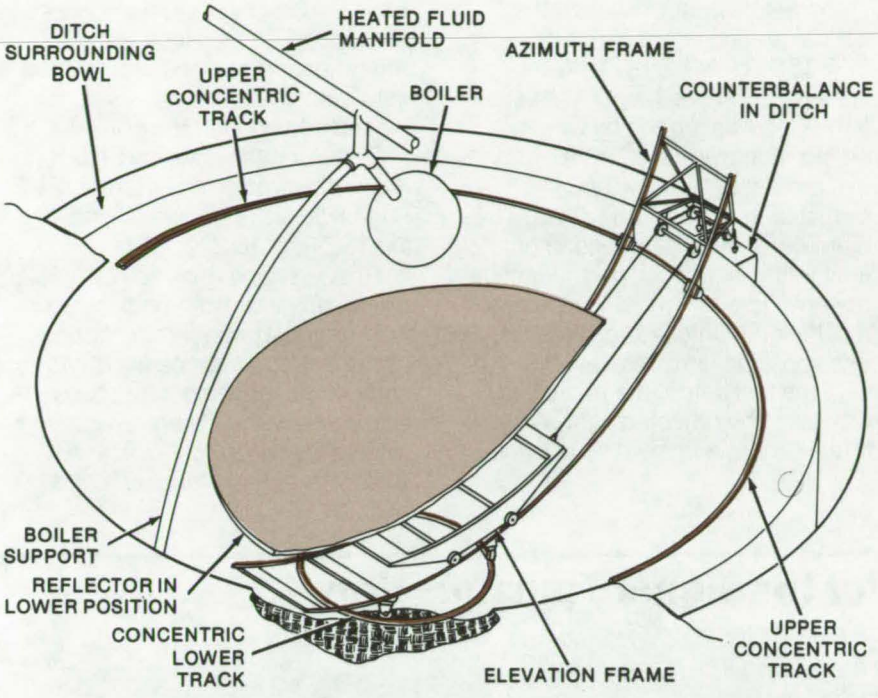

The Two-Axis Movable Concentrating Solar-Energy Collector could be mounted in a spherical hole in the ground. The boiler position would be fixed at the parabolic collector focuses, eliminating the need for flexible or slip connections for transporting high-temperature fluid between the boiler and the heat engine.

The fixed position of the boiler eliminates the high cost of flexible and movable connections and reduces length of the up-and-down piping; thus construction costs can be reduced, maintenance requirements can be lessened, and reliability and flexibility are improved. The low wind profile of this below-ground installation also contributes to overall optimization. An above-ground installation is possible, however, by use of a suitable truss-supporting structure.

This work was done by Gerald S. Perkins of **Caltech/JPL.** *For further information, Circle 22 on the TSP Request Card.*

This invention is owned by NASA, and a patent application has been filed. Inquiries concerning nonexclusive or exclusive license for its commercial development should be addressed to the Patent Counsel, NASA Resident Legal Office-JPL [*see page A8*]. *Refer to NPO-13921*

Wide-Field Schlieren System

The conventional mirror and knife edge are replaced by a diffraction grating and a wire grid.

Caltech/JPL, Pasadena, California

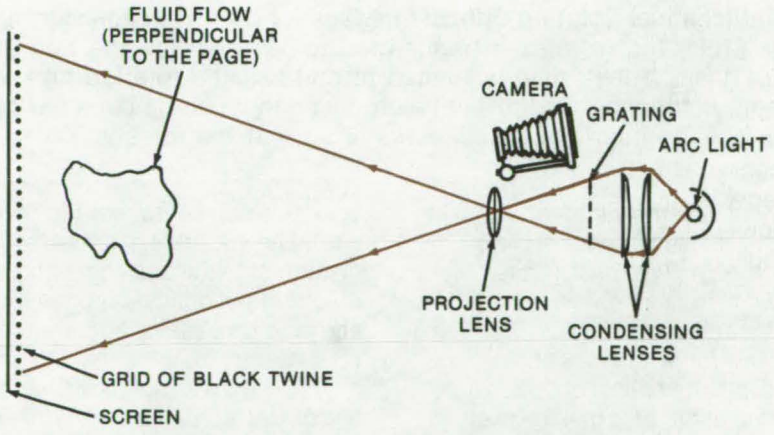

A Novel Schlieren System photographs fluid flow by arranging the flow to disturb a moire pattern. The pattern is formed when light from an optical grating interferes with a wire grid. In tests, the system recorded heat flow rising from a lighted match and mach diamonds in a supersonic air jet.

A new schlieren photography system that requires no mirror or knife edge uses an optical grating and a grid of black twine to form a moire pattern. The system can make much larger schlieren photographs than has been previously possible. Since it obviates the need for a large concave mirror, it is also less expensive.

Schlieren photography is used in wind-tunnel flow studies and in other fluid-flow applications. For nonuniform flow, density gradients produce spatial variations in the refracting properties of the fluid; these spatial variations are recorded as variations in light intensity. In conventional systems, light passing around a knife edge is used to produce these variations of intensity.

(continued next page)

In the new system, shown schematically in the figure, a projection lens forms a magnified image of an optical grating. The image interferes with a grating made by stretching black twine between two threaded rods and forms a moire pattern on the screen. The pattern is photographed by a camera.

The fluid field is located between the two gratings. For uniform flow, the index of refraction is homogeneous across the fluid, and the gratings can be arranged to produce either a uniform dark or bright field. Any departure from uniform flow shows up as a pattern on this field.

In the test system shown, the optical grating was a standard 2- by 2-in. (5.1- by 5.1-cm), 1,000-lines/in. (394-lines/cm) type; the large grid was formed by winding black nylon twine 0.05 in. (0.13 cm) in diameter between 40-in. (101.6-cm) steel rods 1/2 in. (1.27 cm) in diameter. There is no fundamental limit to the size of the grid. It can be made as large as required, provided a sufficiently-intense light source and sensitive film are available.

In the test setup, the photograph was taken by reflected light. A further improvement in sensitivity can be made by using a single or compound Fresnel lens instead of the reflecting screen to focus the light before it enters the camera placed behind the time grid.

This work was done by Shakkottai P. Parthasarathy of **Caltech/JPL.** *For further information, Circle 23 on the TSP Request Card.*

This invention is owned by NASA, and a patent application has been filed. Inquiries concerning nonexclusie or exclusive license for its commercial development should be addressed to the Patent Counsel, NASA Resident Legal Office-JPL *[see page A8].* *Refer to NPO-14174.*

Rotating Optical Coupler for Signal Transmission

An assembly that has no mechanical contacts transmits multichannel data across a rotating interface.

Caltech/JPL, Pasadena, California

An optical coupler transmits data across a rotating interface without sliprings or other mechanical contacts. The device, which uses a rotating Dove prism assembly to form a stationary image of a rotating object (such as the output of multiple optical transmitters), can handle many high-bit-rate data channels. Its potential for high reliability over long and unattended periods makes it suitable for data transfer on interplanetary missions lasting many years and for other signal-transfer applications requiring high reliability.

A Dove prism rotates a transmitted image through 180° when the prism is rotated by 90°. Therefore, the image rotates at twice the rotation speed of the prism. If the prism is rotated at one-half the rotation rate of an object on one side of the interface, its image will appear to be stationary on the other side. The stationary image can then be picked up by receivers.

The Dove prism has some inherent optical drawbacks that can be avoided by the use of a three-element assembly that functions in exactly the same manner. This structure, a Dove prism assembly, is shown in the figure. The same effect can be achieved at lower cost with a triple-mirror arrangement.

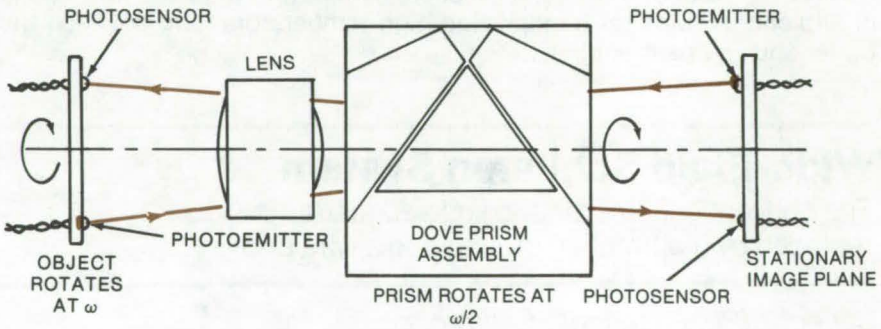

A **Multichannel Rotating Optical Interface for Data Transmission** uses a Dove prism that rotates a transmitted image at twice the rate of the prism itself. If the prism is rotated at one-half the rotation rate of the object, a stationary image will be produced that can be detected by the receiver. The interface is bidirectional so that the roles of object and image can be reversed.

Solid-state optical couplers can operate at bit rates in excess of 2×10^7 bits per second. With this device, many high-density data channels can be transferred across a rotating interface. It should thus be of interest to the designers and manufacturers of optical-communication and data-processing and transfer equipment.

This work was done by Charles V. Ivie of **Caltech/JPL.** *For further information, Circle 24 on the TSP Request Card.*

NPO-14066

Optical Retroreflector

Backscattered radiation is a function of the angle of incidence only.

Marshall Space Flight Center, Alabama

A new planar target material reflects incident optical energy back to the source, such that the retroreflected light intensity is a function of the angle of incidence only. The retroreflective pattern can be tailored to suit specific requirements; for example, it could be used to aline a distant surface normal to a beam of laser light.

The reflector, seen in the figure, consists of a dielectric sheet, transparent to the wavelength of interest, with identical patterns of black (opaque) pigment deposited on both sides in a precisely matching relationship. One of the sides is backed by a white surface having a roughness that makes it a good light scatterer at the wavelength of interest.

Incident light normal to the reflector passes through the two layers of black pigment, seen in perfect register, and illuminates the exposed white surface. Light is diffusely scattered by the white surface and is returned to the direction of incidence. As seen, light incident at an oblique angle illuminates a portion of the white scattering surface, which is smaller as the angle of incidence increases, resulting in a decrease of backscattered energy.

Three methods for generating the random pattern of black pigment have been proposed. In one method, microscopic pigmented resin particles could be dispersed in a chamber and allowed to settle on a clean glass plate until they cover approximately 50 percent of the glass surface. After being fixed by heating the glass substrate, the pattern would be photographically reproduced with suitable change of scale. Alternatively, the photographic plate can be exposed to laser "speckle," developed, and scaled in size. Or, the pattern can be generated by a computer program and printed by a peripheral device, such as a plotter, a CRT, or a photographic camera.

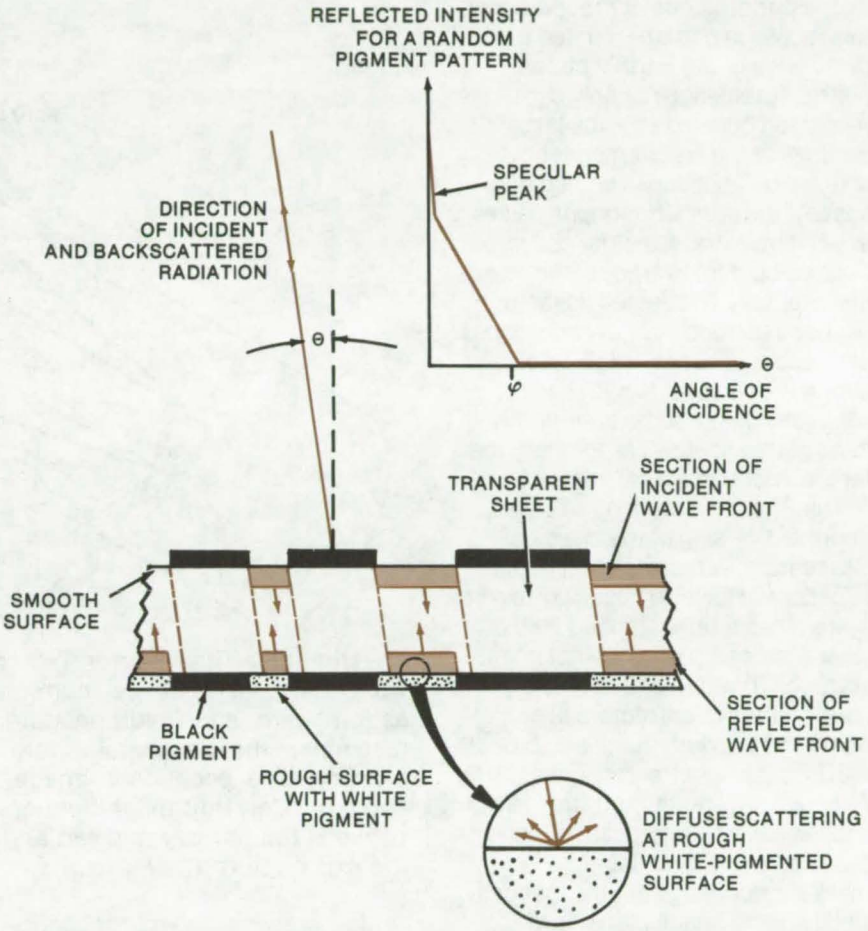

The Reflected Light Intensity depends only on the angle of incidence for this retroreflector. As seen in the insert, light incident at any angle is diffusely scattered by the rough white surface. The light scattered from the rough surface radiates in all directions, independent of the angle of incidence. However, as the angle θ increases, the area of exposed white surface decreases, reducing the reflected wave front and giving the intensity pattern shown. The width (σ) of the reflected peak for a random (isotropic) opaque pattern is proportional to the number of spots per unit area.

In general, if the black pigmented pattern has circular symmetry or a randomness that makes it appear isotropic, then the amount of backscattered energy is a function of the angle of incidence only. The backscattering diagram is related to the autocorrelation function of the black pigmented pattern, making it possible to compute the required pattern when the desired backscattering is known.

This work was done by Frederik Weindling of United Aircraft Corp. for **Marshall Space Flight Center.**

For further information, Circle 25 on the TSP Request Card.

MFS-23282

Anastigmatic Three-Mirror Telescope

Optically corrected instrument has high resolution over a flat image field of 1.5°

Marshall Space Flight Center, Alabama

The performance of ground-based telescopes is primarily limited by the turbulence of the Earth's atmosphere. Turbulence not only degrades resolution but also absorbs large portions of the electromagnetic spectrum. Telescopes placed in space, however, offer opportunities to perform extraterrestrial observations without interference from the atmosphere. To take full advantage of space astronomy, new telescopes are needed that have high resolution over a wide field of view. These telescopes should also be all-reflective, to cover the spectral range from the far ultraviolet to the far infrared.

The Ritchey-Chretien, an improved version of the classical Cassegrain, is today's most popular telescope. However, this two-mirror system has a rather limited field of view and does not have a flat image surface. To widen and flatten the field, refractive correctors are sometimes added, but this approach narrows the spectral response. Although several three-mirror telescopes have been proposed, none provides a practical solution. The main shortcomings are the inaccessibility of the image plane, large central obscuration, and the fast-focal ratio forced by the configurations.

The proposed three-mirror telescope shown in the figure provides very high resolution over a flat field of 1.5°. This is considerably better than the best two-mirror telescope which gives the same resolution over only a few arc-minutes in a curved field. The telescope also suppresses stray-light without an elaborate baffling system, making it well suited for space astronomy and other high-performance and low-light-level applications.

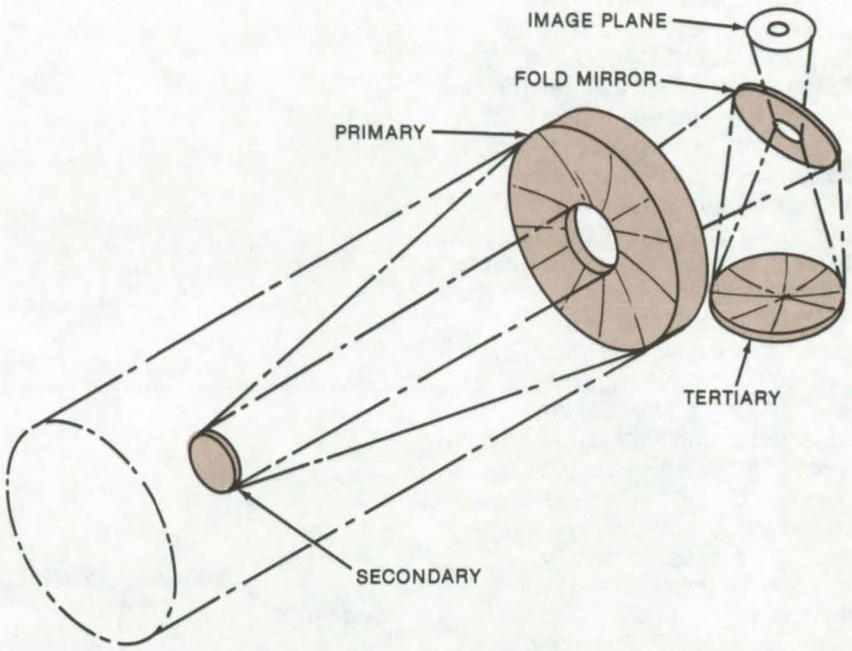

Anastigmatic Three-Mirror Telescope provides high resolution over a wide field. It can be corrected for spherical aberration, coma, astigmatism, and field curvature. The primary/secondary combination resembles the Cassegrain, forming a real image in the hole of the primary. The secondary image is reimaged by a tertiary mirror at approximately unit magnification. A flat perforated fold mirror is placed between the primary and tertiary so that the perforation coincides with the exit pupil of the teritiary.

Most practical two-mirror configurations can be corrected for only two aberrations (usually spherical aberration and coma); this three-mirror telescope is corrected for four aberrations: spherical aberration, coma, astigmatism, and field curvature. The mathematical conditions for correcting these aberrations can be solved for all pertinent design parameters by standard techniques. The parameters can be scaled as desired.

This work was done by Dietrich Korsch of Sperry Rand Corp. for **Marshall Space Flight Center.**

Further information may be found in NASA TMX-73326 [N76-29340], "Starsat - A Space Astronomy Facility," a copy of which may be obtained at cost from the New England Research Application Center *[see page A7]*.

This invention is owned by NASA, and a patent application has been filed. Inquiries concerning nonexclusive or exclusive license for its commercial development should be addressed to the Patent Counsel, Marshall Space Flight Center *[see page A8]*. *Refer to MFS-23675.*

Process Sharpens Micrographic Images

Carbon, deposited by ion glow discharge, enhances the contrast between nonmetallic components.

Lyndon B. Johnson Space Center, Houston, Texas

Image contrast in photomicrographs of nonmetallic composites, such as glass/epoxy printed-wiring boards, is considerably enhanced by an ion glow-discharge technique. The discharge applies an amorphous-carbon layer to the surface after it has been prepared by conventional metallographic methods. Photomicrographs produced by bright-field illumination of the carbon-coated surface are considerably sharper and reveal more detail than those made without the coating or produced by scanning electron microscopy.

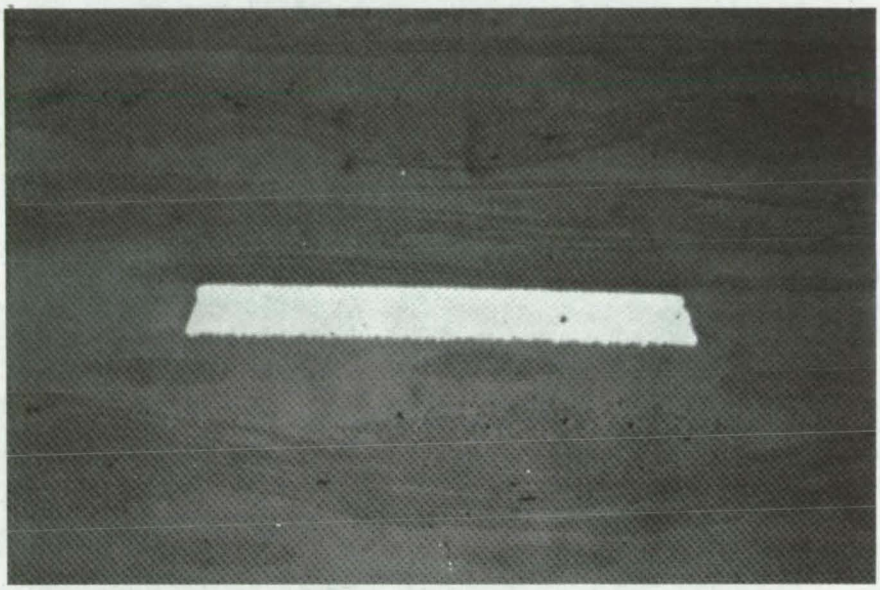

[a]

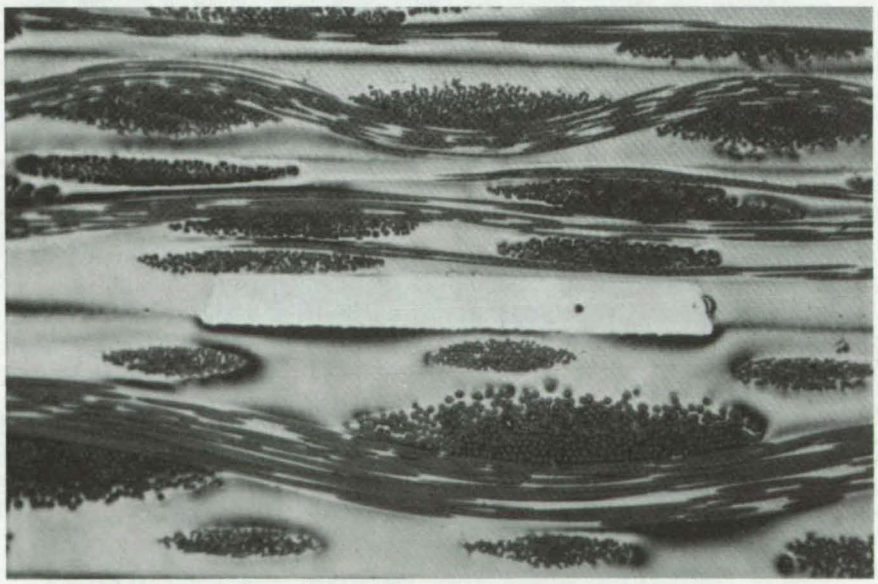

[b]

Image Contrast Is Considerably Improved if a carbon coating is applied to this nonmetallic composite before exposing the micrograph. The image shows the edge of a printed-wiring board magnified 100X: in (a), before carbon treatment, and in (b), after treatment.

The effectiveness of the process was verified in tests on a printed-wiring board. The board edge was subjected to normal metallographic preparation to produce a finely-polished cross section, with vibratory polishing as the final step. Following polishing, the sample was examined by bright-field microscopy [see figure (a)].

The specimen was then silver painted and coated with a layer of amorphous carbon, using an ion glow-discharge apparatus. Examination of the board by scanning electron microscopy revealed a sharper image, but its general appearance was similar to that observed in the figure (a).

With the carbon coating still intact, the specimen was removed from the vacuum chamber of the scanning electron microscope and was viewed by bright-field illumination. The effect of carbon deposition [figure (b)] is apparent. The carbon layer increased the reflectance at the specimen surface and enhanced the contrast between the glass fibers and the epoxy base. The result is considerably sharper definition of the two nonmetallic components.

This work was done by Alan F. Eaton of Sundstrand Corp. for **Johnson Space Center.** *For further information, Circle 26 on the TSP Request Card.*

Inquiries concerning rights for the commercial use of this invention should be addressed to the Patent Counsel, Johnson Space Center [see page A8]. Refer to MSC-16846.

Two Pumps Reduce Maser Weight

Two small complementary vacuum pumps replace a single large pump for scavenging residual gases.

Marshall Space Flight Center, Alabama

In conventional hydrogen masers, a single large ion pump removes hydrogen and residual outgassing products. This type of pump weighs about 90 kilograms owing to the large permanent magnets that provide the strong magnetic fields required for confining electrons in the discharge. The weight and cost of the maser unit are reduced significantly by replacing the large ion pump with a hydrogen sorption pump and a miniature ion pump.

The sorption pump acts as a "getter," having a cartridge with a very large surface area of activated zirconium and aluminum sintered on a thin stainless-steel substrate. The sheet is bent back and forth over itself and is formed into a cylindrical array in the same manner as an automotive oil filter. The cartridge, which is normally stored in an inert gas to prevent contamination, is activated at about 750° C under a vacuum. If the cartridge is to cope with nonhydrogen products, it is kept hot, though at a lower temperature. When the surface becomes saturated with active gas products, a new surface can be prepared by reactivation of the vacuum system. After total saturation, the cartridge is easily replaced with a fresh one. If it is primarily to absorb hydrogen, as in the maser application, the cartridge does not have to be heated. Hydrogen goes into solid solution, and its pumping speed is independent of temperature. It can be released from a saturated cartridge by a rise in temperature.

In the maser system, the miniature ion pump removes residual air, argon, hydrocarbons, and other nonhydrogen gases. A typical ion pump has a capacity of 0.2 l/s and pumps hydrogen as well as other gases. Hydrocarbons are apparently broken up by the ion pump, but eventually only the carbon is pumped, and the sorption cartridge removes the hydrogen. In small quantities, argon is pumped effectively; but if there is a small atmospheric leak, argon can concentrate. If this happens, the ion pump can become unstable, regurgitating the argon and repumping it cyclically.

In one maser system, consisting of well-outgassed metal, a few "O" rings, and large surfaces of Teflon and vacuum epoxy, the combination ion pump and sorption cartridge was operated continuously without failure for nearly a year.

This work was done by the Smithsonian Institution Astrophysical Observatory for **Marshall Space Flight Center.** *For further information, Circle 27 on the TSP Request Card.*

Inquiries concerning rights for the commercial use of this invention should be addressed to the Patent Counsel, Marshall Space Flight Center [see page A8]. Refer to MFS-23265.

Apparatus for Determining Surface Tension

An improved system for determining surface tension measures the pressures required to form bubbles at the openings of two capillaries. A pressure transducer coupled to a bridge supply and a chart recorder registers the pressures more accurately than conventional apparatus that uses a manometer. Errors arising from the lag of the manometer fluid are also eliminated.

(See page 508.)

Recording-Tape Lightning Detector

A simple device uses prerecorded magnetic tape to monitor lightning strikes. The tape stores an audio-frequency signal that is partially erased by the magnetic field around the lightning strike and measures the magnitude of the peak current. The tape is mounted on a plastic strip and held in a plastic tube that can be suspended on a guy wire or other location.

(See page 454.)

Whole-Rock Uranium Analysis by Fission-Track Activation

A new method for uranium analysis does not require that the unknown sample be powdered. Instead, the unknown and a reference sample are simultaneously irradiated along with mica detectors in a special vacuum assembly. The geometry of the assembly and the uranium concentration in the standard allow the unknown concentration to be determined accurately.

(See page 482.)

Photoelectron Spectroscopy by Electron Attachment

A high-resolution method for measuring atomic and molecular energy levels does not require electron optics.

Caltech/JPL, Pasadena, California

A novel technique can detect threshold photoelectrons from atoms and molecules with high resolution, yet requires no electron-optics setup. Instead of detecting the electrons directly, a secondary gaseous species is used to trap threshold-energy photoelectrons. The resulting negative ions are then detected in a mass spectrometer. The technique has several advantages over conventional electron and threshold-photoelectron spectroscopy, including:

- high resolution in final ion states that can easily approach 3 to 5 meV,
- the suppression of autoionization features that give rise to nonthreshold electrons, and
- easy conversion of a conventional photoionization mass spectrometer to the threshold device by the addition of a suitable trapping gas.

Trapping gases such as $CFCl_3$ and SF_6^- have been used with the new technique. The gas is combined with the species being studied, and the mixture is illuminated by narrow-band radiation from a scanning monochromator. Threshold photoelectrons are released when the incident photon energy corresponds to a vibrational or electronic energy level of the primary gas. The electrons attach themselves to the trapping molecules and form negative ions that are detected by a quadrupole mass spectrometer. The transit time of the ions is 50 μs or longer. In the SF_6^- case, this long flight time insures that the only detected ions are those produced by the attachment of electrons with kinetic energies of about 3 meV or less.

A typical photoelectron spectrum obtained with the new method is shown in the figure. In this case, $CFCl_3$, the molecule under study, also serves as the trapping gas; the detected ions were Cl^-, formed by

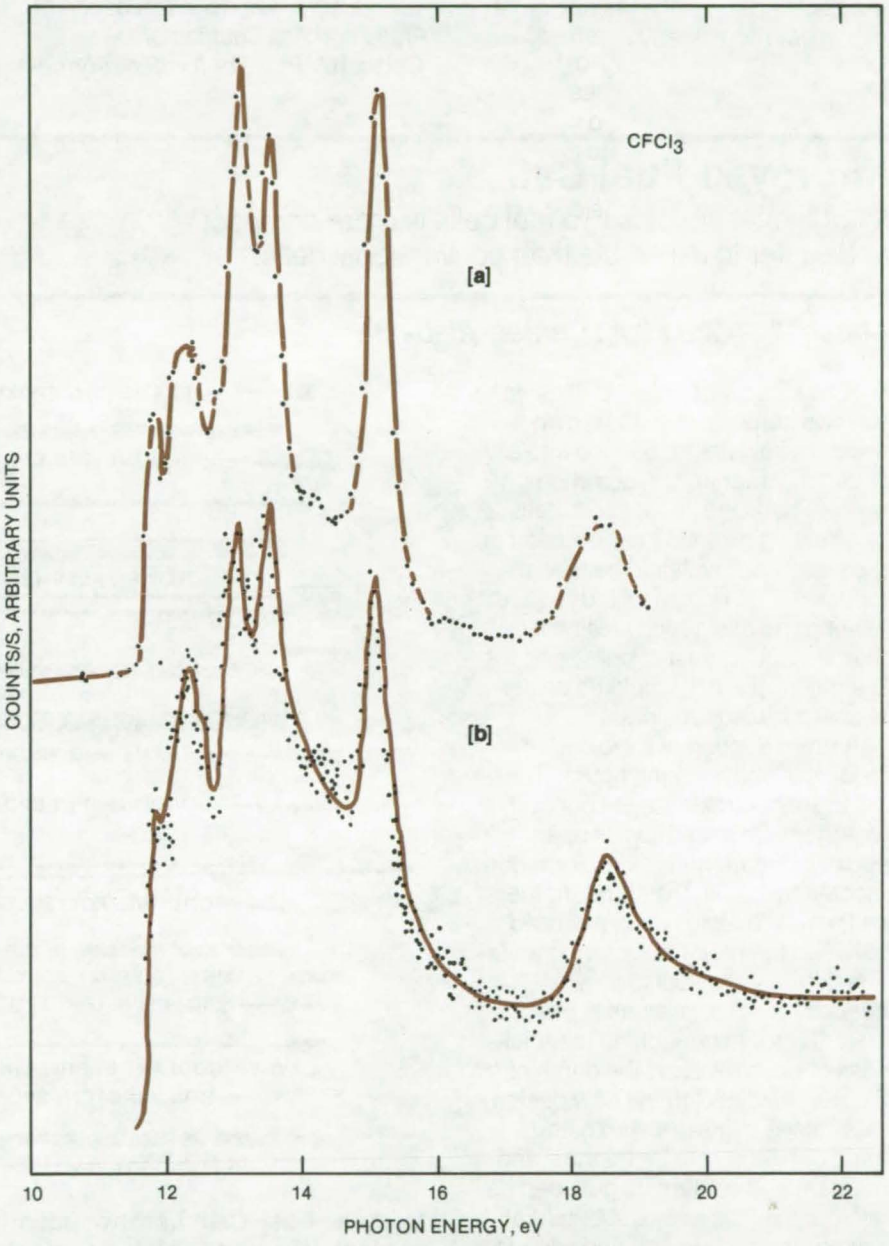

Threshold Photoelectrons are detected with high resolution, using a new technique that mixes a trapping gas with the species under study ($CFCl_3$). Zero-energy electrons attach themselves to the trapping gas molecules (in this case also $CFCl_3$), and the resulting negative ions are detected by mass spectrometry. Curve (a) was obtained, using the new technique; and curve (b), using conventional photoelectron spectroscopy.

(continued next page)

the dissociative attachment of threshold electrons. For comparison, the spectrum obtained, using conventional threshold-electron detection, is also shown. The signal-to-noise ratio is clearly improved with the new technique allowing weak structural features, such as the double peak in the vicinity of 12 eV, to be more clearly resolved.

Spectra taken on xenon and argon also show high resolution. For these atoms, high Rydberg-state features, not seen with conventional threshold-electron spectroscopy, were observed. The Rydberg structure arises as a result of collisional excitation by the trapping gas.

This work was done by Joseph M. Ajello and Ara Chutjian of **Caltech/JPL.** *For further information, Circle 28 on the TSP Request Card.*

This invention is owned by NASA, and a patent application has been filed. Inquiries concerning nonexclusive or exclusive license for its commercial development should be addressed to the Patent Counsel, NASA Resident Legal Office-JPL *[see page A8]**. Refer to NPO-14078.*

Improved Fuel Cell

Module that couples two fuel cells is more compact and easier to assemble than conventional cells.

Marshall Space Flight Center, Alabama

A new concept in fuel-cell design has two cells, each with its own reactant flow fields, bonded into a single modular unit. A common coolant passage serves both cells, and sealing gaskets are only used at the water-removal field between modules. The design would require fewer parts and occupy less space than conventional fuel cells; since it is simpler, the cell would be easier to assemble and maintain.

A cross section of a typical module is shown in the figure. The separate components are bonded together with single layers of an epoxy laminate material to form one module frame. In the standard fuel cell, stack layup gaskets are used between the major cell components. The depth of the seal grooves needed for these gaskets is often a major factor in controlling the thickness of each part and the depth of the flow fields. With the new design, most of the seals are eliminated; parts can therefore be thinner, and reactant and coolant heights can be minimized. This allows substantial savings in stack weight and volume and an overall reduction in costs.

Besides being easier to assemble, the new design would be less susceptible to leakage since it has fewer sealing surfaces. Indications from preliminary tests are that these cell modules could be used in advanced lightweight powerplants.

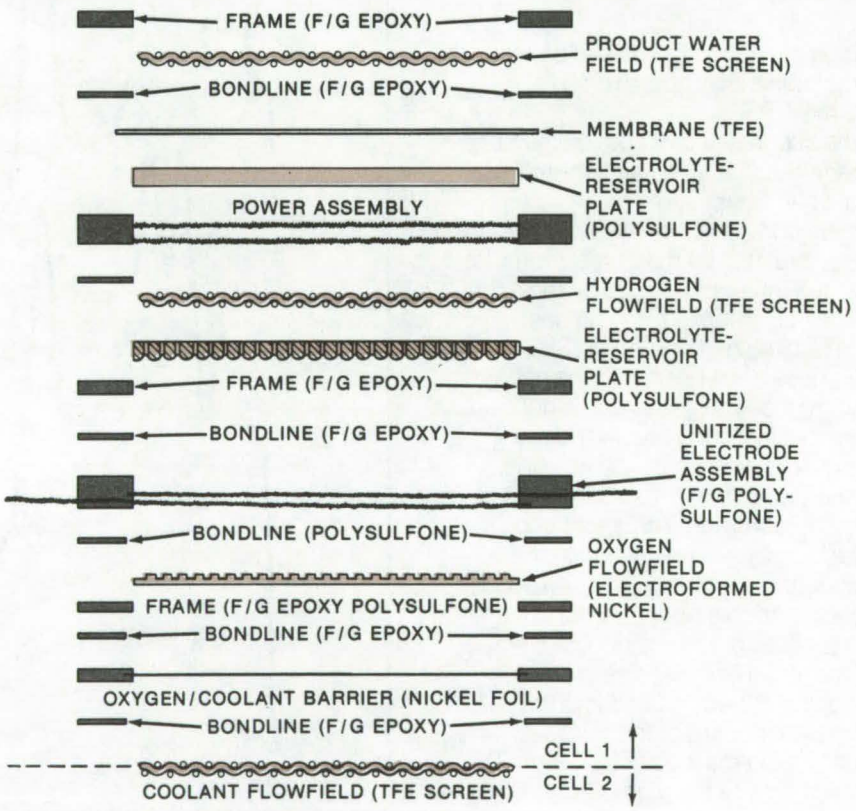

Modular Fuel Cell has two identical cells bonded around a common coolant flow field. Major components are joined by single layers of epoxy laminate material, so that gaskets and seal grooves are eliminated. (Components shown for cell 1 only.)

This work was done by William F. Bell and Nunziato J. Maio of United Technologies Corp. for **Marshall Space Flight Center.** *For further information, Circle 29 on the TSP Request Card.*

Inquiries concerning rights for the commercial use of this invention should be addressed to the Patent Counsel, Marshall Space Flight Center *[see page A8]**. Refer to MFS-23797.*

Negative Deuterium-Ion Source

Negative ions are formed by collisions with surfaces having a low work function.

Caltech/JPL, Pasadena, California

Most proposed controlled thermonuclear reactors (CTR's) require rapid heating and compression of the fuel. However, limits on present heating techniques and mass loss from the confined plasma necessitate the use of auxiliary heating methods. One promising approach has been to inject energetic neutral deuterium into the plasma after the initial compression. The neutral particles penetrate the magnetic fields and further heat the compressed plasma by collisional interaction.

Presently, the neutral beam is created through several steps. Positive deuterium ions are first formed in a gas discharge and then are electrically accelerated to the desired energy. The ion beam passes through a gas cell in which charge-exchange collisions convert the energetic ions to the energetic neutrals. Tens of amperes are readily produced by this method at a few tens of kilowatts, in millisecond-duration pulses. However, future demands of the CTR program will require beam energies of the order of 200 keV; at that level the charge-exchange cross section becomes very small, and neutralization efficiency becomes poor.

The neutralization efficiency is larger for negative ions than for positive ions, because the detachment cross section does not fall off with ion energy nearly as rapidly as the charge-exchange cross section. However, present methods for creating large quantities of negative ions (such as adding two electrons to low-energy positive ions) do not appear to offer the necessary efficiencies and production rates.

A new method that shows promise directly forms negative ions by surface ionization; an atom (or a molecule) strikes a surface of low work function, extracts an electron, and rebounds as a negative ion. By using a low work-function surface of coated porous material, a greater surface area is presented to the source gas, and ionization efficiency is improved.

(continued next page)

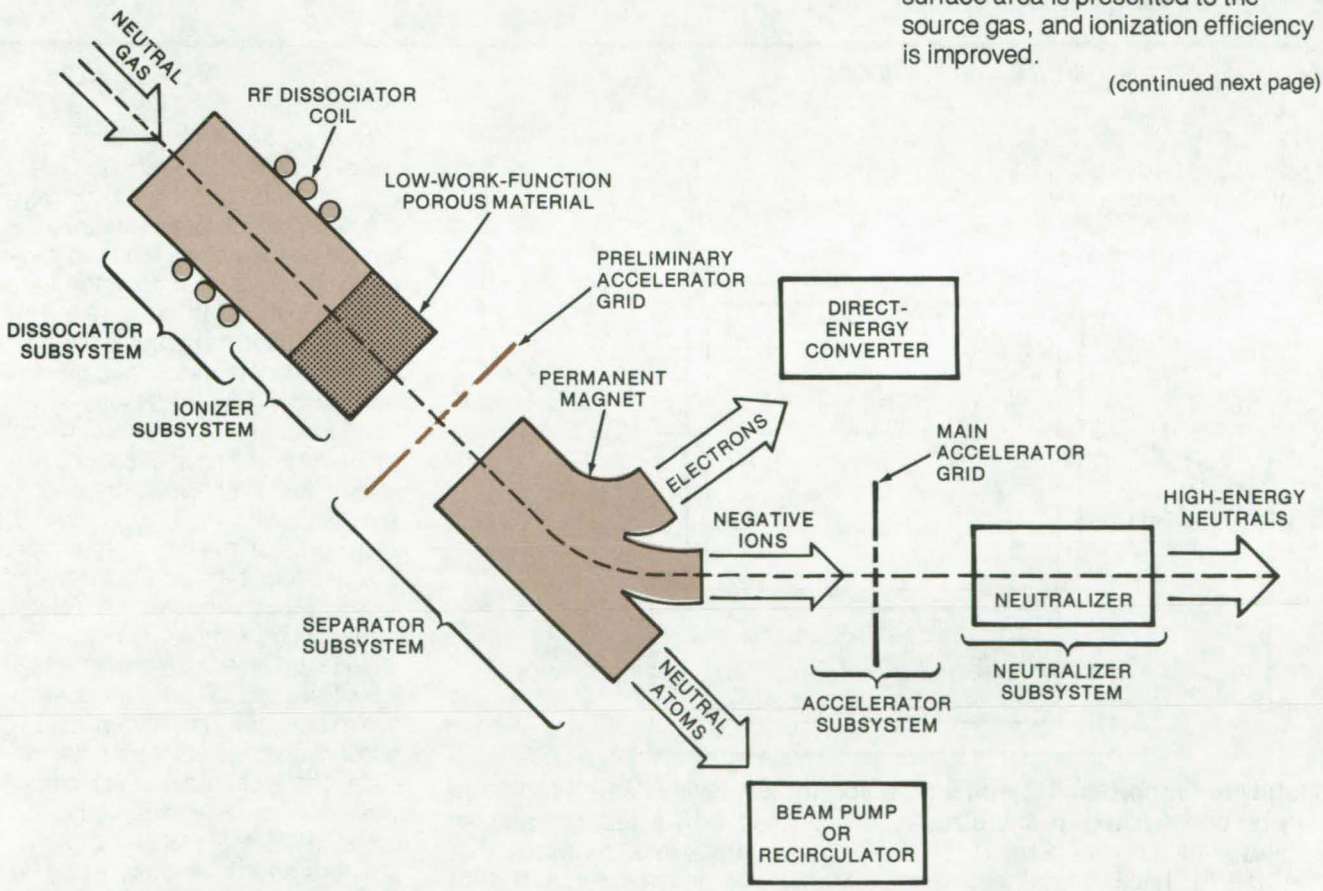

Proposed **Negative Deuterium-Ion Source,** shown here as part of a neutral beam generator for use with controlled thermonuclear reactors, uses a low work-function porous plug in the path of neutral deuterium atoms; the ions are generated by collisions between the atoms and the porous surface. A magnet is used to separate electrons (also generated in the ionizer) and neutral atoms from the negative ions.

A neutral-beam generator employing this approach is shown in the figure. It can be divided into five major subsystems: dissociator, ionizer, separator, accelerator, and neutralizer. The dissociator breaks down diatomic molecules of deuterium into the neutral atoms. It is located a short distance upstream of the ionizer. The actual dissociation takes place either by directing the flow around a heated filament in the flow tube or by an RF discharge created in a cavity in the line by coils or electrodes outside the line. The atomic deuterium flows through the ionizer, a porous plug of tungsten or activated-nickel base metal coated with a low work-function material, and collides with the porous surface.

A transparent accelerating grid and a permanent magnet are used to separate electrons (which are also emitted from the surface), the negative ions, and the neutral atoms. A series of grids focuses and collimates the ions and accelerates them to high energy. The neutralizer subsystem converts the negative ions back to neutrals for injection into the reactor.

Most metals have intrinsic work functions (the amount of energy necessary to remove an electron from the surface) between 4 and 5 eV. However, the work function can be decreased to less than 2 eV by absorbing a thin layer of an electropositive material, such as sodium, potassium, or cesium. Some photoemitter and thermionic-emitter materials have work functions lower than 1.5 eV.

The application of low work-function materials to the production of negative deuterium ions depends on whether the surface is compatible with deuterium gas at its operating temperatures.

This work was done by Raymond Goldstein and James E. Graf of **Caltech/JPL.** *For further information, Circle 30 on the TSP Request Card.*

This invention is owned by NASA, and a patent application has been filed. Inquiries concerning nonexclusive or exclusive license for its commercial development should be addressed to the Patent Counsel, NASA Resident Legal Office-JPL [*see page A8*]. *Refer to NPO-14113.*

Large-Area Radiation Counters for Low-Level Detection

Multiwire proportional counters monitor low beta- and X-radiation levels.

Marshall Space Flight Center, Alabama

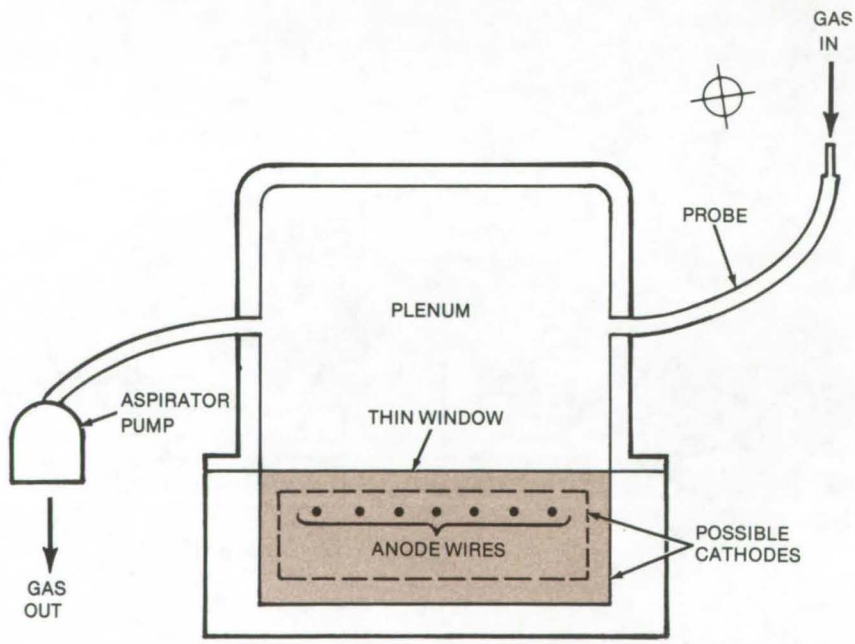

Multiwire Proportional Counter (in color) for low-level β- and X-radiation can be constructed in any size. When coupled with a plenum and an aspirator as shown here, it becomes a sensitive leak detector that "sniffs" for leaking radioactive gas. Multiplane arrangements further improve sensitivity.

Beta (β) and X-ray emitting nuclides may be detected with Geiger or scintillation counters. However, the sensitivity of Geiger counters is limited by their small size and inability to energy-discriminate. Large inorganic scintillators are relatively expensive and have high background counting rates, and plastic scintillators have low efficiency. Semiconductor scintillators, useful for many counting applications, are also limited in sensitivity by their small size.

In contrast, multiwire proportional counters can be made as large and as sensitive as needed. They also have good energy resolution. When used in multiplane arrangements, they can be made relatively insensitive to background and can select β- and X-radiation from a particular nuclide. The technology of these devices has now been adapted to the detection of low-level β- and X-ray emitters, such as in tracers and in leak-detection systems.

The basic multiwire proportional counter, seen in color in the lower portion of the figure, has an arrangement of parallel wires that form the anode. Two possible cathodes are shown. A thin metal-foil or plastic window lets low-energy β-particles enter the chamber. The multiwire technique allows large-area counters to be constructed. Also, since the proportional counters are relatively insensitive to gamma rays, background counting levels are low. This combination (large area, thin window, and insensitivity to background) produces a counter that is very sensitive to low-level β- and X-radiation.

By coupling the basic counter with a plenum above the thin window, and an aspirator to draw gas through a sniffer probe into the plenum, it is possible to construct a low-level detector useful in leak checking and other applications by using a radioactive gas such as krypton-85.

Multiplane, multiwire counters can also be constructed. The planes can be operated in coincidence or anticoincidence modes to optimize detector sensitivity to a particular β- or X-radiation. Absorbers placed between pairs of planes further improve selectivity.

This work was done by Thomas A. Parnell of **Marshall Space Flight Center** *and John C. Gregory of the University of Alabama. For further information, Circle 31 on the TSP Request Card.*
MFS-23304

Airborne Atmospheric Sampling System

Automated system is carried by commercial airlines on regular routes.

Lewis Research Center, Cleveland, Ohio

An airborne atmospheric sampling system economically monitors air quality on a worldwide basis. The system combines sensitive instruments for measuring air constituents with modern aircraft avionics and data-acquisition equipment in a reliable automated system. The system is installed on commercial 747 airliners and is operated during normal passenger service along established airline routes to provide global atmospheric sampling. The project is part of NASA's Global Atmospheric Sampling Program (GASP) with the objective to establish a global air-quality data base. This data base will help to determine whether emissions from jet aircraft and other pollution sources affect the Earth's upper atmosphere.

Air sample measurements include the concentration of gases, such as water vapor, ozone, carbon monoxide, oxides of nitrogens, and chlorofluoromethanes. The number density of particulates and the concentrations of sulfates and nitrates are also measured. In addition to air sample measurements, geographic information, meteorological conditions, and aircraft operational information are recorded and determine the location, and describe the conditions when an air sample is taken.

Existing commercial instruments used to detect carbon monoxide, oxides of nitrogen, and small particles were significantly modified to detect very low concentrations. Instrument sensitivity for carbon monoxide was extended from 400 parts per billion (PPB) to 20 PPB; for oxides of nitrogen, from 10 to 0.05 PPB; and for condensation nuclei, from 300 to 30 nuclei per cm^3. Also, an airline data-management unit was upgraded with a processor for system control. The unit has a bulit-in self-checking capability that helps to verify measurement accuracies and can also recognize certain major failures. In case of a major data-acquisition or system-control problem, a light goes on in the aircraft cockpit requesting the flight engineer to report the GASP system inoperative. Aircraft operations are no way affected by installation and operation of the system. Most data are recorded on magnetic tapes.

At altitude, data are acquired automatically at frequent intervals for ozone, water vapor, carbon monoxide, nitrogen oxide, and particulates. Chlorofluoromethane and other gaseous measurements are obtained by filling four 1-liter bottles at selected times during the flight.

In addition, filter paper is exposed to the atmosphere to obtain samples of sulfates and nitrates. The bottles and filter paper are later analyzed in the laboratory. Data are collected and analyzed every 2 weeks.

This automated atmospheric sampling system could also be used in remote areas for unmanned ground monitoring stations.

This work was done by Ted W. Nyland, Porter Perkins, and Marvin W. Tiefermann of **Lewis Research Center** *and Ulf Gustafsson of United Air Lines, Inc. Further information may be found in NASA TM-X-71790 [N75-31619], "An Automated Atmospheric Sampling System Operating on 747 Airliners," a copy of which may be obtained at cost from the New England Research Applications Center [see page A7].*
LEW-12949

High-Resolution X-Ray Recording and Processing

Two-step technique
resolves detail to 0.001 inch.

Langley Research Center, Hampton, Virginia

Since leads and some defects in microelectronic circuits, printed-circuit boards, and miniaturized components may be 0.001 inch (0.003 cm) or less in thickness, failure analysis often requires high photographic resolution. A new two-step technique for X-ray recording and processing shows detail down to 0.001 inch and resolves density variations to better than 0.2 percent. In contrast, conventional radiography techniques produce images that are resolvable only to 0.002 inch (0.005 cm) with 2 percent thickness resolutions.

The new exposure system uses a generator and a soft X-ray tube with a ¼-mm-thick beryllium window. The sample is placed on extremely-fine-grained photographic film, and a ½- to 4-hour exposure is made. The film is processed by hand, using a developer. The system creates a high-resolution and high-density latitude X-ray, which, however, is too wide ranged to be immediately useful.

The image is therefore projected onto a contrast process film that is processed in a developer. Exposure and development are chosen to produce a high-contrast magnified image with midrange tones in the area of interest. This internegative is printed on photographic paper, using conventional methods, to produce a magnified image similar to the original X-ray but with better spatial resolution and contrast.

This work was done by Thomas L. Tedrow and Alvin A. Weathers of Martin Marietta Corp. for **Langley Research Center.** *For further information, Circle 32 on the TSP Request Card.*
LAR-11722

Materials

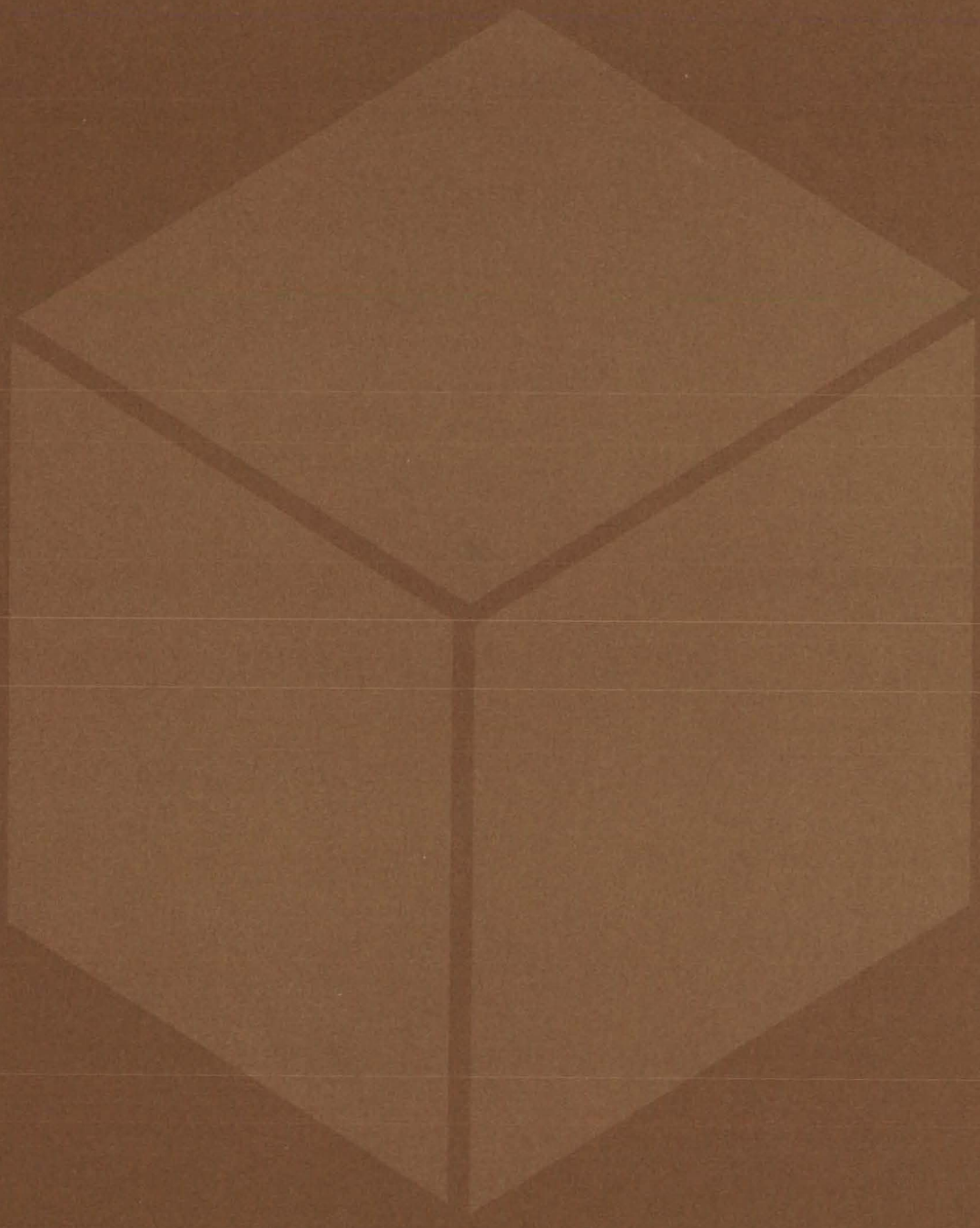

Hardware, Techniques, and Processes

Books and Reports

Screw-Extruded Coal

Versatile technique makes coal more combustible and aids in desulfurization.

Caltech/JPL, Pasadena, California

Coal, the most abundant of fossil fuels, can be made more convenient to use with the aid of screw-extrusion techniques. In one application, a screw extruder (see figure) can feed coal to a furnace operating at near-ambient pressure. Crushed coal is supplied to the hopper. The screw compresses and plasticizes the coal at a pressure of 2,000 to 12,000 psi (14×10^6 to 83×10^6 N/m^2) as it is heated to 734° to 914° F (390° to 490° C). The coal is forced through a die, and as it exits, volatile components abruptly flash off. The devolatilizing coal continuously disintegrates into a fine powder and vapor — a highly combustible combination.

Any mixture of coal sizes that will fit into the screw can be used. A screen over the hopper excludes pieces that are too large. The die shape and the direction of extrusion can be designed to suit the furnace. If a long combustion zone is needed, the coal jet can be extruded roughly parallel to the air jet entering the furnace; or, many orifices can extrude the coal radially and tangentially to promote mixing.

The same principle can be used to pyrolyze coal — that is, to convert coal into char, oil, and gases. These products, instead of being burned as they emerge from the screw extruder, are collected separately for use as chemicals or fuel. If the extrusion rate, extrusion temperature, temperature gradient, die and orifice size and shape, and receiving-chamber pressure and temperature are regulated to suit that particular coal, the coal can be devolatilized to any degree.

Because screw extrusion ejects coal at very high pressure, high-pressure reactions can be carried out in the post-extrusion chamber under conditions of high shear.

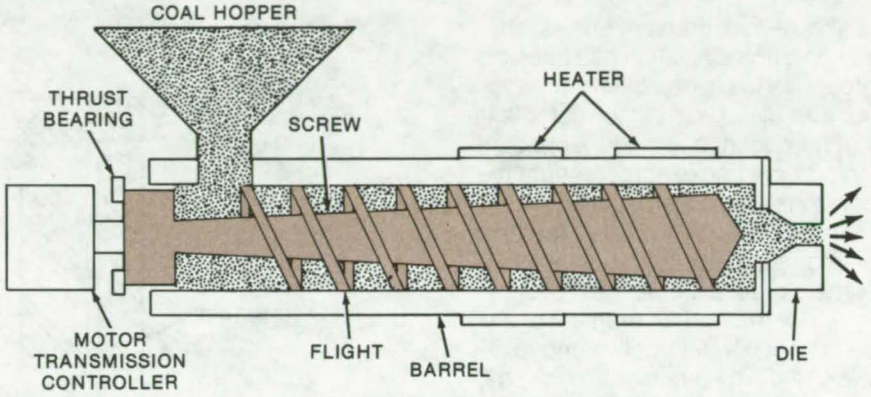

A Screw Extruder Conveys Crushed Coal to a hot, intense-pressure region and ejects it through a die as a fine spray. The spray can be directed at an oxidizer for gasification or directed into a furnace for burning. If the coal is mixed with water in the extruder in the presence of catalysts, liquefaction and desulfurization occur; if it is mixed with powdered metallic ore and fluxing materials, the spray can be used for the continuous reduction of ores.

Pressures approaching 12,000 psi (83×10^6 N/m^2) are possible — far higher than the 300 to 400 psi (2.06×10^6 to 2.76×10^6 N/m^2) possible with conventional pressurized coal systems, such as lock hoppers.

These high pressures and high shear rates may liquefy and desulfurize coal. The coal is screw-extruded into a vessel where temperature and pressure are above the critical points for water — 3,200 psi (22.4×10^6 N/m^2) and 707° F (374° C). Water containing a catalyst (sodium or potassium salts) is pumped into the die. The supercritical water and the coal react. Hydrogen in the water combines with sulfur in the coal, forming hydrogen sulfide gas and upgrading the coal. Both hydrogen and oxygen combine with the carbon, forming various organic gases and liquids. Freshly mined coal can be liquefied while still in the mine, pumped to the surface, and distributed as a liquid.

A similar process can be used to gasify coal. The screw-extruded coal impinges on jets of oxidizer — liquid or gaseous air or oxygen or liquid N_2O_4. Synthesis gas or low-Btu gas results. Reaction time is much shorter than in conventional gasifiers, and reaction volume (and equipment) is much smaller.

In yet another application of screw extrusion, ore is reduced. Ore, coal, and flux are mixed in the extruder and are ejected as a jet of fluid that impinges on a jet of liquid or gaseous oxygen. Reaction occurs immediately. Molten metal and slag form and are collected separately.

This work was done by Porter R. Ryason of **Caltech/JPL.** *For further information, Circle 33 on the TSP Request Card.*

Inquiries concerning rights for the commercial use of this invention should be addressed to the Patent Counsel, NASA Pasadena Office-JPL [see page A8]. Refer to NPO-13769.

Whole-Rock Uranium Analysis by Fission-Track Activation

The concentration of uranium in rock samples is measured rapidly and nondestructively.

Caltech/JPL, Pasadena, California

Whole-rock uranium analysis by fission-track activation has been approached in several different ways, such as by powdering the sample into a homogeneous mixture or counting particle tracks at representative positions on a passive dielectric track detector. While these methods are sound, they either destroy the sample or take a great deal of time.

A new method for uranium analysis is both nondestructive and relatively fast. The technique involves simultaneous irradiation of an unknown rock sample, a standard sample, and mica detectors in a special vacuum assembly. By maintaining a relatively large separation between the rock sample and its detector (compared with the scale of sample nonuniformity), the integrated track density in the detector represents the whole-rock uranium concentration.

As seen in the accompanying figure, a long tube holds the samples, detectors, glass standards, and spacers for irradiation. The entire assembly is placed in a reactor. To avoid material activation and to reduce track background, fused quartz is used for the spacers, and nylon is used for the vacuum tube and caps. The spacers are notched at both ends to allow air to pass during evacuation.

The bottom end of this vacuum-tube assembly has a screwcap O-ring seal; the top is a sliding plug that maintains the compression placed on the samples and detectors during irradiation. The sliding plug is guided by nylon screws attached to the vacuum tube body. The detector material is very-low-uranium mica that has been etched to remove residual tracks.

The assembly may be evacuated before irradiation and sealed off by crimping or by valving. However, it is normally pumped during irradiation by a small forepump, a dry-ice trap, and a length of medium-diameter

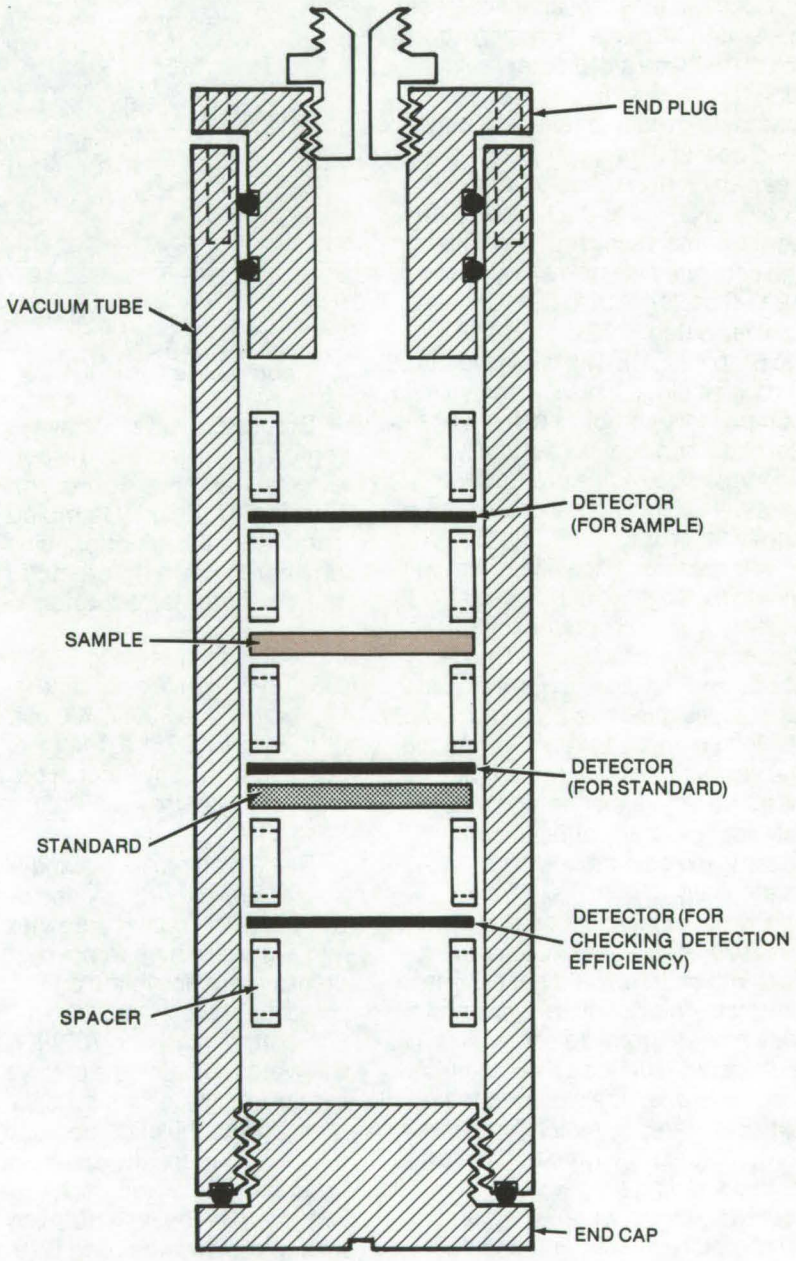

Whole-Rock Uranium Analysis is accomplished nondestructively and relatively fast by this vacuum assembly. An unknown sample rock separated from its detector and a standard sample adjacent to its detector are simultaneously irradiated with neutrons in a reactor. If the standoff distance between the unknown and its detector is large compared with the scale of the sample nonuniformity, then the detector track density accurately represents the whole-rock uranium concentration.

aluminum tubing. Any vacuum below 10^{-3} torr is sufficient. It is monitored by a thermocouple gage near the trap and outside the reactor.

Samples are prepared as thin sections on 2.5-cm-diameter fused quartz disks. In cases where the rock section does not cover the entire area of the disk, an annular mask cut from mica is placed on the sample to expose only the small rock section; geometric factors are then adjusted for the reduced sample diameter.

After exposure, the vacuum tube is disassembled, and the radioactivity is allowed to decay. The detectors are etched with hydrofluoric acid for 5 to 20 minutes to render the tracks visible. They are viewed under a light microscope, and the tracks are counted over the area.

The uranium concentration of the unknown sample is calculated from the known uranium concentration in the standard, and the measured track densities. Detectors for the standard density are in direct contact with the glass standards.

The ratio of the effective fission fragment ranges, which depends on the relative compositions of sample and standard, rarely deviates from unity by more than a few percent for silicate rocks. The efficiency of detection is the product of the ideal detection efficiency and a correction factor used when large detection areas must be scanned.

This work was done by Eldon L. Haines and James R. Weiss of **Caltech/JPL.** *For further information, Circle 34 on the TSP Request Card.*
NPO-13483

Metal/Polyvinyl Pyridine Catalytic Beads

Microspheres with controlled properties form a family of effective catalysts.

Caltech/JPL, Pasadena, California

Tailormade microspheres of polyvinyl pyridine (PVP) and copolymers of PVP with other monomers can be complexed with metallic salts, then exposed to reducing agents to form a metallic outer layer on fine beads of the organic base. Since the porosity and surface area of the beads can be controlled precisely and the amount of complexing can be determined beforehand, the process can produce a wide range of catalytic materials.

In one application, chloroplatinic acid was added to 2,000-Å (diameter) microspheres of PVP; the mixture was then reduced with sodium borohydride. The precipitated solid beads containing free platinum metal were used as a catalyst to hydrogenate 1-hexene. Yields of 100 percent were obtained at room temperature and ambient pressure.

The PVP microspheres are prepared by cobalt γ-irradiation of homogeneous aqueous solutions of PVP and specific cross-linking agents. The porosity of the material increases with the concentration of the cross-linking agents. By using low concentrations of monomer, diameters less than 100 Å can be obtained. Irradiation in the presence of methanol yields larger microspheres.

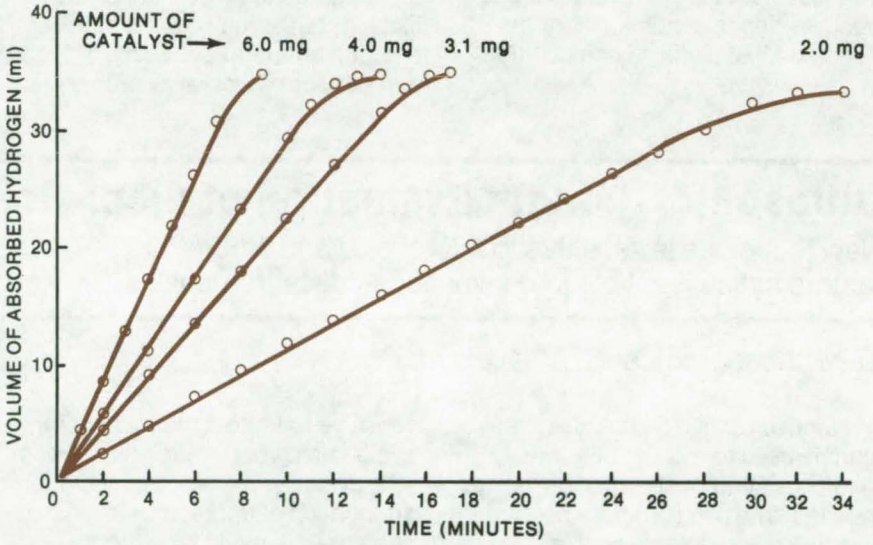

Catalytic Beads of Polyvinyl Pyridine speed the hydrogenation of 1-hexene. In each case the reaction proceeds to 100 percent yield at ambient temperature and pressure. The rate of hydrogenation increases in proportion to the amount of catalyst.

The effectiveness of the beads in the hydrogenation of 1-hexene is illustrated in the figure. Yields were 100 percent in all cases; however, the reaction rate increased as more catalyst was added. The platinum content of the microspheres was approximately 20 percent w/v.

This work was done by Alan Rembaum and Willi Volksen of **Caltech/JPL.** *For further information, Circle 35 on the TSP Request Card.*

Inquiries concerning rights for the commercial use of this invention should be addressed to the Patent Counsel, NASA Pasadena Office-JPL [see page A8]. Refer to NPO-13912.

Homogeneous Eutectic of Pb-Sb

An elusive superplastic
is formed for the first time.

Marshall Space Flight Center, Alabama

The eutectic of Pb-Sb is expected to be a superplastic material that can be used in the formation of shaped charge liners for industrial-explosive metal-forming processes and other applications. Until now, efforts to solidify Pb-Sb eutectic with the expected plasticity and desired average density have not met with success. Although portions of a melt do solidify into a chinese eutectic structure of the proper composition (88.8 percent Pb), invariably there is also some segregation that appears to be primary crystallization. It has been speculated that this occurs because the eutectic tends to supercool, setting up a nonequilibrium condition that shifts its composition.

A new study of the solidification of eutectic Pb-Sb has found that this interpretation of the segregation process is not correct. Microstructures of eutectic, hypoeutectic, and hypereutectic alloys of Pb-Sb were studied after solidification in both "microgravity" and at 1 g. In all cases, the apparent primary crystallization product formed in the solidified material. Centrifuge experiments were conducted to determine the temperature at which these components formed. The experiments conclusively showed that the system forms a "divorced eutectic" that appears to be primary crystallization, but actually forms at the eutectic temperature. Some of the eutectic forms as blocky primary Sb surrounded by eutectic rich in Pb dendrites.

This secondary eutectic phase can be removed by applying a high centrifugal field (1,000 g's) during solidification. The field sweeps the Pb dendrites one way and the primary Sb blocks the other way. A homogeneous spheroidal eutectic is observed when the resulting material solidifies. This material is free of the blocky primary Sb and Pb dendrites that have characterized all previous attemps to form a complete Pb-Sb eutectic.

This work was done by John M. Winter, Jr., of Marvalaud, Inc., for **Marshall Space Flight Center.** *For further information, Circle 36 on the TSP Request Card.*
MFS-23766

Ultrasonic Strength Evaluation of Fiber-Reinforced Composites

New technique is sensitive to microvoids and other
factors not susceptible to conventional measurements.

Lewis Research Center, Cleveland, Ohio

Nondestructive techniques that can be used to evaluate fiber-reinforced composite structures are needed. The problem goes beyond simply finding defects such as delaminations, inclusions, and similar discontinuities. Composites can often be free of overt defects yet still have inadequate strength. These inadequacies may result from poor processing during fabrication or from degradation during use. Lower-than-acceptable strength can, for example, result from microvoids distributed throughout the composite structure. Currently, nondestructive evaluation can find overt discontinuities or gross damage, but better techniques are needed to evaluate the actual strength and endurance properties of composite materials. These new techniques must be sensitive to factors that cannot be evaluated by conventional methods.

Previously, measurement of the attenuation of ultrasonic waves had been used to evaluate strength-related factors in various materials. The method described herein has capabilities that are not available in current ultrasonic methods for evaluating composites. The prime advantage is that a single number produced correlates closely with the strength properties of the composite. Also, the method requires access to only one side of a part, an important advantage when only one surface is readily accessible.

The principle involves the introduction of simulated stress waves in a composite structure. These stress waves are ultrasonic and resemble the resonant waves that would occur from microfractures if the material were to undergo a destructive test, but they cause no damage. However, as the simulated stress waves propagate through the material, their character is strongly affected by the same factors that influence strength properties. After they have propagated a fixed distance through the material, the stress waves are analyzed. One result of analysis is a single numerical value, called "stress-wave factor," that relates to variations in physical properties of the test specimen and thus to strength characteristics such as interlaminar shear strength. This number is a relative value; but by calibrating against a similar object with a known strength, the actual strength of the test object can be stated. The simulated stress waves

can be introduced in a variety of ways, and appropriate modes of analysis can reveal different strength properties.

The apparatus and its method of operation are shown in the figure. A transducer, coupled to the test object by a fluid, repeatedly injects ultrasonic waves into the test object. The transducer in this illustration contains a piezoelectric crystal that is driven by an ultrasonic pulser; frequency and amplitude of the generated waves are constant. These waves are repeatedly injected at a repetition rate controlled by a continuous-wave oscillator. The center frequency of the input ultrasonic transducer is selected to optimize the response of the test object to the input wavelength; i.e., to achieve a resonance or near-resonance condition. Consequently, the test object experiences a continuously repeating series of simulated acoustic emissions emanating from one place on the object and resembling the stress-wave "bursts" that accompany microfractures in a material under stress.

A waveguide pickup is coupled to the surface of the test object at some fixed distance from the input source. A component of the simulated stress wave is transmitted to a receiving transducer at the end of the waveguide. The bandwidth sensitivity of the receiving transducer is selected for optimum response in the frequency domain of the simulated stress wave. Waves arriving at the receiver location are attenuated and dispersed. At the receiver pickup, the amplitude and decay mode are proportional to the energy loss suffered by the wave after having propagated through the test object. The received wave, as modulated by the material, relates to the strength of the material between the input and output probes.

The apparatus shown in the figure provides a simple and effective means of measuring the energy content of the received signals. The method is to count the number of oscillations that exceed a preselected background or threshold (voltage) level after amplification by an appropriate factor. The continuous-wave oscillator and reset clock are adjusted so that a particular number of bursts and their contained oscillations are counted. The totalizer sends signals for digital display. The display indicates the burst energy indirectly by showing a number that is proportional to the number of oscillations above the threshold level per burst. Keeping the relative positions of the input and output probes fixed, one moves the test object (say to the left or right). Any variation in the acoustic propagation properties of the test object becomes apparent in the new data.

Tests made with graphite-fiber composite panel specimens produced strong correlations between the stress-wave energy measurements obtained in the above way and interlaminar shear strength measured directly in destruction.

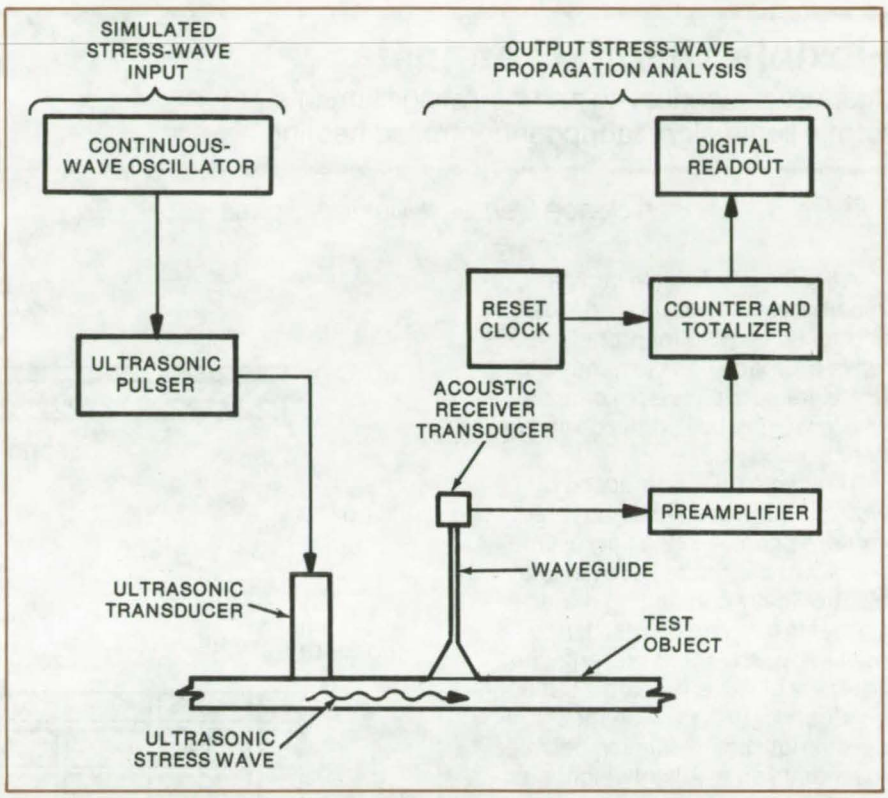

Ultrasonic Test of Composite Strength measures the attenuation of an acoustic signal traveling through a test specimen. The pulsed signal simulates stress-wave bursts that accompany microfracturing in composites under stress. The attenuated pulse is sensed, and the number of oscillations above a threshold are counted. The method is comparative. With the same transducer configuration, the specimen could be moved past the transducers so that variation in output count would indicate a change in propagation properties (and strength).

This work was done by Alex Vary of **Lewis Research Center.** *Further information may be found in NASA TM-X-73646 [N77-23210], "Ultrasonic Evaluation of the Strength of Unidirectional Graphite-Polyimide Composites," a copy of which may be obtained at cost from the New England Research Application Center* [see page A7].

Inquiries concerning rights for the commercial use of this invention should be addressed to the Patent Counsel, Lewis Research Center [see page A8]. *Refer to LEW-12769.*

Flexible Thermal Laminate

Interwoven conducting and insulating filaments form a lightweight fabric for controlled heating.

Lyndon B. Johnson Space Center, Houston, Texas

A lightweight flexible laminate, originally designed to provide localized controlled heating for propellant tanks on space vehicles, may be useful for nonspace applications where weight, bulk, or flexibility are critical concerns.

The laminate is composed of woven or unwoven cross-layered yarns, as shown in the figure. One set of yarns is made from flexible electronically-conducting metal filaments that can be resistance-heated by an electric current. The other set of yarns is flexible but nonconducting; they provide mechanical strength and insulation between the metal yarns. A lightweight electrically-nonconductive plastic film (such as a polyimide) is bonded to the woven fabric for additional strength and to prevent conductive heat loss in nonvacuum applications. A metallic film (such as aluminum, silver, or gold) is deposited on the outside of the nonconducting film for a more uniform distribution of heat load.

The weave can be spaced from 0.1 to 1 cm. A typical metal yarn would be composed of 19 percent Cr, 75 percent Ni, and 4 percent Al in a 12-denier (0.012-mm-diameter) continuous filament, with 91 filaments per yarn in a 3z-ply construction. The plastic film could be 0.012 mm in thickness.

When the laminate is not woven, the metal yarns are placed on the film first, and the nonconductive yarns are placed over the metal yarns. Both layers can be bonded to the base film.

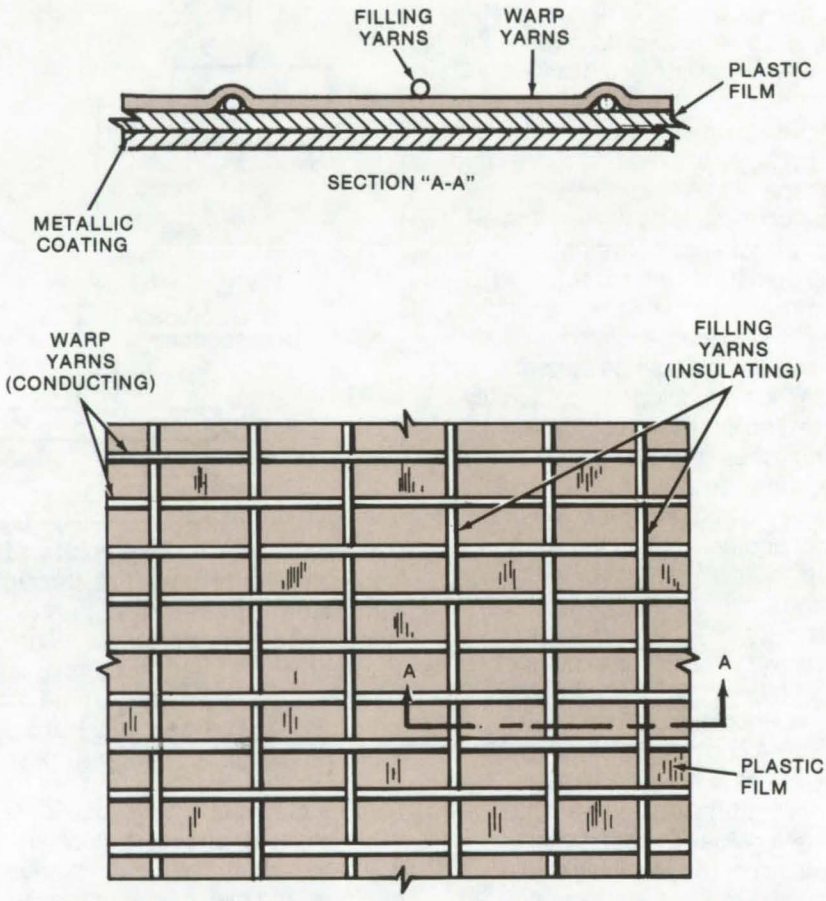

Lightweight Thermal-Control Material is a fabric of cross-layered yarns. The warp yarns are composed of electrically-conducting metal filaments or fibers that can be resistance heated by the application of current. The filling strands are electrically-nonconductive multifilament yarns that provide strength. The plastic film prevents convective heat loss in nonvacuum applications; the metallic film provides a uniform heat load.

This work was done by Frederic S. Dawn and Dale G. Sauers of **Johnson Space Center.** *No further documentation is available.*

This invention is owned by NASA, and a patent application has been filed. Inquiries concerning license for its commercial development should be addressed to the Patent Counsel, Johnson Space Center [*see page A8*]. *Refer to MSC-12662.*

Controlled-Porosity Composite Materials

Porosity is controlled by stitching and later removal of "fugitive" fibers.

Langley Research Center, Hampton, Virginia

A family of lightweight, porous materials can be fabricated by using a new "fugitive-fiber" process. Originally developed to produce lightweight panels for aircraft laminar-flow control systems, the process will allow a wide range of controlled-porosity materials to be manufactured at low cost.

The materials are prepared by stitching fibers (such as nylon, acetate rayon, polyethylene, or polypropylene) through an uncured sheet of graphite-reinforced epoxy prepreg or other composite, then curing the composite, and subsequently removing the fibers by an appropriate method. Nylon, for example, can be leached from the laminate by boiling in 5 percent hydrochloric acid. The degree of porosity can be controlled by the fugitive-fiber diameter and by the density of the stitches (per unit area). The stitching can be done by hand, on a conventional sewing machine or carpet-tufting equipment, or by any other economical method.

The graphite/epoxy prepreg is formed in sheets and is cut into lamina of the correct size and shape. The layers are stacked and encased in Teflon separator sheets 0.5 to 1 mil (0.01 to 0.03 mm) thick. In early tests, this composite was left with a rough surface due to stitched-fiber impressions remaining in the lamina. Therefore, lined polyester-film sheets 8 mils (0.2 mm) in thickness were used to encase the layup; this considerably reduced the stitched-fiber markoff.

Other techniques for obtaining a smooth surface are being explored. One promising method is to abrade excess resin mechanically from the face surface on the side from which the needlepoint exits. As the stitching needle enters the layup, a chamfer is formed; then, as the needlepoint exits from the opposite side, a burr that remains after curing is raised. Smooth surfaces can be produced by abrading this burr.

The technique was found to work well with graphite/epoxy fabric as the base material. Two types of monofilament nylon stitching were tested: fishing lines, rated from 2 through 8 pounds (8.9 through 35.6 newtons) and a 10-mil (0.25-mm) nylon monofilament supplied directly from the manufacturer. Those fibers less than 8 mils (0.2 mm) were found difficult to dissolve.

This work was done by R. T. Beall and A. O. Kays of Lockheed Aircraft Co. for **Langley Research Center.** *No further documentation is available.*

Inquiries concerning rights for the commercial use of this invention should be addressed to the Patent Counsel, Langley Research Center [see page A8]. Refer to LAR-12115.

Welding Thermocouples to Columbium

A new study finds that thermocouples can be attached to columbium metal with high reliability by using titanium weld rod. Several thermocouple materials were tested, and a simple welding procedure was developed. The attachments are strong, durable, and reliable at temperatures up to 4,000° F.
(See page 549.)

Airborne Atmospheric Sampling System

An airborne atmospheric sampling system economically monitors air quality on a worldwide basis. Existing commercial sampling instruments were modified to detect very low concentrations of air constituents, including particulates. The system, which can also be used in unmanned ground monitoring stations, is installed on commercial airliners and is operated during normal passenger service.
(See page 477.)

Large-Area Radiation Counters for Low-Level Detection

Large-area proportional counters are ideal for detecting low-level β- and X-ray emitting nuclides in many applications. The counters can be coupled to a plenum for monitoring tracers and leak checking, and they can be constructed in multiplane arrangements for coincidence and anticoincidence detection of specific nuclides. They are also relatively insensitive to background gamma-ray levels.
(See page 476.)

Improved Silicone-Rubber-to-Silicone-Rubber Bonding

Strongest bonds result when the precured rubber is lightly abraded and left unprimed.

Lyndon B. Johnson Space Center, Houston, Texas

The standard procedure for bonding room-temperature-vulcanizing silicon rubber to itself is to apply a freshly-mixed silicone rubber onto a precured rubber, with a layer of silicone primer applied first. Although this has appeared to give a satisfactory bond, a new investigation indicates that the bond strength can be increased if the primer is eliminated and the surface is lightly abraded.

In a test of this procedure, an aluminum flatwise tensile block was primed and silicone rubber was applied and allowed to cure at room temperature for a minimum of 72 hours. Silicone primer was then applied to the cured silicone rubber and to the surface of a matching aluminum flatwise tensile block. Finally, freshly-prepared silicone rubber was applied to both surfaces of matching blocks. Test specimens without the primer between the rubber-to-rubber interface were fabricated by applying silicone rubber directly to the precured surface.

As the Test I data in the table indicate, the unprimed specimens had considerably higher bond strengths than the primed specimens. The unprimed samples exhibited approximately 30 to 40 percent adhesive failure at the bond interface as evidenced by glassy unbonded areas.

Test I - Silicone-Rubber Surface Not Abraded			
Cured, Not Primed		Cured and Primed	
Specimen	Load (PSI)	Specimen	Load (PSI)
1	325	1	137
2	355	2	196
3	336	3	176
4	136	4	181
	339 (Average)		173 (Average)
30% to 40% Unbonded Area in Rubber-to-Rubber Joint		All Failures in Primed Surface	

Test II - Silicone-Rubber Surface Abraded			
Cured, Not Primed		Cured and Primed	
Specimen	Load (PSI)	Specimen	Load (PSI)
1	375	1	195
2	379	2	190
3	363	3	220
4	348	4	207
	366 (Average)		203 (Average)
90% to 100% Cohesive Failure in Rubber-to-Rubber Joint 0% to 10% Adhesive Failure in Rubber-to-Primed Aluminum Interface		All Failures in Primed Surface	

Flatwise Tensile Data indicate that stronger silicone-rubber-to-silicone-rubber bonds result if the cured rubber is left unprimed (Tests I and II). Bond strength is further enhanced if the surface is lightly abraded (Test II).

A second series of tests, identical to the first except that the precured surfaces were abraded lightly to remove the gloss, produced similar results, as shown in the Test II data. Furthermore, bond strengths for the abraded specimens were consistently higher than for the unabraded specimens, as evidenced by a reduction in the adhesive failure rate to between zero and 10 percent.

The tests indicate that the silicone primer between the rubber-to-rubber bond hinders the bond joint, resulting in a substantially lower bond strength.

This work was done by Kuniyoshi Teramura of Rockwell International Corp. for **Johnson Space Center.** *No further documentation is available.*
MSC-16419

Debonding Agent for Silicone-Rubber Adhesive

Commercially available cleaner is a chemical solvent for adhesive bonds.

Lyndon B. Johnson Space Center, Houston, Texas

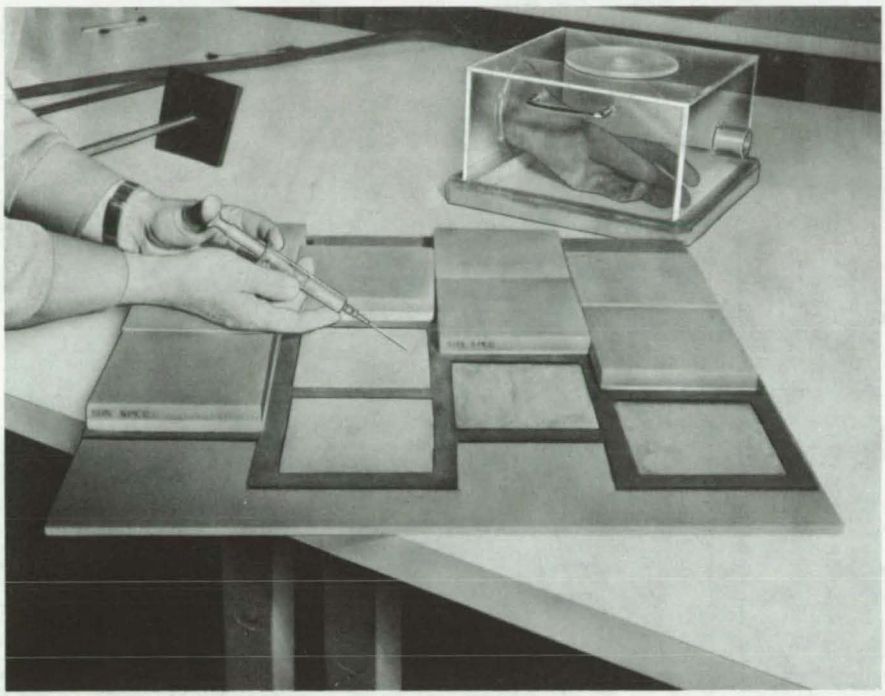

[a]

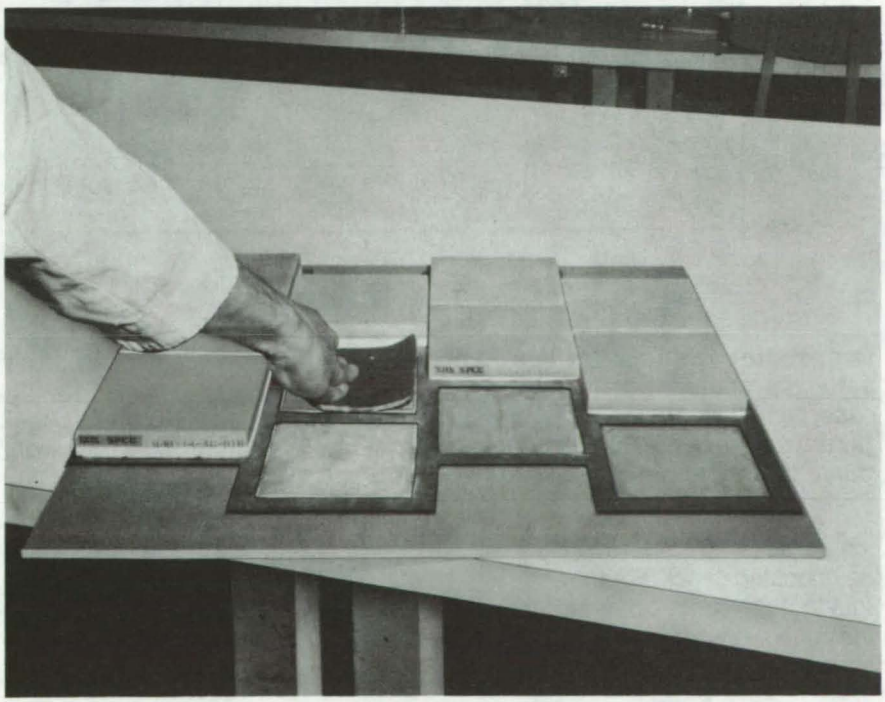

[b]

Solvent Is Injected (a) in controlled amounts along the silicone-rubber adhesive bond line. This felt tile-support pad was debonded within a few minutes, allowing it to be removed manually as shown in (b).

A chemical solvent for silicone-rubber adhesive can break down adhesive bonds without damaging surrounding materials. The solvent, a commercially available blend of methylene chloride in saturated trichlorotrifluoroethane, is widely used in industry for vapor-degreasing and cold-cleaning procedures; it has a natural reactivity with silicone elastomers that is utilized in the debonding procedure.

Conventional chemical solvents often cannot be used to remove bonded components selectively, since the solvents tend to "wick" into surrounding areas by capillary action. Nearby materials can be damaged by this process. Since this solvent has an exceptionally-high room-temperature evaporation rate, wicking is not a serious problem. In addition, the solvent has other desirable properties such as nontoxicity and low viscosity.

In one application, the solvent was used to remove adhesive-bonded felt tile-support pads prior to the installation of replacement tiles. As shown in the figure (a), controlled amounts of solvent are applied with a hypodermic needle to selected areas along the adhesive bond line. The injection points are kept away from the edges of the felt pad to insure further that wicking is not a problem. The chemical action of the solvent degrades the bond and allows the pad to be removed within a few minutes without extensive scraping and without damaging the surrounding tiles.

This work was done by Jack W. Holt and Kuniyoshi Teramura of Rockwell International Corp. for **Johnson Space Center.** *No further documentation is available.*

Inquiries concerning rights for the commercial use of this invention should be addressed to the Patent Counsel, Johnson Space Center *[see page A8].* *Refer to MSC-16933.*

Metallic Coating Reduces Thermal Stress

Plated layer can prevent structural overloads in high-temperature/high-strength materials.

Lyndon B. Johnson Space Center, Houston, Texas

Thermal stress in high-temperature/high-strength materials can be substantially reduced by adding a metallic outer layer that has high thermal conductivity. The layer (silver or copper, for example) is deposited by standard plating processes. The technique can help to prevent structural overloading in turbine blades, heat exchangers, powerplant parts, and other applications where a combination of high temperature and low conductivity can cause large deflections and thermal stress. The layer is applied easily and is inexpensive when compared with other methods, such as adding a thermal-control system or increasing the thickness of the parts.

The effectiveness of the technique is illustrated in the figure, which shows temperature-versus-time curves measured for a heated section of a wing panel for the Space Shuttle Orbiter. The panel is fabricated from an iron/nickel-alloy honeycomb that is closed out by iron/nickel beams. During reentry, these panels can experience a maximum heating rate of 3.8 Btu/ft²-s (1.03 cal/cm²-s), which produces temperatures near 1,300° F (704° C). The conductivity of the alloy is relatively low [12 Btu/h-°F-ft (0.004 cal/s-°C-cm)], and this causes a buildup of localized hotspots.

The figure shows heating curves extracted from two temperature sensors; the dashed curve is for the uncoated panel, and the solid curve is for the panel coated with a silver overlay 10 mils (0.025 cm) in thickness. The silver plate reduces the maximum temperature differential to approximately 210° F (98.9° C) as compared to 1,145° F (618° C) for the uncoated panel. For the Space Shuttle, this reduces thermal stress and deflections for the expected loading conditions to acceptable levels.

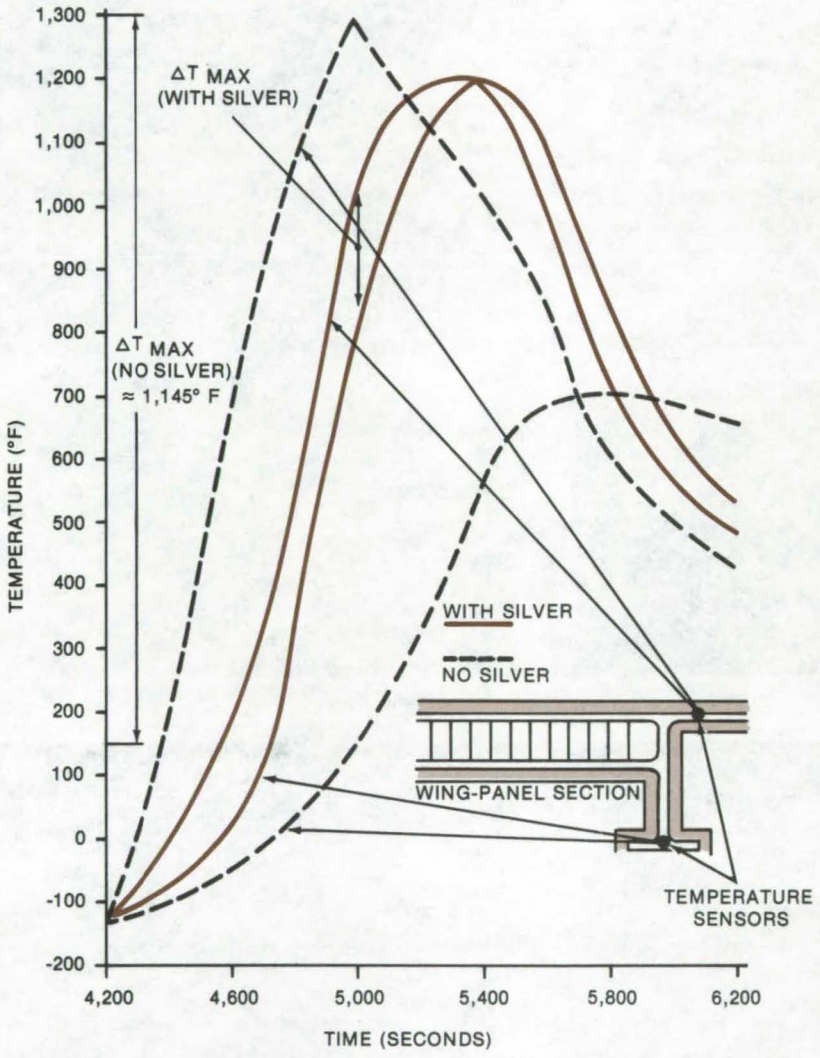

Temperature Differentials Are Reduced by a factor of 5.5 if structural parts are coated with a thin layer of high-conductivity metal. In this case, an iron/nickel-alloy honeycomb wing-panel section has been plated with silver. The dashed curve is for the unplated panel; the solid curve is for the plated panel.

This work was done by R. D. Morgan of Rockwell International Corp. for **Johnson Space Center.** *No further documentation is available.*
MSC-16814

Thermal-Control Coatings for Fabrics

High-emissivity spray-painted coatings remain flexible from -180° to 400° F.

Langley Research Center, Hampton, Virginia

A thermal-control coating for fabrics exposed to extreme temperatures retains its flexibility over a range of -180° to 400° F (-118° to 205° C). The coating — a silicone formulation — cures to a smooth, slightly-pebbled flat white or gray finish without bare spots or streaks. Its emissivity is at least 0.85 at 75°±5° F (23.8°±3° C) for either the gray or white color. Although it was originally developed for the Viking Mars Lander, the coating should be useful in various cryogenic applications.

The surface to be coated is first wiped with a solvent to remove grease and other contaminants; then it is spread with a silicone primer. (The primer turns pink/purple as it dries to indicate the areas that have been covered.)

The thermal-control silicone resin is mixed with zinc oxide (for a white coat) or zinc oxide plus black pigment (for gray). Toluene is added to bring the resin to the proper viscosity. Finally, a small amount of dibutyl tin dilaurate catalyst is added, and the mixture is strained.

The resin mixture is applied to the fabric with a siphon-feed spray gun in several light coats until a thickness of 0.010 in. (0.25 mm) is built up for sand and dust resistance. Each coat is applied lightly [thickness 0.001 to 0.002 in. (0.025 to 0.050 mm)] and is allowed to dry for at least 30 minutes to prevent a gloss from forming. When painting is complete, the coating is cured for at least 24 hours at 65° to 100° F (18° to 37° C) before it is handled.

This work was done by Lyle E. Johnson of Martin Marietta Corp. for **Langley Research Center.** *For further information, Circle 37 on the TSP Request Card.*

This invention is owned by NASA, and a patent application has been filed. Inquiries concerning nonexclusive or exclusive license for its commercial development should be addressed to the Patent Counsel, Langley Research Center [see page A8]. *Refer to LAR-11756.*

Simplified Systematic Production of Graphite Polyimide Prepreg

Technique is ideally suited for researchers and small-lot producers of composite structures.

Langley Research Center, Hampton, Virginia

The rapidly changing emphasis from heavier metal alloys to lighter structural materials has stimulated the development at Langley Research Center of a simple, systematic method for producing a preimpregnated polyimide/graphite material. The resin system used involved the polymerization of monomeric reactants (PMR) with methyl alcohol as the solvent at a formulated molecular weight of approximately 1,500, the result commonly designated as PMR 15. The reinforcement material was HTS graphite; the technique, however, is believed to be readily adaptable to other resin systems and fibers.

In preparing the polyimide resin system, ester acids were formed by reacting 5-norbornene-2,3-dicarboxylic anhydride (NA) and 3,3′,4,4′-benzophenonetetracarboxylic acid dianhydride (BTDA)

(continued next page)

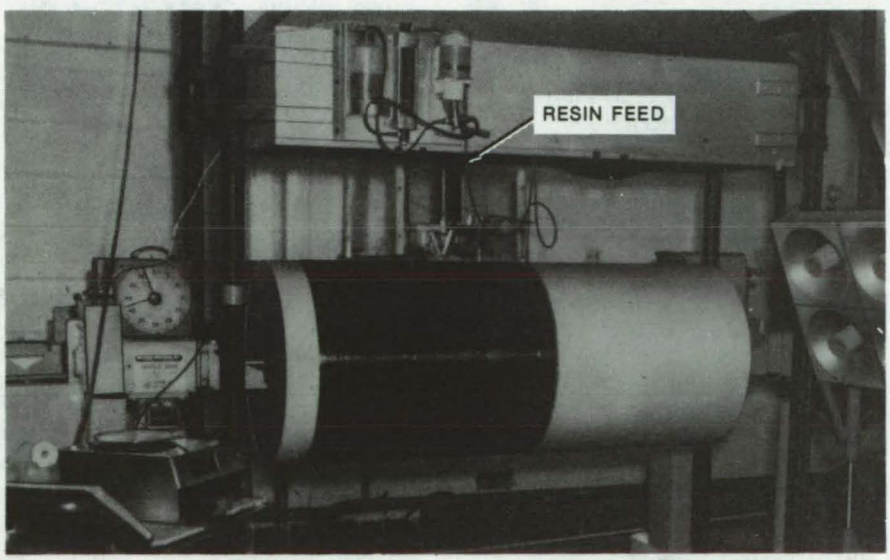

The **Drum-Winding Machine** simultaneously winds the HTS graphite and impregnates it at a typical speed of 10 revolutions per minute. After the desired size is reached, heat lamps are used to drive off volatiles, and the prepreg is covered with a transparent film of Teflon. When the prepreg has been sliced and removed, it may be stored indefinitely at 0° F (-17.8° C).

with excess methyl alcohol. Then, 4,4′-methylenedianiline (MDA) was dissolved in methyl alcohol to form the third reactant. Finally, the ester acids were mixed with the MDA solution to yield the PMR precursor.

The prepreg was prepared on a drum-winding machine 23.75 in. (60.33 cm) in diameter and 58.50 in. (148.59 cm) in width. For resin delivery, a metering pump was employed, and the resin was applied through a delivery tube mechanism. The winding drum, lead transverse travel, and resin pump were synchronized and calibrated to wind and impregnate simultaneously. The length of the sheets produced was 74.6 in. (189.5 cm). Widths were varied to accommodate laminate size requirements. The setup is shown in the photographs. The desired cured laminate parameters of 7 mils (0.018 mm) per ply thickness, 63 percent fiber weight, and 37 percent resin weight were obtained by precision control of 55 percent fiber, 30 percent resin, and 15 percent volatiles in the prepreg operation and by maintaining 50 percent solids by weight in the PMR 15 formulation.

This method has proved to be both precise and repeatable and is well suited to the researcher or small-lot producer of prepreg materials. By following the systematic, detailed procedures developed with this method, even inexperienced personnel can successfully produce prepreg materials of consistent quality.

This work was done by Samuel E. Harper, William E. Stoops, and Maywood L. Wilson of **Langley Research Center.** *For further information, Circle 38 on the TSP Request Card.*
LAR-12266

Books and Reports

These reports, studies, and handbooks are available from NASA as Technical Support Packages (TSP's) when a Request Card number is cited; otherwise they are available from one of NASA's Industrial Application Centers or the National Technical Information Service.

Ammonia-Compatible Elastomers and Alloys

Results of mechanial tests after long-term immersion in liquid anhydrous ammonia

The effects of long-term immersion in liquid ammonia on the mechanical properties of two metal alloys and two elastomers are reported in a new study. The alloys, Inconel 718 and Ti-6Al-4V, were found to be ammonia-compatible and suitable for use in storage vessels, fluid lines, and other system components. The elastomers, varieties of ethylene propylene terpolymer rubber, are also resistant to degradation by ammonia and could be used for valve seats, seals, and gaskets.

Ten samples of each alloy were prestressed to nearly 60 percent of their yield strengths and were immersed in liquid anhydrous ammonia for 90 days at 125° F (52° C). The samples had reduced middle sections and provisions for pin loading the ends for tensile testing. Half of the samples were TIG (tungsten/inert-gas) welded in the centers of the reduced sections. An additional 20 samples were retained as controls.

The samples showed no measurable weight changes, within 1 mg, and no visible surface damage under 400X micrographic analysis. Yield strength, ultimate tensile strength, and elongation were virtually unaffected.

Five samples of each elastomer were fabricated into tensile-test specimens along with five each of tear and compression-set samples. An equal number were retained for controls. The samples were immersed in liquid ammonia under the same conditions as the metal specimens. The preimmersion ammonia analysis showed 3,190 ppm water and 4 ppm oil.

After exposure, the exposed tensile samples and unexposed controls were tensile tested. Tear and compression-set samples were also tested along with their controls. Effluent liquid anhydrous ammonia was analyzed separately for metal and rubber samples.

The rubber specimens exhibited a marked change in color upon exposure, with a relatively insignificant increase in weight (0.06 to 0.24 percent). As with the metal samples, the mechanical properties were relatively unaffected. The ammonia analysis showed an increase in moisture to 4,692 ppm and of oil to 28 ppm.

This work was done by M. T. Bantrell and D. A. Rietdorf of Fairchild Industries Inc. for **Johnson Space Center.** *To learn how to obtain a copy of the report, Circle 39 on the TSP Request Card.*
MSC-16559

Detection of Hydrogen Chloride Gas in Air

Summary of HCl detection techniques in instrument development program

Launch vehicle effluent (LVE) monitoring is part of NASA's overall tropospheric and stratospheric environmental study program. The goal of the LVE monitoring program is to assess the applicability and accuracy of diffusion models for predicting the dispersion of exhaust effluents from current and future NASA launch vehicles. Early in the LVE program, it was determined that detection techniques for HCl gas (a major exhaust product in most solid rocket motors) were inadequate. This requirement for a high-performance HCl detector to monitor ambient air concentrations led to work on the development of suitable new detectors. Nine techniques were evaluated or developed, and

the results have been published in a report cited at the end of this article. The techniques are briefly discussed below and are compared in the accompanying table.

The first three methods are fairly standard and are frequently employed for HCl dosage (ppm-s) detection:

1. *Bubbler Method* (a standard laboratory and field sampling technique for many gas species): However, HCl detection capability of the bubbler is only about 50 ppm-s and is limited by the background chloride concentration of the bubbler solution.
2. *pH Measurements* (based on the fact that HCl is hygroscopic and readily forms an acid with water): These include standard lab techniques, such as the use of pH-sensitive papers, pH electrodes, and the like. Such methods are limited, with lower detection sensitivities of about 60 ppm-s.
3. *Indicator Tubes* (available commercially for HCl detection and generally contain a granular material, typically a silica gel, impregnated with a substance that changes color upon exposure to HCl): Silica gel indicator tubes are most suited for problem estimation, being capable of detecting 1 ppm over a 2- to 5-minute period. Other indicator tubes (not available commercially) are coated with various other substances that capture the HCl for laboratory analysis. These techniques have a lower detection limit of about 10 ppm-s.

These three standard techniques are all limited in accuracy and/or require laboratory analysis. The following six techniques are relatively newly developed, involve in situ sampling, and require no laboratory analysis to obtain HCl concentration or dosage data.

4. *Microcoulometers* (a continuous-mode technique where the incoming HCl bubbles through an electrolyte): Silver ions in the electrolyte react with the HCl, precipitating AgCl and thus reducing the silver ion concentration of the electrolyte. The consequent generation of replacement silver ions at generating electrodes can be accurately related to the quantity of HCl introduced to the system. This method is operational and has a lower detection limit of about 0.08 ppm.
5. *Modified Condensation Nuclei Counter* (HCl is converted to NH_4Cl by passing the air sample over a solution of NH_4OH): The NH_4Cl particles are detected by a conventional condensation nuclei counter and are related by calibration to the HCl concentration. The instrument, existing as a breadboard unit, has some potential for detecting as low as 1 to 2 ppm with a response time of a few seconds.
6. *Dual-Isotope Infrared Absorption* (nondispersive infrared analysis): An IR beam is passed alternately through a cell containing HCl^{35} and one containing HCl^{37}. Each cell filters out the wavelengths absorbed by its molecule. The filtered/chopped beam is passed through the sample cell, where the nonfiltered wavelengths are absorbed in an amount dependent on the ambient HCl isotope concentrations and on other factors (cell constants, temperature, and so forth) that are the same for each beam. Since ambient HCl contains a known and constant ratio of the two isotopes, the attenuation of the two beams can be electronically processed to produce a readout signal proportional to HCl concentration. This detector currently exists as a breadboard unit capable of detecting 0.3 ppm HCl in 8 seconds to 90 percent of reading.
7. *Gas-Filter Correlation* (a modification of the nondispersive infrared analyzer): An open-cell gas-filter correlation instrument that is designed to operate onboard an aircraft has been constructed and is being tested. It has a lower detection limit of about 5 ppm with a response time of 10 seconds to 90 percent of reading.
8. *Chemiluminescent Nitric Oxide Detection* (the reaction of HCl gas with NH_3 and the conversion of the remaining NH_3 to NO): The NO is then measured, using a conventional chemiluminescent NO detector, and the measurement of NO is related by calibration to the concentration of HCl in the sample. The breadboard unit has a lower detection limit of 1 to 2 ppm with a response time of a few seconds to 90 percent of reading.
9. *Chemiluminescent Luminol-Oxidation Detection* (based on a chemiluminescent reaction in which visible light is generated in an alkaline solution of luminol during oxidation by H_2O_2): The visible light is monitored by a photomultiplier tube and is proportional to the HCl concentration of the airstream. The alumina tube that conducts sample gas to the reaction cell is coated with $NaBrO_3$ and NaBr. This coating reacts with the HCl to produce a series of bromine/chlorine compounds that catalyze the luminol oxidation. This detector is commercially available and has a lower detection limit of about 0.05 ppm with a response of 1 to 20 seconds.

Summary of Measurement Methods

Method (See Text)	HCl Conc. Meas.	Lower Det. Lim. (ppm)	Time to 90% of Reading (Seconds)
1	No	*50	—
2	No	*60	—
3	No	*10	—
4	Yes	0.08	>60
5	Yes	1 to 2	<5
6	Yes	0.3	8
7	Yes	5	<10
8	Yes	1 to 2	<5
9	Yes	<0.05	1 to 20

*(ppm-s)

Complete data on specificity and interference by other species are not yet available. Thorough interference tests have not been performed for most of the techniques discussed. The instruments range, in stage of development, from breadboard units requiring additional laboratory study to operational techniques (bubbler, microcoulometer, and chemiluminescent luminol) currently in use in NASA's LVE program.

(continued next page)

This report was prepared by Gerald L. Gregory of **Langley Research Center.** *Further information may be found in NASA TN-D-8352 [N77-16310], "Measurement Techniques Investigated for Detection of Hydrogen Chloride Gas in Ambient Air," a copy of which may be obtained at cost from the North Carolina Science & Technology Research Center [see page A7].*
LAR-12218

Mechanical Properties of Low-Nickel Stainless Steel

Ambient and low-temperature data for Nitronic 33 stainless

The demand for improved corrosion-resistant steels, coupled with the increased emphasis on conserving strategic metals, has led to the development of a new family of stainless steels in which manganese and nitrogen are substituted for a portion of the usual nickel content. One such steel, 18-3 Mn (Nitronic 33) stainless contains approximately 18 percent chromium, 3.5 percent nickel, 0.05 percent carbon, 13.5 percent manganese, and 0.3 percent nitrogen. Compared to 304 stainless steel, which contains 8 percent nickel, 18.3 Mn has been purported to offer the following advantages:

- Approximately-doubled yield strength in the annealed condition,
- Better resistance to stress-corrosion cracking,
- The retention of low magnetic permeability even after severe cold working,
- Excellent strength and ductility at cryogenic temperatures,
- Superior resistance to wear and galling, and
- Excellent high-temperature properties.

A report that presents the results of a detailed study of the ambient and low-temperature mechanical properties of this material is now available. Included in the study were the ambient and liquid hydrogen temperature (20.5 K) tensile properties and the ambient stress-corrosion resistance of annealed-parent and tungsten/inert-gas (TIG) welded specimens.

Tensile tests on longitudinal and transverse specimens of both parent and welded specimens indicated excellent mechanical properties at test temperatures down to -200° F (144.26 K). At lower temperatures, the elongation rapidly decreased to less than 6.0 percent at liquid hydrogen temperature. The notched tensile properties of the longitudinal and transverse parent-metal specimens indicated a progressive increase in notched tensile strength (NTS) from ambient to liquid nitrogen temperature. Below -320° F (77.6 K) the NTS decreased rapidly. The notched/unnotched tensile ratio of the longitudinal and transverse material specimens remained above 0.9 from ambient to -200° F. At lower temperatures the tensile ratio decreased steadily, yet remained above 0.6 at liquid hydrogen temperature for both specimens.

Stress-corrosion tests were performed on the as-received and on the welded longitudinal and transverse specimens in four different environments: noncorrosive atmosphere, alternate immersion in a 3.5-percent NaCl bath, a humidity cabinet, and a salt-spray cabinet. Tensile tests made after exposure for 180 days indicated that only the specimens exposed to the salt-spray were corroded (pitting) causing a degradation in mechanical properties. The angle of exposure proved to be more influential than the specimen direction (longitudinal or transverse) or the applied stress in determining the extent of degradation.

This work was done by J. W. Montano of **Marshall Space Flight Center.** *Further information may be found in NASA TM-X-73309 [X68-18883], "The Stress Corrosion Resistance and the Cryogenic Temperature Mechanical Behavior of 18-3 Mn [Nitronic 33] Stainless Steel Parent and Welded Material," a copy of which may be obtained at cost from the New England Research Application Center [see page A7].*
MFS-23543

Life Sciences

Hardware, Techniques, and Processes

Versatile Communications Terminal

Radio and telephone communications are controlled from a single, easily operated console.

Lyndon B. Johnson Space Center, Houston, Texas

Many widely separated parties can be linked into an efficient communications network by a versatile new control terminal, shown in the figure. The terminal can handle voice and data communications via both telephone lines and radio-frequency channels. It includes telephone-to-radio "patch," a telephone autodialer, and other advanced features to provide rapid communications for applications such as emergency medical services (EMS) operations. The system combines commercially available subassemblies into an attractive package that is easily operated by nontechnical personnel.

A prototype of the terminal has been used for several months at the Odessa, Texas, Medical Center to assist in EMS operations. The prototype controls three radio channels and three telephone lines. It includes a 32-number telephone autodialer and the telephone-to-radio patch.

The radio channels may be any frequency in the VHF or UHF range. Signals are transmitted through three remote unmanned radio-frequency base stations. Communications between the terminal and the base stations are along dedicated telephone lines. One channel is reserved for EKG transmissions; a second handles hospital to hospital and ambulance to hospital communications in the region serviced by the EMS; and the third is a local ambulance to hospital communications channel that uses a locally assigned frequency.

A subaudible tone is automatically sent from the ambulance when transmitting to the hospital over the local channel. The base station is muted until this address tone is received; the tone automatically activates the receiver. With this arrangement, the ambulance medical technician is not troubled by mechanical dialing when communicating on the local channel and the hospital medical personnel hear no unwanted messages. The muting system can be overridden in special situations (such as a disaster) so that all parties transmitting at the designated local frequency can be heard at the control unit.

Emergency Communications Control Unit handles telephone and radio communications between many parties. A "patch" is included to link the radio and telephone circuits. Other features include a 32-number telephone autodialer and a tone-code dialer on the radio panel that calls other similar terminals via a coded address system. The terminal also has an auxiliary control unit that allows personnel to radio/transmit via the station from a remote location. In one application, the remote unit was located in the hospital sleeping quarters of an on-duty emergency physician for rapid response during off-peak hours.

For the regional channel, each hospital has a three-digit address that is dialed to contact that hospital. By using the three-digit code, the operator can contact other hospitals equipped with similar terminals. Also, each ambulance is equipped with a tone-code dialer to contact the regional hospitals via this channel.

The telephone circuits are standard, commercially available items. One line is a "hotline" to an emergency dispatch center (911 network); a second is an incoming EKG line that can interface with a cardioscope and strip-chart recorder; and the third is a programable telephone dialer that stores up to 32 numbers (to special-care centers, poison-control centers, a blood bank, and other services). The console operator initiates communications to one of these centers without dialing, simply by pressing a button.

All terminal functions are clearly marked and accessible on the front of the console. Three speakers are mounted for receipt of the radio communications. Each has an indicating light that flashes when the corresponding channel is activated by an incoming call. When this signal is received, the operator rotates the select switch to engage in two-way communications on that channel.

This work was done by Norman Belasco, Sam L. Pool, and Richard L. Sinderson of **Johnson Space Center.** *For further information, Circle 40 on the TSP Request Card.*
MSC-16823

Miniature Diaphragm Valve for Medical Equipment

Plunger is isolated from fluid to prevent failure of valve subjected to sterilization temperatures.

Langley Research Center, Hampton, Virginia

When systems containing small or miniature fluid valves are sterilized, it is essential that the fluid that the valves control not change its viscosity during the high heat exposure. Should a fluid, for example, contain a nutrient that becomes gummy and sticky when heated (as occurred in one of the Viking spacecraft biological instruments), the residue of the nutrient will lodge within the plunger cavity and hinder or prevent the proper functioning of the valve.

A proposed valve assembly (shown in the diagram) keeps the nutrient out of the moving parts of the valve by physically isolating the plunger from the fluid. The poppet and the diaphragm are molded together, and the latter is shaped to act as a static seal, which remains seated during the valve operation. As the plunger moves, the diaphragm also moves to form a separate cavity for the nutrient and thus isolates it from the plunger cavity and the latching mechanism. When the plunger changes direction, the diaphragm returns to its at-rest position, and the nutrient is expelled through the outlet ports into a manifold, a line, or a reservoir.

The diaphragm/poppet combination functions as a mechanical lock as well; this results in a positive seating and unseating action of the diaphragm on the valve seat. The valve should not be adversely affected by gross pressure of up to 180 psig (1.3×10^6 N/m^2) and is designed to be rugged enough to withstand a planetary landing.

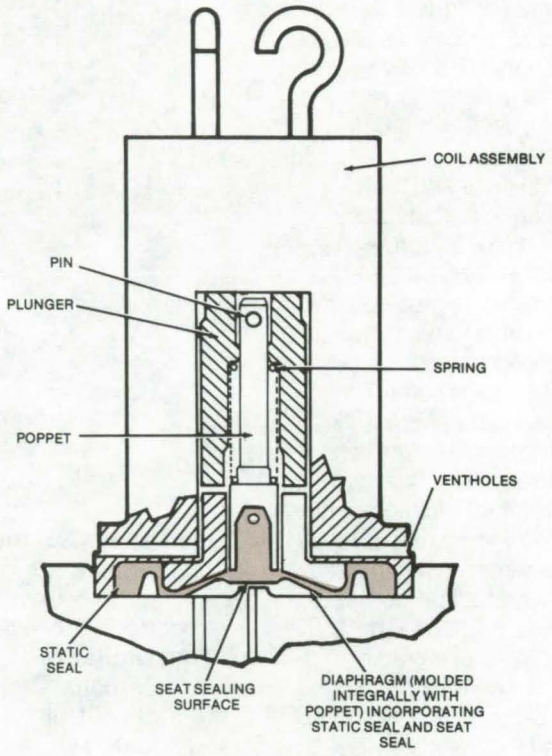

In the Miniature Diaphragm Valve, the poppet and diaphragm are molded together. The movement of the diaphragm during activation of the plunger forms a separate cavity for the nutrient or other substance, isolating it from the plunger cavity and the latching mechanism and thus preventing a possible malfunction of the valve.

This work was done by Thomas J. Stadler and James R. Taylor of TRW, Inc. for **Langley Research Center.** *No further documentation is available.*
LAR-11775

Calibration Faceplate for X-Ray Image Intensifiers

Convenient x-y reference system

Ames Research Center, Moffett Field, California

Medical X-ray systems containing image intensifiers are designed to produce film or video images that are to be assessed qualitatively. When quantitative measurements are to be made of the resultant dynamic images, it is necessary to provide an x-y reference system external to the object being recorded.

This can be accomplished by the use of lead crosshairs embedded in a detachable, radiolucent intensifier faceplate. [This device can be used with the alinement tool described in the following article (ARC-11017).] The face of the intensifier was selected for the location of the

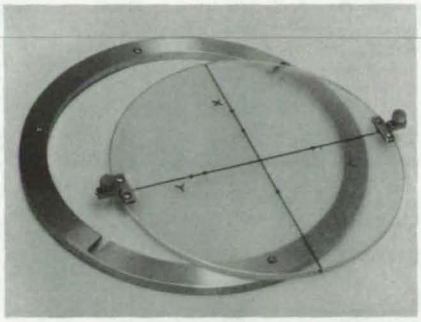

The **Calibration Faceplate** can be used to provide an x-y reference system external to the device being photographed.

coordinate system because this is the point in the video chain where there is no distortion.

Intersecting x-y coordinate lines are accurately cut 1 mm deep in a 6-mm clear plastic plate that fits inside a ring on the face of the intensifier (see photo). The fiducial markers are drilled on the coordinate lines at about one-third and two-thirds of the outside radius of the faceplate. The x-y labels and lines on the plate are filled with lead-containing putty that is sanded smooth when dry. Keyways are cut at each end of the y-axis on the periphery of the plate, and screw holes are placed and tapped so that aluminum locating keys with spring-loaded locking pins can be fastened to the plate.

This work was done by Daryl Rasmussen and John Rietman of **Ames Research Center** *and Sally Marquis of Stanford University. For further information, Circle 41 on the TSP Request Card.*
ARC-11146

Alinement Tool for X-Ray Image Intensifiers

Gage indicates amount and direction of skew in images.

Ames Research Center, Moffett Field, California

The **Alinement Gage** consists of an upper plate and a lower plate connected by an aluminum post marked with a metric scale. The upper plate is identical to the calibration plate except for the post flange. The lower plate is made of aluminum and is grooved for x-y coordinates and a pattern of concentric rings that aid in the recognition and measurement of nonlinearity. The x-y coordinates on the upper and lower plates match exactly.

Image intensifiers have found increased application in medical X-ray systems where the X-ray image is to be analyzed quantitatively. In such systems, however, it is not uncommon for significant errors to be caused by distortion introduced by the image intensifier electro-optics and by skew due to misorientation of the image intensifier with respect to the X-ray source.

Greater accuracy in making calculations from resultant images can be obtained with a detachable alinement gage that shows the amount and direction of skew. The alinement tool, as shown in the photograph, consists of an upper plate and a lower plate separated by an aluminum post. Both plates are grooved in a pattern of concentric rings and coordinate lines. The gage is mounted on the face of the image intensifier. Skew is corrected by viewing the gage on the video monitor and adjusting the image-intensifier position and tilt angle. The circular patterns on the lower plate show the amount and type of distortion caused by the electro-optics.

This work was done by Daryl Rasmussen and John Rietman of **Ames Research Center** *and Sally Marquis of Stanford University. For further information, Circle 42 on the TSP Request Card.*
ARC-11017

Biotelemetry System for Ambulatory Patients

Multichannel system uses CMOS integrated circuits for minimum size and weight and uses PCM for high signal fidelity in applications such as EEG and EKG monitoring.

Ames Research Center, Moffett Field, California

A newly developed transmitter for multichannel telemetry of medical data is so compact that it can be carried in a patient's belt. Pulse-code modulation (PCM), is used for a high-quality signal, and low-power CMOS integrated circuits make miniaturization possible. The transmitter is useful for electro-encephalograms (EEG) and electro-cardiograms (EKG) and other bio-medical patient-monitoring situations.

A block diagram of the part of the telemetry system that is carried by the unrestrained subject is shown in Figure 1. (The receiver and demodulator that recover the analog data are powerline operated and are not miniaturized.) The system is configured with eight low-noise pre-amplifiers for multichannel EEG applications or EKG with reduced amplifier gains. Of course, any transducer (such as pressure, blood flow, respiration, oxygen consumption, or dimension) that has a suitable signal conditioner to provide an analog output in the ±1.0-V range can be connected to the multiplexer.

After time multiplexing the resultant composite analog signal is converted to a pulse-width-modulation (PWM) format, as seen in the typical waveforms of Figure 2. The analog signal is converted to PWM by inputting it and a ramp function to a comparator amplifier. The sample interval is approximately 100 μs per channel, which results in a frame repetition rate of 1,000/s (eight channels plus one zero reference and one frame sync interval).

The PWM signal is converted to pulse-code modulation (PCM) by gating a 5-MHz oscillator on and off with the PWM signal and counting the number of 5-MHz cycles. The counted cycles at the end of each word are parallel shifted to a shift register, and the counter is reset to zero, ready to accept the next word. While the next word is being counted, the previous word is serial shifted out of the shift register as a PCM signal. The final stage is a transmitter for RF transmission at 88 to 108 MHz.

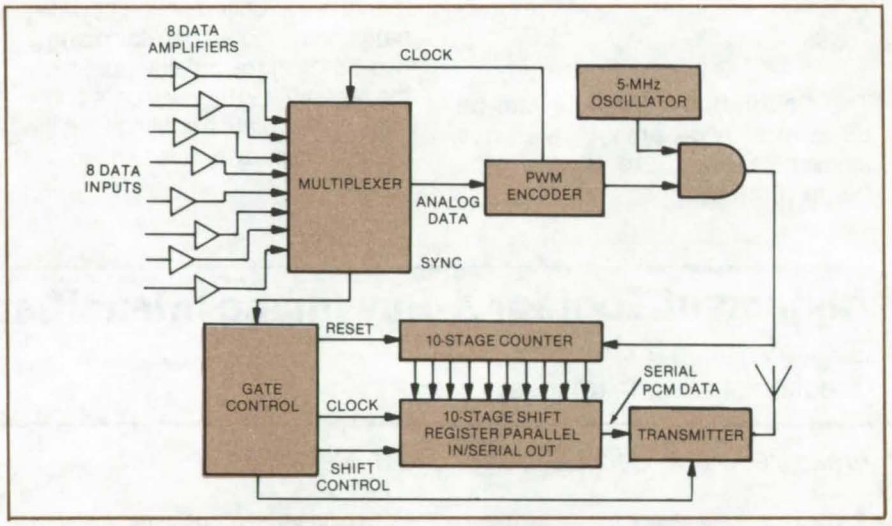

Figure 1. **Multichannel PCM Telemetry System,** shown in block diagram form, uses CMOS large-scale integrated circuitry to minimize size, weight, and power requirements.

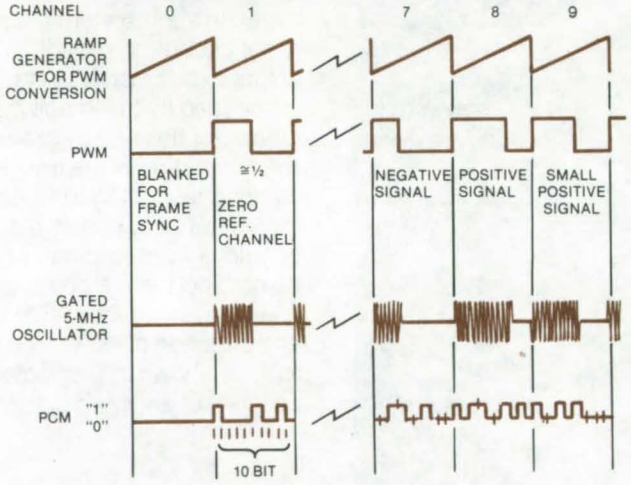

Figure 2. **Typical Waveforms** in the portable telemetry system show that data are initially converted to pulse-word modulation, which gates a 5-MHz signal. The 5-MHz cycles are counted to produce pulse-code modulation for transmission.

The transmitter electronics are packaged in three small units, each about 2 by 5 by 8 cm in size, that are placed in small pouches attached to a belt. A fourth pouch has two 9-V batteries and the RF transmitter. Although the entire unit could be placed in one larger package, this arrangement is less bulky and most easily conforms to various body contours.

This work was done by Thomas B. Fryer of **Ames Research Center.** *Further information may be found in: "A Multichannel EEG Telemetry System Utilizing a PCM Subcarrier," Thomas B. Fryer, Biotelemetry, Vol. 1, No. 4, p. 202, 1974. No further documentation is available.*
ARC-11142

Mechanics

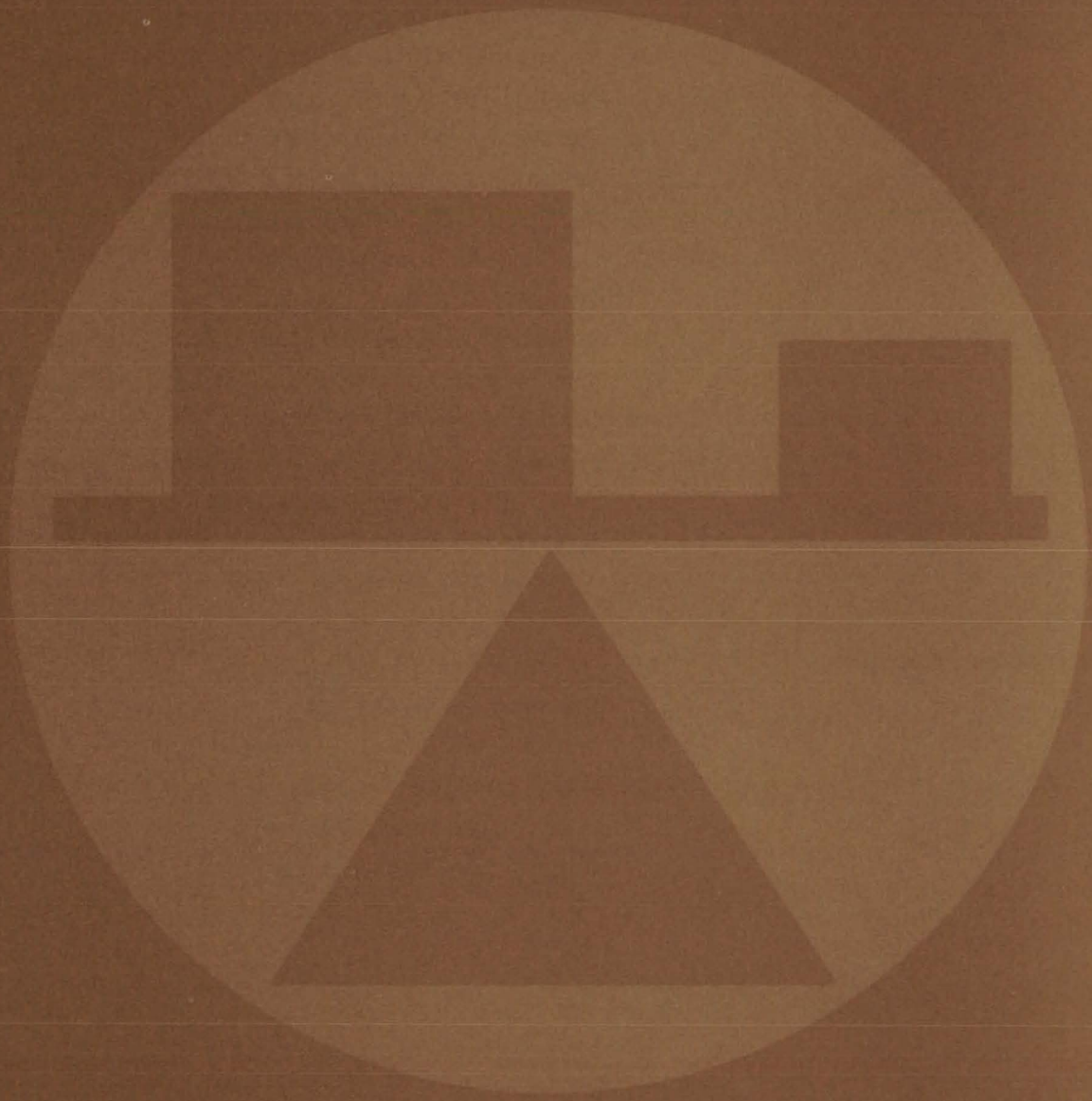

Hardware, Techniques, and Processes

Computer Programs

Multipurpose Miniature Drag-Force Anemometer

Inexpensive probe
measures speed and direction.

Lewis Research Center, Cleveland, Ohio

A simple, rugged, and accurate probe has been developed to measure steady-state and dynamic velocity head, steady-state and dynamic flow angle, and turbulence intensity in flowing fluids at subsonic velocity. The probe is much simpler in design and calibration, and more durable, than hot-wire and hot-film anemometers and is not affected by flow contamination. It is very much less expensive and complex than laser anemometers. The associated electronics are as simple as those of strain-gage pressure transducers.

The probe (see figure) consists of a cantilevered silicon beam 0.10 in. (2.5 mm) long, 0.06 in. (1.5 mm) wide, and 0.01 in. (0.25 mm) thick, with an integrated, diffusion-bonded, strain-gage bridge at the base as the force-measuring element. (The silicon beam is a commercially available item.) The outer 0.06-in. (1.5-mm) length of the beam, which is exposed to the flow, is equal to the width of the beam and therefore comprises a square plate element. Two longitudinal strain gages measure tension or compression on the beam. Two transverse strain gages complete a Wheatstone bridge. The proximity of the four strain gages provides inherent temperature compensation. Water-cooling passages in the supporting tube allow use of the anemometer at moderately elevated temperatures and reduce thermal stress between the components. Under dynamic flow conditions, the anemometer has a frequency response like that of a highly-underdamped second-order system with a natural frequency of 42 kHz and a damping coefficient of 0.007.

To measure velocity head, the probe is oriented with the wide side of the beam nearly perpendicular to the flow. In this position, the output of the strain-gage bridge is proportional to the velocity head. Over the range of mach numbers from 0 to 0.6, the output is linear with velocity head to within the accuracy of measurement. The anemometer can measure velocity head in either forward or reverse flow.

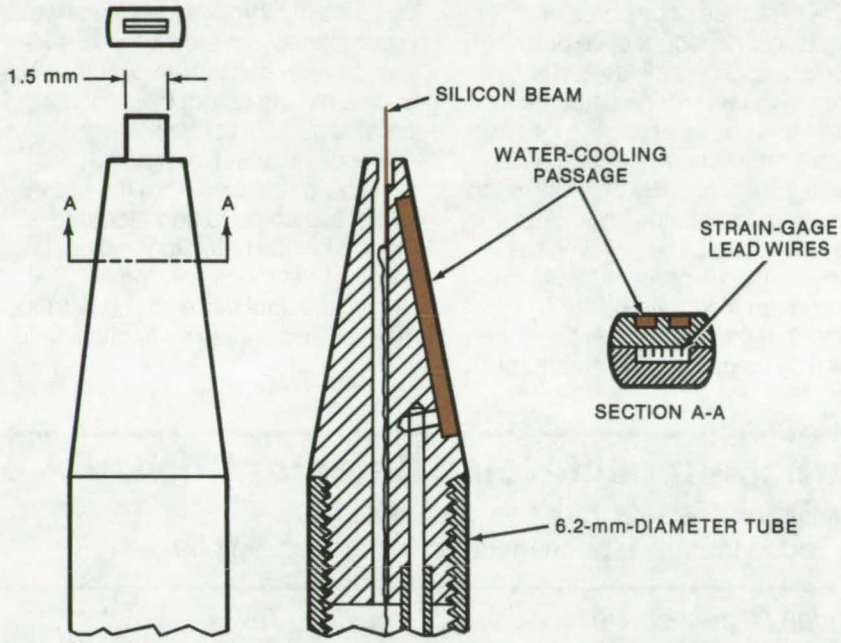

Drag-Force Anemometer measures air (or other fluid) speed and direction, using a silicon beam and strain-gage bridge. With the wide side of the beam perpendicular to flow, output depends on fluid speed; with the wide side nearly parallel to flow, output depends on speed and direction.

To measure flow angle, the probe is oriented with the wide side of the beam nearly parallel to the flow. In this position, the output of the strain-gage bridge is proportional to both the flow angle and the velocity head. Thus to measure flow angle, the velocity head must be determined as described above, either by orienting the beam in two positions or by using two probes oriented 90° to each other. The anemometer can measure flow angles in excess of ±40°.

To measure turbulence intensity, the probe is oriented with the wide side of the beam nearly perpendicular to the flow. The turbulence intensity is simply the root-mean-square value of the strain-gage bridge output divided by twice the mean value.

The anemometer has performed satsfactorily in two applications. In the first application, the anemometer was used to measure turbulence intensity in a free jet. The results agreed with those measured with a hot-wire anemometer. In the second application, the anemometer was used as a diagnostic instrument during fan flutter tests of a fan-jet engine. Non-engine-order as well as engine-order frequencies were detected in the rotor-blade wakes.

This work was done by Gustave C. Fralick and Lloyd N. Krause of **Lewis Research Center.** *Further information may be found in NASA TM-X-3507 [N77-25487], "Miniature Drag Force Anemometer," a copy of which may be obtained at cost from the New England Research Application Center [see page A7].*

Inquiries concerning rights for the commercial use of this invention should be addressed to the Patent Counsel, Lewis Research Center [see page A8]. Refer to LEW-12790.

Testing Internal Coatings in Metal Vessels

Defects are detected by measurement of electrical conductivity.

Lyndon B. Johnson Space Center, Houston, Texas

The presence of pinholes or defects in a nonconductive protective coating on the inside surface of a closed vessel can be detected if that vessel has one opening into which a small stainless-steel probe can be introduced. By inserting such a probe and attaching another to the outside surface, and by filling the vessel with a 10-percent NaCl solution (an electrolyte), the integrity of the coating will be determined by measuring the electrical conductivity through the vessel wall. A completely-covered internal surface is very resistant electrically, but even a minute defect in the coating creates a "short circuit."

Should a defect be present, the solution is removed from the vessel, which is then dried and recoated. The conductivity-testing and coating sequence is then repeated as necessary until there are no defects. This method should be applicable to any metallic container that is coated internally with a nonconductive resin system for protection against corrosive stored fluids. A standard dc ohmmeter with a 0- to 1,000-megohm scale is sufficient for detecting any defects.

This work was done by Armand Ruby and Peter Perkins of United Technologies Corp. for **Johnson Space Center.** *No further documentation is available.*
MSC-16532

Particle-Impact Noise Detector [PIND]

Nondestructive test for loose particles in IC packages that have been installed in page assemblies

Lyndon B. Johnson Space Center, Houston, Texas

Integrated circuits (IC's) can fail if loose particles become trapped in their packages during their fabrication. Often this failure mode is not detected until after the IC has been installed in its page assembly. Packages with this defect can now be screened at the page level by the ultrasonic-test system shown here. The technique, which involves subjecting the page to acoustic vibration and detecting the impact noise as particles strike the interior of the package, might also be used to detect other assembly flaws, such as loose screws, slapping wire harnesses, and loose mounting hardware. It can be particularly effective when testing assemblies that could be damaged by electrical or mechanical test probes.

The detection apparatus includes a vibration-testing machine, which subjects the page containing the package to low-frequency (40-Hz) transverse vibration. The vibration amplitude is gradually increased to approximately 5 g's. A miniature acoustic transducer is attached to each IC in turn, using double-backed tape. The tape has sufficient adhesive quality to remain in place during the test and transmits vibrations in the acoustic range. The transducer output is fed to an acoustic loose-particle detector and is also displayed on an oscilloscope. Vibrations caused by particle impacts can be "seen" above background on the scope and "heard" as an audible signal from the detector.

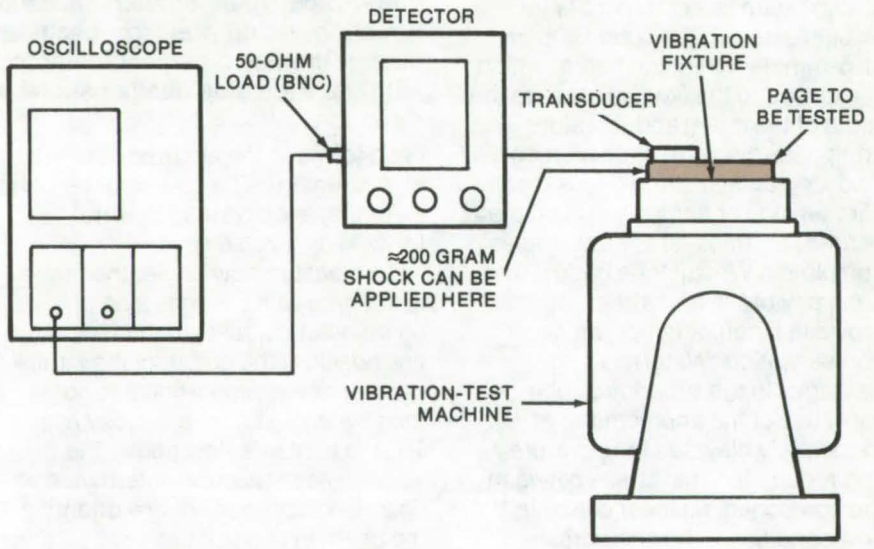

Loose Particles in IC Packages Are Detected by Ultrasonics, using this setup. The package, in its page assembly, is subjected to low-frequency (40-Hz) vibration, and the noise generated by particle impacts is picked up by the transducer. Test procedure calls for three transverse shocks to be applied to the page to dislodge any trapped particles.

Particle impact-noise detection has been used to detect flaws at the component level for some time; however, it has only recently been adapted as a practical technique at the page level. One difficulty has been the generation of electrostatic charge that can cause particles to adhere to the inside of the package. This effect appears to be most pronounced when the page is vibrated at high frequencies (above 200 Hz) or for prolonged periods at lower frequencies. The vibrations also cause particles to lodge in cavities inside the package. Both effects prevent the particles from creating noise and therefore reduce the acoustic signal. The new technique minimizes this problem by applying a light (approximately 200-gram) shock to the page assembly, perpendicular to the plane of vibration, to dislodge the inactive particles.

Another difficulty that exists when page assemblies are tested is spurious background noise due to slapping leads and vibrating mounting hardware. This problem is reduced by arcing leads away from the page and using rubber inserts for the mounting screws.

When these procedures are adhered to, the ultrasonic technique can detect flaws at the page level with the same efficiency as at the component level.

This work was done by R. J. Barr, D. E. Jackson, W. D. Leaf, R. G. Meza, and G. E. Rader of IBM Corp. for **Johnson Space Center.** *For further information, Circle 43 on the TSP Request Card.*
MSC-16626

Ablative Liner Locates Hotspots

Material measures heat flux in combustion chambers by depth of ablation.

Lyndon B. Johnson Space Center, Houston, Texas

An ablative liner can quantify local-heating effects in combustion chambers and other applications. By identifying hotspots and helping to map heat-flux patterns, the liner can be a useful tool for research in engine design. Unlike other materials that give only qualitative indications of hotspots through their discoloration or melting, this liner permanently records the heat flux at each point by the depth of ablation due to local heating. The technique can be used to determine the best locations for thermocouples for more extensive testing.

In the figure, typical polytetrafluoroethylene liner is shown installed in a combustion chamber. For this application, a cylindrical liner is used and held in place by an ordinary silicone-rubber adhesive. After a hot-fire test, the heat load at each point on the chamber wall is permanently recorded as the depth of ablation of the liner material. The ablation rate is determined from the manufacturer's data and from previous hot-fire test calibration.

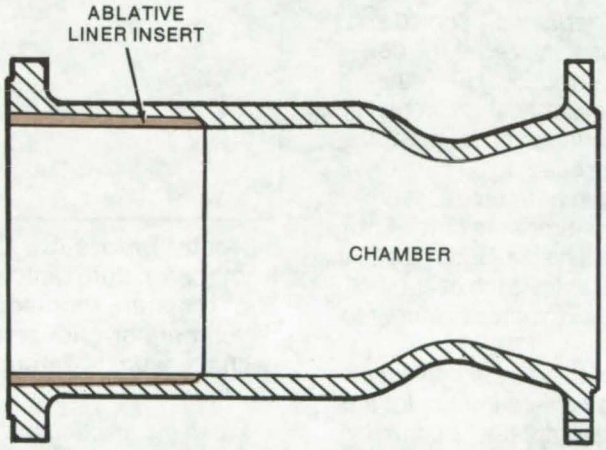

Ablating Liner of polytetrafluoroethylene is installed in a combustion chamber during hot-fire tests. After testing, the liner is a permanent record of the heat flux in the chamber. The heat flux correlates with the depth of ablation at each point.

The test results can be complemented by thermocouple measurements to give an accurate picture of the heat flux in the chamber. For example, rows of thermocouples might be placed around the areas of highest flux indicated by the liner.

This work was done by Stephen D. Mercer and Thomas J. Tierney of Aerojet Liquid Rocket Co. for **Johnson Space Center.** *No further documentation is available.*

Inquiries concerning rights for the commercial use of this invention should be addressed to the Patent Counsel, Johnson Space Center [see page A8]. *Refer to MSC-16981.*

Improved Dewpoint-Probe Calibration

Pressure-control technique is fast and accurate.

Lyndon B. Johnson Space Center, Houston, Texas

Relatively-simple pressure-control apparatus can calibrate dewpoint probes considerably faster than conventional methods, with no loss of accuracy. The technique requires only a pressure measurement at each calibration point and a single absolute-humidity measurement at the beginning of the run. Several probes can be calibrated at one time, and unlike other methods, points can be checked above room temperature.

Until now, the standard probe-calibration technique has required that the temperature of a mirror be accurately controlled and measured. The mirror is repeatedly cooled and heated until it stabilizes at the dewpoint of the surrounding air. When this occurs, condensation droplets form on its surface and cause a reflected light beam to be interrupted. The temperature must be cycled several times until the mirror reaches thermal equilibrium, so that it is not unusual for each calibration point to take 45 minutes or longer to complete.

The new method substitutes faster and simpler pressure control for the moisture and temperature control required in the mirror method. It is based on the principle that once the moisture content (absolute humidity) of the air is known, then the dewpoint is uniquely determined at each pressure.

The calibration apparatus is shown in the figure. Also required is a sling psychrometer to determine the absolute humidity of the air prior to the start of the calibration run. An air psychrometric chart is used to determine the moisture content from the dry- and wet-bulb readings.

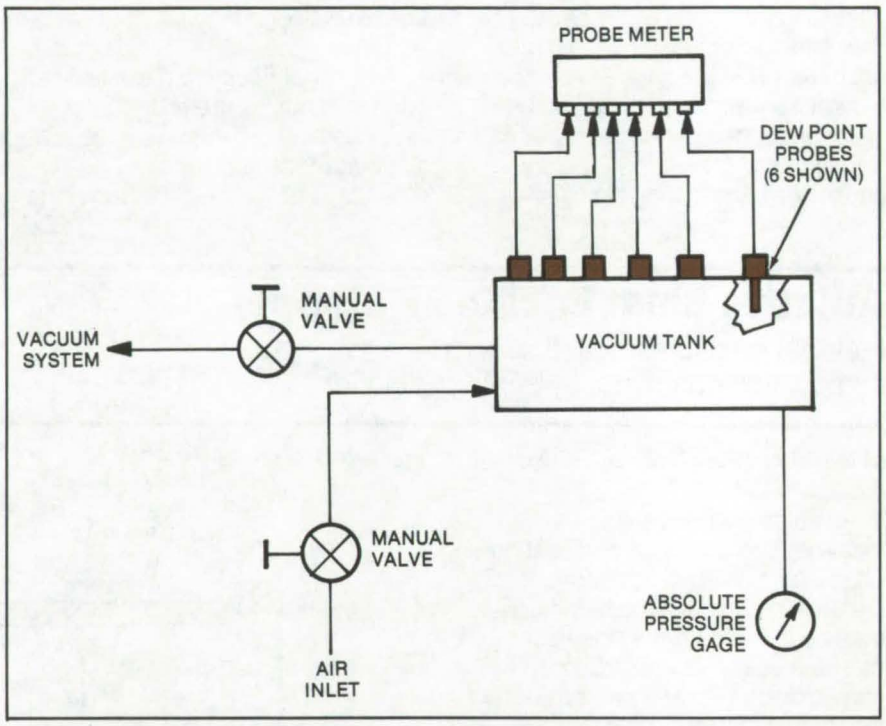

Dewpoint Probes Are Calibrated, using this apparatus, by removing air from the vacuum tank in steps and measuring the pressure at each step. The moisture content of the air is determined by using a sling psychrometer prior to the start of the calibration run. The dewpoint at each pressure is determined from these data, using an air psychrometric chart.

When the ambient moisture content is known, the vacuum tank is evacuated, then filled with air at atmospheric pressure. The air is then removed in steps, and the pressure is measured at each step. Since the absolute humidity (mass percentage of water) in the tank does not change as it is emptied, the dewpoint temperature at each pressure can be read directly from the psychrometric chart. The temperatures can then be compared with the readings on the probe meter. The calibrations can be extended above room temperature by heating the vacuum tank and introducing high absolute humidity.

This work was done by James G. Stephenson and Eugene A. Theodore of Rockwell International Corp. for **Johnson Space Center.**
For further information, Circle 44 on the TSP Request Card.
MSC-16811

Neutron Radiographic Testing for Hydrogen Embrittlement

"N-ray" inspection can often detect inhomogeneities more easily than X-rays.

Marshall Space Flight Center, Alabama

Neutron radiography (N-ray) inspection is similar to X-ray inspection in that both depend on variations in attenuation to achieve object contrast. However, the effectiveness of these methods differs significantly when certain combinations of elements are examined.

The attenuation of X-rays is determined largely by the electron density of the material; thicker and denser materials appear more opaque. The mass attenuation coefficient for N-rays is a function of both the scattering and capture probabilities for each element; thus the density or thickness of a material is less important in determining its transparency to neutrons.

The mass attenuation coefficients of different elements for X-rays present a nearly linear increase with increasing atomic number. In contrast, the (thermal) neutron attenuation coefficients show no such proportionality. High attenuation coefficients are exhibited by elements scattered throughout the periodic table. Hydrogen, boron, cadmium, and gadolinium with atomic numbers of 1, 5, 48, and 64, respectively all have exceptionally large coefficients. (Hydrogen has the highest scattering probability, while the other three have high neutron-capture probabilities.)

For the case of hydrogen in titanium, as an example, the titanium neutron attenuation coefficient is only 0.2 percent that of hydrogen; the titanium X-ray absorption coefficient is 79 percent, or much closer to that of hydrogen. Thus, substantially better contrast is obtained when neutrons are used to test for hydrogen embrittlement in titanium than when X-rays are used. Other combinations of elements that give only marginal resolution with X-rays, can be distinguished clearly by using neutrons.

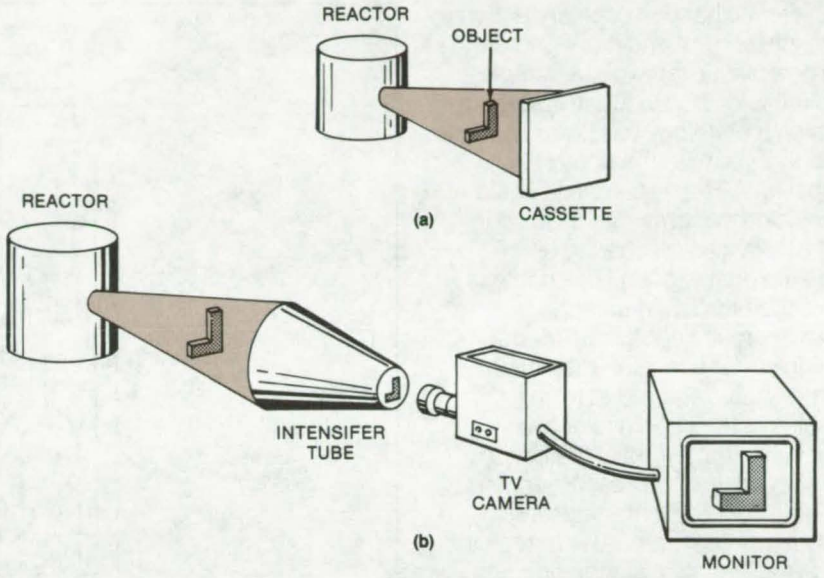

Neutrons Are Transmitted through an object to probe its inhomogeneties. Elements having different neutron attenuation coefficients are resolved on a photographic cassette (a) or on a TV monitor (b). The resolution of hydrogen in titanium, for example, is much better when using neutrons than it is when X-ray radiography is used.

Standard photographic and non-photographic imaging techniques can be used with neutrons (see figure). The source could be a small port on a nuclear reactor. The specimen under study would be positioned to intercept neutrons on their way from the source to a photographic plate or a TV camera. In the direct photographic method, the film is exposed and processed in the same way as for X-rays; in the transfer photographic method, two films can be exposed in one cassette and processed in a darkroom.

This work was done by John Dunstan of Rockwell International Corp. for **Marshall Space Flight Center.** *For further information, Circle 45 on the TSP Request Card.*
MFS-24193

Apparatus for Determining Surface Tension

Improved system for studying capillary action uses a pressure transducer and chart recorder instead of a manometer.

Caltech/JPL, Pasadena, California

Systems that use capillary action for liquid control and management are potentially lightweight, simple, and reliable. Consequently, surface tension technology has been applied in recent years to the control of propellants in space-vehicle liquid propulsion systems. In industry, this technology can be used to determine the quality of liquids such as petrochemicals and paints.

An improved apparatus for determining surface tension measures the pressure required to form bubbles at the openings of two capillaries immersed in the liquid at the same depth. A pressure transducer is coupled to a bridge supply and a strip-chart recorder to register the pressures to avoid the difficult task of simultaneously reading two levels of a manometer at the instant of bubble separation. Errors arising from the lag of the manometer fluid are also eliminated. The apparatus gave an error of only 0.2 percent in a recent study of hydrazine.

The new system is shown in the figure. The pressurized gas (compatible with the liquid being studied) is adjusted for a slow flow rate (to give approximately 2 to 4 bubbles per minute) and is passed through a copper coil (not shown) at the temperature of the liquid. Initially, the stopcock is opened, and the gas passes through the larger capillary. The transducer records the pressure for several cycles of growth and release of the bubbles. Next, the stopcock is closed, and the pressure recordings are made as the gas passes through the smaller capillary. The recordings allow the pressure at the exact instant of detachment to be determined accurately.

The surface tension (γ) is related to the difference between the maximum pressure required to detach a bubble from each of the two tubes (ΔP), according to the following expression [developed by Sugden (1924)]:

$$\gamma = \Delta P\left(1 + 0.69\,\frac{rgD}{\Delta P}\right)A$$

where r is the radius of the widest tube, g is the acceleration due to gravity, D is the density of the liquid, and A is a characteristic constant of the apparatus (all in the MKS system of units).

The apparatus enables the measurements to be made under controlled atmospheres. It also may be remotely operated. These features are particularly useful when dealing

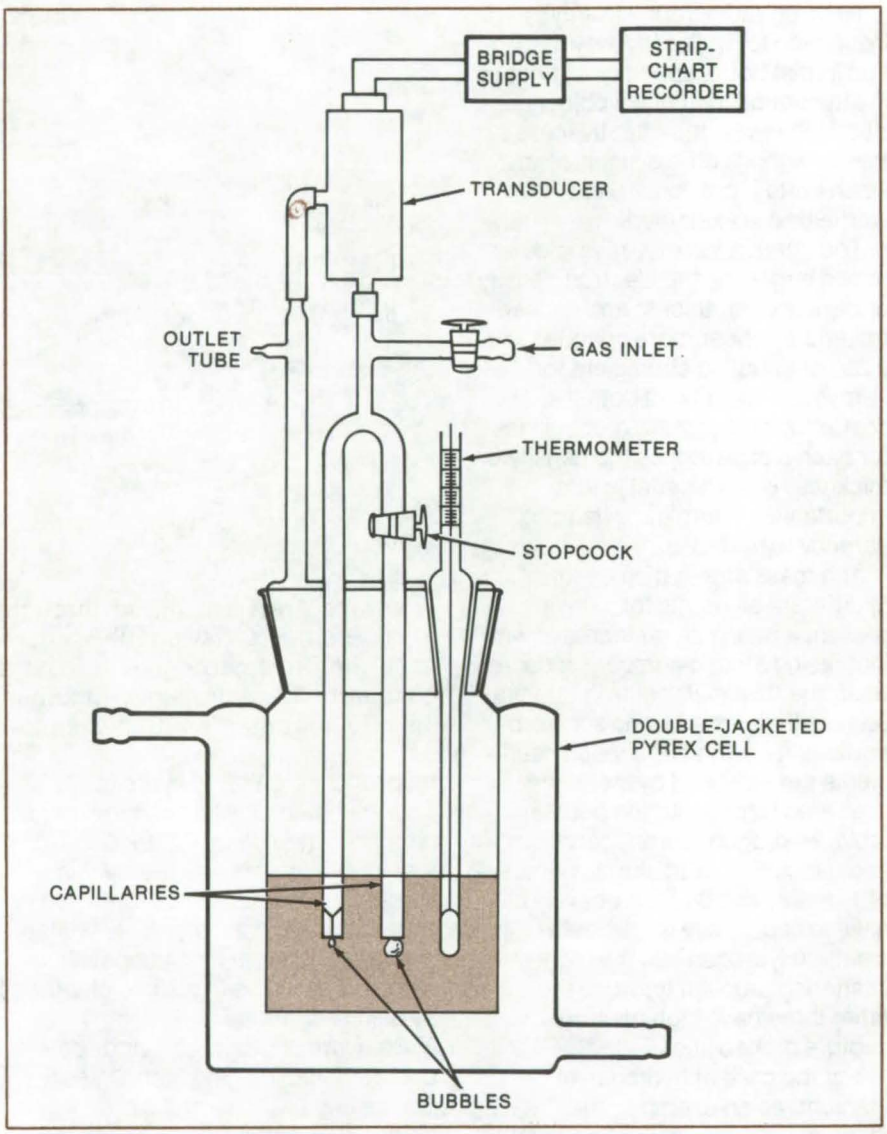

Surface Tension Is Determined Accurately by this apparatus that uses a transducer to measure the pressure necessary to detach a gas bubble from each of two capillaries of different sizes. The outlet tube contains a small vent to maintain atmospheric pressure on the reference side of the transducer.

with noxious liquids and for the study of surface tension under high-pressure conditions that require the use of all-metal apparatus.

This work was done by Rashad E. Razouk of **Caltech/JPL.** *For further information, Circle 46 on the TSP Request Card.*

Inquiries concerning rights for the commercial use of this invention should be addressed to the Patent Counsel, NASA Resident Legal Office-JPL [see page A8]. Refer to NPO-13294.

Leak Detector Uses Ultrasonics

A probe located on the outer wall of vacuum-jacketed fluid lines can detect leaks on the inner wall.

Lyndon B. Johnson Space Center, Houston, Texas

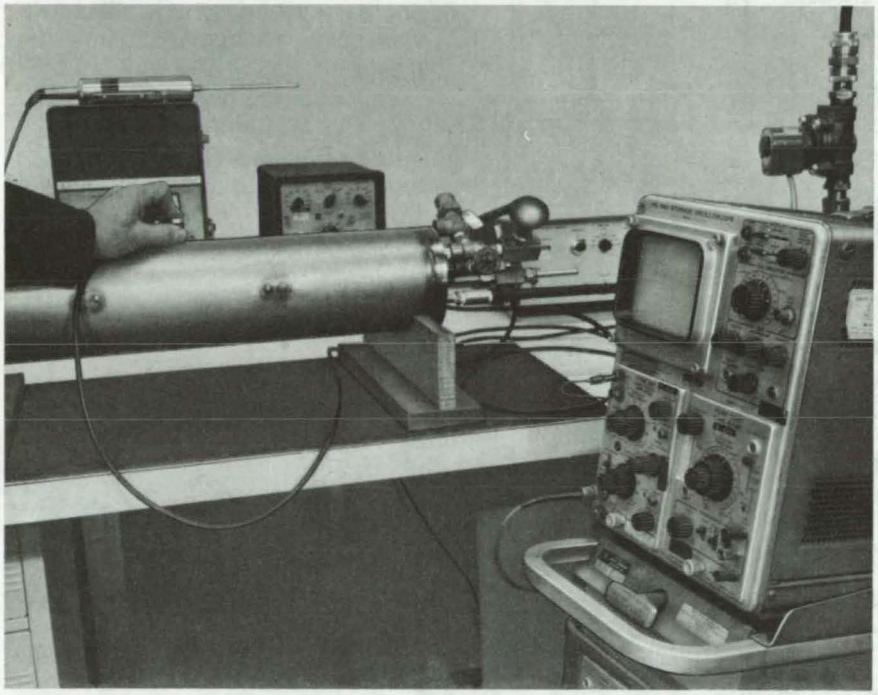

Figure 1. An Ultrasonic Probe Can Detect Leaks on the inner wall of this mockup of a vacuum-jacketed fluid line. The probe picks up vibrations when gas rushes through the leak into the jacket. Gas at low pressure is introduced into the jacket to maximize turbulence of the gas jet.

A new leak-detecting system uses an ultrasonic probe to "listen for" tiny leaks in vacuum-jacketed fluid lines. The probe picks up and amplifies vibrations that occur when gas rushes through the leak and converts them to an audible signal or a CRT disply. It can detect leaks on the inner wall of the jacket from outside the fluid line (Figure 1) and can therefore detect leaks that would be inaccessible to conventional leak testers. The system is considerably simpler to use than helium leak detectors and allows rapid leak checks to be made as part of routine maintenance.

When helium leak detectors are used, the tester must bleed helium gas into the system from one side of the leak and attach the detection system, usually a mass spectrometer, to the other side. Besides being tedious, this method is not applicable to welded lines since the inner wall is inaccessible. In addition, the helium may be incompatible with the "getters" used to prevent contamination.

Two forms of the ultrasonic detector have been developed. The first (Figure 2a) picks up the turbulent-jet signal with an ultrasonic microphone and mixes it with a local oscillator signal to generate an audible frequency. The audio signal is amplified and used to drive a speaker. This method can detect leaks through holes as small as 0.007 in. (0.018 cm) and requires no direct coupling to the fluid line. The operator simply moves the probe over the outer surface to pick up leaks on the inner wall.

To obtain greater sensitivity, a piezoelectric-crystal sensor is coupled to the outer wall of the vacuum jacket (Figure 2b). A coupling fluid, which could be soap and water, is used to improve contact between the probe and fixture. The signal is passed through a low-noise amplifier, is filtered, and then

(continued next page)

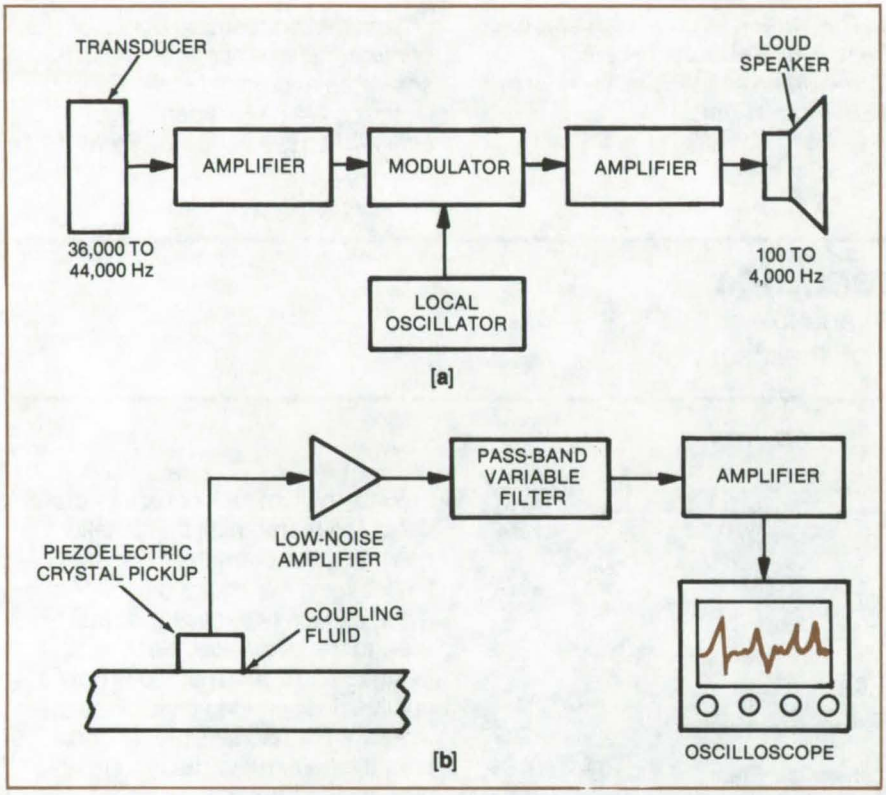

Figure 2. **Two Detection Circuits Can Be Used** with the ultrasonic probe. In (a), the ultrasonic signal is mixed with that from a local oscillator to generate an audio signal. This technique requires no direct coupling to the jacket outer wall but is less sensitive than the circuit in (b), which uses a saturated amplifier to display the detected signal on a CRT. With this system, leaks through orifices as small as 0.0015 in. (0.038 cm) can be detected within a 2-in. (5.08-cm) radius.

is amplified a second time. The final signal is displayed on an oscilloscope. The signal can be maximized by operating the second amplifier above its saturated level. With this system, leaks through orifices as small as 0.0015 in. (0.038 cm) were located within a 2-in. (5.08-cm) radius in mockup fluid lines.

The ultrasonic signal is optimized by introducing gas at low pressure into the vacuum jacket to increase turbulence and the coupling between the vibrations and the outer wall. In the test system, the fluid line was pressurized to several atmospheres, and atmospheric pressure was maintained in the vacuum jacket.

This work was done by Robert M. Heisman, William F. Iceland, and Andrew R. Keir of Rockwell International Corp. for **Johnson Space Center.** *For further information, Circle 47 on the TSP Request Card.*
MSC-16803

Cryogenic Liquid-Level Detector

Continuous reading sensor and signal conditioner accurately detect liquid levels under adverse conditions.

Marshall Space Flight Center, Alabama

A cryogenic liquid-level detector used in the Space Shuttle propellant-loading system should be useful in the handling and storage of cryogenic liquids for other applications. The continuous capacitance sensor and analog-signal conditioner, in an improved version of a design used in the Saturn 1B rocket stage, give an accuracy of 0.75 in. (1.91 cm) when used with liquid oxygen and 1.02 in. (2.59 cm) when used with liquid hydrogen. The improved detector has been designed for quick assembly, fast response, and good performance under vibratory stress. Its basic parallel-plate open configuration can be adapted to any length and allows its calibration scale factor to be predicted accurately. When compared with discrete level sensors, the continuous reading sensor was found to be superior if there is sloshing, boiling, or other disturbance.

A cross section of the sensor, showing its electrodes and spacer structure, is seen in Figure 1. A grounded guard circuit is provided in each spacer by an eyelet that is spring-loaded against the stud. The stud in turn is grounded to the sensor guard. The center electrode is designed with window cutouts between the studs that compensate for nonlinearity caused by the electrode spacers. This design gave a nonlinearity of 0.04 in. (0.10 cm) or better over most of the length of the unit used in the Shuttle application. Fringing effects increased the nonlinearity to 0.2 in. (0.51 cm) near the ends. The instability caused by vibration at 0.05 and 0.2 g^2/Hz from

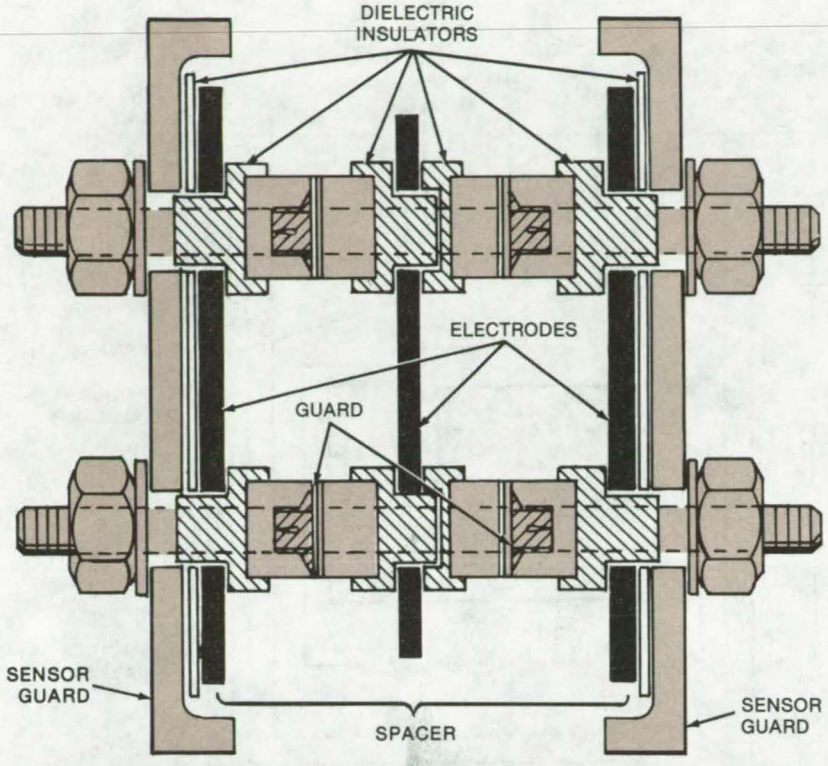

Figure 1. Spacer structure for the **Cryogenic Level Sensor** allows quick assembly and prevents stress buildup during low-temperature operation. The spacers are positioned at intervals along parallel-plate electrodes.

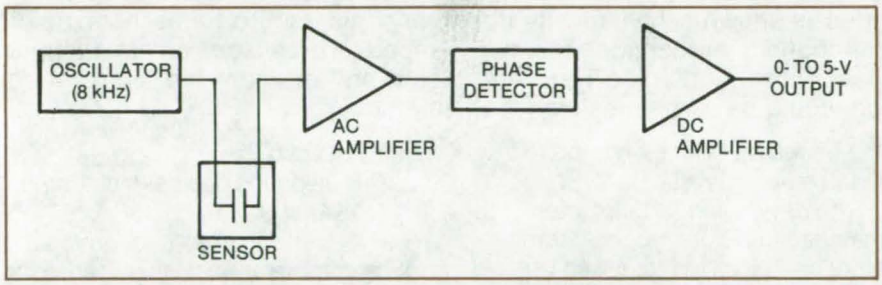

Figure 2. One of **Four Analog Signal Conditioners** tested with the sensor of Figure 1. Other circuits used (1) a different oscillator frequency, (2) a rectifier in place of the phase detector and a feedback capacitor in the ac amplifier, or (3) a bridge/feedback circuit following the ac amplifier. All gave better than 1 percent accuracy.

20 to 2,000 Hz along three mutually perpendicular axes was 0.04 percent. The maximum dynamic variation was 0.5 percent and symmetrical, allowing easy filtering.

Tests were performed with liquid nitrogen (to simulate liquid oxygen) and with liquid hydrogen. The maximum temperature instability was 0.63 percent at liquid hydrogen temperature and 0.03 percent at liquid nitrogen temperature. Temperature coeficients were 0.67 percent (hydrogen) and 0.05 percent (nitrogen). Since the sensor measures the instantaneous liquid level, a measurement of the average level, which is desirable for tanking, can be obtained by integrating and averaging the output.

Several signal-conditioner circuits were evaluated and tested; one is shown in Figure 2. It was concluded that any of the designs can yield an overall accuracy of 1 percent. The major error source for all circuits is temperature errors, which could be reduced by temperature-compensation circuits.

This work was done by John Hamlet of **Marshall Space Flight Center.** *Further information may be found in NASA TM-X-64914 (N75-19626), "Shuttle Propellant Loading Instrumentation Development," a copy of which may be obtained at cost from the New England Research Application Center (see page A7).*

MFS-23253

Measuring Cryogenic-Refrigerator Cooling Capacity

A temperature-sensing bridge determines liquid reserve level in the low-temperature heat exchanger.

Caltech/JPL, Pasadena, California

The cooling capacity of a closed-cycle helium (maser-cooling) refrigerator can be determined by applying heat from an electrical heating element mounted on the liquid-helium stage. However, any electrical power in excess of the cooling capacity of the refrigerator causes rapid heating of the refrigerator; any lesser amount allows the refrigerator to accumulate a liquid (helium) reserve and a reserve cooling capacity. Nonetheless, the refrigerator will warm up slightly, even with reserve cooling capacity. In addition, the absolute measurement of the continuous cooling capability (eliminating liquid reserve power) necessitates boiling away the liquid reserve, which would interfere with the maser operation.

(continued next page)

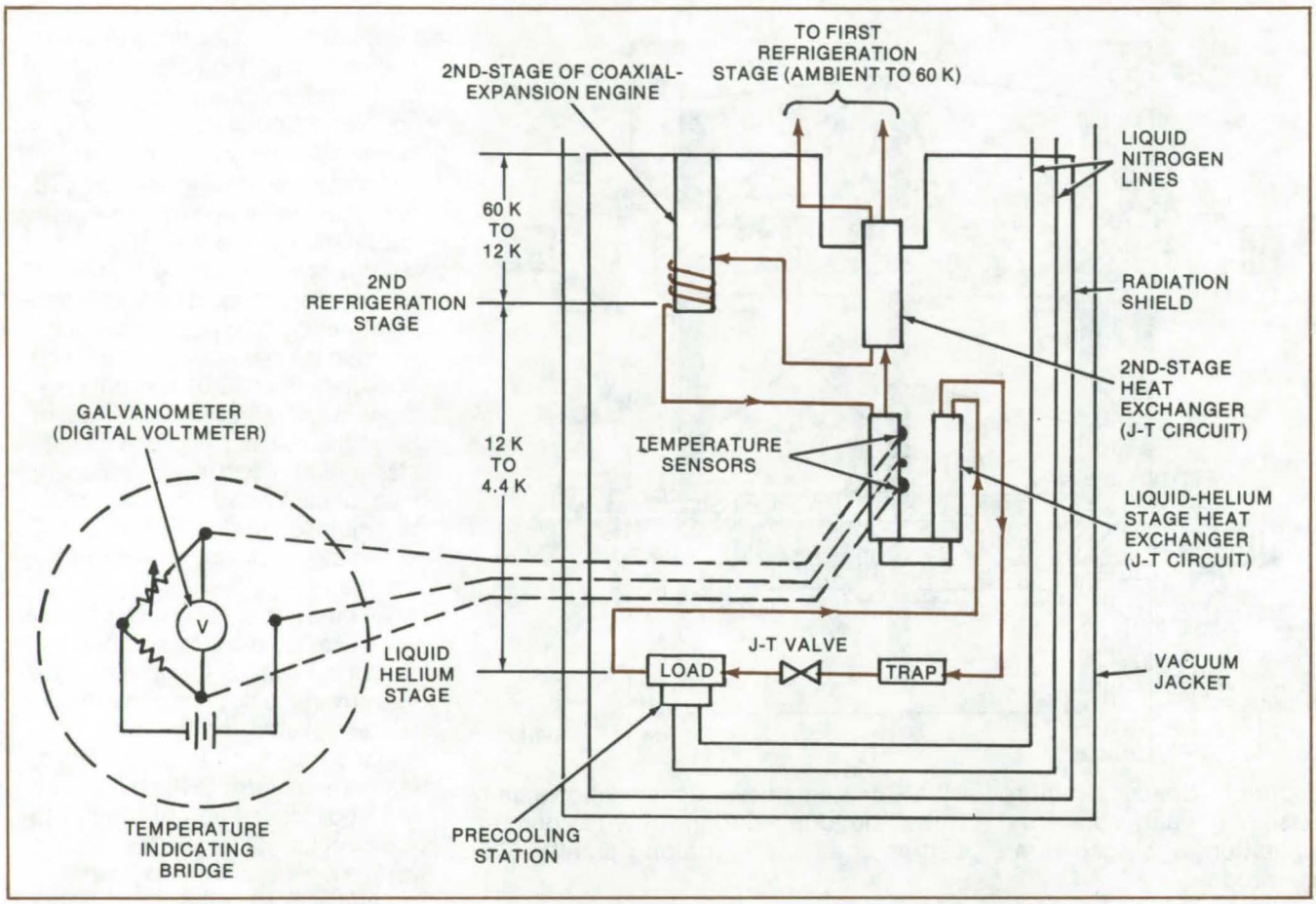

The **Temperature-Gradient Sensing Bridge** is shown schematically in the inset diagram to this schematic of the low-temperature stages of a maser-cooling refrigerator. The two temperature sensors are in thermal contact with the liquid-helium stage heat exchanger (Joule-Thomson circuit) and measure the temperature gradient along its length. These sensors could be carbon resistance thermometers.

A temperature-gradient sensing bridge avoids these difficulties. The device determines the liquid-reserve level in the final counterflow (low-temperature) heat exchanger by sensing the temperature difference along a short length of final heat-exchanger near its warmer (15 K) end. The temperature difference causes a voltage difference across the bridge that can be related to the liquid reserve level.

The device should be of interest to manufacturers of cryogenic refrigerators as well as to those who use them in conjunction with the operation of electronic equipment like masers or Josephson junctions.

This work was done by Ervin R. Wiebe of **Caltech/JPL.** *For further information, Circle 48 on the TSP Request Card.*

This invention has been patented by NASA [U.S. Patent No. 3,914,950]. Inquiries concerning nonexclusive or exclusive license for its commercial development should be addressed to the Patent Counsel, NASA Resident Legal Office-JPL [see page A8]. Refer to NPO-13435.

Vapor-Modulated Heat Pipe for Improved Temperature Control

Dryout induced by vapor throttling makes control of equipment temperature less dependent on variations in sink environment.

Ames Research Center, Moffett Field, California

A vapor-modulated heat pipe continues to provide efficient control of source temperature even when the temperature of heat sink approaches that of the source of heat. This mechanism for maintaining equipment temperature closely despite variations in the sink environment, developed for use in spacecraft and satellites, can be useful wherever ambient temperatures fluctuate widely.

The new mechanism, shown in the figure, controls the flow of vapor in the heat pipe by using a valve in

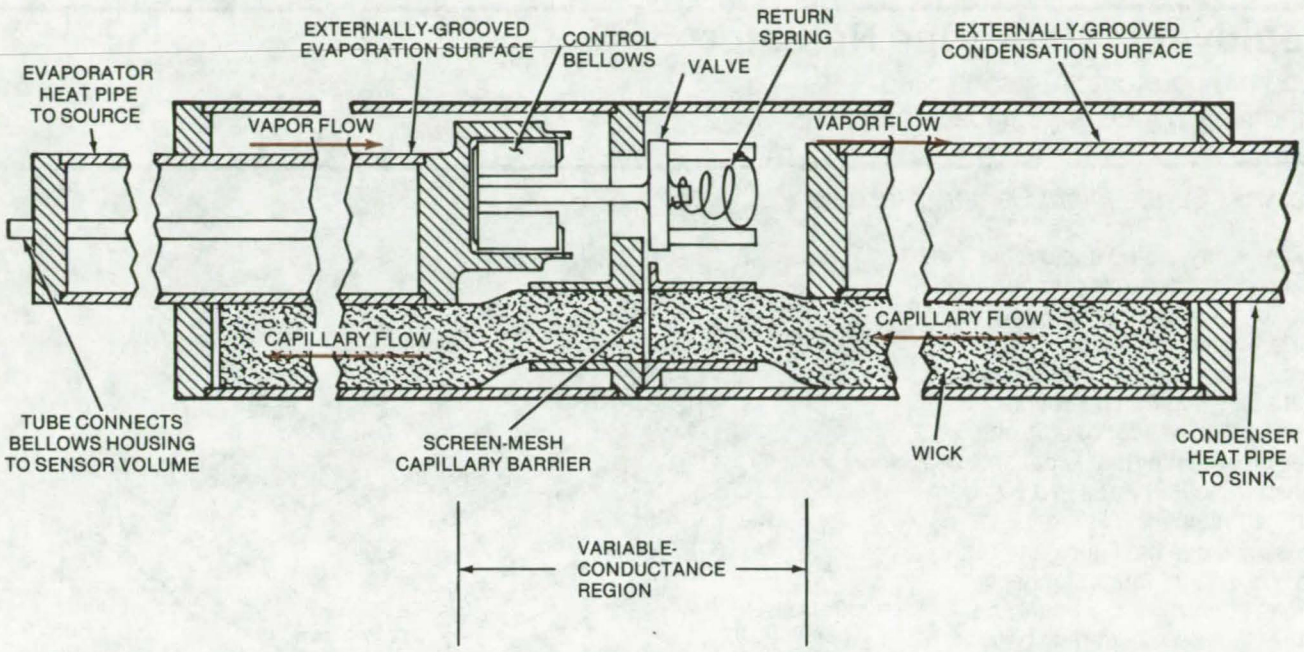

A Control Valve in the Vapor Path of the heat pipe closes to let the wick dry out when the source temperature approaches the sink temperature. The source temperature then rises again, and the valve reopens. This mechanism allows the heat pipe to control source temperature closely despite variations in sink temperature.

the return path to build a difference in pressure and also a difference in saturation temperature of the vapor. The valve is actuated by fluid expansion and contraction in a sensor bulb that is in thermal contact with the equipment to be temperature controlled. Thus, the equipment temperature is maintained closely, independent of variations in the sink environment.

When water is used as the working fluid, the vapor-modulated heat pipe is limited to applications in which the water will not freeze. However, methanol and ammonia can be used as well as water.

In a heat pipe that uses ammonia (see figure), a variable-conductance section approximately 10 inches (25 cm) long and 1 inch (2.5 cm) in diameter connects two conventional heat pipes. When the valve is fully open, liquid is evaporated from the externally grooved surface of the evaporator heat pipe. The vapor flows through the valve and condenses on the externally grooved surface of the condenser heat pipe. Thus, with the valve fully open, the two conventional heat pipes are coupled with a small temperature difference between them.

When the heat sink is colder than the source, the heat-pipe system causes the source temperature to fall until it reaches a set point. At At this point, liquid in the sensor volume, which is thermally coupled to the source, contracts and closes the valve. The vapor is throttled, and the pressure buildup on the evaporator side of the bulkhead exceeds the capillary-pressure limit of the grooves and wick. As a result, the liquid flows out of them to the other side of the bulkhead. The evaporator side dries out, and a large temperature difference is incurred between the condenser and evaporator heat pipes. The pressure buildup is large enough to "blow through" the capillary barrier consisting of a few layers of fine-mesh screen that separates the wicks at the bulkhead. Blowthrough does not affect performance because by the time it occurs, the wick structure on the evaporator side is dried out. The capillary barrier reestablishes isolation before the pressure difference is low enough to allow the wick to rewet.

With the valve closed then, the overall conductance of the system is low, and the heat source increases in temperature. When it rises above the set point, liquid in the sensor volume expands, and the valve opens. With the pressure relieved, the wick and grooves become wet again, and high conductance between the source and sink is reestablished. The source then begins to cool, and the cycle repeats. In steady state, the valve closes just enough to produce a partial dryout that achieves the required temperature drop.

This work was done by Donald K. Edwards, James E. Eninger, and Edward E. Ludeke of TRW, Inc., for **Ames Research Center.** *For further information, including the details of valve design and operation, Circle 49 on the TSP Request Card.*

Inquiries concerning rights for the commercial use of this invention should be addressed to the Patent Counsel, Ames Research Center [*see page A8*]. *Refer to ARC-11001.*

Deployable Heat-Pipe Radiator

Loop temperatures are controlled effectively under varying load conditions.

Marshall Space Flight Center, Alabama

A recently-tested deployable heat-pipe radiator controls pumped-fluid loop temperatures under varying loads. It has an aluminum panel containing variable-conductance heat pipes that can be coupled to either a fluid header or a flexible heat-pipe header that is capable of transporting 850 watts in a 90° bent configuration.

As shown in the figure, the radiator consists of four detachable pieces of hardware: a heat-pipe panel, a flexible heat-pipe header, a heat exchanger, and a fluid header. The panel contains six L-shaped longitudinally-grooved aluminum heat pipes; the long condenser leg is adhesively bonded to the panel, and the short evaporator leg is clamped to the fluid or heat-pipe header. Flats across the pipes are the thermal-contact interface for the clamped connections to the header. The area of control is increased by jogging the evaporator section in the middle so that two consecutive evaporator sections can be clamped side by side on the header. Stainless-steel reservoirs are welded to each pipe through an aluminum/stainless-steel transition piece. Valved charge tubes are used in place of a permanent seal to allow single-fluid or variable-conductance heat-pipe (VCHP) operation.

The flexible heat-pipe header consists of an evaporator section (an aluminum tube), a flexible transport section (a stainless-steel bellows hose assembly overwrapped with wire braid and designed for a 90° inside bend radius), a condenser section (a thick-walled aluminum tube), and a stainless-steel reservoir welded to the condenser.

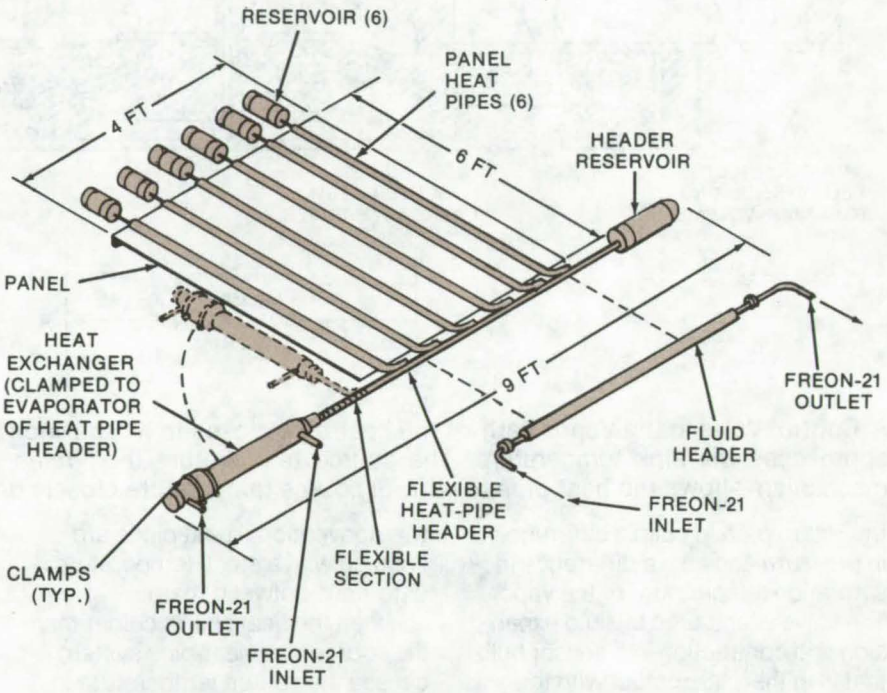

A **Deployable Heat-Pipe Radiator** has four separate pieces of hardware: a heat-pipe panel, a flexible heat-pipe header, a heat exchanger, and a fluid header. Single-fluid transport capacities of about 850 watts, corresponding to 51,000 watt-inches, have been achieved in a 90° bend orientation of the heat-pipe header.

The heat exchanger is a two-piece aluminum clamshell design that clamps over the circular evaporator. The heat-exchanger effectiveness between Freon 21 (or equivalent), which flows through an annular section, and ammonia vapor in the header has been estimated at over 80 percent.

The fluid header is made of aluminum and clamps directly to the six evaporators of the panel feeder pipes. The outer surface of the fluid header is identical to that of the heat-pipe header condenser; it has a flat machined surface that rests against the flats on the panel heat-pipe evaporators.

This work was done by Fred Edelstein of Grumman Aerospace Corp. for **Marshall Space Flight Center.** *For further information, Circle 50 on the TSP Request Card.*
MFS-23292

Influence of Lubricant Starvation on Mechanical Parts

Predict the effects of lubricant starvation on pressure and film thickness.

Lewis Research Center, Cleveland, Ohio

A formula has been developed for determining the effect of lubricant starvation on pressure and film thickness within the conjunction of ball bearings, gears, cams, and similar components. The formula was the result of a study to determine the complete theoretical solution of the isothermal elastohydrodynamic lubrication of fully-flooded and starved elliptical contacts. It was not until recently that the influence of lubricant starvation upon elastohydrodynamic behavior received serious consideration.

Prior to this time, it was assumed that the inlets were fully flooded. Maintaining a fluid film of adequate thickness is extremely important to the operation of machine elements. The film thickness in a starved conjunction is less than that of a fully flooded conjunction. This means that starved conjunctions have increased wear and decreased fatigue lives when compared to fully flooded conjunctions.

The formula is based on the computed area in and around the Hertzian contact. In Figure 1, the coordinate X is made dimensionless with respect to the semiminor axis b of the contact ellipse, and the coordinate Y is made dimensionless with respect to the semimajor axis a of the contact ellipse. The ellipticity parameter k is defined as the semimajor axis divided by the semiminor axis of the contact ellipse ($k = a/b$). Because of the way the coordinates X and Y are made dimensionless, the Hertzian contact ellipse becomes a Hertzian circle regardless of the ellipticity parameter. This Hertzian contact circle is shown with a radius of unity. The edges of the computing area, where the pressure is assumed to be ambient, are also denoted. The dimensionless inlet distance m, which is equal to the dimensionless distance from the center of contact to the inlet edge of the computing area, is also shown.

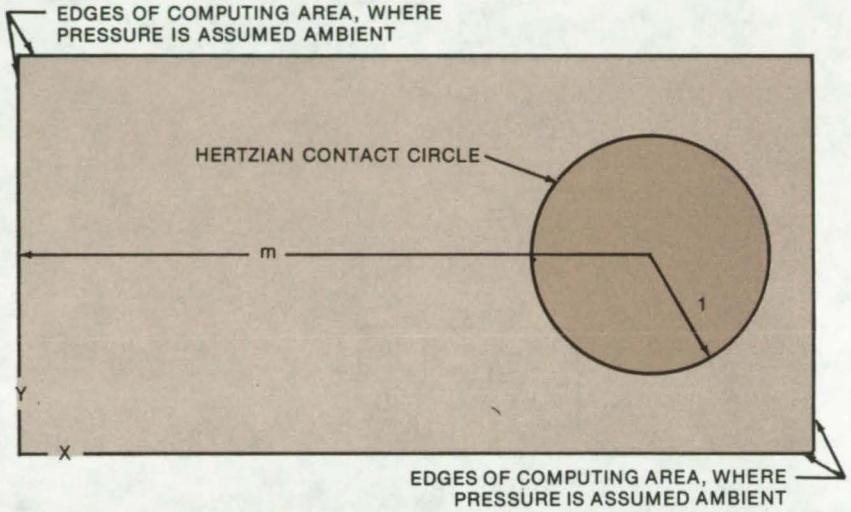

Figure 1. The Area in and Around the Hertzian Contact Circle is computed to derive a formula for determining the effects of lubricant starvation on pressure and film thickness. X and Y are dimensionless with respect to the semiminor and semimajor axes, respectively, of the contact ellipse. The contact ellipse is a circle shown here with a radius of 1. The inlet distance, m, is dimensionless.

Lubricant starvation can be studied simply by reducing the dimensionless inlet distance. A fully flooded condition is said to exist when the dimensionless inlet distance ceases to influence in any significant way the minimum film thickness. When starting from a fully flooded condition and decreasing m, the value at which the minimum film thickness first starts to change is called the fully flooded/starved boundary and is denoted by m^*. Therefore, lubricant starvation was studied by using the elastohydrodynamic lubrication point-contact theory and observing the effect of reducing the dimensionless inlet distance.

The expression for the fully flooded/starved boundary can be written as shown in Figure 2. A fully flooded condition exists when $m \geq m^*$, and a starved condition exists when $m < m^*$.

Having fully established the limiting location of the inlet boundary for the fully flooded condition, the equation defining the dimensionless film thickness for lubricant starvation conditions can be written as shown in equation (8) in Figure 2 on the next page.

Therefore, whenever $m < m^*$, where m^* is defined by equation (1) in Figure 2, a lubricant starvation condition exists, and the dimensionless minimum film thickness should be expressed by equation (8) in the text. If $m \geq m^*$, where m^* is defined by equation (1) in Figure 2, a fully flooded condition exists, and the dimensionless minimum film thickness will be obtained.

The importance of this technique is that engineers will be able to use

(continued next page)

$$m^* = 1 + 3.34\left[\left(\frac{R_X}{b}\right)^2 H_{min,F}\right]^{0.56} \quad (1)$$

where

$$b = \left\{\frac{6EF}{\pi x E'\left(\frac{1}{R_X} + \frac{1}{R_Y}\right)}\right\}^{1/3} \quad (2)$$

$$E = 1 + \frac{3R_X}{5R_Y} \quad (3)$$

$$x = 1.03\left(\frac{R_Y}{R_X}\right)^{0.64} \quad (4)$$

$$E' = \frac{2}{\left[\frac{1-\nu_A^2}{E_A} + \frac{1-\nu_B^2}{E_B}\right]} \quad (5)$$

$$\frac{1}{R_X} = \frac{1}{r_{AX}} + \frac{1}{r_{BX}} \quad (6)$$

$$\frac{1}{R_Y} = \frac{1}{r_{AY}} + \frac{1}{r_{BY}} \quad (7)$$

$$H_{min,s} = H_{min,F}\left(\frac{m-1}{m^*-1}\right)^{0.25} \quad (8)$$

Figure 2. The **Equation for a Fully Flooded/Starved Boundary** (m^*) is shown above, where r is the radius of curvature, ν is Poisson's ratio, E is the modulus of elasticity, F is the applied load, and $H_{min,F}$ is the dimensionless minimum film thickness for a fully flooded conjunction.

this equation to predict the effect of lubricant starvation on pressure and film thickness for ball bearings, gears, and cams.

This work was done by Bernard J. Hamrock of **Lewis Research Center** *and Duncan Dowson of Leeds University. Further information may be found in NASA Tech Brief "Determining Minimum Lubrication Film for Machine Parts" [LEW-12885] in this issue and in the following reports:*

NASA TN-D-8049 [N75-30565], "Isothermal Elastohydrodynamic Lubrication of Point Contacts, I — Theoretical Formulation," and

NASA TN-D-8318 [N76-33509], "Isothermal Elastohydrodynamic Lubrication of Point Contacts, IV — Starvation Results."

Copies of these reports may be obtained at cost from the New England Research Application Center [see page A7].

LEW-12884

Determining Minimum Lubrication Film for Machine Parts

Formula predicts the minimum film thickness required for fully flooded ball bearings, gears, and cams.

Lewis Research Center, Cleveland, Ohio

A formula has been developed for determining the adequate fluid-film thickness in ball bearings, gears, cams, and similar components. The formula was the result of a study to determine the complete theoretical solution of the isothermal elastohydrodynamic lubrication of fully-flooded elliptical contacts. Prior to the development of this new formula, approximation formulas were used with limited success.

Maintaining a fluid film of adequate thickness is extremely important to the operation of machine elements. An adequate fluid-film thickness will reduce wear and increase fatigue life and thereby avoid early damage to the machine elements.

This formula is based on two solids having different radii of curvature in a pair of principal planes (x and y) passing through a single point contact between the solids with no applied load. Such a condition is called "point contact" and is shown in the figure where the radii of curvature are noted by r's.

It is assumed that for convex surfaces, the curvature is positive but that for concave surfaces, the curvature is negative. The curvature sum in the x and y directions can be written as:

$$\frac{1}{R_x} = \frac{1}{r_{Ax}} + \frac{1}{r_{Bx}}$$

$$\frac{1}{R_y} = \frac{1}{r_{Ay}} + \frac{1}{r_{By}}$$

When a normal load (F) is applied to the ellipsoidal solids shown in the figure, the point expands to an ellipse with "a" as the semimajor axis and "b" as the semiminor axis. For the special case where $R_x = R_y$,

the resulting contact is a circle rather than an ellipse.

The ellipticity parameter (k) is the semimajor axis divided by the semiminor axis and is expressed in terms of the curvatures sums in the x and y directions as:

$$k = 1.03\left(\frac{R_y}{R_x}\right)^{0.64}$$

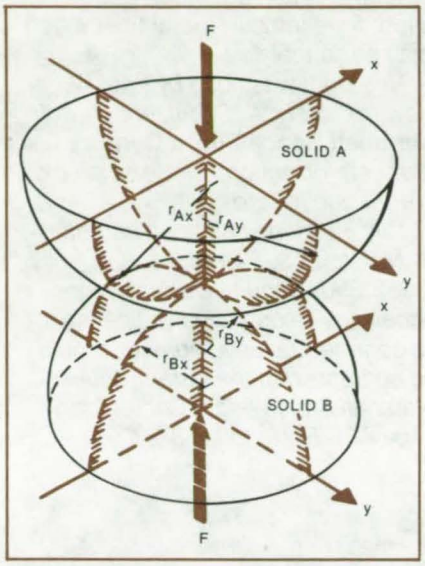

A Point Contact situation is used to derive the formula for the minimum necessary thickness of a lubricating film on machine parts. The two solids have different radii of curvature in the x and y planes that pass through their single point of contact.

The minimum film thickness in a fully flooded conjunction is a function of the ellipticity parameter (k) as well as the following dimensionless parameters:

Speed: $U = \frac{\eta_0 u}{E' R_x}$

where η_0 = atmospheric viscosity
u = surface velocity in x-direction

$$E' = \frac{2}{\left[\frac{1-\nu_A^2}{E_A} + \frac{1-\nu_B^2}{E_B}\right]}$$

ν = Poisson's ratio
E = modulus of elasticity

Load: $W = \frac{F}{E' R_x^2}$

Material: $G = \alpha E'$

where α = pressure viscosity constant.

The minimum film-thickness formula for fully-flooded elastohydrodynamic elliptical contacts can be written as:

$$H_{min,F} = \frac{h_{min,F}}{R_x} = 3.63U^{0.68}G^{0.49}W^{-0.073}(1-e^{-0.68k})$$

The importance of this technique is that engineers will be able to use this equation to predict the minimum film thickness for ball bearings, gears, and cams.

This work was done by Bernard J. Hamrock of **Lewis Research Center** *and Duncan Dowson of Leeds University. Further information may be found in NASA Tech Brief "Influence of Lubricant Starvation on Mechanical Parts" [LEW-12884] in this issue and in the following:*

NASA TN-D-7774 [N74-31951], "Numerical Evaluation of the Surface Deformation of Elastic Solids Subjected to a Hertzian Contact Stress,"

NASA TN-D-8049 [N75-30565], "Isothermal Elastohydrodynamic Lubrication of Point Contacts, I — Theoretical Formulation," and

NASA TN-D-8317 [N77-11400], "Isothermal Elastohydrodynamic Lubrication of Point Contacts, III Fully Flooded Results."

Copies of these reports may be obtained at cost from the New England Research Application Center [see page A7].

LEW-12885

Quiet Wind Tunnel

Wire mesh hushes whistling air and makes measurements more accurate.

Marshall Space Flight Center, Alabama

One advance in wind-tunnel design, the use of porous walls, has turned out to be a mixed blessing. By lining the tunnel walls with a perforated material, designers have eliminated the problem of shock-wave reflections, which distort load measurements on the aerodynamic model. However, air flowing over the sharp edges of the pores creates enough noise to influence measurements of the fluctuating pressure around the model.

A simple and inexpensive technique suppresses background noise generated by the pores and makes aerodynamic data more accurate and reliable. The porous walls are covered with a wire-mesh screen (see figure). The screen offers a smoother surface to the airflow and damps vortexes and resonance caused by the wall perforations; yet it provides enough open area for the perforations to cancel shock waves generated by the model.

The screen can be bonded to the porous wall with an adhesive or can be attached with fasteners, such as screws. The screen does not interfere with adjustments of variable-porosity walls, in which the perforated layers can be moved into or out of alinement to accommodate different mach numbers.

In a developmental model, the screen was made of woven stainless-steel wire. The mesh was 40

(continued next page)

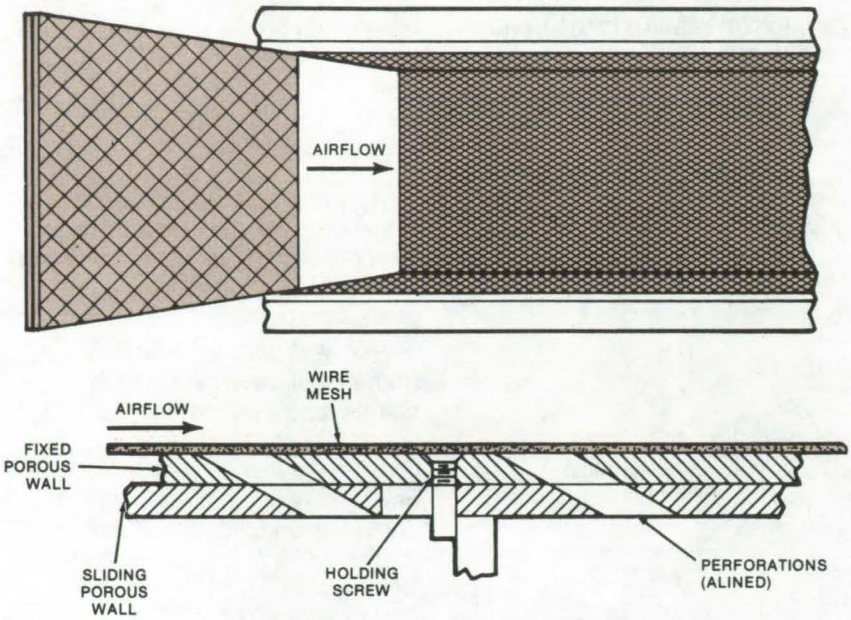

Transonic **Air Flows More Quietly** over walls lined with wire-mesh screen. The screens do not interfere with relative motion of wall sections when porosity is adjusted for different airspeeds. Here, the perforations are alined for maximum porosity.

wires per in. (approximately 16 wires per cm); wire diameter was 0.01 in. (0.254 mm); mesh opening was 0.015 in. (0.381 mm), for an open area of 36 percent. Materials other than stainless steel may be used; for example, metal fiber mesh may be suitable.

This work was done by Paul W. Howard and L. A. Schutzenhofer of **Marshall Space Flight Center.** *For further information, Circle 51 on the TSP Request Card.*

This invention has been patented by NASA [U.S. Patent No. 3,952,590]. Inquiries concerning nonexclusive or exclusive license for its commercial development should be addressed to the Patent Counsel, Marshall Space Flight Center [see page A8]. Refer to MFS-23099.

"Either-Side-Up" Inflatable Liferaft

Easy access, safety features, and economical fabrication make this one-man liferaft ideal for many applications.

Langley Research Center, Hampton, Virginia

A new one-man inflatable liferaft can be thrown into the water and boarded, regardless of which side falls up. The new raft, which incorporates several additional safety and convenience features, is designed for simplicity. As such, it should be economical to manufacture and easy to use.

The "both-sides-up" feature is made possible by positioning the floor midway between the top and the bottom of the inflatable float tube. As shown in the figure, the raft is symmetrical about a horizontal plane through its midheight and can be ridden on either side.

Another interesting feature is a zippered entry door through the floor. On most rafts a portion of the inflatable tube is tapered, so that it is lower and one can more easily climb over the side and into the raft at that point. The tapered section, however, requires special construction and adds measurably to the cost of the raft. With the much more

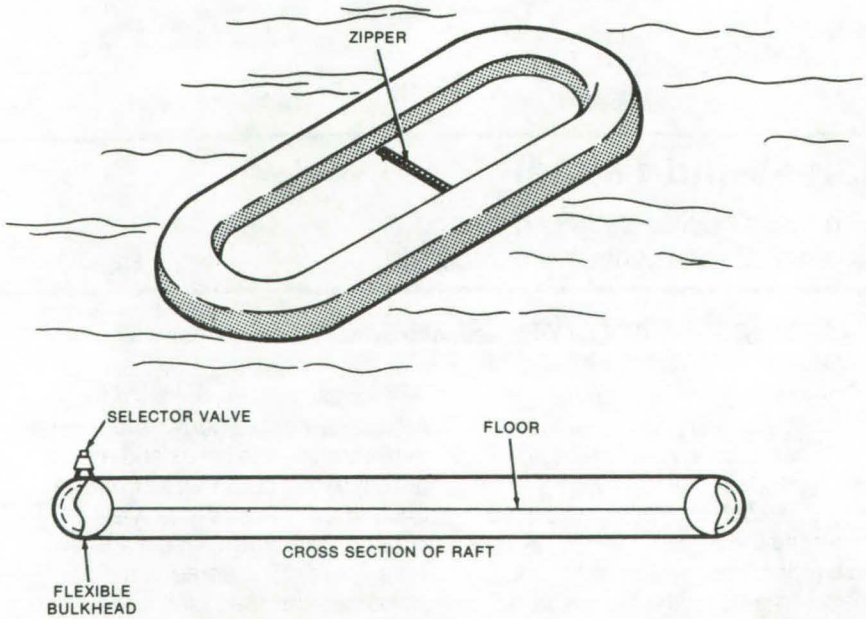

"Either-Side-Up" One-Man Liferaft can be thrown into the water without concern for how it lands. The floor is halfway between the top and bottom of the inflatable tube. A zippered door, which can be opened from either side, makes boarding easier. The double sectioned tube provides an extra margin of safety against punctures.

economically-fabricated zippered door, a swimmer can lift the raft over his head and board through the center at a point barely above water level.

Finally, the raft is made safer by a double-tube flexible bulkhead construction in the float. The inflatable tube is divided into two parallel tubes by a bulkhead that runs around the circumference of the raft. The bulkhead is flexible and has enough extra material so that if one wall is punctured, the bulkhead can be expanded to a single tube of the original size.

The selector valve for inflation allows either or both sections to be inflated, and an extra cartridge can be carried to reinflate the raft in the event one wall is punctured.

This work was done by Ernest J. Soter of **Langley Research Center.** *Further information may be found in the patent [U.S. Patent No. 3,781,933] and may be purchased for $0.50 from the U.S. Patent Office, Washington, D.C. 20231.*

This invention has been patented by NASA. Inquiries concerning nonexclusive or exclusive license for its commercial development should be addressed to the Patent Counsel, Langley Research Center [see page A8]. Refer to LAR-10241.

Computer Programs

These programs may be obtained at very reasonable cost from COSMIC, a facility sponsored by NASA to make new programs available to the public. For information on program price, size, and availability, circle the reference letter on the COSMIC Request Card in this issue.

Automated Predesign of Aircraft

Design of box-beam structures

APAS III (Automated Predesign of Aircraft Structure) uses a multistation structural-synthesis to size and design box-beam structures for transport aircraft. The program optimizes static strength and scales up to satisfy fatigue and fracture criteria. It has multimaterial capability and a library of materials properties, including advanced composites. APAS III can be used to evaluate the impact on the weight of variables such as materials, types of construction, structural configurations, minimum gage limits, applied loads, fatigue lives, crack-growth lives, initial crack sizes, and residual strengths.

Up to six external static-strength loading conditions can be input. Each condition consists of a set of 3 forces and 3 moments for up to 20 stations along the structure. Any convenient reference axes may be adopted. Internal computations automatically transfer the loads to the section elastic axis. The internal distribution of loads is calculated by a multicell box-beam analysis subroutine. Shear and bending stresses are found by assuming that plane sections remain plane. Torsional moment and direct shear can have prescribed distributions.

The geometry is defined by discrete nodes on the contour of the surface. The structure is represented by structural panels that join adjacent nodes. A variety of construction types are available to the user, including various integral and builtup skin-stiffener panels and metallic and advanced-composite faced sandwich panels. With a special symmetry-grouping feature, the user can constrain selected panels to be alike. Thus, advantage is taken of the fuselage center-plane symmetry and of cases where adjacent panels are identical.

The user may choose from a library of materials in the program or input properties for materials not in the program. A maximum of three metallic materials and three composite materials may be used simultaneously.

The program calculates margins of safety, using the internal stresses due to the applied loads and the allowable stresses. The allowable stresses for static strength are calculated, using buckling, crippling, and net-tension analyses. The allowable stresses for the fatigue, crack-growth, and residual-strength criteria are calculated, using Miner's analysis and fracture mechanics. The stress spectra for these analyses are generated at each analysis station, using the flight profile for a medium-range, large, commercial transport.

The optimization procedure for static strength is a two-step process that proceeds systematically from one rib or frame location to another. In the first step of the synthesis process, initial sizes of structural members are adjusted iteratively until each element has a zero margin of safety for at least one loading condition or until a minimum-gage constraint is encountered. In the second step, the margins of safety are maximized by changing element geometry and holding structural weight constant. Using the new design as the initial design, the two steps are repeated until the design converges.

This optimized design is then successively checked for the fatigue, crack-growth, and residual-strength criteria. If any criterion is not met, the structure is scaled up in size, and a new pass is made through the static-strength, fatigue, crack-growth, and residual-strength analyses. This procedure is repeated until all criteria are met.

A Fletcher, Powell, Davidon technique is used to maximize the margin of safety, rather than to minimize the weight, to allow constrained-function optimization methods to be used. With this approach, structural-member sizes can be constrained within practical limits of material sizes and manufacturing capability, multiple failure modes can be taken into consideration for each structural element, and positive margins of safety can always be maintained.

This program is written in FORTRAN and uses the CDC FIN OVERLAY feature. The program has been implemented in a CDC 6000-series computer with a central

(continued next page)

memory requirement of approximately 56K (octal) of 60-bit words.

This program was written by Clarence C. Poe, Jr., of **Langley Research Center** *and G. S. Kruse, C. J. Tanner, and P. J. Wilson of General Dynamics. For further information, Circle B on the COSMIC Request Card.*
LAR-12258

Thermal Hydraulic Analyzer

Solves separate or combined thermal and hydraulic problems

The Thermal Hydraulic Analyzer Program (THAP) solves thermal, hydraulic, or combined thermal and hydraulic problems. It can handle transient and steady-state thermal problems, steady-state hydraulic problems, and combined thermal/hydraulic transient or steady-state problems. A physical system of interest is approximated to most any degree of accuracy with a lumped-parameter representation, using elements provided by the program.

Any complex thermal/hydraulic system can be modeled by proper synthesis of program elements connected between nodes. Elements are provided to handle conduction, radiation, heat inputs, line pressure drops, pumps, flow-rate inputs, film conduction, fluid-motion heat conduction, and fluid-flow heat capacity. The dependent variables (temperature and/or pressure) are calculated at the nodes between elements. Material properties or fluid properties can be input by means of curves. A variables block allows the user to do unique calculations and testing, using the program parameters, program keywords, and curve data. The output block allows particular outputs to be printed selectively, including graphics when using CRT's.

Several innovative techniques make this program more accurate and less costly to run. The one-and-a-half "Step Method" has been developed for steady-state iterative solution of both thermal and hydraulic problems. The methods use next-neighbor nodes for those already calculated in the current iteration and next-neighbor plus next-to-next-neighbor nodes for those nodes not yet calculated in this iteration. This allows the errors to be reduced much more rapidly throughout the steady-state network. Convergence time is likewise reduced.

A forward option for thermal fluid-flow transient problems allows time-increment steps to 100 times the fluid-flow time between adjacent nodes with less than 5 percent error in the results. Additional techniques include the alternating-direction method for the thermal-transient calculation and the matrix method for the steady-state hydraulic solutions. The matrix method can also be used as the first approximation to the nonlinear steady-state hydraulic equations, followed by use of the iterative method until convergence occurs. Many non-branched pipes can be combined into a larger pseudoelement to reduce significantly the computer time required to balance the hydraulic system.

The user's input defines the thermal/hydraulic model, initial conditions, and control information. The objective has been to make the input as natural, simple, and compact as possible, thus to reduce input errors and the number of document references required.

This program is written in FORTRAN and IBM OS Assembler. It has been implemented on an IBM 370 computer with a central memory requirement of approximately 390K 8-bit bytes.

This program was written by Thomas C. Core, Erculano E. Garcia, and Donald Jelinek of Rockwell International Corp. for **Johnson Space Center.** *For further information, Circle C on the COSMIC Request Card.*
MSC-16797

Optimizing Simulated Trajectories

Six-DOF program for flight mechanics

POST (6 DOF), a general-purpose rigid-body six-degrees-of-freedom program, can be used to solve a wide variety of atmospheric flight mechanics and orbital transfer problems. Written for the analysis of powered or unpowered vehicles operation near a rotating oblate planet, typical applications of POST (6 DOF) include:

- Guidance and flight-control system simulation and analysis,
- Loads and dispersion-type analysis,
- General-purpose six-degrees-of-freedom simulation of controlled and uncontrolled vehicles, and
- Six-degrees-of-freedom performance validation.

POST (6 DOF) features a NAMELIST-type input feature that significantly reduces input deck setup time (and cost); it is readily used by trajectory engineers without specialized training in such areas as systems programing and optimization theory. This program is also capable of using general-purpose discrete-parameter targeting and optimization to solve a broad spectrum of problems related to the impact of the control system design on the performance characteristics of aerospace vehicles.

The basic simulation flexibility is achieved by decomposing the trajectory into a logical sequence of simulation segments. These trajectory segments, referred to as phases, enable the trajectory analyst to model both the physical and the nonphysical aspects of the simulation accurately and efficiently. By segmenting the mission into phases, each phase can be modeled and simulated in the manner most appropriate to that particular flight regime. For example, the planet model, the vehicle model, and the simulation options can be changed in any phase to be compatible with the level of detail required in that phase.

Every computational routine in the program can be categorized according to five basic functional elements: the planet model, the vehicle model, the trajectory simulation model, the auxiliary calculations module, and the targeting and optimization module. The planet model comprises an oblate spheroid model, a gravitational model, an atmosphere model, and a winds model. These models define the

environment in which the vehicle operates. The vehicle model comprises mass properties, propulsion, aerodynamics and aeroheating, an airframe model, a navigation and guidance model, and a flight-control system model. These models define the basic vehicle simulation characteristics.

The trajectory simulation models are the event-sequencing module that controls the program cycling, table interpolation routines, and several standard numerical-integration techniques. These models are used in numerically solving the translational and rotational equations of motion. The auxiliary calculations module provides for a wide variety of output calculations. For example, conic parameters and range calculations are among the many output variables computed.

The targeting and optimization module provides a general discrete-parameter iteration capability. The user can select the optimization variable, the dependent variable, and the independent variables from a list of more than 400 program variables. An accelerated projected gradient algorithm is used as the basic optimization technique. This algorithm is a combination of Rosen's projection method for nonlinear programing and Davidon's variable metric method for unconstrained optimization. In the targeting mode, the minimum norm algorithm is used to satisfy the trajectory constraints. The cost and constraint gradients required by these algorithms are computed as first differences calculated from perturbed trajectories. To reduce the costs of calculating numerical sensitivities, only that portion of the trajectory influenced by any particular independent variable is reintegrated on the perturbed runs. This feature saves a significant amount of computer time when targeting and optimization are performed.

POST (6 DOF) is written in FORTRAN IV and has been implemented on a CDC 6000-series computer with a central memory requirement of approximately 107K (octal) of 60-bit words. A key feature of POST (6 DOF) is an easy-to-use NAMELIST-type input procedure. This feature significantly reduces input deck setup time (and cost).

This program was written by G. L. Brauer, A. R. Habeger, and R. Stevenson of Martin Marietta Corp. for **Langley Research Center.** *For further information, Circle D on the COSMIC Request Card.*
LAR-12089

Transonic Flow About Airfoils

Viscous analysis for speeds near that of sound

A new program analyzes airfoils that permit transonic flow for subsonic free-stream mach numbers. The term transonic refers to aircraft speeds less than the speed of sound but close enough so that on the top of the wing, where airflow is the fastest, the mach number becomes greater than 1. For aircraft designed to fly near the speed of sound, it is desirable that these supercritical wing sections be designed such that the transonic flow is shockless or that the shock wave be as weak as possible. This program should be of aid in the design phase of a new airfoil and in the analysis of existing airfoils.

The program was first developed for off-design analysis of supercritical airfoils, but it can be used as a stand-alone program to analyze the flow field about any airfoil. It calculates weak solutions of equations of motion that include one or more isentropic shocks. The flow equations, including a semiempirical turbulent boundary-layer correction, are solved by a rotated finite-difference scheme in a more-or-less arbitrary curvilinear-coordinate system. This allows the prediction of shock waves as far back on the airfoil as desired. Inputs are the airfoil geometry (coordinates) and one or more sets of prescribed mach numbers and angles of attack. Outputs are the flow field about the airfoil.

The program has yielded results that agree very well with experimentally obtained data. Recently the analysis results have been compared to schlieren photographs with very suitable agreement. The program provides numerical and plotted output for further processing.

This program is written in FORTRAN IV for the CDC 6000-series computer and has a core requirement of approximately 113K (octal) 60-bit words. The program can use a tape drive to stop and later restart a flow calculation. If plotted output is requested, a CALCOMP Plotter is required. Experimental data can be included on the pressure distribution plot for comparison with the theoretical results.

This program was written by Frances Bauer, Paul Garabedian, Anthony Jameson, and David Korn of New York University for **Langley Research Center.** *For further information, Circle E on the COSMIC Request Card.*
LAR-12265

Design and Analysis of Supersonic Aircraft

Package of modular programs is relatively easy to use.

An integrated system of computer programs, developed for the design and analysis of supersonic configurations, uses linearized-theory methods to calculate surface pressures and uses supersonic area-rule concepts in combination with linearized theory to calculate aerodynamic force coefficients. The programs are easily used for design and analysis and include constraints on linear theory methods to provide physical realism. The package should prove useful for any type of supersonic configuration.

The integrated system consists of an executive "driver" and seven basic computer programs including a geometry input module. The individual modules provide data for configuration design or analysis. Skin friction is computed using turbulent flat-plate theory. Wave drag is calculated with either far-field (supersonic area rule) or near-field (surface pressure integration) methods. The far-field method is

(continued next page)

used for wave-drag coefficient calculations and for fuselage optimization according to area-rule concepts.

The near-field method is used primarily as an analysis tool where detailed pressure distributions are of interest. Lifting pressure, drag due to lift, pitching moment, and trim drag are computed from the lift analysis program, which breaks arbitrary wing/fuselage/canard/nacelles/horizontal-tail configurations into a mosaic of "Mach-box" rectilinear elements that are employed in linear theory solutions. A complementary wing-design and optimization program solves for the wing shape required to support an optimized pressure distribution at a specified flight condition.

A geometry module handles all configuration geometry for the system. All "paneling" of the configuration for theoretical analyses is accomplished within the programs, and the user prepares only "drawing-type" geometry specifications for input. A plot module draws configuration pictures according to size and view requests. Thus the basis of the system is supersonic linearized theory, modified with the "Whitham" correction-to-disturbance positioning being used in the propagation of body pressure fields, an optional limiting-pressure feature to control the permissible level of upper-surface pressure coefficient, and a constraint to limit the upper-surface streamwise pressure gradient.

The entire design and analysis system is a single overlaid program. The executive level of the system controls module execution by means of special identification cards in the input data. Data in the system are transferred between modules by disk storage and common blocks. The system was developed with an interactive graphic capability, but this ability was developed specific to the NASA Langley Research Center CRT display system and its associated software. This part of the system is considered inoperative in the distributed code because of the lack of supporting software.

A user may be able to revive the interactive graphics segment if they already have existing interactive graphics capabilities. The program also provides offline plotting abilities that require a Calcomp plotter. The Langley Research Center graphic library routines are provided in relocatable form as a plot library.

This program is written in FORTRAN and has been implemented on the CDC 6000-series computer with a central memory requirement of approximately 77K octal of 60-bit words.

This program was written by R. G. Coleman, J. L. Lundry, and W. D. Middleton of The Boeing Co. for **Langley Research Center.** *For further information, Circle F on the COSMIC Request Card.*
LAR-12237

Compressible Laminar Boundary-Layer Flow

Suction transition analysis for yawed wings

STAYLAM, which stands for Suction Transition Analysis of a Yawed Wing Laminar Boundary Layer, is a new program developed for the computation of the compressible laminar boundary-layer flow over a yawed infinite wing including distributed suction. These computations are useful in efforts to implement boundary-layer suction on a wing to maintain laminar flow in order to reduce net drag. Based on the current state of the art for boundary-layer computations for finite swept wings and that for transition estimates, a rigorous computation would be complex and difficult to use. Hence, STAYLAM contains a number of approximations to simplify the analysis; yet the results are accurate enough to be useful, particularly in the preliminary design phase.

STAYLAM is based on a previous program for the calculation of the incompressible laminar boundary layer and prediction of transition on an infinite sheared wing. It includes distributed wall suction and compressibility effects. To allow for discontinuous changes in the suction distribution, the boundary layer is computed by using a first-order accurate finite-difference scheme in the streamwise marching variable. The Stewartson transformation is used to account for compressibility effects. The Prandtl number is assumed to be unity, and the total temperature is assumed to be the same as the free-stream value. A further approximation in the treatment of the streamwise pressure gradient term allows the incompressible, infinite, swept-wing equations to be obtained after the Stewartson transformation. This latter approximation restricts the use of STAYLAM to speeds in the transonic range or less.

The boundary-layer results are analyzed to determine whether leading-edge instability or crossflow instability occurs. The Owen-Randall criterion is used for the crossflow instability test. The Tollmien-Schlichting instability is estimated by using a correlation of the critical Reynolds number as a function of the external pressure gradient. The point where transition is completed is estimated by the Granville correlation. Input quantities to these tests are the actual compressible values, not the incompressible values given by the Stewartson transformation.

Input to the program includes geometric description of the airfoil, free-stream information, compressibility parameters, and various parameters controlling the numerical techniques used in the program. Output includes displacement and momentum thickness, skin-friction values, and results of the transition estimates at each location on the airfoil where a boundary-layer calculation is made.

This program is written in FORTRAN IV and has been implemented on a CDC 6000-series computer with a central memory requirement of approximately 24K (octal) of 60-bit words.

This program was written by James E. Carter of **Langley Research Center.** *For further information, Circle G on the COSMIC Request Card.*
LAR-12254

Machinery

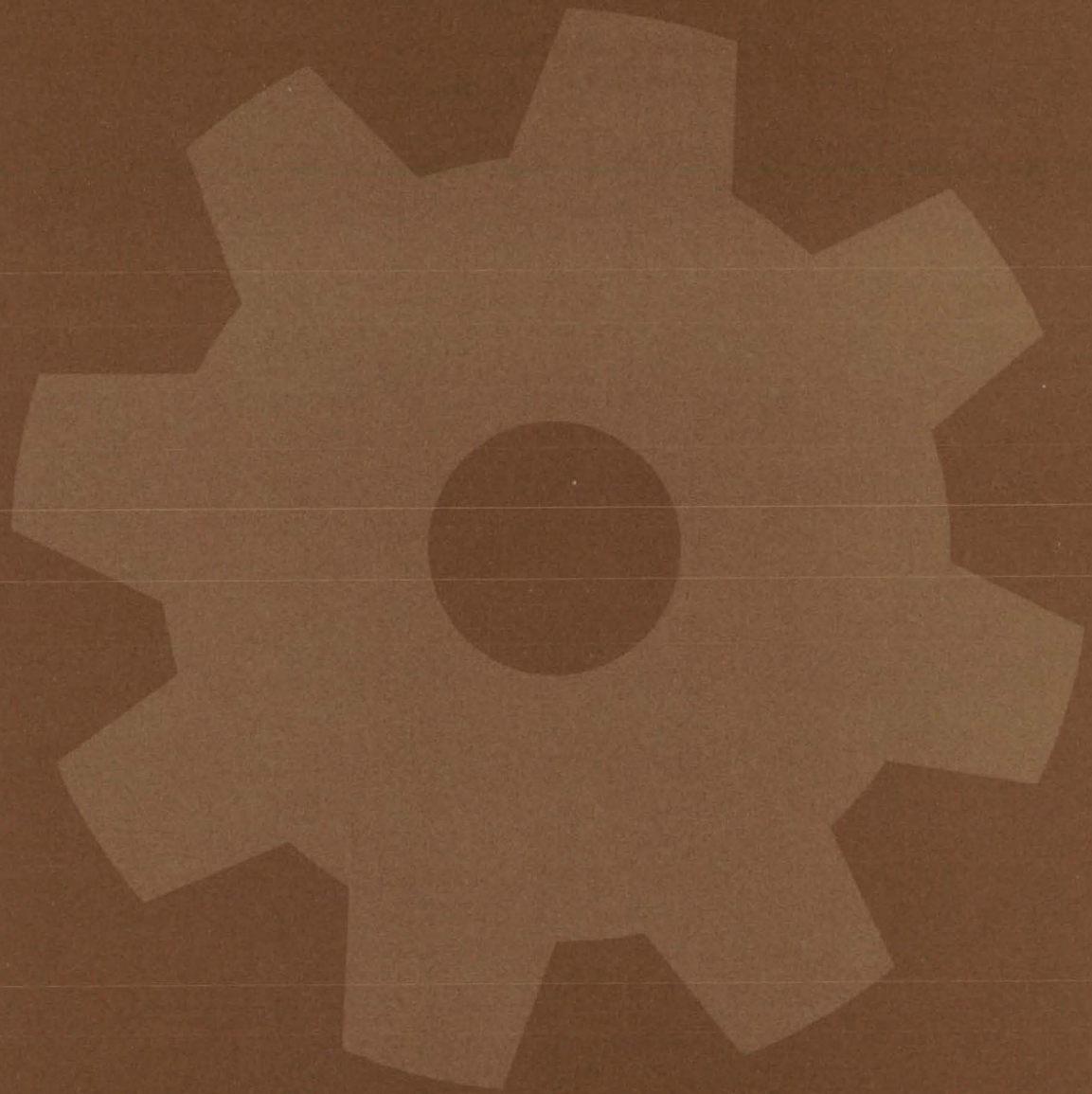

Hardware, Techniques, and Processes

Books and Reports

Foldable Beam

Triangular-truss beam folds flat
for stowage in a helical configuration.

Langley Research Center, Hampton, Virginia

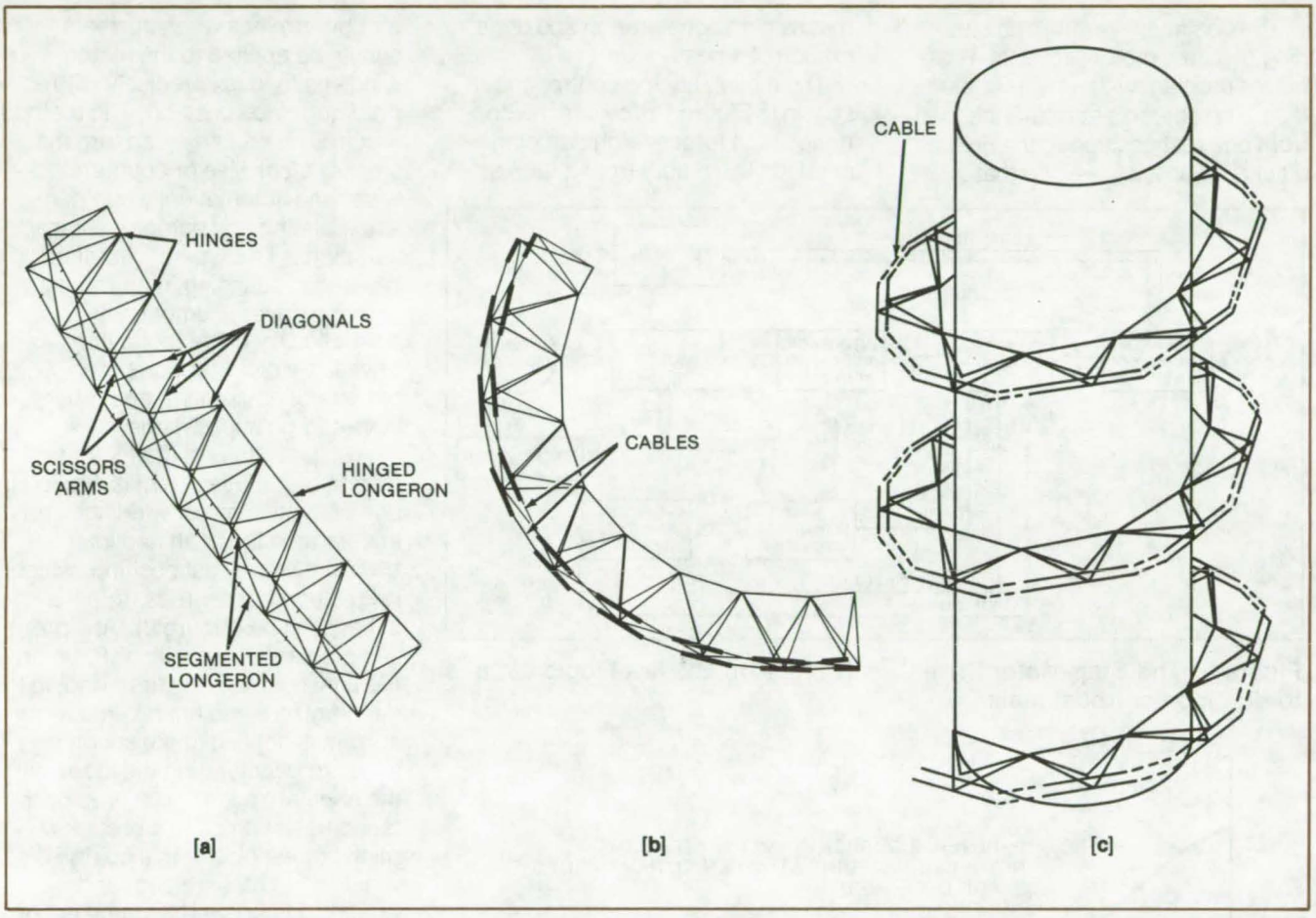

This Foldable Triangular-Truss Beam, shown in the deployed (a), partially stowed (b), and fully stowed (c) configurations, is designed for compact stowage in a helix around a circular cylinder. The beam is locked by applying tension to the cables. During stowage the segmented longerons collapse to lie adjacent to each other.

An articulated beam that becomes a rigid triangular truss when deployed, is stored by folding it flat as it is heliced about a cylinder. The beam, shown in its deployed, partially stowed, and fully stowed configurations, is composed of longerons, diagonals, and scissors arms.

On one side of the beam the longerons are hinged; on the opposite side they are segmented and have cables reeved through them. The scissors arms are attached to the segmented longerons so that when the latter separate during stowage the arms rotate, causing the sides of the beam to move next to one another. This produces a flat envelope that allows more beams to be stowed on the cylinder than would be possible if the beams did not fold flat.

The beam is deployed by retracting the cables until the segmented longerons are pulled together. The cables are loaded to lock the longerons together. The beam is stowed by releasing the tension on the cables and wrapping the beam around the cylinder.

This work was done by John V. Coyner, Jr., and John M. Hedgepeth of Astro Research Corp. for **Langley Research Center.** *For further information, Circle 52 on the TSP Request Card.*

Inquiries concerning rights for the commercial use of this invention should be addressed to the Patent Counsel, Langley Research Center [see page A8]. Refer to LAR-12077.

Step Motor Damping for High-Inertia Loads

Brushless tachometer generates signals
for moving large and varying loads precisely.

Goddard Space Flight Center, Greenbelt, Maryland

The continual starting and stopping of a step motor presents a particular problem with a high-inertia load. The object is to rotate the load from one rest position to the next as quickly as possible — and that means high acceleration and deceleration of a heavy load.

The digital/analog control circuit shown in Figure 1 provides the controlled high torque/high damping needed. The output from a tachometer determines when currents should be applied to the motor windings to index precisely with a predetermined position. The method requires no brushes, can turn the stepper clockwise or counterclockwise, and automatically compensates turning and damping for load variations. This type of circuit could be used in scanning instruments, antenna drives, numerically-controlled machine tools, film drives, x-y plotters, computer peripheral equipment, and other stop-and-go applications.

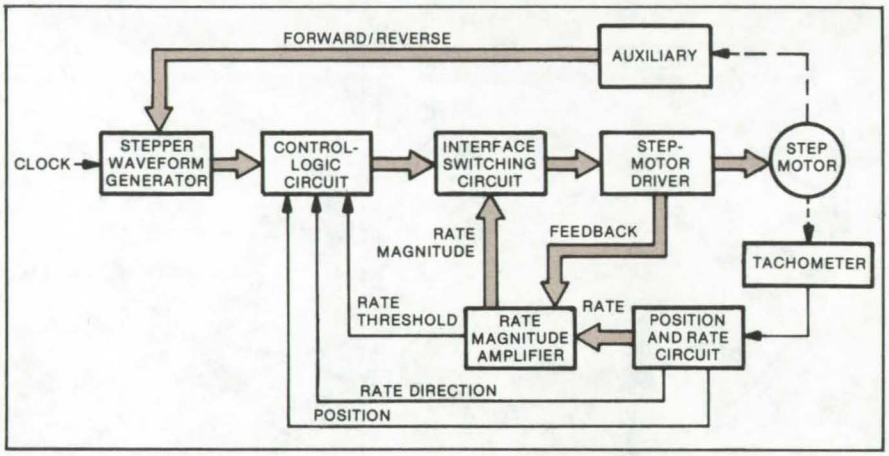

Figure 1. The **Step-Motor Drive Circuit** employs low-level logic circuits to develop control signals.

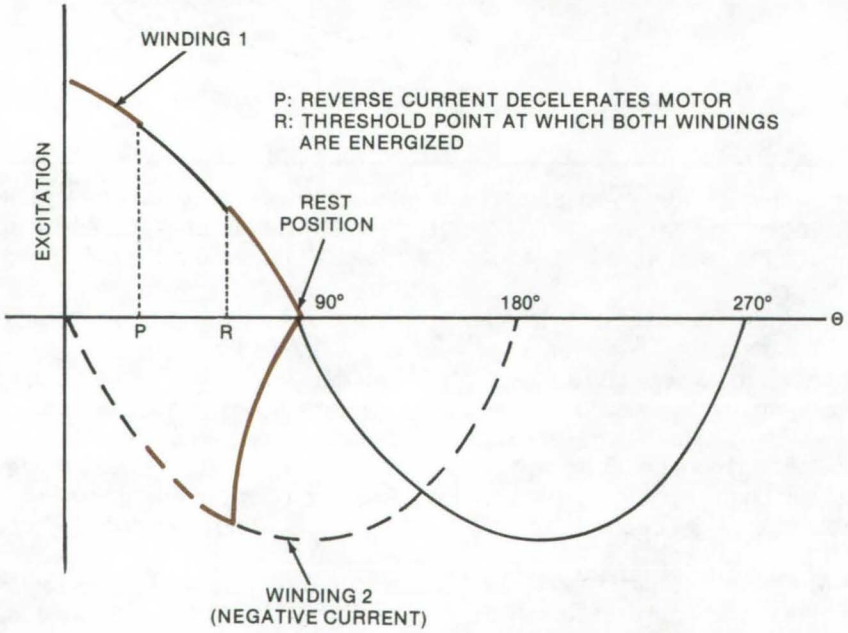

Figure 2. **Waveforms** illustrate the principle of the damping method. Full excitation on winding 1 accelerates the load until it reaches set point P; then reverse excitation on winding 2 decelerates the motor quickly for a short period. When the speed drops below a predetermined threshold, proportional damping (both windings energized) brings the load to a smooth stop.

A step starts with the motor and load at rest. Full current is applied to one of the two motor windings and accelerates the shaft and load toward the new rest position, which is 90 electrical degrees from the initial position (Figure 2). At a preselected angular position, P, before the final position, the first winding is deenergized, and full reverse current is applied to the second winding, decelerating the load until the angular speed (measured by the tachometer) drops to a predetermined threshold. At this point, R, winding 1 is reenergized, and winding 2 is allowed to come out of saturation. Winding 2 thus damps essentially proportionally, stopping the shaft at the new position.

Whether a load is heavy or light, the desired damping can be obtained by adjusting the circuit gain.

In operation, the motor step is initiated by a 50-millisecond clock pulse applied to a stepper waveform generator (Figure 1). (The clock pulse duration is long enough for the step to be completed and fully damped.)

The stepper waveform generator sends a short sequence of pulses to instruct a control logic circuit to perform its function — that is, to select the proper windings and directions of excitation to drive and damp the motor. The control logic

circuit bases its decisions on the following logic signals, derived from the tachometer:

- Rate Direction,
- Rate Threshold, and
- Position.

The control logic circuit output is applied to an interface switching circuit, which serves as the connecting link between the low-power logic circuitry and the high-power step-motor driver circuit. The direction of motion can be reversed by a logic signal from an auxiliary circuit.

This work was done by Leo J. Veillette of **Goddard Space Flight Center.** *For further information, Circle 53 on the TSP Request Card.*
GSC-11871

Self-Alining Valve Poppet and Seat

Novel design traps particles before they enter the seal area.

Langley Research Center, Hampton, Virginia

A poppet-and-seat combination, originally designed for miniature latching solenoid valves in the gas chromatograph on the Viking spacecraft, may be useful in any fluid-control system that has to operate at high temperatures with low leak rates. In conventional valves, the poppet and seat are normally mounted in line with the flow stream. During the closing cycle, the flow is abruptly stopped, and contaminants can adhere to the surfaces adjacent to the seal. When the poppet moves away from the seat, the adhering particles tend to be attracted onto the sealing surfaces. These particles can cause leakage after only a few cycles.

In the design shown in the figure, contaminants in the flow stream are removed before they reach the sealing surfaces by altering the direction of the flow several times before it enters the poppet-and-seat flow passage. Particles are separated and are deposited on surfaces not affecting sealing performance.

The valve has a metallic spherical seat and a nonmetallic poppet in a metallic enclosure. To eliminate excessive wear due to parts misalinement, the poppet swivels on the spherical surface of the seat. The poppet guide is provided with ample lateral clearance, allowing it to float and to seek its center on the seat during the closing cycle.

The poppet is made of a polyimide that can withstand high compressive loads and remains dimensionally stable at high temperature. In addition, polyimides are resilient and relatively soft, can accept embedded particles without destroying the sealing surfaces, and can be machined to the necessary surface finishes. Although they are permeable to helium, they are one of the least permeable of relatively-soft nonmetallic materials.

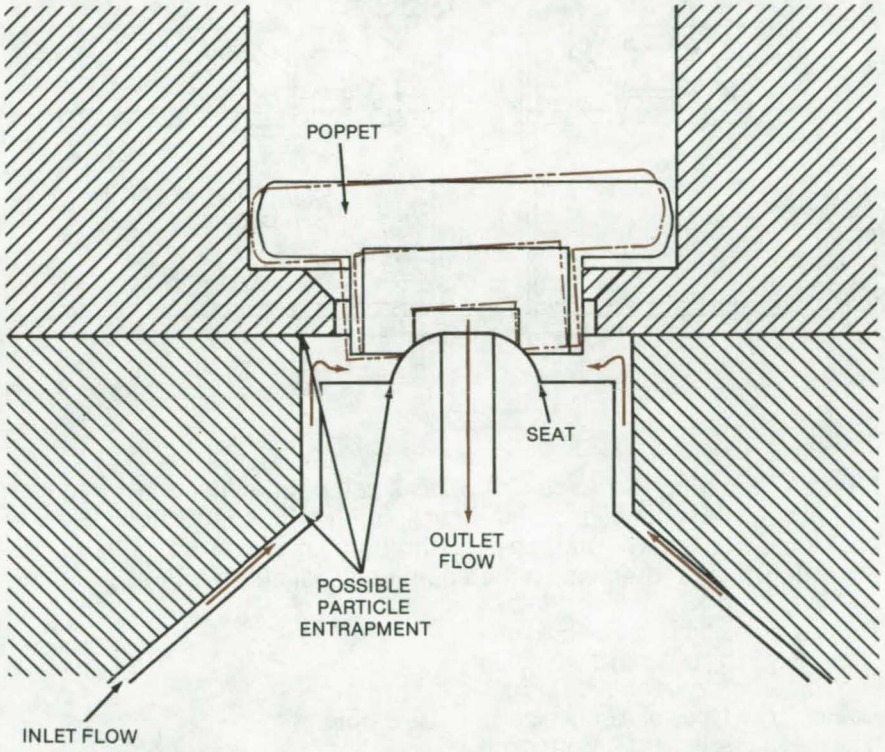

Self-Alining Poppet-and-Seat Combination is designed with several changes in direction in the inlet flow path to trap contaminants before they settle on the active seal area. The poppet has clearance to allow it to "float" and seek its center on the seat, thus preventing leaks due to misalinements.

This work was done by U.P. Olivas of Beckman Instruments, Inc., for **Langley Research Center.** *For further information, Circle 54 on the TSP Request Card.*
LAR-11623

Floating Nut for Spacecraft Applications

New nut overcomes mechanical mismatch from accumulated tolerances and maintains assembly even if mounting screw loosens.

Marshall Space Flight Center, Alabama

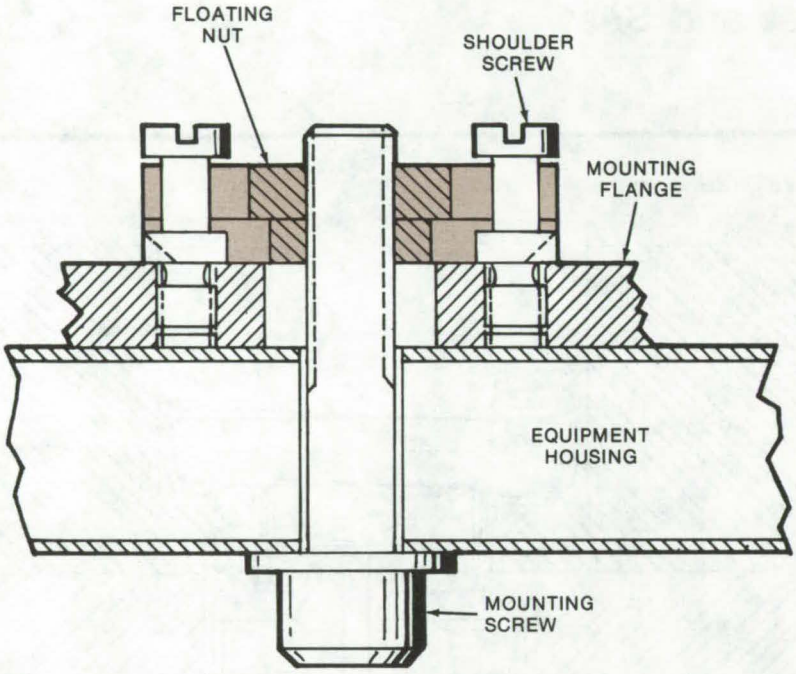

Figure 1. **Floating Nut Assembly** uses a pair of shoulder screws to lock the nut while allowing some float. The main connection is to a back-mounted screw that passes through an oversized hole in the mounting flange attached to the equipment housing.

A novel floating nut can hold an assembly in place even if the mounting screw becomes loose. This nut is useful for all types of mechanical and electronic assemblies in which accumulated tolerances can add up to a sloppy fit at the chassis side of the equipment. In the case of stacks of electronic assemblies, for instance, individual mounting-hole tolerances can add and subtract so that screw-mounting them to a less flexible structure (e.g., a cabinet or honeycomb deck) requires the floating nut.

As shown in Figure 1, the main structural connection is made with a back-mounted screw that passes through an oversized hole in the mounting flange attached to the equipment housing. The nut is rectangular, and is slotted to accommodate a pair of shoulder screws as shown in Figures 1 and 2. Each of these screws has two shoulders — one to rest on the top of the rectangular nut, and the other to slide in a groove cut into the bottom of the nut. The threaded portion of the shoulder screw enters the mounting flange on the equipment housing.

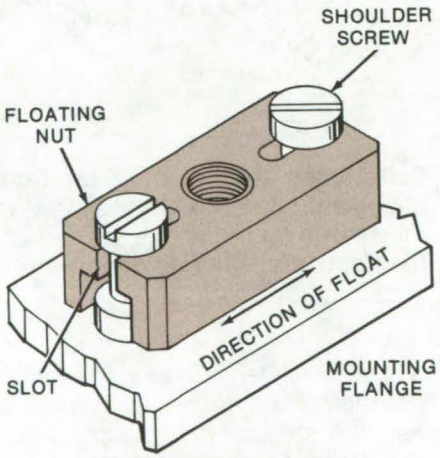

Figure 2. **Slots** in the rectangular floating nut allow it to move relative to the shoulder screws for alinement with the mounting screw (Figure 1).

Thus, while the mounting screw is relatively inflexible, the floating nut that secures the equipment to it, via the mounting flange, can be moved laterally to accommodate the accumulated tolerances. Furthermore, if for some reason the mounting screw should become loose, the shoulder screws will keep the nut assembly in place because the rectangular nut cannot turn any further than the bottom shoulders allow it. In fact, the nut will tend to lock onto the bottom shoulders.

To facilitate further a reliable connection, the nut and screws can be painted with a bonding agent to insure a lock. If the assemblies are to be removed a number of times, the nut and screws can be made of steel to reduce wear and tear on the threads and the risk of faulty threads.

This work was done by Lawrence J. Ell and Robert B. Mathewson of TRW, Inc., for **Marshall Space Flight Center.** *For further information, including detailed parts drawings, Circle 55 on the TSP Request Card.*
MFS-23248

No-Spill Touchup Paint Container

Added part prevents spillage if can is overturned.

Lyndon B. Johnson Space Center, Houston, Texas

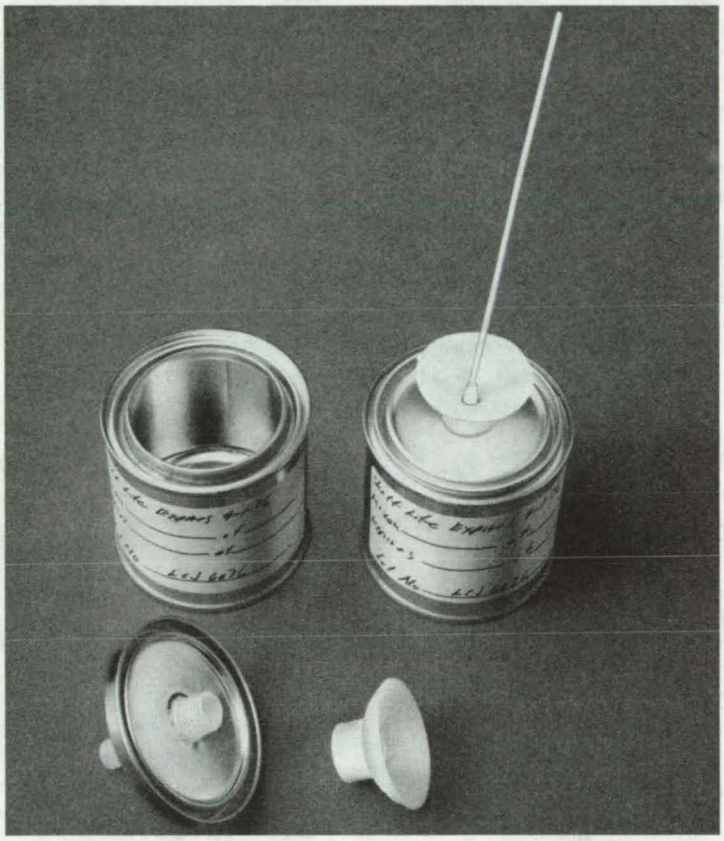

No-Spill Touchup Paint Container has a two-piece threaded device that is installed in a hole in a standard metal lid. In addition to preventing spillage, the device provides a better brush support and wiper edge.

Small paint cans used for touchup painting can be easily converted to "spillproof" containers. By screwing a spout made from readily available hardware into the lid of the can, a touchup brush can be inserted, yet the paint will not spill if the container is tipped over. The spout is simple enough to be made in most shops and should also be of interest as a consumer product.

The two-piece threaded device is installed in a hole in a standard metal lid, as shown in the figure. The central tubular part extends almost to the bottom of the container to adapt it for use with a small touchup brush. The funnel that makes it easier to dip the brush is made of a solvent-resistant plastic. (These funnels were made by adapting an existing flow nozzle.) The container not only saves cleanup cost but also reduces fire hazard and solvent loss by restricting the open area above the liquid.

This work was done by Richard L. Peters of Rockwell International Corp. for **Johnson Space Center.** *No further documentation is available.*
MSC-16269

Books and Reports

These reports, studies, and handbooks are available from NASA as Technical Support Packages (TSP's) when a Request Card number is cited; otherwise they are available from one of NASA's Industrial Application Centers or the National Technical Information Service.

Measurement of Friction and Wear

A review of tools and techniques

A report has been written that reviews the various techniques and surface tools available for the study of the atomic nature of the wear of materials. The atomic nature of solid surfaces plays an important role in the wear behavior for materials in solid-state contact.

While those solids that undergo wear can consist of a wide variety of materials both crystalline and noncrystalline, wear is most frequently encountered with crystalline solids. With elemental metals, the surface will consist of the interface between the outermost layer of atoms, which is not bound by a layer of like atoms, and the foreign medium to which the layer is exposed. For alloys, the surface may be more complex, containing a number of different elements or a particular element that, because of energy considerations, chooses to segregate at the surface.

There are a number of tools that can be extremely useful in the study of wear. They range from such unsophisticated techniques as simple chemical etching to the use of the field ion microscope with atom probe.

The surface tools, their use, and the results obtained and described in the report are: chemical etching, X-ray diffraction, electron diffraction, scanning electron microscopy,

(continued next page)

low-energy electron diffraction, Auger emission spectroscopy analysis, electron spectroscopy for chemical analysis, field ion microscopy, and the atom probe. These devices provide useful information as simple analytical tools to examine wear surfaces as well as to conduct in situ dynamic monitoring of wear studies.

Analysis of wear surfaces and the wear process with these tools has indicated the anisotropic nature of the wear process. Revealed are properties of surfaces and wear surface regions that affect wear, such as surface energy, crystal structure, crystallographic orientation, mode of dislocation behavior, and cohesive binding. A number of mechanisms involved in the generation of wear particles are identified with the aid of these tools.

The use of these surface tools has done much to help clarify basic mechanisms involved in the friction and wear behavior of materials. Continued and expanded use of these devices in the future will help to provide the necessary fundamental understanding of material surfaces, resulting in a reduction of friction and minimizing maintenance costs associated with wear.

This work was done by Donald H. Buckley of **Lewis Research Center.** *Further information may be found in NASA TM-X-73437 [N77-19901], "The Use of Analytical Surface Tools in the Fundamental Study of Wear," a copy of which may be obtained at cost from the New England Research Application Center [see page A7].*
LEW-12910

Disconnects, Couplings, Fittings, Fixed Joints, and Seals

Design criteria monograph

A design monograph has been written to organize and present significant experience and knowledge accumulated by NASA in development and operational programs. The purpose is to assist system designers. It reviews and assesses current design practices and from them establishes guides for achieving greater consistency in design, increased reliability in the end product, and greater efficiency in the design effort.

Rocket engine and space vehicle programs have utilized various kinds of disconnects, couplings, fittings, fixed joints, and seals for many purposes. The current configurations for many of these components have resulted from solutions to operational problems with earlier designs and from the need to satisfy new and more stringent performance requirements. In general, the components have become more sophisticated to meet the ever-increasing requirements for performance and reliability. The monograph treats component design rather than the procedure or process by which a part is made.

The problem most prevalent in valve-type disconnects is leakage, which may be caused by the misalinement of components, extreme environment, extreme fluid requirement, or mechanical loads.

The primary problem with couplings and seals also involves leakage, which may arise from structural deflection, differential thermal expansion, inadequate control of surface finish and dimensions, or handling damage.

Problems with fittings that lead to leakage or inadequate functioning have been due primarily to initial design inadequacies, such as improper flow levels and flow distribution, excessive pressure loss, and undesirable thermal gradients.

Problems with fixed joints include leaks, corrosion due to improper cleaning and purging, poor dimensional control of parts to be joined, excessive weld dropthrough that restricts flow, and structural failures due to inadequate support or higher-than-predicted vibrations.

Since the primary problems related to the components discussed in the monograph are concerned with design details, emphasis is placed on experience with particular detail problems and on successful problem solutions.

The monograph comprises two major sections: "State of the Art," and "Design Criteria and Recommended Practices." References complement the text.

Both major sections are divided into six subjects: "Disconnects" (design configuration and integration); "Couplings" (design configuration and intergration); "Fittings" (configuration); "Fixed Joints" (welded, brazed, bonded, soldered, and interference-fit); "Seals" (static-seal configuration and integration and dynamic-seal configuration and integration); and "General Considerations for Design" (material selection, handling, and testing).

This monograph is one of a series being published on space vehicle chemical propulsion, environment, structures, and guidance and control. A list of all monographs issued prior to this one is presented on the final pages of the report.

This work was done by the Space Propulsion and Power Division of **Lewis Research Center.** *Further information may be found in NASA SP-8119 [N77-24191], "Liquid Rocket Disconnects, Couplings, Fittings, Fixed Joints, and Seals," a copy of which may be obtained at cost from the New England Research Application Center [see page A7].*
LEW-12948

Fabrication Technology

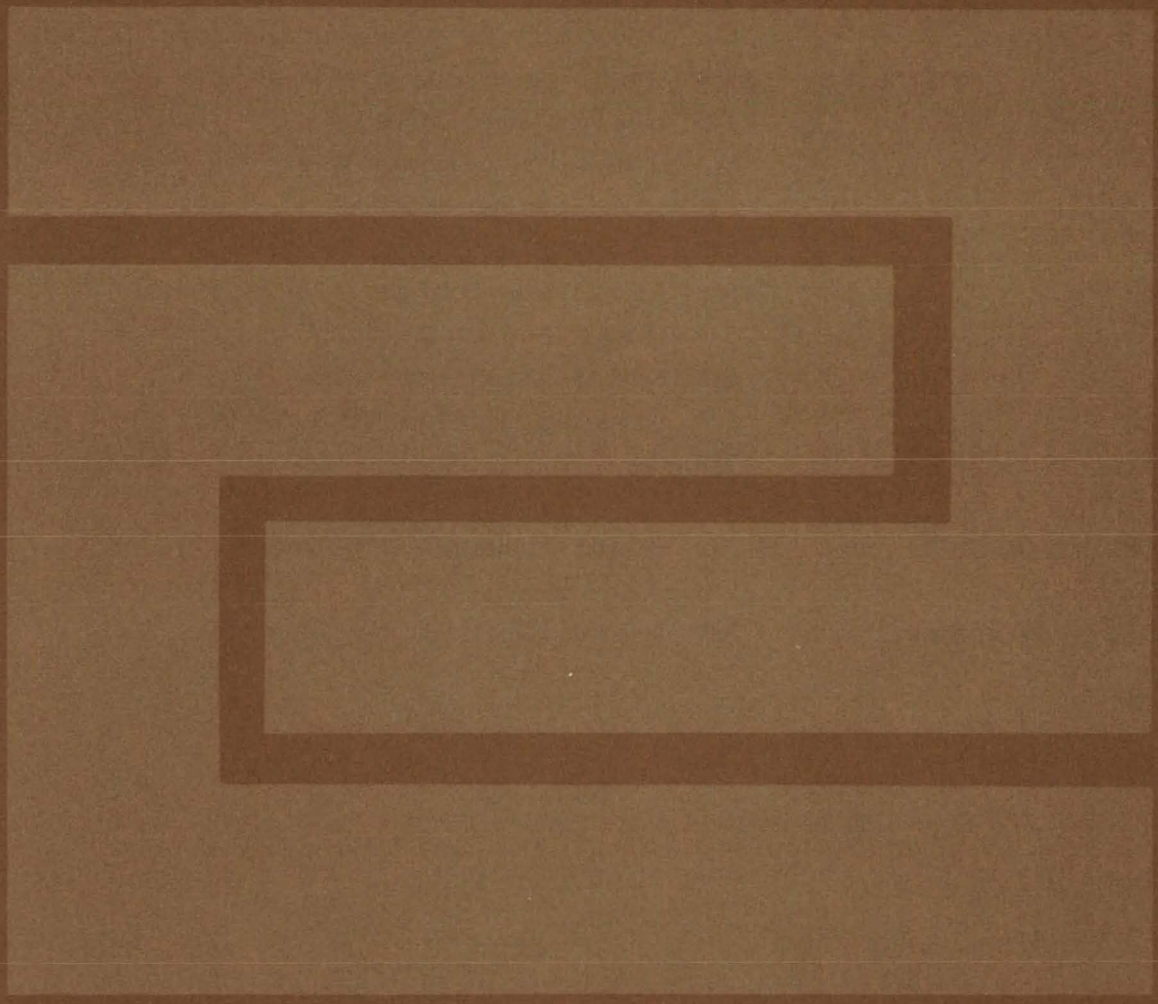

Technology of Welding Aluminum Alloys - I

Systems approach to
high-quality welding programs

Lyndon B. Johnson Space Center, Houston, Texas

This is the first of four consecutive articles that describe systems and techniques for obtaining aluminum alloy welds of the highest quality. In fabricating the crew module for the Space Shuttle it was necessary to develop techniques to produce weldments of high integrity and durability under severe conditions. The magnitude of this program, illustrated in Figure 1, indicates the need for a systematic approach.

The crew module is made from aluminum alloys of the 2219 series and is designed for automatic welding by the gas tungsten-arc process. This process, with 100-percent helium gas, produces a narrow straight-sided bead that minimizes distortion and avoids weld peaking.

The design philosophy is to use square-butt joints, kept away from sharp contour changes. Intersecting welds are configured for T-type intersections rather than crossovers. Differences in panel thickness are accommodated with transition step areas where the thickness increases or decreases within the weld, but never at an intersection.

High quality in the welds requires accurate dimensional control of parts and assemblies. In the machining of the parts, allowance is provided for growth during aging and for transverse shrinkage during welding. Longitudinal shrinkage is considered in the tooling for subassemblies.

The tooling is a key element in controlling dimensions. It must be rigid and massive, as shown in Figure 2, to maintain moldline control during welding. Yet, it must allow complex sculptured parts and subassemblies to be loaded, trimmed, cleaned, welded, and removed without disassembly of the tooling.

Stainless-steel fingers and backup bars or contour backup members hold the parts in place. Penetration is controlled by a groove in the

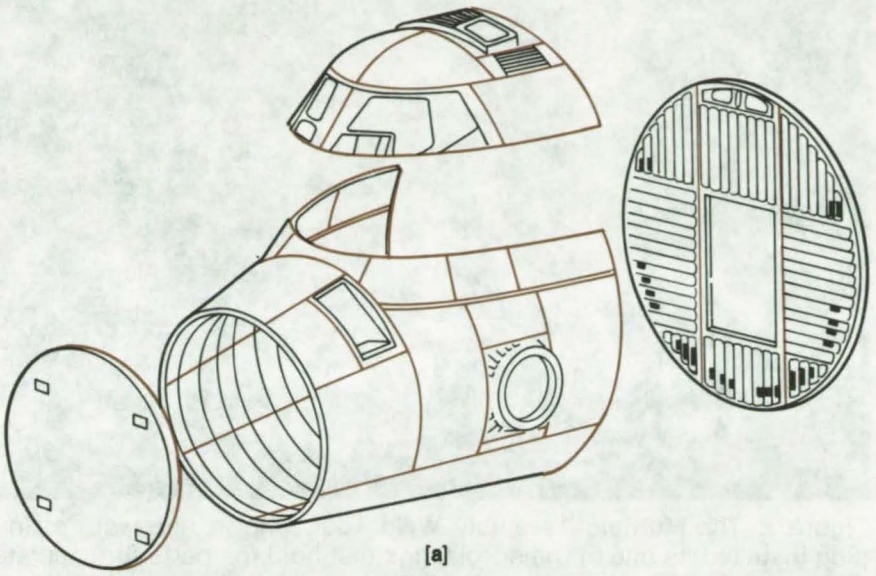

[a]

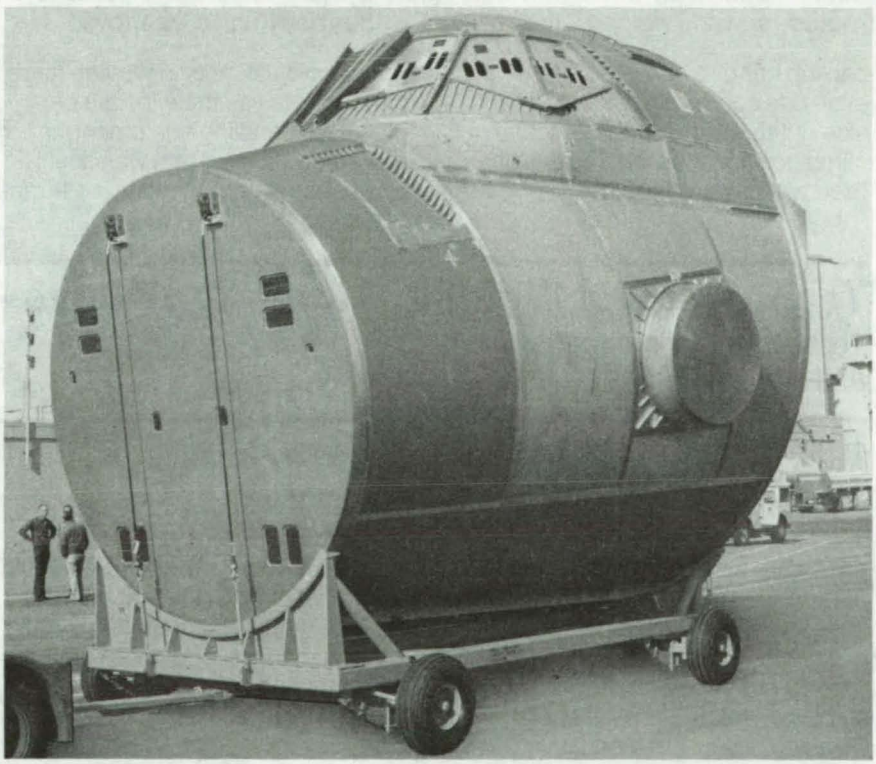

[b]

Figure 1. Fabrication of the **Space Shuttle Crew Module** required development of a systems approach to high-quality aluminum welding. The 36 welds, some of which can be seen in color in (a), were performed accurately, reliably, and automatically with the aid of massive tooling. The completed module (b) is essentially a large pressure vessel.

(continued next page)

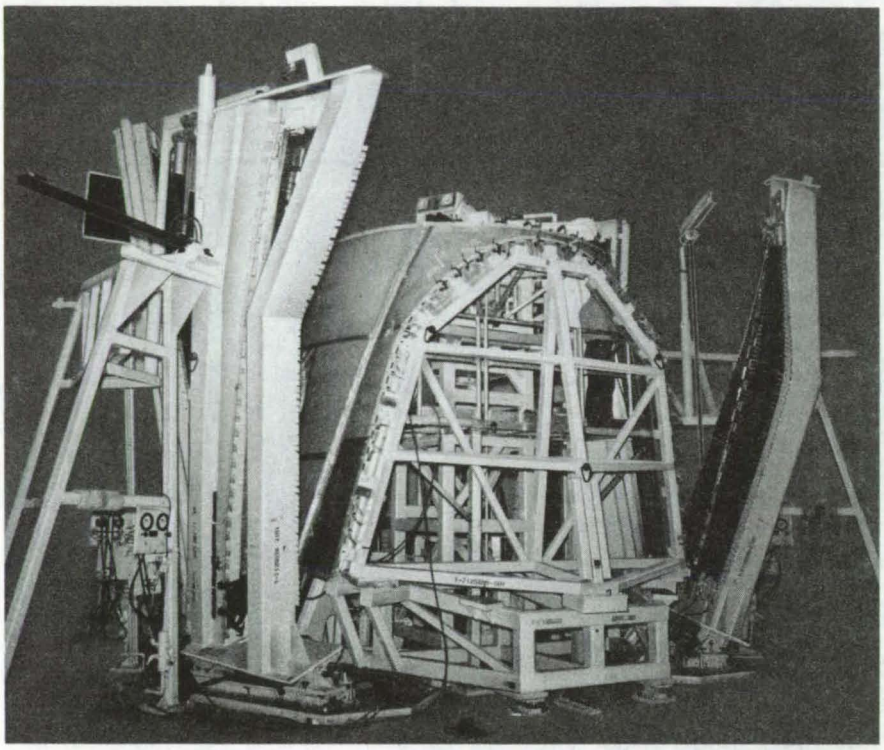

Figure 2. The **Multiple Assembly Weld Tool,** shown here with sizing plug installed, is one of the special jigs that hold the parts for accurate dimensional control. A universal skate system allows the parts to be routed, sawed, welded, and X-rayed without having to be moved.

backup bar or by a welder with an over-ride control on the penetration side of the weld. Flat or vertical-climb positions for welding are utilized whenever possible.

To avoid the risks in moving large parts, as well as the expense of elaborate handling equipment, a universal skate system was developed. This precision skate-and-track arrangement allows routing, sawing, welding, and x-raying in all positions. Joints are first tacked intermittently and then tacked continuously with a partial penetration. The fill-penetration pass is either followed by or combined with a cover pass. The weld beads are ground nearly flush to prevent cracking.

The universal skate welder is discussed separately in "Technology of Welding Aluminum Alloys - IV" (MSC-18084), in this issue. The other two topics that are treated individually are techniques for manual and machine welding in "Technology for Aluminum Welding - II" (MSC-18082) and the control of porosity in aluminum welds in "Technology for Aluminum Welding - III (MSC-18083).

This work was done by James R. Harrison, Lawrence J. Korb, and Carl E. Oleksiak of Rockwell International Corp. for **Johnson Space Center.** *For further information, including alloy selection, welding design and philosophy, weld strength and criteria, manufacturing considerations, dimensional control, tooling concepts, and welding equipment, Circle 56 on the TSP Request Card.*
MSC-18081

Technology of Welding Aluminum Alloys - II

Techniques for manual and machine welds

Lyndon B. Johnson Space Center, Houston, Texas

As part of the welding improvement program described in the preceding article, step-by-step procedures were developed for high integrity manual and machine welding of aluminum alloys. These procedures start with prewelding steps for preparation of the joint, cleaning, fit-up into tooling fixtures, selection and testing of shielding gas, and selection of the filler alloy. Detailed instructions are given for each of these steps with tables and graphs to specify materials and dimensions.

The welding is performed by either the gas tungsten-arc or gas metallic-arc process. After the tack welds, if any, and the first welding run, the work is inspected in a prescribed manner. The bead may be contoured and cleaned if necessary, and then the welding steps are repeated until the operation is completed.

The finished weldment is removed from the tooling, and the head is flushed if required. After inspection, parts are packaged, stored, or routed to the next operation.

Throughout this work sequence, the processing procedure designates manufacturing verification points and inspection points. The quality assurance requirements are spelled out in detail and illustrated by many drawings; a typical example is shown in the figure. Quality procedures for tests, inspections, and record-keeping are specified with the same thoroughness as the processing procedures.

Manual and machine welding practices are similar, but differ in two respects. One is that the

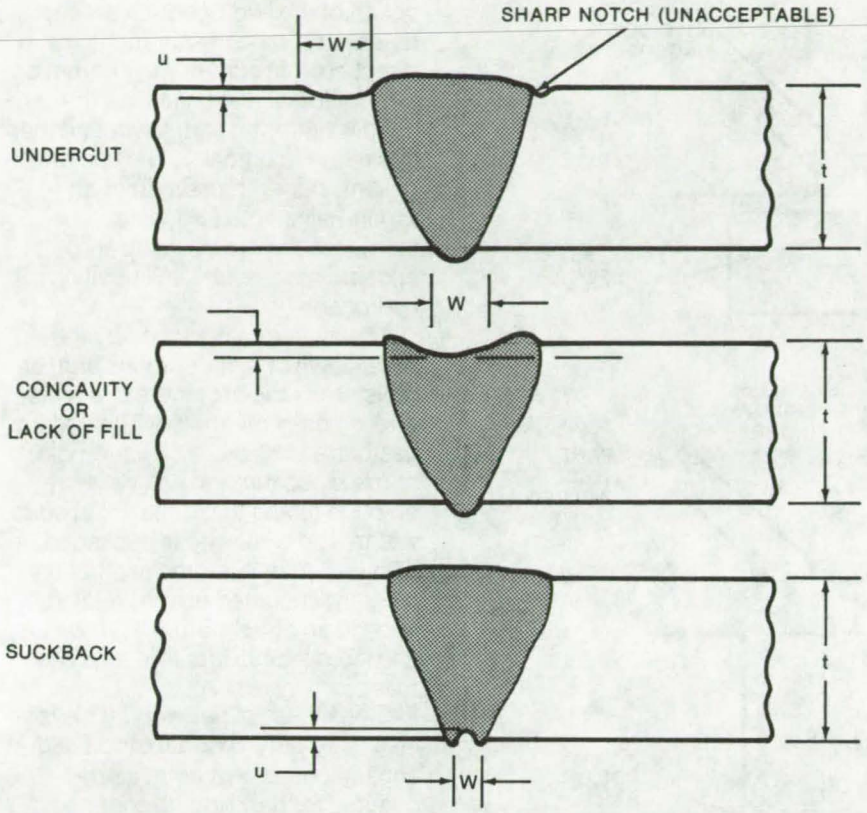

Detailed quality requirements on **Undercut, Concavity, and Suckback** exemplify the painstaking procedures and standards that produce reliable high-quality welds. The maximum allowable depth "u" is the lesser of 2 percent of "t" or 0.020 inch ("t" being the thickness of the thinnest member). When undercut or concavity exists in an area in conjunction with a suckback condition, the depth dimensions shall be additive. All sharp notches (defined by depth greater than width) are unacceptable. For undercut, concavity, and suckback, the maximum allowable width "w" is the lesser of t/4 or 0.125 inch (smoothly blended).

mechanized procedure starts with a verification test weld to establish the repeatability of the welding equipment. The other major difference is inclusion of steps for adjustment of the skate welder to assure proper alinement and smooth operation.

This work was done by Rockwell International Corp. for **Johnson Space Center.** *For further information, including processing procedures, tables and graphs of gap limitations, charts of filler alloys for various base-metal combinations, and quality requirements and procedures, Circle 57 on the TSP Request Card.*
MSC-18082

Technology of Welding Aluminum Alloys - III

Control of porosity in aluminum welds

Lyndon B. Johnson Space Center, Houston, Texas

Control of porosity in weld beads was a major objective in the development of the aluminum welding program described in the two preceding articles. Porosity, the most difficult defect to control, is caused by hydrogen gas unable to escape from the bead during solidification. Either conventional spherical pores or long stringerlike defects are produced when the hydrogen bubbles follow the molten bead as they try to surface.

To allow the hydrogen gas to bubble out of the molten bead as much as possible, the ideal welding position is either flat or a vertical climb for the bead. The horizontal position is undesirable for welding because hydrogen rising to the upper edge of the weld nugget is trapped by the solid metal above the bead and therefore forms a pore.

Boiloff of the hydrogen is also facilitated by a high bead temperature. Hard welding, in which the joint rests against a grooved backup plate, produces fewer pores than free-fall welding, in which there is no metal behind the joint (see figure). The chilling effect of the backup bar allows more heat to be put into the weld bead and thus allows greater

(continued next page)

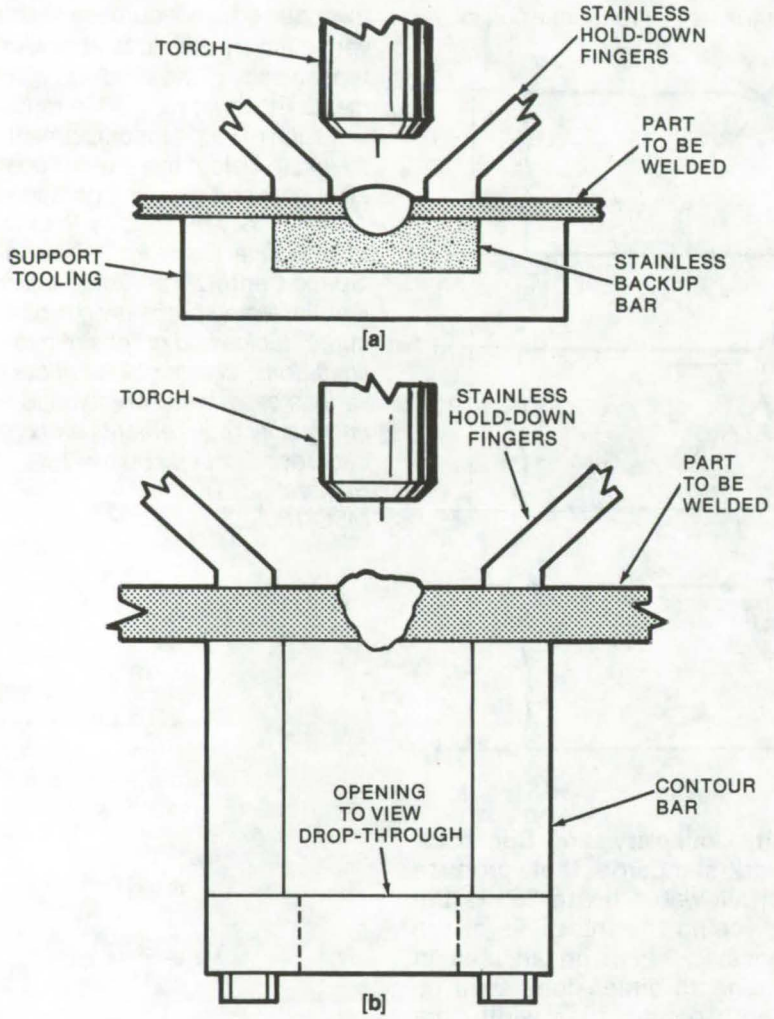

The type of **Tooling Affects Porosity** in an aluminum weld bead. Hard tooling (a) allows a hotter bead than free-fall tooling (b) so that hydrogen bubbles can boil out instead of forming pores. Welding position, moisture, and cleanliness are other important factors in control of porosity.

boiloff of the hydrogen. Likewise, defect-control considerations make direct current superior to alternating current for welding because the bead is hotter and narrower and thus has reduced porosity. The use of helium, rather than argon or an argon-helium mixture, also increases the arc intensity and appears more effective in boiling off hydrogen.

The hydrogen is formed by the breakdown of hydrocarbons and/or moisture in the arc; therefore moisture is tightly controlled. The helium gas has a -78° F (212 K) dew point and is piped through polyvinyl chloride tubing that does not absorb water. The weld wire is packaged with desiccants, stored in a hot dry-box, and mounted on the welding head in an airtight drum from which it is fed out by rollers through Nylon tubes.

Cleanliness of parts and tools is also extremely important for avoidance of pores. Systematic procedures for handling, preparing, cleaning, and inspecting parts before welding thus contribute to high quality in aluminum welding.

This work was done by James R. Harrison, Lawrence J. Korb, and Carl E. Oleksiak of Rockwell International Corp. for **Johnson Space Center.** *For further information, including data on the effects of various factors that influence porosity, and quality control inspection techniques, Circle 58 on the TSP Request Card.*
MSC-18083

Technology of Welding Aluminum Alloys - IV

A universal skate welder

Lyndon B. Johnson Space Center, Houston, Texas

As part of the welding improvement program described in the three preceding articles, a skate-weld carriage and track assembly were developed for controlled fusion welding on compound-curvature surfaces. Unlike the fixed-position carriage used for vertical, horizontal, and circumferential welding, this carriage has a suspension system that permits angular positioning of the weld head on the carriage. It also has a carriage-and-drive track mechanism capable of traveling over compound curvatures, which is not possible with the rack-and-pinion drive mechanism in existing skate welders. Figure 1 shows the complete skate welder.

Previous track welders were limited to coplanar curved paths. Flexible-type skate drives have been available, but they could not provide positive tracking over compound curves.

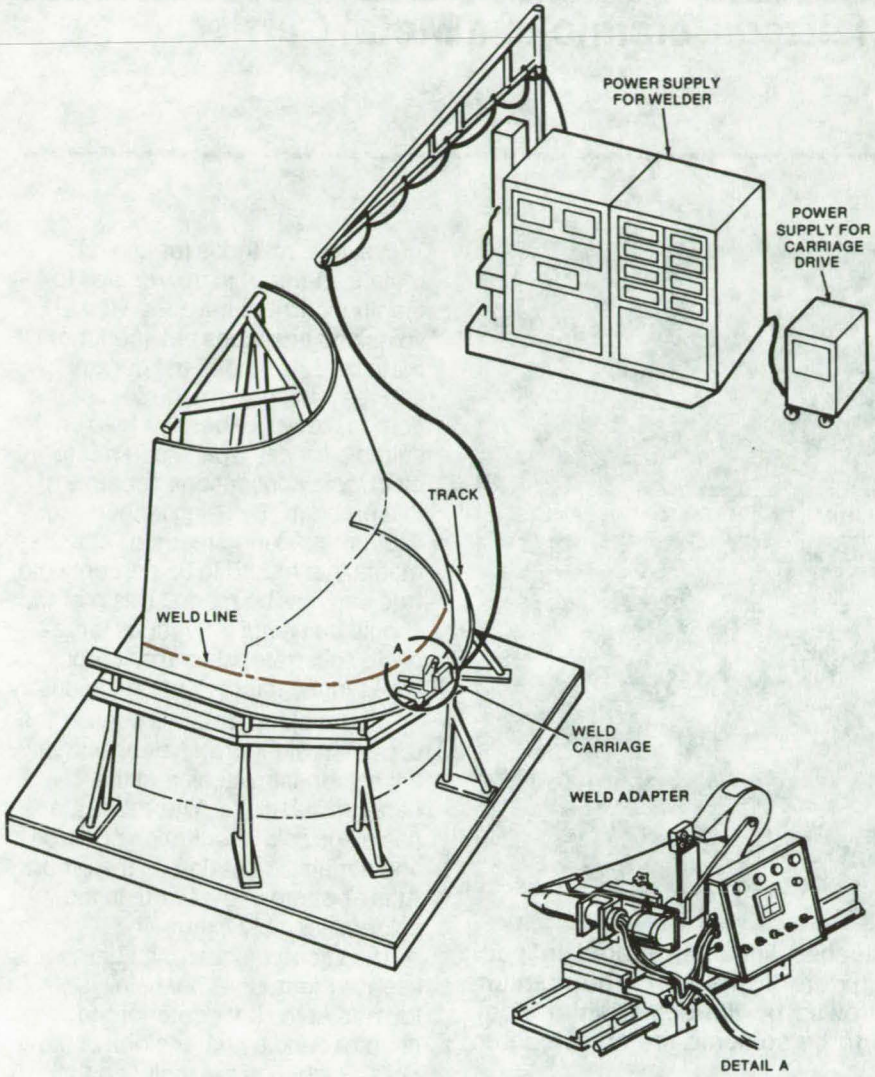

Figure 1. The **Universal Skate-Welder** carriage can carry a trim tool, a welding torch, or an X-ray head over compound curvatures on any assembly. The three units can be interchanged without need for any adjustment or alinement. The carriage follows a bar on a track, as shown in Figure 2.

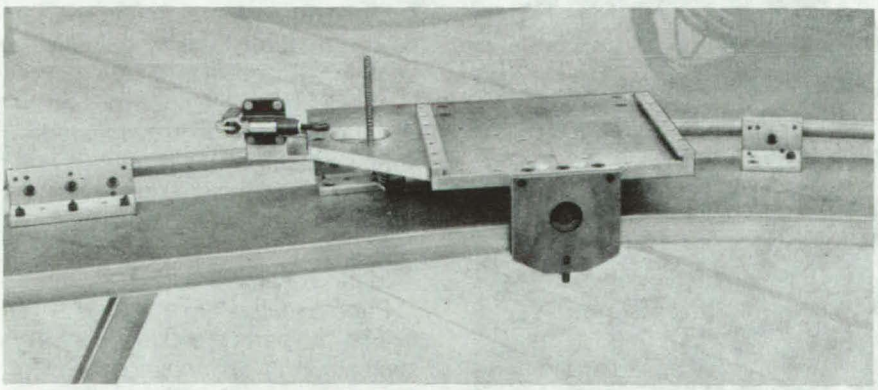

Figure 2. The **Carriage Rides the Track** to any location or position, including overhead. The electric motor that drives the carriage is not in place in this photo, but the gears can be glimpsed below the left end of the platform. Grooves for mounting tools on the carriage platform are seen, as well as the brackets for adjusting the guide rail along the track.

The carriage incorporates a three-point suspension system that allows angular positioning of the carriage. This is accomplished by two followers on the carriage. The followers engage a guide bar on the outboard side of the track, as shown in Figure 2. The bar is positioned by adjustable supports and is formed to the contours of the surface to be welded. Rack-and-pinion drive is replaced with a contoured drive track that has special teeth that mate with a compatible drive gear on the carriage. This driving mechanism provides positive tracking over the curved contours where the welding must be done. Spring-mounted rollers even hold the skate drive engagement in vertical or overhead weld positions.

The carriage is designed with a universal mounting platform so that a trim tool, a weld head, or an X-ray unit can be interchanged without need for any realinement. Since all three of these are required in each weld operation, their simple interchangeability saves time and assures precision.

This work was done by Rudolph Ginez, Jack R. Lewis, Alma U. Millett, Karl A. Saenger, John K. Skelly, Vernon E. Standiford, and James O. Whiteman of Rockwell International Corp. for **Johnson Space Center.** *For further information, including detailed drawings and photographs of the carriage, track, and heads, Circle 59 on the TSP Request Card.*
MSC-18084

Vacuum Soldering a Metalized Ceramic to a Metal Carrier

Method reduces voids
by 85 to 95 percent.

Caltech/JPL, Pasadena, California

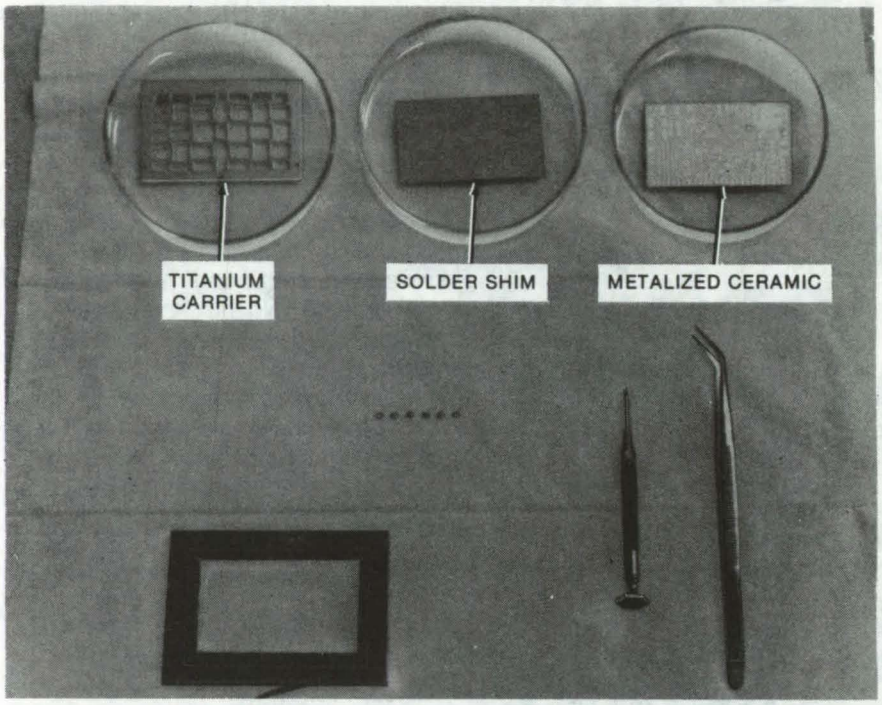

Figure 1. **Parts To Be Soldered** are cleaned and then stored in petri dishes prior to assembly in the solder fixture (lower left). The titanium carrier is placed in the fixture first, followed by the solder-shim stock and the metalized carrier. The surfaces to be soldered are spray-coated with flux.

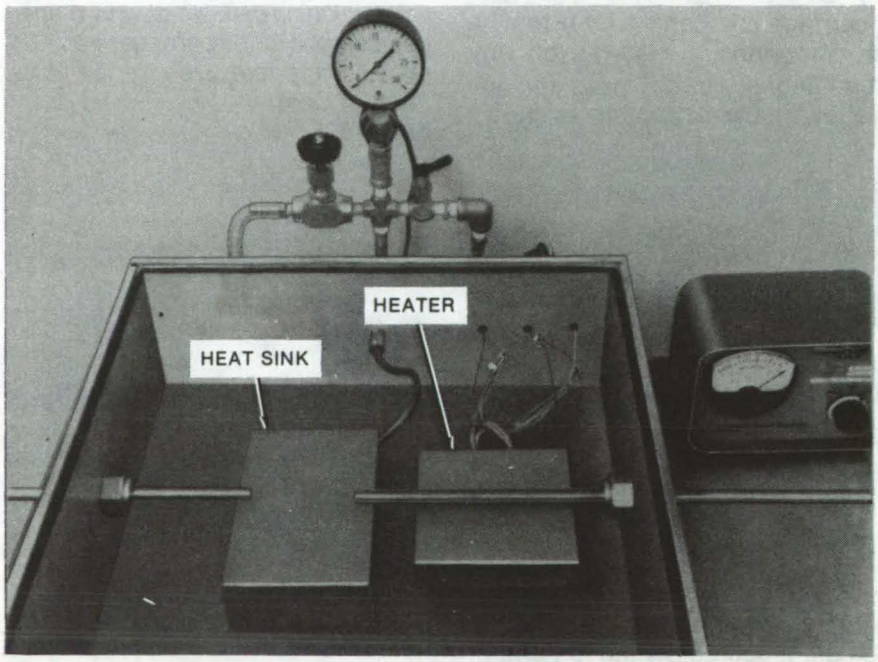

Figure 2. The **Vacuum-Soldering Chamber** contains a heater, a heat sink, and push rods for manipulation of the solder fixture.

Previous methods for joining metalized-ceramic microstrips to titanium carriers have resulted in voids and airspaces between the metalized surface of the ceramic and the carrier. In many cases, the composites have been judged unsuitable for aerospace and microelectronic applications because of this problem. By using a new vacuum-soldering method, attachments that are 85 to 95 percent void free can now be made. This method should be useful for various large-scale substrate attachment processes in the microelectronic industry.

The titanium carrier is seen at the upper left of Figure 1, along with the flat solder shim stock and the ceramic substrate. The substrate has electronic circuitry on one side and a metallic coating on the other. At the bottom of the figure is the solder assembly fixture.

The vacuum-soldering chamber is seen in Figure 2. A heat sink is located at the left center of the chamber and a heater block at the right. Push rods are included to transfer the solder assembly between the heater and the heat sink. The parts are assembled and placed on the heat sink, as seen in Figure 3. Also shown are asbestos pads that are placed over the assembly and a weight used to exert a downward force. The weighted assembly is transferred to the heater by manipulating the push rods after the chamber has been evacuated. After solder flow, the push rods are used to return the soldered assembly to the heat sink, and positive pressure is applied to the vacuum soldering chamber.

Prior to their being mounted in the fixture, the parts are cleaned ultrasonically in 1,1,1-trichloroethane for 10 minutes, are rinsed in fresh 1,1,1-trichloroethane and then in isopropyl alcohol, and are blown dry with dry nitrogen gas. They are placed in a clean petri dish and are covered with distilled water.

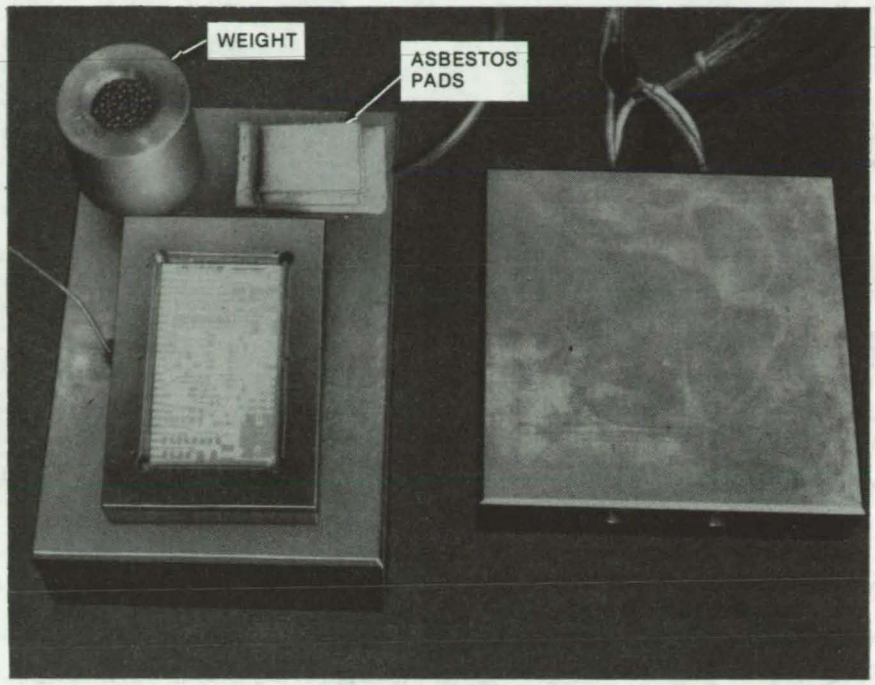

Figure 3. The **Assembled Fixture** will be covered by asbestos pads, weighted, and then transferred to the heater by manipulation of the push rods, after the chamber has been evacuated.

The surface of the ceramic substrate is scrubbed with a felt-tipped applicator for the removal of residual films, is rinsed in isopropyl alcohol, and is blown dry with dry nitrogen. It is then ultrasonically cleaned in trichloroethane for 2 minutes, is rinsed in isopropyl alcohol, and is blown dry.

This work was done by Brian D. Gallagher, Arthur W. Kermode, and Robert C. Mayne of **Caltech/JPL.** *For further information, Circle 60 on the TSP Request Card.*
NPO-14037

Linear Dimension Establishes Weld Integrity

Simple visual test replaces radiographic inspection in most cases.

Caltech/JPL, Pasadena, California

To provide high reliability and minimum weight, tubes designed to carry fluids between components of a spacecraft must be butt-welded on assembly rather than attached with screws. In some instances the two ends to be welded are deep within a subsystem. With numerous components crowded nearby, radiographic inspection of the weld is very costly and time consuming and may be impossible in many cases.

However, a new study finds that when an automatic in-place tube-welding head is used to butt-weld two stainless-steel tubes together, the welding process can be made so reliable that when the weld exceeds a certain minimum dimension, penetration of the weld can be assumed to be complete. A detailed procedure for tube welding has been developed that considers the effects of arc gap, shielding gas, welding speed, and other parameters related to weld reliability. When the procedure is adhered to, the minimum dimension criterion becomes a simple visual test of the weld quality.

The test is performed by verifying that:

- The welded tubes are alined axially according to specifications;
- Oxide discoloration of the tubes is not darker than "straw" color;
- The weld concavity is within specifications; and
- The weld width at any point around the tube exceeds a minimum-dimension criterion that depends on the tube diameter and thickness.

When these criteria are not met, radiographic inspection is necessary.

A new inspection tool [described on page 540 of this issue in "Tube-Weld Inspection Tool" (NPO-13978)] greatly aids the visual inspection procedure, which should be applicable to other high-performance weld situations.

This work was done by Joseph C. Lewis of **Caltech/JPL.** *For further information, Circle 61 on the TSP Request Card.*
NPO-13977

Tube-Weld Inspection Tool

Calibrated notch and fiber optics
are used to determine weld integrity.

Caltech/JPL, Pasadena, California

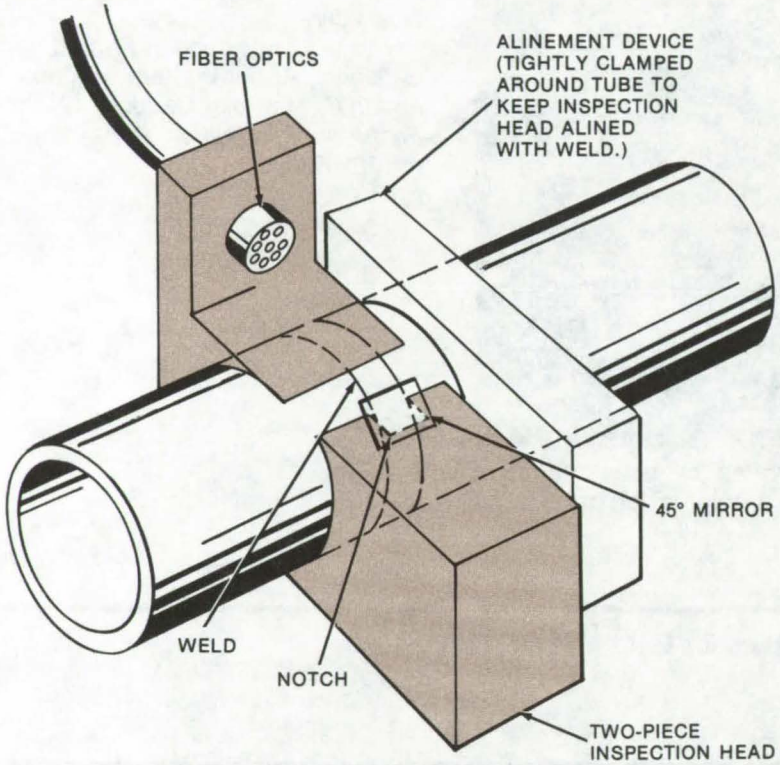

This **Tube-Weld-Dimension Inspection Tool** compares the weld width with a notch width. The weld is considered satisfactory if the weld is wider than the notch. The figure is schematic, enlarged, and somewhat distorted to show significant elements. The fiber optics permit the inspection head to be completely rotated around the tube for complete inspection of the weld. A 45° mirror over the notch aids in comparing the notch and weld widths.

In crowded systems, tube welds may be inaccessible to conventional X-ray radiographic inspection. A new tool that uses a calibrated notch and fiber optics can be used for simple visual inspection of welds in hard-to-reach areas.

The inspection head is clamped (slip-fit) around the tube and is alined with the weld as shown in the figure. Light is transmitted through the fiber optics to illuminate the weld area. The operator then looks into a magnifying eyepiece that compares the width of the weld to the width of a notch in the inspection head (which lie in the same optical plane). If the weld width exceeds the notch width, the weld is considered satisfactory. [See "Linear Dimension Establishes Weld Integrity" (NPO-13977) on page 539 of this issue.] The fiber optics permit the operator to rotate the inspection head completely around the tube to compare the width of each increment of weld to the width of the tube.

This work was done by Howard B. Stanford of **Caltech/JPL.** *No further documentation is available.*
NPO-13978

Heat-Dissipating Aluminum Wire

"Pointed-star" cross section increases
heat dissipation while reducing weight and cost.

Marshall Space Flight Center, Alabama

A length of aluminum wire must have at least 1.5 times the volume of copper wire to have equivalent current-carrying capacity and surface heat dissipation. Surface area, and consequently heat dissipation, can be considerably increased by using a star-shaped, rather than a round cross section (see figure). When used with modern high-temperature insulating materials, the pointed-star wire is suitable for applications where low-cost lightweight wire is required.

Standard 12-gage copper wire has a circumference of 251 mils (0.64 cm). Round aluminum wire of the same gage has a circumference of 380 mils (0.97 cm). By going to a 6-, 8-, or 12-pointed-star configuration, the circumference can be increased to 0.492, 0.544, and 0.672 in. (1.24, 1.38, and 1.71 cm) respectively, without increasing the outside diameter. The resulting wire has improved surface heat dissipation yet uses less material; cost and weight are therefore reduced.

High-temperature insulating materials, such as polyimides

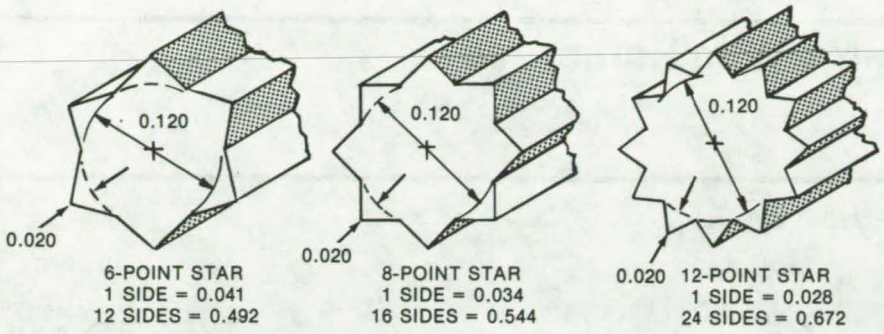

NOTE: ALL DIMENSIONS IN INCHES.

Heat-Dissipating Wire increases in surface area as the number of star points increases. Each side gets smaller as the number rises; nonetheless, the total surface area of all the sides, and therefore the surface heat dissipation, increases. The diameter of 0.120 in. is characteristic of 12-gage round wire.

(199° C) and tetrafluoroethylene (343° C), can be used with the wire to minimize fire hazard and overheating. The proposed conductor configuration would increase surface area and allow adequate insulation thickness to be maintained.

This work was done by James D. Doyle and Eugene J. Stringer of Rockwell International Corp. for **Marshall Space Flight Center.** *For further information, Circle 62 on the TSP Request Card.*
MFS-24274

Cable-Clamp Installation Tool

Tiny vise simplifies the installation of cable clamps in confined spaces.

Caltech/JPL, Pasadena, California

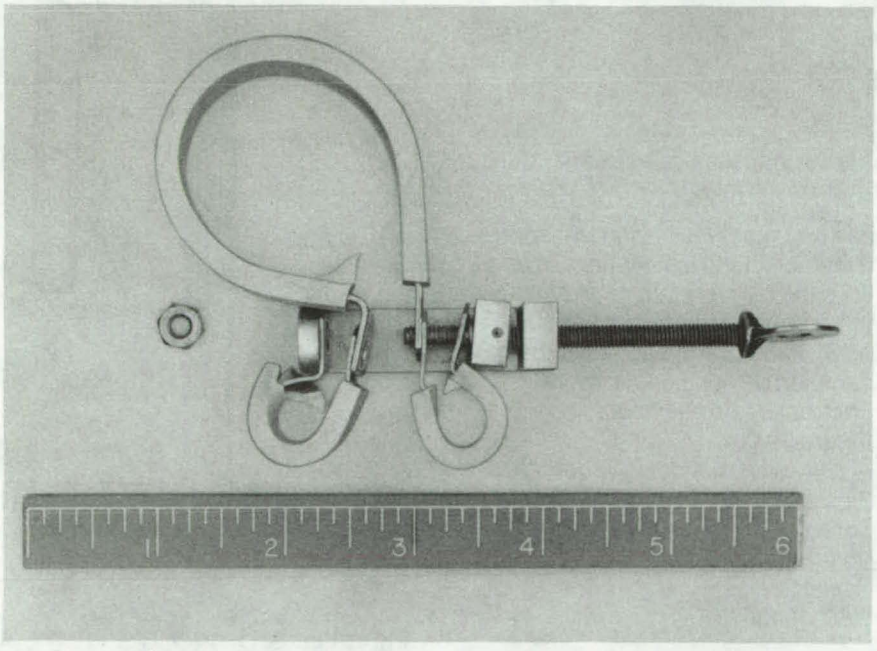

Cable Clamps Are Bolted together with a tool constructed like a tiny bench vise. As the thumbscrew is tightened, the ears of the clamps are forced together, and the bolt passes through all the lugs and into the hole in the stationary jaw.

It is difficult to install cable clamps in confined spaces when short bolts must be used. The ears of the clamps are often too small to be easily grasped with pliers or other conventional tools.

A new tool, resembling a tiny bench vise, clamps the ears tightly together and then passes the assembly bolt through the alined boltholes. The tool is shown in the figure in its most open position, with the bolt and three standard cable clamps ready to be tightened. The movable jaw of the tool is recessed to accommodate the head of the bolt, while the stationary jaw has a hole large enough to accommodate the nut.

As the thumbscrew is tightened, the lugs of the cable clamps come together, and the bolt is passed through all the lugs and into the hole in the stationary jaw. After a few threads appear through the hole, the nut can be easily threaded onto the bolt; the tool is then removed.

This work was done by Milton B. Noel of **Caltech/JPL.** *For further information, Circle 63 on the TSP Request Card.*
NPO-13976

Positioning Bars for Large Wire Harnesses

Bars prevent damage and reduce transport and installation times.

Lyndon B. Johnson Space Center, Houston, Texas

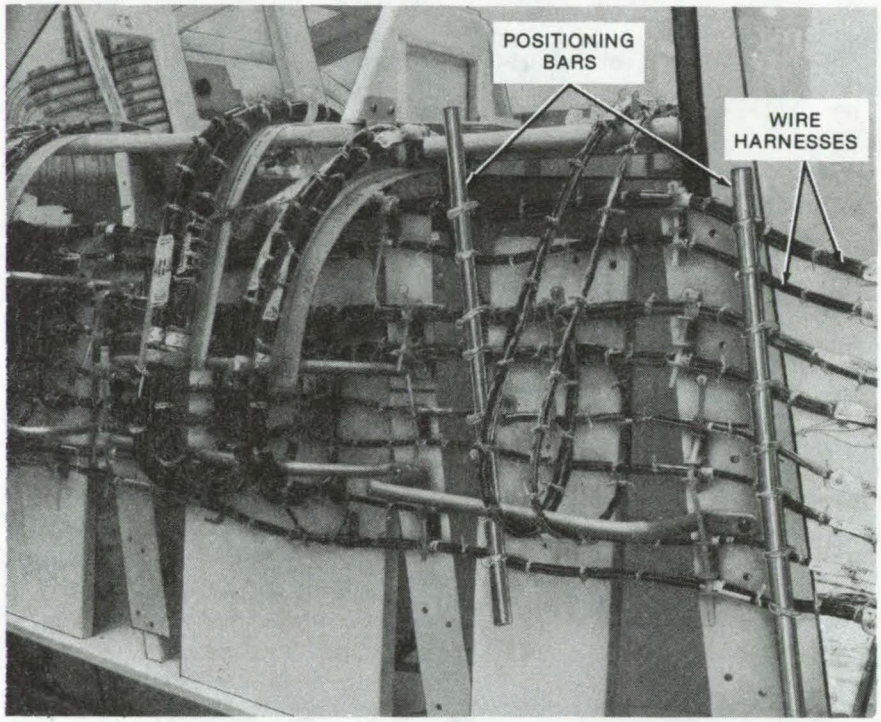

Figure 1. **Positioning Bars** preserve wire harness alinement during transport between the jig board and final assembly.

Large wire harnesses for electronic assemblies are usually bundled for transport from the breadboard setup to the final installation. This bundling and the subsequent opening of the bundle during installation can frequently damage the harness and nearby components. In addition, the repositioning of the opened bundle for attachment to the supporting brackets requires considerable time.

By tying positioning bars to the harness (Figure 1), its configuration can be preserved during transport, thus facilitating installation. In addition, the harness can be stowed temporarily by placing a hanging hook at the end of each bar; the bar can then be hung on movable "hatracks" or wall hooks, as in Figure 2.

This work was done by John R. Glessner of Rockwell International Corp. for **Johnson Space Center.** *No further documentation is available.*
MSC-16420

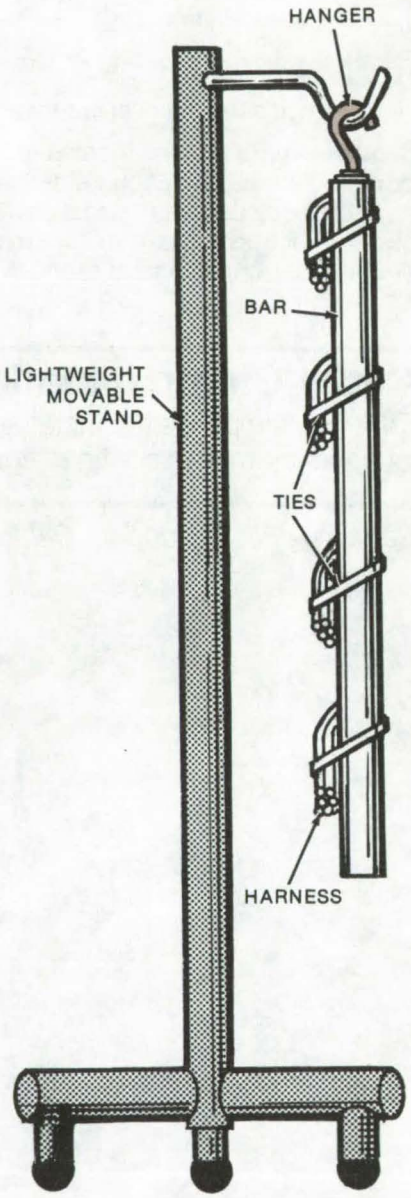

Figure 2. A **Hanger** at the end of the bar allows it to be stowed on movable "hatracks" or wall hooks.

Adding Through-Bolt Holes to Pin-Fin Cold Plates

Standard plates can be modified inexpensively by overlap spot welding.

Lyndon B. Johnson Space Center, Houston, Texas

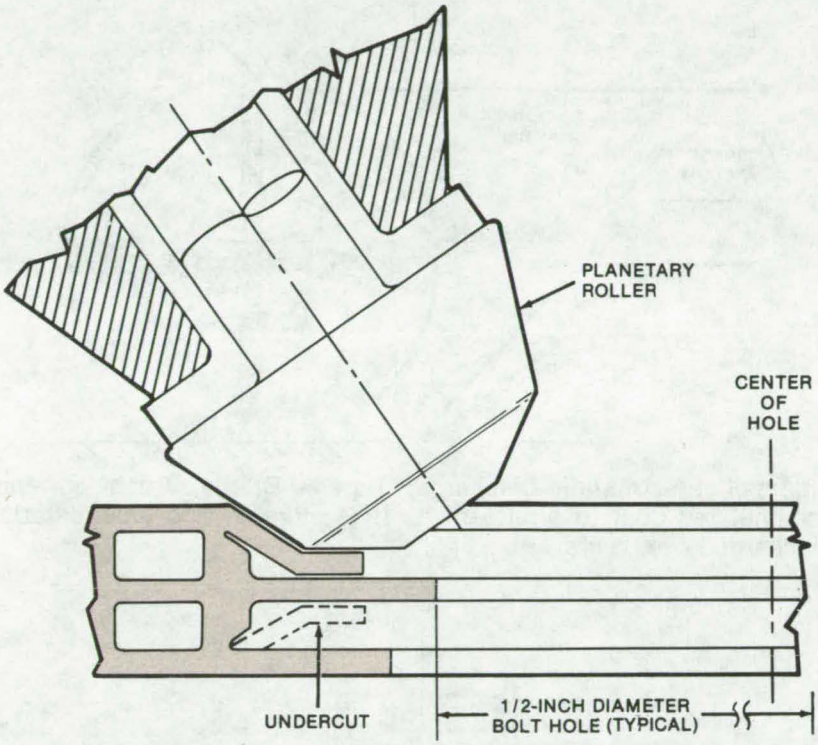

Figure 1. **Inner Flanges for Overlap Spot Welding** are formed as the planetary roller closes the face sheets onto the core sheet. Previously, the roller had been used to form edge-contact closures over shallower undercuts for brazing or electron-beam welding.

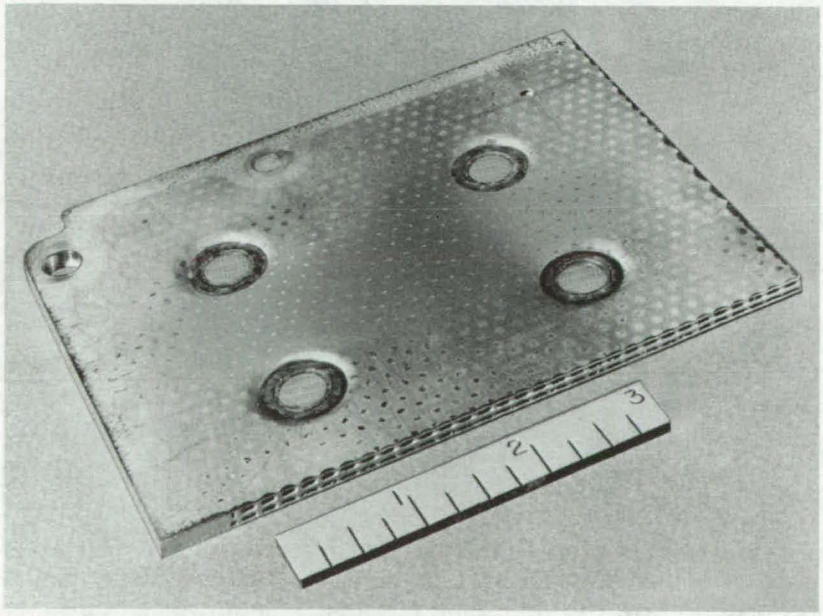

Figure 2. These **Four Through-Bolt Holes** were formed in a test cold plate by the new method.

A spot-welding technique for adding through-bolt mounting holes to pin-fin stainless-steel cold plates is less expensive than secondary-brazing and electron-beam methods. With the new procedure, standard plates can be modified in quantity for various mounting configurations without the need for special tooling.

After a hole is bored through the plate, the area around it is undercut with special cutters. As shown in Figure 1, a planetary roller closes the face sheets onto the core sheet with inner flanges for overlap spot welding. Figure 2 shows a test cold plate with four through-bolt holes added by the new method. These holes tested satisfactorily at 140 psi (960×10^3 N/m^2) pressure during a 10-μ helium leak check. The pressure tests indicated that washers can be used but are not required.

This work was done by Emil P. Ruppe of Rockwell International Corp. for **Johnson Space Center.** *No further documentation is available.*
MSC-16421

Space-Age Vacuum Cleaning

Varied concepts for brushes and air handling remove dirt more effectively.

Caltech/JPL, Pasadena, California

In the aerospace industry, cleanliness is all-important. Dust and dirt can damage delicate instruments and destroy integrated circuits — and ruin an entire mission. Biological matter could introduce fungi and bacteria into space. Consequently, imaginative vacuum-cleaning concepts have been proposed and developed. Many of these concepts, while not appropriate for household cleaning, may find use in industry, research, and medicine. Among them:

- **Electrostatic-Discharge, Tapered-Bristle Brush** (Figure 1): Tapered bristles have a rougher surface and greater length in contact with the surface to be cleaned; therefore, they dislodge and entrap dust particles more efficiently. The brushes are mounted to interfere with air flowing into the vacuum chamber — until they pass over a series of vents, where the rushing air shakes the bristles and dislodges the dust, sweeping it into the vacuum chamber. At the same time, a ground connection removes electrostatic charge that the bristles have accumulated in moving over the surface to be cleaned; the particles therefore tend to cling less to the bristles.

  Air entering the brushes is smooth flowing and nearly at atmospheric pressure. The bristles therefore do not have to withstand strong wind forces and do not have to be as stiff (and scratchy) as conventional vacuum-cleaner bristles.

  The brush device can remove up to 98 percent of surface particles as small as 5 microns. It is suitable for cleaning delicate instruments or equipment that could be damaged by a strong airflow or stiff bristles. Another possibility is cleaning "clean" rooms where semiconductor devices are processed.

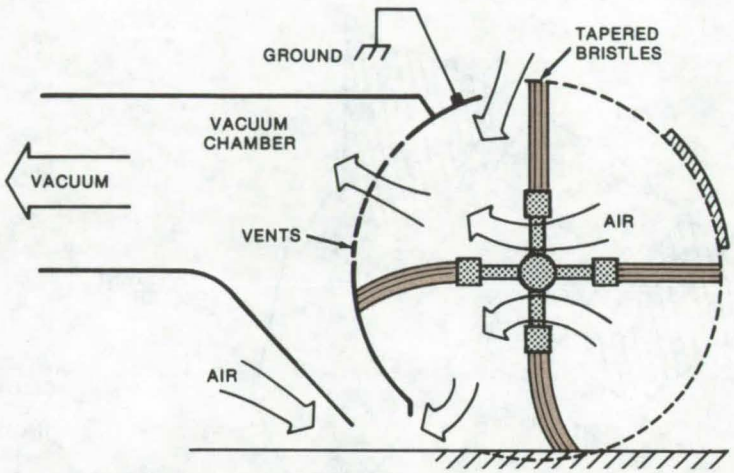

Figure 1. **Electrostatic-Discharge, Tapered-Bristle Brush** surrenders accumulated dust to airstream as it is vibrated and electrostatically discharged over vents.

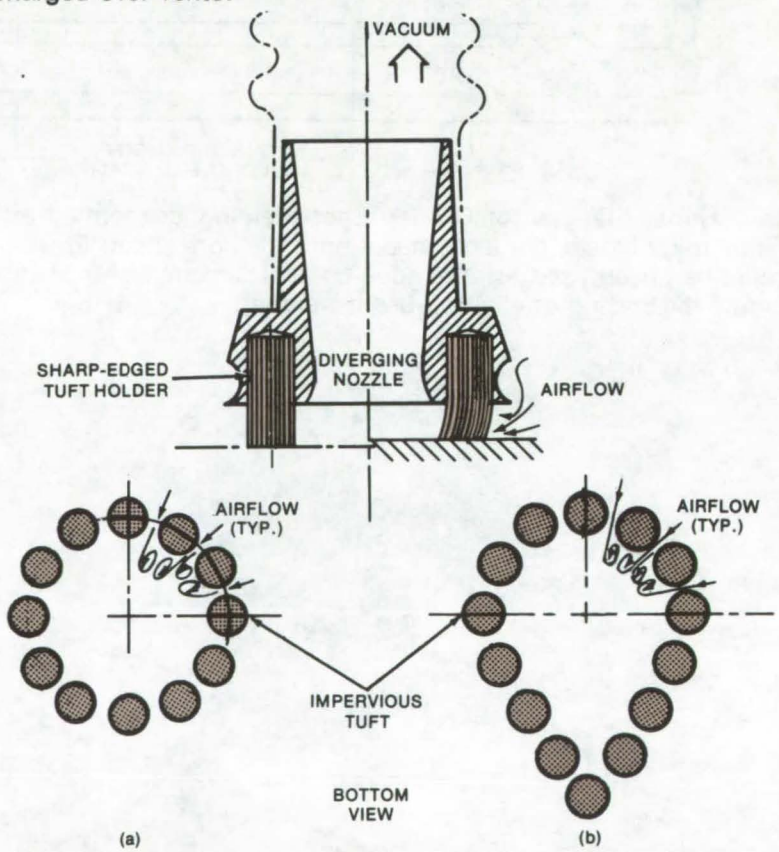

Figure 2. **Aerodynamically Designed Brush** forces turbulent air close to surface and then lets air flow to vacuum chamber with minimum impedance to flow. (In right side of cross section, vacuum cleaner is "on" and on left side it is "off.") The tufts can be arranged in a conventional circular pattern (a) or in teardrop form (b), which is advantageous for cleaning in corners.

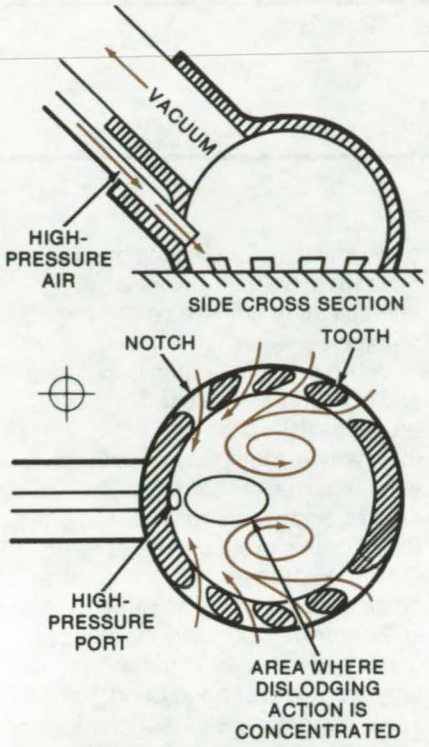

Figure 3. **Notched-Nozzle Cleaning Head** directs airflow so that twin vortexes are formed. Air jet at high pressure aids particle removal.

- **Aerodynamically Designed Brush** (Figure 2): A low, sharp-edged tuftholder forces air close to the surface being cleaned, where it can entrain more dirt dislodged by the bristles. The interior of the brush is shaped like a diverging nozzle so that air flows through with minimum energy loss. The tufts are stiff and impervious to the airflow so that air is forced between the tufts for maximum velocity and turbulence — and effectiveness.
- **Notched-Nozzle Cleaning Head** (Figure 3): Designed for cleaning hard-to-reach areas, the cleaning head has teeth instead of brushes. The notches between the teeth are oriented at such an angle that they induce the inrushing air to form twin counterrotating vortexes. The high velocity and low pressure between the vortexes detach and entrain particles from the surface. To enhance the detachment process, a jet of high-pressure air can be directed at the surface between the vortexes.
- **Cross-Sweeping Brush** (Figure 4): This brush sweeps in two directions simultaneously, because it is both rotated and tumbled. It can therefore get at particles that are normally difficult to dislodge — for example, particles in scratches at right angles to vacuum-cleaner motion. The brush necessarily has a small width, but many brushes can be combined to give overlapping coverage in a single vacuum-cleaning machine. The angle of the cross sweeps is determined by the ratio of the tumbling-pulley diameter to the rotating-pulley diameter. A ratio of 1 gives right-angle sweeps. Less than 1 makes the crossing angle narrow, and more than 1 makes it wide.

The cross-sweeping brush is suitable for cleaning biological materials from large areas. Reportedly, it removes 99 percent of the biological matter on steel surfaces, whether rough or smooth.

These new vacuum-cleaning concepts may be used in combination. For example, the cross-sweeping brush might also be an electrostatic-discharge, tapered-bristle brush.

This work was done by Horst W. Schneider of **Caltech/JPL.** *For further information, Circle 64 on the TSP Request Card.*

Inquiries concerning rights for the commercial use of this invention should be addressed to the Patent Counsel, NASA Resident Legal Office-JPL [see page A8]. Refer to NPO-14008.

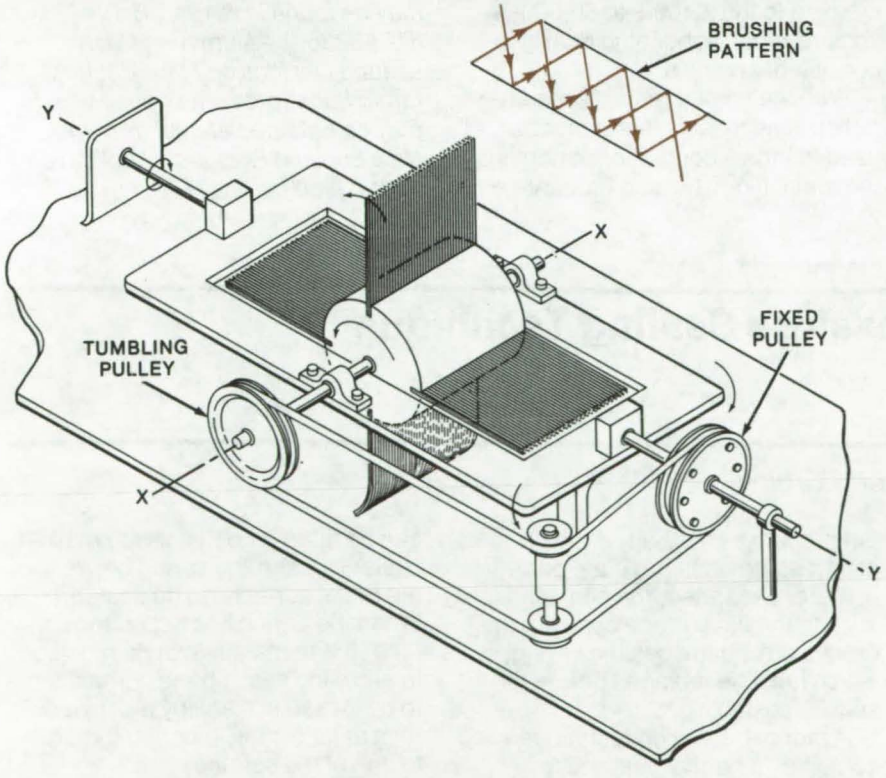

Figure 4. **Cross-Sweeping Brush** uses pulleys and belt or gears to rotate around x-x axis and tumble around y-y axis. The result is the crisscross brushing pattern shown in the insert.

Bonding Aluminum Beam Leads

Aluminum can replace gold in beam-lead devices with only minor changes in equipment and processes.

Marshall Space Flight Center, Alabama

Beam-lead integrated circuits, in which the silicon chip is connected to the "outside world" by leads that also provide support, have used gold almost exclusively for the beam leads. Aluminum, however, is an excellent substitute. It makes reliable beam leads and can be used with minor modifications in existing processing equipment. However, many of the physical and chemical properties of aluminum are quite different from those of gold and must be taken into account if the less expensive metal is to be used successfully.

A report, based on a study of attachment methods for IC's with aluminum beam leads, makes it relatively easy for hybrid-circuit manufacturers to convert to IC chips with aluminum beam leads. The report covers: techniques for handling the tiny chips; proper geometries for ultrasonic bonding tips; the best combinations of pressure, pulse time, and ultrasonic energy for bonding; and the best thickness for the metal films to which the beam leads are bonded. The report is based on an investigation of bonding techniques and tests of bonded devices.

A major difference from gold beam-lead bonding is the layer of oxide on the aluminum. If this layer is not penetrated by the bonding tip, the bond is not reliable. If the tip penetrates too deeply, the beam is weakened and can break. The solution is to use a small hemispherical sapphire tip, 75 mm in diameter.

Another major difference is that aluminum beam leads attach best to relatively thick metalization on the hybrid substrate. The accepted standard in the semiconductor industry for ultrasonic bonding is a 12,000-angstrom nickel-chromium-aluminum interconnection pattern. However, when aluminum beam leads are bonded to such films, holes are created in the beam leads. When the film thickness is increased to the 25,000- to 60,000-angstrom range, bonding quality is consistent and reliable.

With the thicker metal, a modification is necessary in the process used to etch a conductor pattern in the metal film. The acid etchant ordinarily used undercuts the thick metal film. Substitution of a hot agitated alkaline etchant solves the problem.

When proper bonding conditions and procedures are used, the bonded units easily pass electrical and mechanical tests. Environmental tests (thermal shock, vibration fatigue, and step stress) of 144 units, for example, produced no failures. Over the entire test program, transistor beta varied by no more than ±2 percent. Operators quickly became proficient and produced a very high yield of good bond. Nearly 1,000 beams were ultrasonically bonded with less than 0.2 percent bond failures.

This work was done by F.S. Burkett of Electronic Communications, Inc., for **Marshall Space Flight Center.** *Further information may be found in NASA CR-124434 [N73-32369], "Aluminum Beam Leaded Devices on Microcircuit Ceramic Substrates," a copy of which may be obtained at cost from the New England Research Application Center [see page A7].*
MFS-23183

Adhesiveless and Grooveless Sealing Technique

A steel spring holds O-rings in place without heating or curing.

Langley Research Center, Hampton, Virginia

When two metal parts are sealed with an O-ring, one of the parts is usually grooved to accommodate the O-ring and to effect the seal. However, if the parts are heat-sensitive, the ring-sealing adhesive cannot usually be cured in situ, because thermal deformation may alter critical dimensions of the groove and seal.

An often-used alternative procedure, to bond the seal adhesively into the groove, is difficult to carry out properly, especially if the parts are small. In addition, if the parts are later separated, the seal tends to stick to the flat surface opposite the groove. This damages the O-ring, which must be replaced before the seal is reestablished.

A proposed sealing technique combines a normal seal with a spring, as shown in the figure. When tiny O-rings are involved, the spring is a steel disk around which the ring is molded. (An optional "handle" can be fitted onto the disk to make it easier to insert the spring between the metal surfaces to be sealed.) When the O-ring lies flat on the surface, the technique can be modified to allow the seal/spring combination to be locked in place by a screw or rivet at its center, mooring the disk to one of the surfaces.

In addition to O-rings, the technique may be applied to soft or hard seals or to other geometries, such as triangular seals. In some cases, a

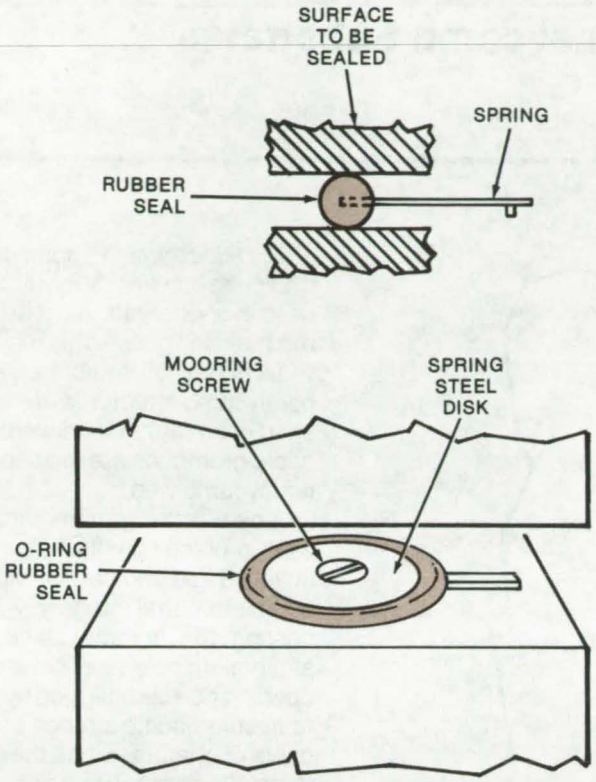

The **Adhesiveless and Grooveless Sealing Technique** is illustrated, using two different types of springs. The O-ring is molded around the spring much like a tire on a rim. The metal disk can be fastened in place to hold the O-ring firmly. A handle on the spring helps one to put the spring/seal combination between the surfaces to be sealed.

steel with a high spring constant (which holds the seal in place by tension) may retain the seal better.

This sealing technique not only eliminates the groove or the adhesive bonding and its attendant heating and curing, but it also probably does away with the need to finely finish at least one of the surfaces to be sealed. The seal could be mounted either inside or outside the seal line, and it could be installed in final assembly without exposing the part to the heat and pressure of curing.

This work was done by Jon W. Martin and Harry M. Elmendorf of TRW, Inc., for **Langley Research Center.** *No further documentation is available.*
LAR-11779

Metallic Coating Reduces Thermal Stress

Thermal stress in high-temperature/high-strength materials can be substantially reduced by adding a metallic outer layer that has high thermal conductivity. The layer can be deposited by standard plating processes. In tests, wing-panel sections of the Space Shuttle were exposed to high heating rates, typical of reentry; temperature differentials were reduced by a factor of 5.5 by this relatively simple technique.
(See page 490.)

Controlled-Porosity Composite Materials

A family of lightweight, porous materials can be fabricated by using a new "fugitive-fiber" process. Fibers such as nylon are stitched through an uncured sheet of graphite-reinforced epoxy prepreg or other composite, cured, then removed by a suitable technique such as leaching. The process should allow a wide range of controlled porosity materials to be manufactured at low cost.
(See page 487.)

Improved Silicone-Rubber-to-Silicone-Rubber Bonding

Flatwise tensile-test results indicate that stronger silicone-rubber-to-silicone-rubber bonds result if the rubber is left unprimed and the cured surface is lightly abraded before the uncured layer is applied. Average maximum tensile loads for several specimens were more than doubled by this procedure, indicating that standard bonding methods should be modified.
(See page 488.)

Cast-in-Place Grommets for Honeycomb Substrates

Cable grommets are easily installed without weakening subchassis.

Caltech/JPL, Pasadena, California

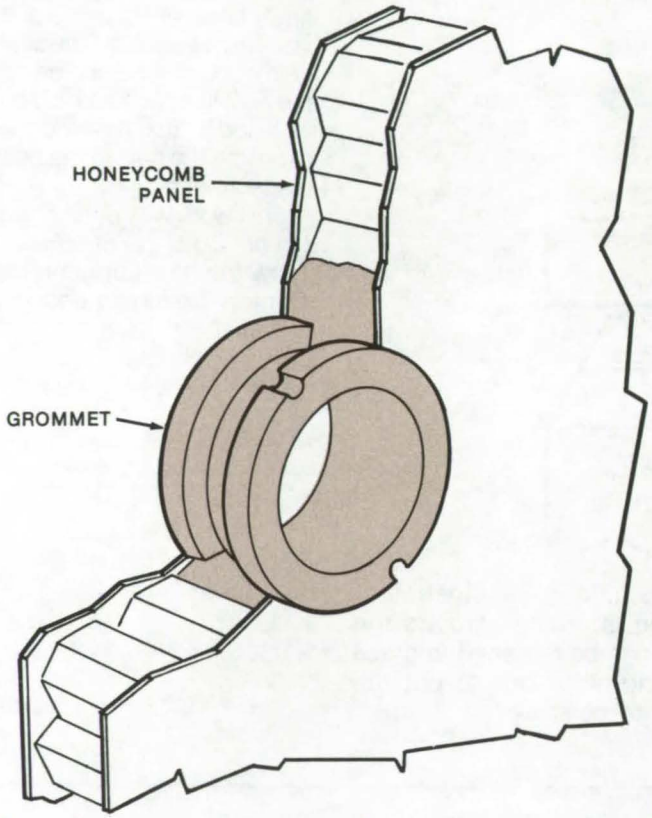

Cast-in-Place Grommet is structurally compatible with lightweight honeycomb substrates. The size of the hole, set at a minimum during casting, can be enlarged by drilling to accommodate a range of cable diameters.

To reduce weight, some electronic assemblies, such as those used in spacecraft, must be mounted in lightweight, relatively-weak honeycomb subchassis. These honeycomb structures are weakened even further if conventional cable grommets are installed in the honeycomb web.

A new Teflon grommet that is cast-in-place (see figure) is easily installed and compatible with honeycomb structural integrity. After casting, the grommet blank has only a minimum hole size; however, the opening can be enlarged by drilling to accommodate a range of larger cable diameters. Since the grommet is installed flush with adjacent mounting surfaces, it cannot fall out.

This work was done by Mervin K. Parker of **Caltech/JPL.** *No further documentation is available.*
NPO-13868

Books and Reports

These reports, studies, and handbooks are available from NASA as Technical Support Packages (TSP's) when a Request Card number is cited; otherwise they are available from one of NASA's Industrial Application Centers or the National Technical Information Service.

Welding Thermocouples to Columbium

Special thermocouples and attachment techniques are required for rocket engines and other applications.

Columbium (niobium) has proved itself to be an almost indispensable metal in rocket engines. However, until now, it has been impossible to attach thermocouples to columbium thrust chambers for testing. Conventional welding methods (capacitance-discharge spot welding and heliarc welding with stainless-steel rod and even with high-columbium-content rod) used for stainless-steel or molybdenum chambers has been ineffective. Test engineers have resorted to spring-loading tungsten-rhenium thermocouples so that their exposed junctions pressed against the chamber wall; but the data that resulted seemed highly suspicious because they differed widely from the expected temperature readings.

To solve the problem, an investigation was made of thermocouple welding, with the goals of finding a suitable welding method, evaluating thermocouple materials, and developing a welding procedure. Using titanium weld rod turned out to be the answer to the attachment problem. A small bead of titanium, heliarc-welded to the columbium chamber (with or without its coating being ground off), adhered so tightly that it could not be dislodged with a

hammer and chisel. Next, various thermocouples were tested for responsiveness and durability when titanium-welded to columbium. The results:

- Chromel-Alumel couples are easily attached and durable, but they are limited to temperatures of about 2,500° F (1,300° C).
- Tungsten-rhenium extension-wire couples have approximately the same properties as Chromel-Alumel couples.
- Tungsten-5 percent rhenium/tungsten-26 percent rhenium couples are easy to attach and usable up to 4,000° F (2,200° C) — but they are so brittle that engine vibration is likely to break them.
- Platinum-6 percent rhodium/platinum-30 percent rhodium couples perform ideally in measuring temperatures up to 3,300° F (1,800° C) — a high enough range for the temperatures that occur in the columbium chamber.

Although the platinum-rhodium alloys clearly make the best thermocouple, they are extremely expensive. The long run of thermocouple wire to reach a reference junction box — standard practice with Chromel-Alumel and other common thermocouple materials — would be prohibitive. Instead, a short length of platinum-rhodium wire can be connected to a copper extension wire that leads directly to the instrumentation; but this means that the reference junction (the thermocouple-wire-to-copper-wire junction) will be at ambient temperature. It is important, therefore, to protect this junction so that it will not be influenced by heat radiated from the engine. Usually, merely insulating or shielding it is enough.

The procedure developed for attaching thermocouples is simple and explicit. It includes such steps as preparing the columbium surface by cleaning it, depositing a globule of titanium, and remelting the globule and inserting the thermocouple wires in it.

This work was done by Frank R. DeMonbrun, Lawrence A. Goudie, and Jesse C. Huguley of Northrop Services, Inc., for **Johnson Space Center.** *To learn how to obtain a copy of the report, Circle 65 on the TSP Request Card.*
MSC-16676

Computer Programs

These programs may be obtained at very reasonable cost from COSMIC, a facility sponsored by NASA to make new programs available to the public. For information on program price, size, and availability, circle the reference letter on the COSMIC Request Card in this issue.

Automated Process Planning System

Aid to manufacturers of machined parts

The CAM-I Automated Process Planning (CAPP) System helps process engineers set up manufacturing plans for machined parts. Typically, a process engineer will need to draw up a sequential list of individual steps needed to manufacture a part in a particular facility. The CAPP System allows one to develop and store a library of similar parts characteristics, as related to a particular facility. This information is then used in an interactive system to help develop manufacturing plans that meet required standards.

The basic system logic for CAPP is derived from "group technology" methods of coding and classifying populations of machined parts for the purpose of segregating them into family groups. Each part family comprises "like" parts having characteristics sufficiently common to prescribe basically the same method of fabrication. Before using the program, the individual parts must be classified and coded, and parts families must be established by the user. These data are then loaded into the CAPP System files.

Part families are symbolically represented in system storage by matrix structures. The set of classification codes that, after analysis, has been deemed to constitute a part family group is then input in matrix format via a file-management utility program. The common manufacturing method established for a specific part family is termed the "standard plan" for that part family. One standard plan for each part family is loaded into the CAPP System files. Standard plan generation is the responsibility of the user and occurs external to CAPP. The CAPP System includes a set of utility programs for generating and maintaining the system files that comprise the part family and standard plan data bases.

Once the CAPP System files are established, the generation of new process plans using the system may begin. Input of an individual classification code, representing the new part to be planned, results in a validity check of the code. If the code is valid, a search of the Part Family Matrix File is made in an attempt to establish the existence of a matrix representing a part family to which the input code should logically belong. If no concurring matrix is found, a negative message is returned from the search. If a matrix concurrence exists, the identification number of the part family represented by the matrix will be returned. In the negative-search situation, the user will manually have to generate the process plan for that part. The process plan can then be entered into the CAPP System so that it is available for future searches.

When a search yields a part family concurrence, the user may retrieve the standard plan for that part family for use in development of a specific process plan for the new part. The

(continued next page)

standard plan is displayed in a series of menus based on three defined hierarchical levels of operation planning information. Using the editing capabilities of the CAPP System, the user modifies and/or extends the standard plan to suit his specific new part. If the part family refinement and standard plan specification are satisfactory, there should be little modification or new data required.

The user also has the option to retrieve and display completed part-dependent process plans from within the part family. A "create same as, except" mode may then be used under the assumption that minimal editing of the process plan will be involved. When a new process plan that satisfies part requirements is complete, the new process plan can be stored in the CAPP System permanent online storage. It is then available for future reference. An interface routine is provided to retrieve a sequential listing of a specific process plan by part number key.

The CAPP System is written in FORTRAN IV and IBM OS Assembler for implementation on an IBM 360/370 system with Time-Sharing Option (TSO). It requires at least one direct access device and approximately 50K of central memory. The display terminal device supported is the Hazeltine, Model 2000.

This program was written by Walter Mann of **Ames Research Center.** *For further information, Circle H on the COSMIC Request Card.*

ARC-11145

Mathematics and Information Sciences

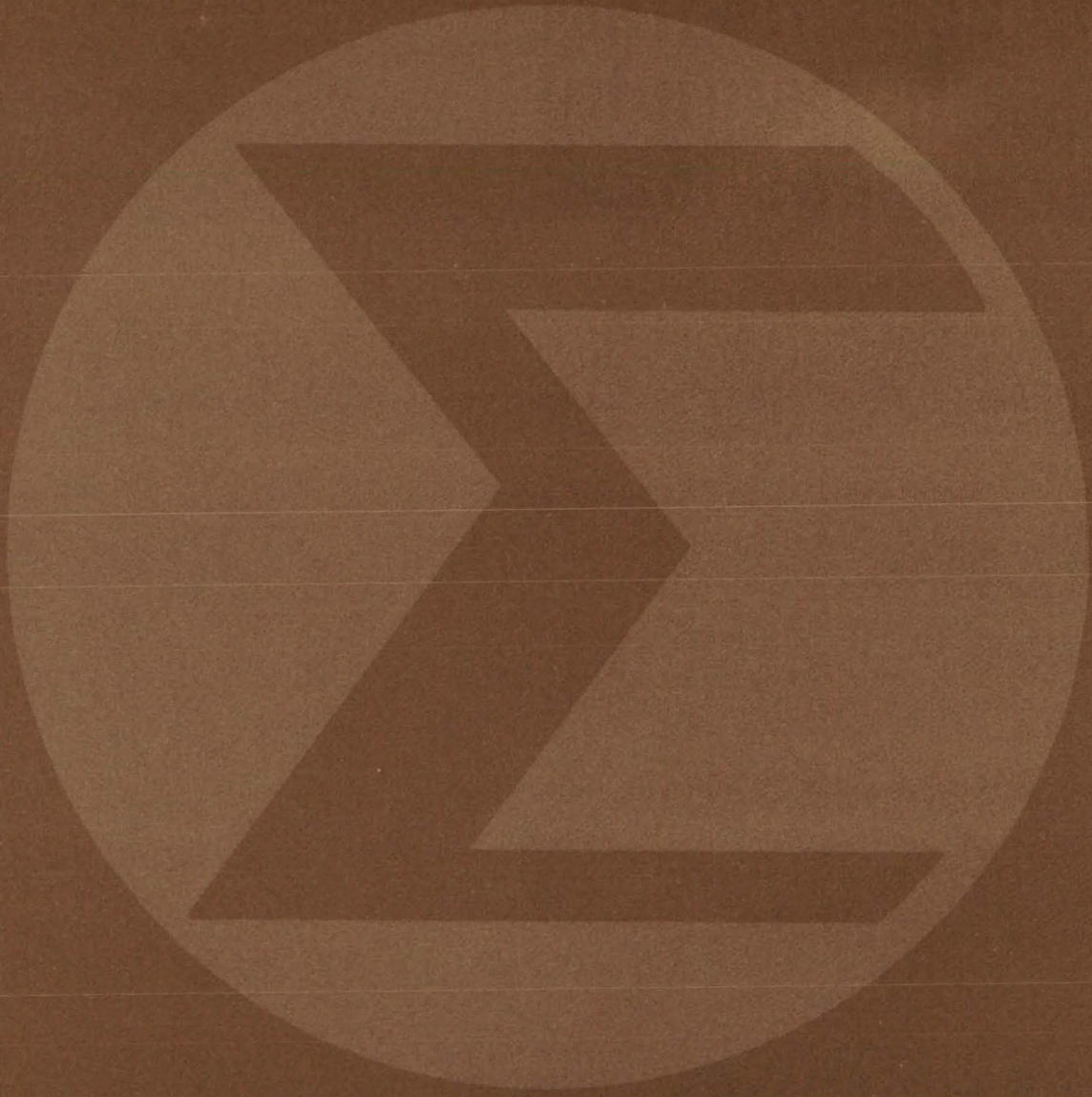

Calculating Parts Factors for Redundant Systems

Reliability analysis simplifies calculations and is easily programed.

Marshall Space Flight Center, Alabama

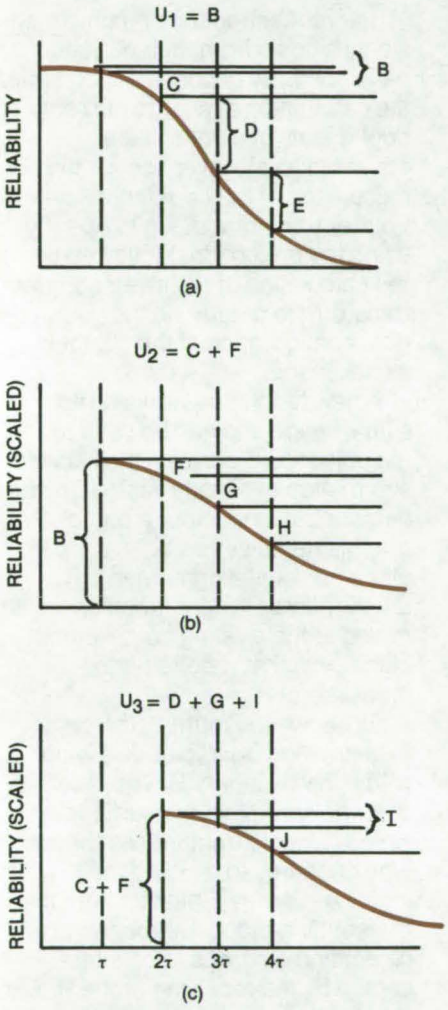

Module Reliability Curve is scaled and displaced after each service interval to determine the reliability curve for the next interval. The reliabilities for each module can then be used to calculate the parts factor for the system, useful in estimating repair and service costs. The symbols are defined in the text.

In systems such as spacecraft that require periodic replacement of redundant elements, the estimation of service and repair costs involves the determination of a constantly-varying parts factor, which is the fraction of the system replaced during each servicing operation. A new method that is easily programed simplifies the calculation of the parts factor. The individual module unreliabilities are computed as a function of the number of service intervals and service interval length.

The parts factor is then calculated from

$$pf = \sum_{i=1}^{n} \frac{\left(\begin{matrix}\text{module}\\ \text{unreliability}\end{matrix}\right)\left(\begin{matrix}\text{module}\\ \text{weight}\end{matrix}\right)}{\text{total system weight}}$$

where the summation is across all modules in the system of interest. The module unreliabilities are evaluated at the servicing time. It is assumed that on the average (over a large number of identical modules), the number of failed modules divided by the initial number of modules is the unreliability. The concept is then extended to say that, on the average, a part of each module, equivalent to its unreliability, will be replaced. The unreliability can thus be examined on a per-module basis.

In the figure, (a) represents the module reliability (R) curve starting from zero time. The unreliability (U) is given by 1 − R. The quantities B, C, D, and E represent the change in unreliability from one servicing interval to the next for those modules that are never replaced. At time τ, modules are replaced, on the average, to the extent of the unreliability B. The change in the reliability of these replaced modules with time is shown in (b). The reliability function has been scaled by the number (B) of modules replaced, and the curve has been shifted to the right by one servicing period. The unreliability at 2τ then becomes C plus F. These are replaced by C-plus-F new modules that start their decay from unity reliability at time 2τ, as shown in (c).

At each service interval, the unreliability is the sum of the unreliabilities of the replaced and original modules. It must be calculated for each module (or module with a different reliability function) to obtain the parts factor.

This work was done by W.L. DeRocher, Jr., of Martin Marietta Corp. for **Marshall Space Flight Center.** *For further information, Circle 66 on the TSP Request Card.*
MFS-23413

Obtaining a Tomographic Image From Transmission Projections

Object configuration is obtained by a simple summation of density values.

Caltech/JPL, Pasadena, California

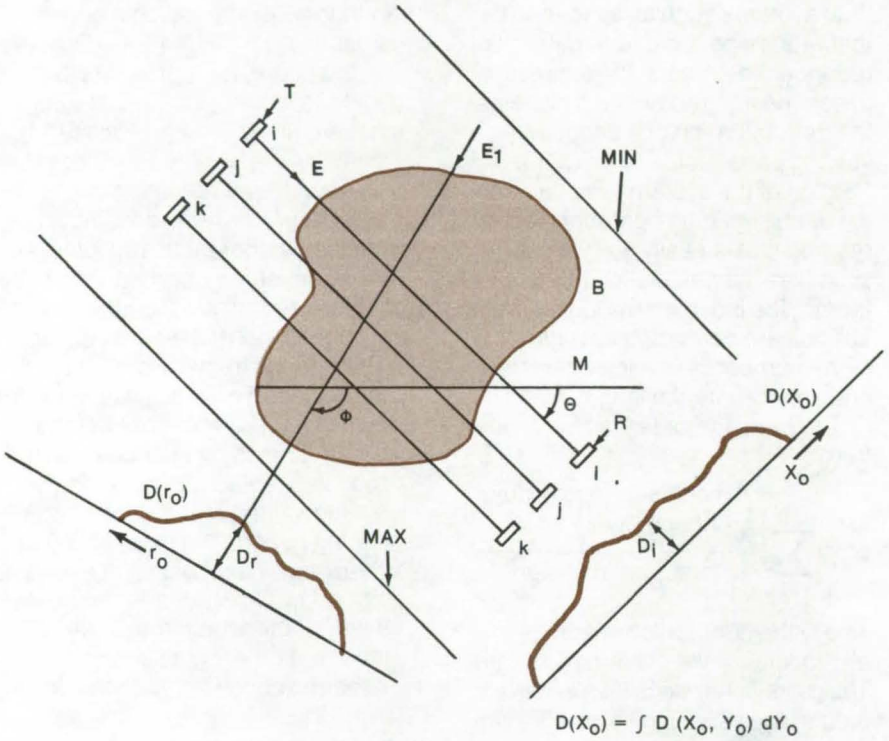

Figure 1. The **Projection Density Values** [$D(X_o)$, $D(r_o)$, etc.] of a scanned object are recorded as a function of scanning position. The transmitting and receiving probes (T and R) are translated perpendicular to the path of energy between them, and then the direction of propagation (θ, ϕ, etc.) is varied.

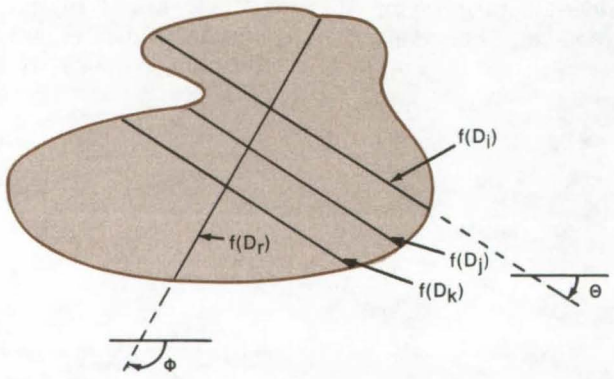

Figure 2. A **Tomographic Image** is obtained by using first the density values D_i of the original scan to compute an appropriate value of intensity on the reconstruction plane as a constant value $f(D_i)$ of the original scanning path. Every other processed intensity line $f(D_r)$ is then superimposed on the plane.

The reconstruction of multidimensional signals from their projections has previously depended upon either the calculation of a large number of coefficients of a set of linear equations in signal space, or the calculation of the two-dimensional Fourier transform of the image (by using the projections) followed by the calculation of the inverse Fourier transform to determine the geometrical configuration of the object in signal space.

A new technique works directly in signal space and can be used to find the object configuration by a simple summation of density values. In one demonstrated version, a photographic negative has been used in place of a digital computer. In another embodiment, addition replaces the existing complicated algorithms that require large processors.

As shown in Figure 1, the object to be imaged is indicated as lying within the boundary B. The object lies wholly within a medium M, which is itself structureless for the type of energy to be used for imaging. Energy E passes from the transmitting probe T through the test object and emerges to be intercepted by the receiving probe R. For proper imaging, the energy should be sensibly undeflected in its passage through the test object. The direction of propagation bears some angular relationship Θ with a fixed coordinate axis on the test object.

To obtain a tomographic section, the two probes are translated perpendicular to the path of energy between them and may, for example, assume successive places, such as i, j, k, etc.; the minimum and maximum positions of the line of energy must be outside the boundary B. Attached to the two

probes are devices, such as sine/cosine and position potentiometers, which indicate the geometrical relation between the instantaneous position of the probes and the reference geometry of the scanned object. The projected density $D(X_O)$ is processed to represent a continuum of values as a function of probe position for a particular angle of projection. Further sets of projections are then taken at different scan angles, e.g., Φ.

The image is reconstructed by the precise inverse of scanning. Signal values corresponding to the density of projection are added as constant terms along the line corresponding to the original path between the two probes that give rise to that density value. The tomograph is thus built up as a superposition of density values corresponding to each angular projection view, as shown in Figure 2. Such superposition may be accomplished by a computer or by any imaging device capable of the appropriate time-exposure reciprocity, such as film or scan converter displays. The tomograph may be enhanced by subtracting the constant background level from the constructed image.

This work was done by Richard C. Heyser and Robert Nathan of **Caltech/JPL.** *For further information, Circle 67 on the TSP Request Card.*

Inquiries concerning rights for the commercial use of this invention should be addressed to the Patent Counsel, NASA Pasadena Office-JPL. Refer to NPO-13739.

Image Registration Using Binary Boundary Maps

Simpler, faster method for alining digital images

Marshall Space Flight Center, Alabama

Procedures for alining ground-scene images recorded at different times, or with different detectors, play an important role in the analysis of remotely-sensed Earth observation data. When the image is recorded as digital data, the matching procedures (registration) can be used to detect changes in ground features as a function of time. For instance, registration based on satellite imagery is used to estimate cloud velocities for global weather information. For multispectral camera data, images from the different camera stations must be registered before analysis can be performed.

Since image registration typically involves large quantities of raw data, it is desirable to make the procedure more efficient and shorten computer run time. A registration technique that matches binary boundary maps extracted from the raw data, rather than matching the actual data, is considerably faster than other techniques [such as the fast Fourier-transform (FFT) correlation routine]. The boundary maps, which are digital representations of regions where the image amplitudes change significantly, typically represent a data compression of 60 to 70 percent. Additional data simplifications are made by working with sequences of boundary points. Since the binary boundary maps contain only "0's" and "1's", computational factors needed for registration, such as average-amplitude products, are always positive and are sharpened so that the removal of means and normalization is not necessary. Furthermore, the maps allow the average products to be computed with addition rather than multiplication, further reducing computation time.

The program that generates the boundary maps runs about 13 minutes on a large computer, for an area of 1,000 row scans by 255 columns. This includes time to read and compile the program in addition to the calculation time. The program calculates the average change in the data at each row and column intersection for displacements by a single row or column. The spectroscopic changes in the x (scan) and y (column) directions are stored in a joint histogram. These changes may be selected as boundary points if they are large compared to the x and y modes of the joint histogram. In this comparison "largeness" is decided by a discriminating criterion with several decision input parameters. The selected points are assigned the value "1"; the remaining points are assigned "0" to form the boundary map that corresponds to the image.

Pairs of boundary maps are registered according to a correlation and registration procedure that compares one map (the "picture") with local areas ("windows") on the other map. It is assumed that the images can be registered through translations and rotations only, that the images have the same scale, and that little or no distortion exists. It is further assumed that by working with several local areas, rotation effects in the local areas can be neglected; by treating misalinements of the local areas as translations, rotational and translational misalinements of the larger images can be determined. This procedure can be repeated until the desired degree of registration is achieved. When correlating, sequences of boundary points on the window and the picture are compared, and row and column shifts are made until coincidence is maximized.

This work was done by J. F. Andrus, C. W. Campbell, and R. R. Jayroe of **Marshall Space Flight Center.** *Further information may be found in NASA TN-D-7607 [N74-19035], "Digital Image Registration Method Based on Binary Boundary Maps," a copy of which may be obtained at cost from the New England Research Application Center* *[see page A7]*.

Inquiries concerning rights for the commercial use of this invention should be addressed to the Patent Counsel, Marshall Space Flight Center *[see page A8]*. *Refer to MFS-23043.*

Defining Structural Limit Loads

In terms of the probability distribution of largest loads occurring in a time interval

Marshall Space Flight Center, Alabama

Fluctuating dynamic loads such as wind gusts and wave forces are usually described by the power spectral density (PSD) function of a stationary and ergodic Gaussian random process with zero mean and standard deviation σ. Limit loads describing the extreme design condition are typically defined as percentile values (e.g., 3σ) of the nominal load probability distribution.

A new method for defining limit loads uses the probability distribution of the largest load occurring during given time intervals. The method is compatible with both deterministic and probabilistic structural design criteria. It also rationally accounts for the fact that the longer a structure is exposed to a random loading environment, the greater is the possibility that it will experience an extreme load.

The lognormal distribution is proposed as an acceptable approximation to the exact distribution of normal extremes. Referring to equation 1 in the figure, the design limit load

$$\ln x_p = \ln(\check{y}\cdot\sigma) + K_p\cdot\delta \quad (1)$$

$$\text{where } p = \frac{1}{\sqrt{2\pi}}\int_{-\infty}^{K_p} e^{-t^2/2}dt$$

$$F(\check{y}) = \exp\left[(\ln 0.5)\,[1 - F(\hat{u})]\right] \quad (2)$$

$$\delta = 0.00199\hat{u} - 0.0633 + 0.6634\hat{u}^{-1} - 0.2648\hat{u}^{-2} \text{ for } 1 < \hat{u} < 16 \quad (3)$$

$$\hat{u} = \left[2\ln(T\cdot E[N_+(0)]\right]^{1/2} \quad (4)$$

Equations Defining the Design Limit Load [x_p] are discussed in the text.

(x_p) is defined as the pX100 percentile value of the lognormal variate representing the random extreme largest load. In equation 1, σ represents the standard deviation of the nominal load probability distribution. The standardized extreme median ($\check{y}$) and the parameter δ are expressed in equations 2 and 3 in terms of the standardized characteristic largest value ($\hat{u}$) given in equation 4. In this equation, $E[N_+(0)]$ is the expected rate of zero crossings with positive slope, as given by Rice's standard formula, and T is the given time duration for which the largest load is desired. The method is primarily a comprehensive interpretation of load quantities that are typically calculated as part of conventional structural analyses for random loading conditions.

This work was done by David H. Merchant of The Boeing Aerospace Co. for **Marshall Space Flight Center.** *No further documenation is available.*
MFS-23582

Autonomous Rendezvous and Feature Detection System

Algorithms and equations have been developed for converting standard television-image data into steering signals for spacecraft. Accurate relative position is obtained by scanning a ground area that "overlaps" the spacecraft edge, then converting the images into threshold maps. The data can augment primary spacecraft guidance, navigation, and attitude-control equipment.
(See page 451.)

Optimizing Simulated Trajectories

A general-purpose, six-degrees-of-freedom program solves a variety of rigid-body flight-mechanics problems. The program is composed of functional elements that define the vehicle environment and the output format and perform targeting and optimization calculations. It has a novel input listing feature that saves deck setup time and cost.
(See page 520.)

Automated Process Planning System

A new computer program helps process engineers set up manufacturing plans for machined parts. The system classifies "like" parts into populations having a similar method of fabrication. When considering a new part, the user retrieves the standard plan for the appropriate family and modifies or extends it as necessary. The system can be updated as new parts or families are developed.
(See page 548.)

Books and Reports

These reports, studies, and handbooks are available from NASA as Technical Support Packages (TSP's) when a Request Card number is cited; otherwise they are available from one of NASA's Industrial Application Centers or the National Technical Information Service.

Nonlinear Finite Elements

Handbook provides rapid access to wide variety of element types.

A comprehensive survey of past and current literature on geometrically-nonlinear finite elements has been organized into handbook form and can serve as a valuable reference when solving problems in nonlinear structural mechanics. The handbook provides rapid access to a wide variety of element types and can facilitate the evaluation of different elements as to their features, probable accuracy, and complexity. The compilation can serve as a guide in the choice of nonlinear elements for specific problems and as background to provide directions for new element developments. It should be particularly useful in generating computer codes for finite elements.

The elements are classified according to type as beams, plates, shells, and solid or three-dimensional elements. Within each type, the elements are further identified by the assumed displacement shape and form of the nonlinear strain equations. Solution procedures are deemphasized, except when a particular element formulation poses special problems or capabilities.

Each handbook description includes a brief definition of the element, followed by the displacement function equations and a concise description of the element in narrative form. This is followed by an identification of the reference in which the element was derived, variations from the basic element, and any known advantages or disadvantages it may have. The strain displacement equations are given to indicate how the geometric nonlinearities are introduced into the strains and what nonlinearities are included in the formulation. Finally, there is a discussion of the element that presents user-oriented information concerning material description, coordinate systems, and solution procedures.

This work was done by R. E. Jones and J. W. Straayer of The Boeing Aerospace Co. for **Marshall Space Flight Center.** *Further information may be found in CR-144276 [N76-22582], "Survey and Developments of Finite Elements for Nonlinear Structural Analysis," a copy of which may be obtained at cost from the New England Research Application Center [see page A7].*
MFS-23664

Computer Programs

These programs may be obtained at very reasonable cost from COSMIC, a facility sponsored by NASA to make new programs available to the public. For information on program price, size, and availability, circle the reference letter on the COSMIC Request Card in this issue.

WOLF Contouring and Plotting Package

Flexible and easily used with printers and CRT's

The WOLF Contouring and Plotting Package is a general-purpose plotting and contouring package for producing line-printer, SC4020, Gerber, Calcomp, and SD4060 plots. Tasks ranging from a quick simple plot (which requires only one call to the package) to highly sophisticated plots (including motion picture plots) can be easily generated with only a basic knowledge of FORTRAN and the plot commands. Designers preparing a software system that requires plotted output will find that this package offers many advantages over the standard hardware support packages available.

The WOLF package is divided into a plot segment and a contour segment. The plot segment can produce output for any combination of line-printer, SC4020, Gerber, Calcomp, and SD4060 plots. The line printer allows the user to have plots available immediately after a job is run at a low cost.

Although the resolution of line-printer plots is low, the quick results allow one to judge whether a high-resolution plot of a particular run is desirable. The SC4020 and SD4060 provide high-speed high-resolution cathode-ray plots, with film and hard-copy output available. The Gerber and Calcomp plotters provide very-high-quality (of publishable quality) plots of good resolution. Being bed- or drum-type plotters, the Gerber and Calcomp plotters are usually slow and not suited for large-volume plotting.

All output for any or all of the plotters can be produced simultaneously. The types of plots supported are: linear, semilog, log/log, polar, tabular data using the FORTRAN WRITE statement, 3-D perspective linear, and affine transformations. A labeling facility prepares horizontal labels, vertical labels, diagonal labels, vector characters of a requested size (special character fonts are easily implemented), and rotated letters. Gridding routines label the gridlines according to user specifications. Special line features include multiple lines, dashed lines, and tick marks.

(continued next page)

The contour segment of this package is a collection of subroutines that can be used to produce contour plots and perform related functions. The package can contour any data that can be placed on a grid and any data that are regularly spaced, including any general affine or polar grid data. The package includes routines that will grid random data. Contour levels can be specified at any values desired.

Input data can be smoothed, with undefined points being acceptable where data are unreliable or unknown. Plots that are extremely large or detailed can be automatically output in parts, to improve resolution or overcome plotter size limitations. The contouring segment uses the plot segment for actual plotting; thus all the features described for the plotting segment are available to the user of the contouring segment.

Included with this package are two data bases for producing world map plots in Mercator projection. One data base provides continent outlines only, and another provides continent outlines and national borders in great detail.

This package is written in FORTRAN IV and IBM OS Assembler and has been implemented on an IBM 360 with a central memory requirement of approximately 140K of 8-bit bytes. The Assembler routines are basic plotter interface routines.

This program was written by Geofrey T. Masaki of **Goddard Space Flight Center** *and Ron Williamson of Wolf Research, Inc. For further information, Circle J on the COSMIC Request Card.*
GSC-12326

SUBJECT INDEX

National Aeronautics and
Space Administration

Washington, D.C.
20546

Official Business
Penalty for Private Use. $300

SPECIAL FOURTH-CLASS RATE
BOOK

FOURTH-CLASS MAIL
POSTAGE & FEES PAID
NASA
WASHINGTON, D.C.
PERMIT No. G 27

NASA

Rapid and mobile communications are the purpose of a new radio and telephone communications terminal designed by engineers at NASA's Johnson Space Center in Houston, Texas. Tested for emergency medical services operations at the Odessa, Texas, Medical Center, the terminal transmits medical-instrument data and voice communications over three telephone and three radio lines. See page 497 for a description of this terminal.

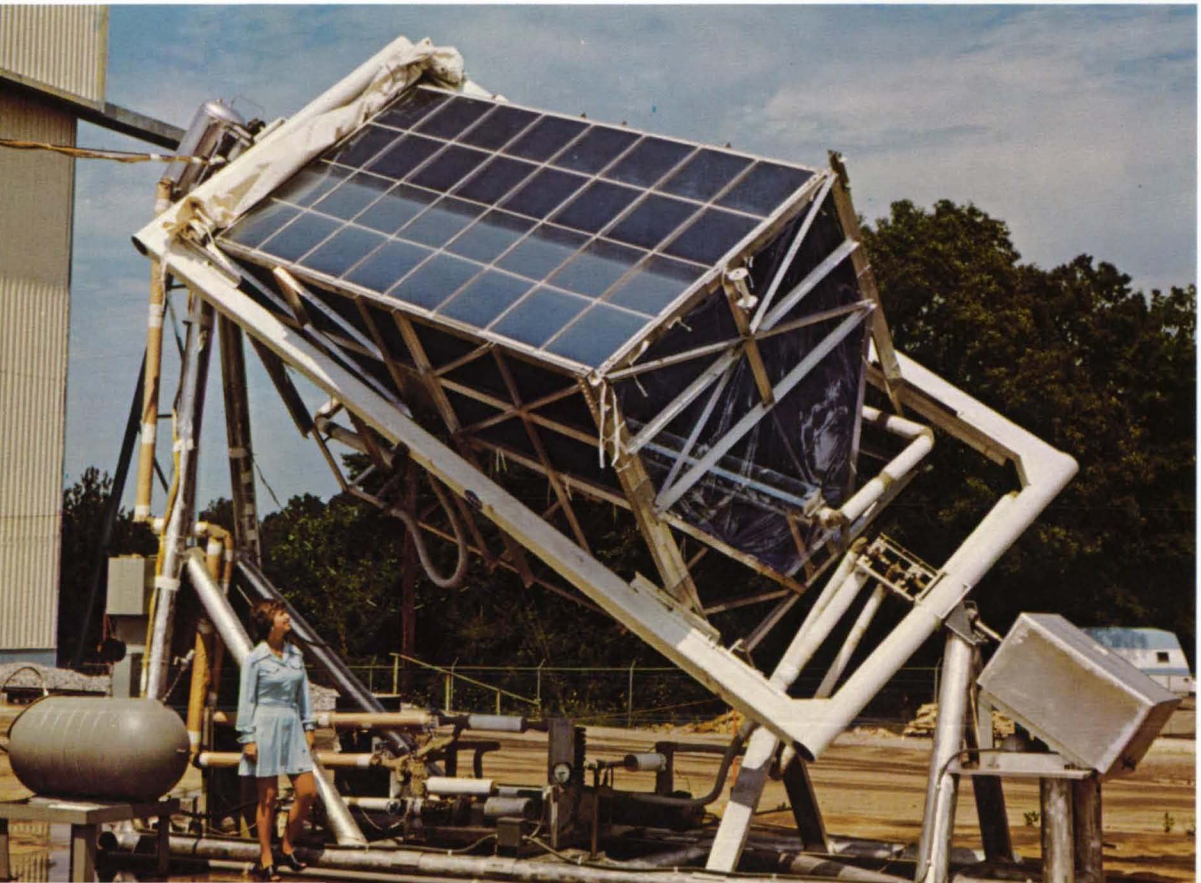

Aerospace power requirements led to an early interest by NASA scientists in solar-energy systems. Today, NASA continues to design and test systems, including many for terrestrial uses, such as the solar thermal concentrator at the left. Developed at NASA's Marshall Space Flight Center in Alabama, this tracking concentrator, which uses Fresnel lenses, is described on page 461.